Doctoral theses at NTNU, 2021:128

Tor Inge Reigstad

Optimal control of variable speed hydropower

Utilising model predictive control and virtual inertia for delivering power system services

Doctoral thesis

NTNU
Norwegian University of Science and Technology
Thesis for the Degree of
Philosophiae Doctor
Faculty of Information Technology and Electrical Engineering
Department of Electric Power Engineering

NTNU
Norwegian University of
Science and Technology

Tor Inge Reigstad

Optimal control of variable speed hydropower

Utilising model predictive control and virtual inertia for delivering power system services

Thesis for the Degree of Philosophiae Doctor

Trondheim, May 2021

Norwegian University of Science and Technology
Faculty of Information Technology and Electrical Engineering
Department of Electric Power Engineering

NTNU
Norwegian University of
Science and Technology

NTNU
Norwegian University of Science and Technology

Thesis for the Degree of Philosophiae Doctor

Faculty of Information Technology and Electrical Engineering
Department of Electric Power Engineering

ISBN 978-82-326-5323-2 (printed ver.)
ISBN 978-82-326-5870-1 (electronic ver.)
ISSN 1503-8181 (printed ver.)
ISSN 2703-8084 (online ver.)

Doctoral theses at NTNU, 2021:128

Printed by NTNU Grafisk senter

Preface

This PhD project was has been conducted at the Department of Electric Power Engineering at NTNU in Trondheim, Norway. It was part of task 2.5 “Flexible hydropower unit” in WP 2 “Turbine and generators” of the FME research project HydroCen. The main objective of HydroCen is to enable the Norwegian hydropower sector to meet complex challenges and exploit new opportunities through innovative technological solutions. The project is financed by the Norwegian Research Council under grant number 257588 and several industry partners, however, the PhD was financed by NTNU.

Acknowledgments

This thesis summarises and concludes the research performed during my PhD study, which was carried out at and financed by the Department of Electric Power Engineering at the Norwegian University of Science and Technology (NTNU). The PhD is a part of the FME research project HydroCen founded by the Norwegian Research Council and partners within the hydropower industry. The main objective of the project is to enable the Norwegian hydropower sector to meet complex challenges and exploit new opportunities through innovative technological solutions.

I'm extremely grateful to my supervisor, Kjetil Uhlen, for his essential support and for his confidence in my work. He is also the creator of the innovating project description, boosting the progress of my work from the very first day. Special thanks go to my co-supervisor Arne Nysveen for his knowledge-sharing and contact network within the hydropower industry.

I am also grateful for all technical discussions that have been of considerable importance for my thesis. Many thanks go to my NTNU colleagues Torbjørn K. Nielsen, Pål Tore Storli, Bjørnar Svingen, Trond Toftevåg, Olimpo Anaya-Lara, Thomas S. Haugan, Raghbendra Tiwari, Gilbert Bergna-Diaz, Dan El Andres Montoya Andrade, Olav B. Fosso and Lars Imsland, and my SINTEF Energy colleagues Olve Mo, Karl Merz, Thuc Dinh Duong, Raymundo E. Torres-Olguin, Jon Are Suul, Salvatore D'Arco, Santiago Sanchez-Acevedo and Sigurd Hofsmo Jakobsen.

Last but not least, I want to thank the most important peoples in my life, my exceptional wife and mentor Gunhild and my clever daughters Ingvild and Signe. Gunhild, thank you for your guidance, motivation, pushing, patience, encouragement, support and love. You have made this work easier for me.

Summary

Variable speed operation of hydropower plants can be of benefit to the security and flexibility of power system operation. This thesis focuses on system services related to power balancing and frequency control. By utilising the flexibility of the converter control system and the kinetic energy of the rotating generator and turbine, variable speed hydropower (VSHP) plants can provide system services like virtual (synthetic) inertia, damping and fast frequency reserves (FFR). In this thesis, a new VSHP control scheme is developed, aiming at significantly improving system frequency stability and increased damping of power oscillations.

The shift towards a more sustainable energy system demands thermal power plants with high inertia to be replaced by converter-based renewable energy. The reduction of system inertia challenges system stability, especially frequency stability but also the rotor angle stability. Since wind and solar power plants have almost no energy storage and no possibility to increase production when operating at maximum power point tracking, the possibility of delivering virtual inertia or fast frequency containment reserves is limited. In contrast to most other renewables, VSHP has a significant amount of energy stored in its rotation masses available for power system services. By proper control, the power-electronic converter can utilize this energy immediately to stabilise the power system. The turbine rotational speed will deviate from its optimal value as a result of this action. However, it is regained within seconds by controlling the turbine guide vane opening and thereby the turbine power.

An innovative control scheme is proposed in this thesis to optimise VSHP system services. Virtual inertia control is implemented on the grid-connected converter to counteract frequency deviations and damp oscillations. Two promising control schemes are analysed and compared: the grid-following virtual synchronous generator (VSG) and the grid-forming virtual synchronous machine (VSM). Further development of the VSM has been necessary to improve its frequency containment reserves supply. Moreover, the virtual inertia controllers are parametrised to

increase the damping of power oscillations by small-signal analysis.

A model predictive controller (MPC) is developed to optimise the control of the VSHP and coordinate the turbine control with the virtual inertia control. The MPC considers the constraints in both the hydraulic and electric systems to prevent damage to the system. Thus, it can optimise the turbine rotational speed to maximise the efficiency and minimise the guide vane operation. This reduction of the guide vane operation limits oscillations in the hydraulic system and reduces wear and tear. The MPC primarily controls the guide vane opening to adjust the turbine rotational speed. However, in extreme cases, it also adjusts the power reference of the virtual inertia controller to avoid the turbine rotational speed exceeding its limits.

Precise models of the VSHP were needed, both for simulations and for designing the MPC dynamic model. These comprised the development of a detailed VSHP model, including an advanced hydraulic model for grid integration studies. The hydraulic model is based on the Euler turbine equations and the 1-D momentum and continuity balance for a water-filled elementary pipe. As a result, the turbine power is modelled as a non-linear function of both the turbine flow, the turbine rotational speed and the guide vane opening.

The proposed control system, with MPC and virtual inertia controller, is tested on both the Kundur two-area system and the Nordic-44 system. The transient analysis shows the potential for significant reductions in frequency deviation after disturbances in the Nordic power system; a 40% reduction when the rated power of the VSHP power plants equals 5% of the total produced power in the power system. In addition, both the critical fault clearing times and the damping of oscillations are increased. Small-signal analysis verifies how appropriate tuning of the VSG reduces power oscillations. It also demonstrates negligible dynamic interaction between the hydraulic system and the electrical system. This conclusion applies for both:

- the proposed MPC control system as long as the cost function of the MPC is defined such that the costs of deviations in the hydraulic system are low compared to the cost of deviation in the VSG power reference, and;
- a VSHP with conventional PID controllers, where the grid-connected converter controls the VSHP output power, the generator-connected converter controls the dc-link voltage, and the guide vane controls the turbine rotational speed.

Consequently, the virtual inertia controller can be tuned without considering small-

signal stability issues related to the hydraulic system, synchronous generator or generator-connected converter.

The control scheme proposed in this thesis can benefit both the frequency control of the modern electrical power system and the development of a pump storage hydropower plant with variable speed operation. With economic initiatives, VSHP can profit by providing virtual inertia and/or fast frequency resources to the power system operator, thereby increasing the gain of new projects. At the same time, the system services provided by VSHP allows for further integration of renewable energy sources, such as wind and solar.

Contents

List of Abbreviations

aFRR Automatic Frequency Restoration Reserves

AGC Automatic Generation Control

AVR Automatic Voltage Regulator

BESS Battery Energy Storage System

CIGRE International Council on Large Electric Systems

CPC Constant Power Controller

DAE Differential-Algebraic Equations

DC Direct Current

DFIG Double-Fed Induction Generator

DFIM Double-Fed Induction Motor

DI Dimensioning Incident

ESS Energy Storage System

FCR Frequency Containment Reserves

FCR-D Frequency Containment Reserves for Disturbances

FCR-N Frequency Containment Reserves for Normal operation

FFR Fast Frequency Reserves

FRR Frequency Restoration Reserves

HVDC High-Voltage Direct Current

IEEE Institute of Electrical and Electronics Engineers

mFRR Manual Frequency Restoration Reserves

MHE Moving Horizon Estimator

MIMO Multiple-Input, Multiple-Output

MO Modulus Optimum

MPC Model Predictive Controller

PCC Point of Common Coupling

PD Proportional-Derivative

PID Proportional-Integral-Derivative

PLL Phase-Locked Loop

PMU Phasor Measurement Unit

POD Power Oscillation Damper

PV Photovoltaics

PWM Pulse Width Modulation

QP Quadratic Programming

QSEM Quasistationary electrical SM model

RES Renewable Energy Source

RL Resistance, Inductance

RLC Resistance, Inductance, Capacitance

ROCOF Rate Of Change Of Frequency

RR Replacement Reserves

SEM Spectral Element Method

SG Synchronous Generator

SM Synchronous Machine

SO Symmetrical Optimum

SVC Static VAR Compensator

TSO Transmission System Operator

VI Virtual Inertia

VSC Voltage Source Converter

VSG Virtual Synchronous Generator

VSG-PID Power-frequency PID controller with permanent droop

VSHP Variable Speed Hydropower

VSM Virtual Synchronous Machine

VSM-PD VSM with power-frequency PD controller

VSM-PID VSM with power-frequency PID controller

WF Wind Farm

Chapter 1

Introduction

The goal of the Paris Agreement to limit the global temperature rise to well below two degrees Celsius requires comprehensive alternations of the electrical power system. The development of renewable energy is massive and increasing. Around 75 % of all the net power capacity growth is now renewable [1]. It is expected that the renewable electrical capacity increases by 1220 GW worldwide toward 2024, a 50% increase compared to 2018. Solar power contributes the largest share of this increase; approximately 100 GW is built each year and is expected to grow to 130-170 GW per year by 2024. Wind power increases by around 60 GW per year, while approximately 20 GW new hydropower is added each year [1]. In Europe, the EU has proposed "The green deal" [2] which is a set of policy initiatives to make Europe climate neutral by 2050 and implies developing a power sector based largely on renewable resources. The ambitions are elaborated in the report "Clean Energy for all Europeans" [3]; Some of the main issues highlighted in this report, like the acceleration of the clean energy transition and increasing energy security, are also important motivations for the investigation of new ancillary services.

The growth in renewable energy challenges the electrical power system in many ways. One of the main issues is that solar power, wind power and some of the hydropower are uncontrollable; we cannot decide when and how much power the power plants should produce at a certain time [4]. Therefore, more flexible production and loads are required to control the balance of the grid. Variable speed hydropower (VSHP) can contribute to faster power balancing and frequency control than conventional hydropower by utilising the energy stored in the variable speed machinery based on converter technology. The VSHP is thereby a suitable source for delivering a wide spectrum of additional ancillary services to the grid.

VSHP offers many advantages and is used for different applications, with the most relevant being pumped-storage hydropower; however it can also be applied in small hydropower and in HVDC-connected plants. In pumped-stored plants, variable speed operation is necessary for effective control of the pumping power [5]. Pumped-stored plants are the most efficient large-scale energy storage with 70-85% efficiency [6]–[8]. They are primarily used for balancing the power production and load demand in the grid and may allow the thermal and nuclear power plants to operate at constant power at their maximum efficiency.

With the increasing integration of renewables with fast varying production that is hard to predict, more flexible energy storages are needed in the power system. A potential use of VSHP is to provide this flexibility and compensates the production of variable renewables. The hypothesis is that VSHP can offer additional ancillary services, contributing to the frequency control and improving the grid stability, thus allowing for higher penetration of renewables in the grid. The advantages compared to conventional pumped-storage hydropower with constant rotational speed are better utilisation of the rotation energy in the turbine and generator and improved power control in pumping mode. The efficiency at low power output and the operating range of variable speed hydropower will also be higher. Moreover, they can contribute to frequency control both in production and pumping mode [5]. By allowing the turbine rotational speed to deviate temporarily from its optimal speed, the VSHP is able to vary its output power quickly due to the converter technology [9]. In the first seconds after a disturbance, the energy is delivered to or taken from the kinetic energy in the turbine and generator. Subsequently, the governor will react to the deviation in the turbine rotational speed and adjust the guide vane opening to regain the optimal speed of the turbine. Through doing so, the VSHP can contribute more effectively to primary frequency control and the maintenance of grid stability. The VSHP plants will be able to provide fast frequency reserves (FFR) both in production and in pumping mode, and the efficiency and operating range will potentially be higher than for conventional hydropower and other variable renewable sources without storage. [5]

Additionally, the converter technology offers faster control of reactive power and higher reactive power capability, which benefits the voltage control. However, the converter short circuit current is limited and this can be challenging during faults.

Frequency control is an important part of the ancillary services and is fundamental for the quality of a power system. This thesis will primarily focus on the frequency containment reserves (FCR) and FFR. The FCR aims to manage imbalances through automatic decentralised control of production [10], [11]. The governor of thermal and hydropower plants is controlled to counteract frequency deviations within 5-30 seconds. However, this is too slow to reduce the minimum

frequency after a disturbance. The Nordic transmission system operators (TSOs) have therefore suggested implementing FFR. These reserves are fast enough to reduce the maximum frequency deviation and thereby reduce the requirements for inertia [12].

The direct-connected synchronous generators contribute with kinetic energy to the power system due to its inertia. The inertia of the synchronous machines reduces the frequency deviation in the first seconds after a power imbalance. Thermal and nuclear power plants have until now contributed the main part of the inertia to most of the power systems. Hydropower has less inertia; however, the FCR is faster and can contribute within seconds. In the future, there will be less rotation masses in the Nordic power system due to the increased amount of wind turbine and small-scale hydropower, reduced nuclear power and more HVDC connections. This will imply a decrease in the system inertia, which may cause problems for frequency regulation during disturbances. Today, the TSOs in the Nordic countries ensure that the FCR requirements are fulfilled by a marked system; however, the system inertia is assumed to be sufficient. This may not be the case for a system at low load and less thermal and nuclear power production [13], [14]. Virtual inertia or synthetic inertia control of converters in the system will solve such problems by controlling the active power supply after a disturbance. In fact, utilising FFR and virtual inertia is shown to be more effective than increasing the rotation masses [15].

Virtual inertia control of grid-connected converters will increase the total inertia in the power system and thereby reduce the frequency deviation after a disturbance. It has been a popular area of research for the last few years and many different layouts and applications of virtual (or synthetic) inertia have been investigated [16]. However, to achieve a large effect on the system frequency and stability, the converter has to be able to increase the power output quickly. For this to happen, the production of the power plant must be increased in a matter of milliseconds or a large amount of energy must be stored. A DC capacitor in for instance a PV plant will only be able to store and deliver a small amount of energy. Moreover, the production of the PV plant cannot be increased and PV is therefore not suited for virtual inertia control. A variable speed wind turbine is able to increase the output power by 5-10 % temporarily for several seconds by reducing the rotation speed in the case of an under frequency event. Since the optimal rotational speed must be retained to maximise the efficiency of the turbine, a recovery period with reduced power is followed [17], [18].

A VSHP stores energy in the rotation masses, and will therefore be able to deliver virtual inertia similar to the variable speed wind turbines. It has the advantage that the recovery period is not required since the VSHP can increase the mechanical

power by increasing the turbine flow. However, very little research has been performed on virtual inertia control of VSHP and especially on the limitations given by the turbine and waterway and how to maximise the frequency reserves. A relevant research question is thereby how virtual inertia control of VSHP can improve frequency services and grid stability and which virtual inertia structure is best fitted for the purpose. For this reason, we will need new knowledge on how the waterway, turbine, generator, converter control and grid interfere with each other in a VSHP, which raises new research questions. Firstly, how should the dynamics of VSHP plants for the purpose of grid integration studies be modelled? And secondly, how can the VSHP control system be designed to avoid small-signal interaction between the hydraulic system of the VSHP and the rest of the power system? This knowledge will be the basis for the development of optimal control strategies for control of the VSHP.

An advanced control system has been developed in this thesis to utilise the potential of the VSHP for virtual inertia and frequency control. The objective of the control system is to optimise the operation of the power plant while considering the constraints in the electric and the hydraulic systems. This can be achieved by combining virtual inertia control for improving the power response to frequency deviations with model predictive control (MPC) for handling the internal control of the VSHP. The proposed controller structure allows for quicker changes of the VSHP output power by utilising the rotational energy of the turbine and generator compared to a conventional power plant, where the slow governor response will limit the ancillary service capabilities. Through this, new possibilities such as faster frequency control and other grid ancillary services present themselves, but this also necessitates proper co-ordination of the controls - and there will be new constraints that must be taken into account. The thesis will answer how both linear and nonlinear MPC can increase the VSHP plants' contribution of FFR and virtual inertia and what the potential for frequency and rotor angle stability improvements would be. Another research question to be answered is: How can small-signal analysis of the VSHP with the suggested MPC be performed to avoid small-signal interaction between the hydraulic system of the VSHP and the rest of the power system?

1.1 Objectives and Main Contributions

The focus of the PhD work is to investigate the interactions between the VSHP plant and the electric power system and how variable speed operation can benefit the security and flexibility of the power system operation. The main research task has been to explore the control possibilities from a system perspective while considering the limitations given by the hydraulic system. This comprises the de-

velopment of nonlinear time-domain simulation models including constraints for the hydraulic system with waterway, turbine, governor, generator, generator-side converter, grid-side converter and representative test grids. These models are used for testing the developed control systems, both for dynamical analysis and small-signal analysis. Well-proven converter control schemes are compared to virtual inertia control methods such as the virtual synchronous generator (VSG) and the virtual synchronous machine (VSM).

Variable speed operation allows the possibility for better utilisation of the energy of the rotation masses in the generator and turbine during faults and transients. When the synchronous generator is connected directly to the grid, the rate of change of power output is limited by the maximum speed of the governor, the maximum pressure in the waterway and over the turbine blades and the stability properties of the governor and hydraulic system. In a VSHP plant, the power output of the grid converter can be controlled faster by utilising the rotational energy of the generator and the turbine. New control schemes for coordinating the control of the governor and the grid converter are developed. Model predictive control (MPC) is found to be well suited for the purpose since the control system needs to consider the constraints in the hydraulic system, the turbine speed and the power output of the converters and at the same time optimise the control from a power system perspective.

The objectives of the thesis are to:

- Develop dynamic models of hydropower plants that are applicable for VSHP plants including waterway, turbine, generator, converters and controllers for grid integration studies.
- Develop models for small-signal analysis and parametric sensitivity of VSHP, including virtual inertia control.
- Investigate the performance of different types of virtual inertia control for VSHP plants and compare them to conventional converter control concerning the availability to deliver frequency services and to maintain the stability of the grid.
- Develop MPC control systems for utilising the kinetic energy of the VSHP for FFR and inertia support, based on a linear system model. The hydraulic and electric constraints of the VSHP will be considered.
- Increase the precision of the MPC controller by developing an MPC control system based on a nonlinear system model. Investigate the possibility for including a power oscillation damping function in the MPC.

- Develop a method for small-signal analysis of the VSHP with MPC control to study possible oscillations between the hydraulic system of the VSHP and the rest of the power system.
- Investigate the potential for frequency and rotor angle stability improvements of implementing a VSHP with the proposed control system in the Nordic grid.

The main contributions of this thesis are:

1. Propose and analyse a nonlinear hydraulic model for grid integration studies of VSHP plants:

   The proposed hydraulic model is based on the Euler turbine equations and a one-dimensional model of the waterway system, including modelling of water hammering in the penstock presented by an IEEE working group. This model is compared to conventional grid simulation models of turbine and waterway by utilising both small-signal and dynamic analyses. Primarily, the accuracy of the proposed model is higher, especially the calculation of the turbine power. The main reason is that the Euler turbine equations are nonlinear and include the turbine rotational speed as input.

2. Development and documentation of detailed converter model for VSHP:

   A VSHP model that can aid the design of optimal controllers is designed and tested. A detailed model is needed since the controller is intended to maximise the utilisation of the power plant for the provision of ancillary services, considering the limitations given by the hydraulic system. The model is tested and analysed with more or less conventional controllers to identify critical modes, adverse interactions or other limitations that must be taken into account in the future design of more advanced controllers for VSHP. Dynamic tests are performed by simulating step responses in power demand and by comparing the responses of the model with the VSHP and a conventional hydropower plant.

3. Analysis and verification of the non-existence of small-signal interaction between the VSHP hydraulic system and the grid for the control layouts from the previous point:

   A participation factor-based interaction analysis shows that there is no small-signal interaction between the hydraulic system of the VSHP and the rest of the grid. This simplifies the tuning of the control system. However, the analysis concludes that some oscillatory modes associated with the hydraulic

system become much more excited when operating at variable speed; which is due to the larger deviation in turbine rotational speed. Additional awareness when designing the control system is therefore needed to keep the hydraulic system variables within their limits.

These conclusions apply for a control layout where the grid converter controls the output power from a power reference, for instance provided by a virtual inertia controller, the synchronous generator converter controls the generator power to ensure that the DC-link voltage follows its reference and the governor controls the guide vane opening to reduce the deviation in turbine rotational speed.

4. Further development of virtual inertia controllers for adaptation to VSHP:

   Two virtual inertia control structures, the VSG and the VSM, are further developed to fulfil the main objective of the control; to maximise the grid support from the VSHP by utilising the turbine and generator rotational energy. They are evaluated by two main criteria; their ability to deliver instantaneous power (inertia) to reduce the rate of change of frequency (ROCOF) and their contribution to frequency containment control (steady-state frequency droop response). At the same time, the impact on the hydraulic system is considered to fulfil the objectives for internal control of the plant; i.e. to optimise the turbine rotational speed, minimise water hammering and mass oscillations, minimise guide vane servo operation and minimise hydraulic and electric losses.

5. Development of linear and nonlinear MPCs for coordinating the governor control and the virtual inertia control of VSHP and optimising the contribution to frequency containment reserves:

   The MPC coordinates the turbine controller with the VSG control of the power electronics converter to optimise the plant's performance. Its main objective is to deliver fast power responses to frequency deviations while keeping the electric and hydraulic variables within their constraints. The VSG delivers fast power response by utilising the rotational energy of the turbine and the generator. Simultaneously, the MPC controls the guide vane opening of the turbine to regain the nominal turbine rotational speed. If this is not possible due to the constraints of the hydraulic system, the MPC adjusts the VSHP output power by changing the VSG power reference. The benefits of using a nonlinear MPC compared to a linear MPC are improved estimation of turbine head and more accurate modelling of the turbine power. This ensures that the turbine pressure does not exceed its limit and reduces the overshoot in the turbine speed after a disturbance.

6. Development of a method for small-signal stability analysis of VSHP with MPC:

   The aim of developing a method for small-signal analysis of the proposed VSHP control system is to parametrise the cost function of the MPC to minimise oscillation modes between the hydraulic system of the VSHP and the power system. In order to be able to linearise the system, a state-space representation of the MPC is required. This state-space representation is developed by assuming that the system is in a stable and steady-state operation point equal to the reference values of the MPC cost function, and no constraints are active.

7. Investigation of the VSHP's performance to improve the frequency stability of the Nordic grid:

   The proposed VSHP controller with MPC and VSG or VSM virtual inertia control is implemented in a Nordic grid model to demonstrate the grid support capacity of the VSHP. By active power control, the VSHP is shown to improve both the frequency stability and the transient rotor angle stability by contributing to virtual inertia, fast frequency reserves and power oscillation damping.

The relationships between the papers that are part of this thesis and the main contributions are shown in Figure 1.1. The Euler turbine model (Contribution 1) and the VSHP model (Contribution 2) presented in, respectively, Paper I and Paper II are utilised as basic models in all the following papers. This is also the case for the virtual inertia controllers presented in Paper III and Paper IV which contribute with new virtual inertia control layouts adapted for VSHP (Contribution 4).

The first four papers are the basis for the development of the linear and nonlinear MPC controllers presented in, respectively, Papers V and VI (Contribution 5) and compared in Paper VI. The hydraulic and electric models from Paper I and Paper II are necessary for both designing and testing the MPC controller. The virtual inertia controllers from Papers III and IV are combined with the MPC in order to be able to deliver both virtual inertia and primary frequency control.

The final two papers, Papers VII and VIII, are based on the nonlinear MPC from Paper VI. A method for small-signal analysis of the MPC is developed in Paper VII (Contribution 6) while Paper VIII investigates how the frequency and rotor angle stability of a large grid, in this case the Nordic grid, can be improved by the implementation of VSHP with MPC and virtual inertia controllers (Contribution 7).

1.2 Scope

The PhD work focuses on primary frequency control, FFR and virtual inertia support in the transmission grid. The assumptions and simplifications of the models developed in the project are adapted for this purpose. The work includes a rather detailed model of the waterway and the turbine from an electrical point of use; however, these models will not be suited for other uses, such as the design of hydropower plants.

The work does not cover protection and harmonics studies.

1.3 Methodology

The research content of the PhD is the models and methods described in Chapters 2 to 6. The research methods applied are:

- Literature search
- Development of simulation models
- Analysis of simulation results
- Development of control schemes by utilising optimisation methods

MATLAB and Simulink are used to model the VSHP including the controllers and hydraulic system and the two-area Kundur model. The Nordic model is originally created in PSS/E; however, the model is implemented in ePHASORSIM to be simulated together with MATLAB/Simulink on OpalRT. The linear MPC controller is solved by the `quadprog`-function in MATLAB while CasAdi [19] in both MATLAB and Python versions are used for solving the nonlinear MPC problem.

All results in this thesis are based on models of the power hydropower plant and the power system. Thus, their quality depends on the accuracy of these models. Verification in a laboratory test set-up or on a real power plant is, therefore, a natural next step for strengthening the results of this thesis. This applies in particular for the results of the proposed MPC since the MPC design is based on the same models as it is tested upon. The laboratory test should include a more detailed model of the hydraulic system and, preferably, real VSHP converters and generator.

The power system stability is analysed to evaluate the investigated control structures. However, the stability analyses are limited to rotor angle stability and short-term frequency stability, as indicated in Figure 2.1. Long-term frequency stability is not included in the scope of this thesis since secondary and tertiary frequency control is not a part of the proposed control structures. Voltage stability could have

been included since the VSHP grid converter can control reactive power. However, as most converters have this ability, the voltage control is not found to be especially interesting for VHSP. Thereby, the voltage stability analysis is excluded to limit the scope of the thesis.

1.4 List of publications

The results in this PhD work are published in:

Paper I T. I. Reigstad and K. Uhlen, 'Modelling of variable speed hydropower for grid integration studies', *Presented at IFAC World Congress 2020, Germany, to be published in IFAC-PapersOnLine*,

Paper II T. I. Reigstad and K. Uhlen, 'Variable speed hydropower conversion and control', *IEEE Transactions on Energy Conversion*, vol. 35, no. 1, pp. 386–393, March 2020

Paper III T. I. Reigstad and K. Uhlen, 'Virtual inertia implementation in variable speed hydropower plant', *Presented on the Modern Electric Power System conference (MEPS'19), September 9-12, 2019, Wroclaw, Poland*,

Paper IV T. I. Reigstad and K. Uhlen, 'Variable speed hydropower plant with virtual inertia control for provision of fast frequency reserves', *International Journal of Power and Energy Systems*, vol. 35, no. Volume 41, issue 2, 2021

Paper V T. I. Reigstad and K. Uhlen, 'Optimized control of variable speed hydropower for provision of fast frequency reserves', *Electric Power System Research, Special issue: Proceedings of the 21st Power Systems Computation Conference (PSCC 2020)*, vol. 189, 2020

Paper VI T. I. Reigstad and K. Uhlen, 'Nonlinear model predictive control of variable speed hydropower for provision of fast frequency reserves', *Electric Power Systems Research*, vol. 194, p. 107 067, 2021

Paper VII T. I. Reigstad and K. Uhlen, 'Stability properties of non-linear model predictive control of variable speed hydropower', *IET Renewable Power Generation*, 2020

Paper VIII T. I. Reigstad and K. Uhlen, 'Variable speed hydropower for provision of fast frequency reserves in the nordic grid', *Submitted to IEEE Transaction on Power Systems*, 2020

1.5 Outline of the thesis

The background theory of this thesis is divided into four categories as given in Chapters 2 to 5, of which Chapters 3 to 5 also present some of the contributions of this thesis. Chapter 2 provides a short introduction to power system stability, with the primary emphasis on frequency and rotor angle stability. The VSHP model is presented in Papers I and II; however, Chapter 3 provides a short introduction to and additional theory on hydraulic system modelling. Chapter 4 introduces the virtual inertia control schemes. These are presented in more detail in Papers III and IV. An introduction to the MPC theory and objectives for the controller are given in Chapter 5. Papers V to VIII present the MPC utilised in the respective papers in more detail.

A summary of the discussion of the results is given in Chapter 6, classified by the main contributions and related to each paper. Finally, in Chapter 7, the conclusions and suggestions for further works are given.

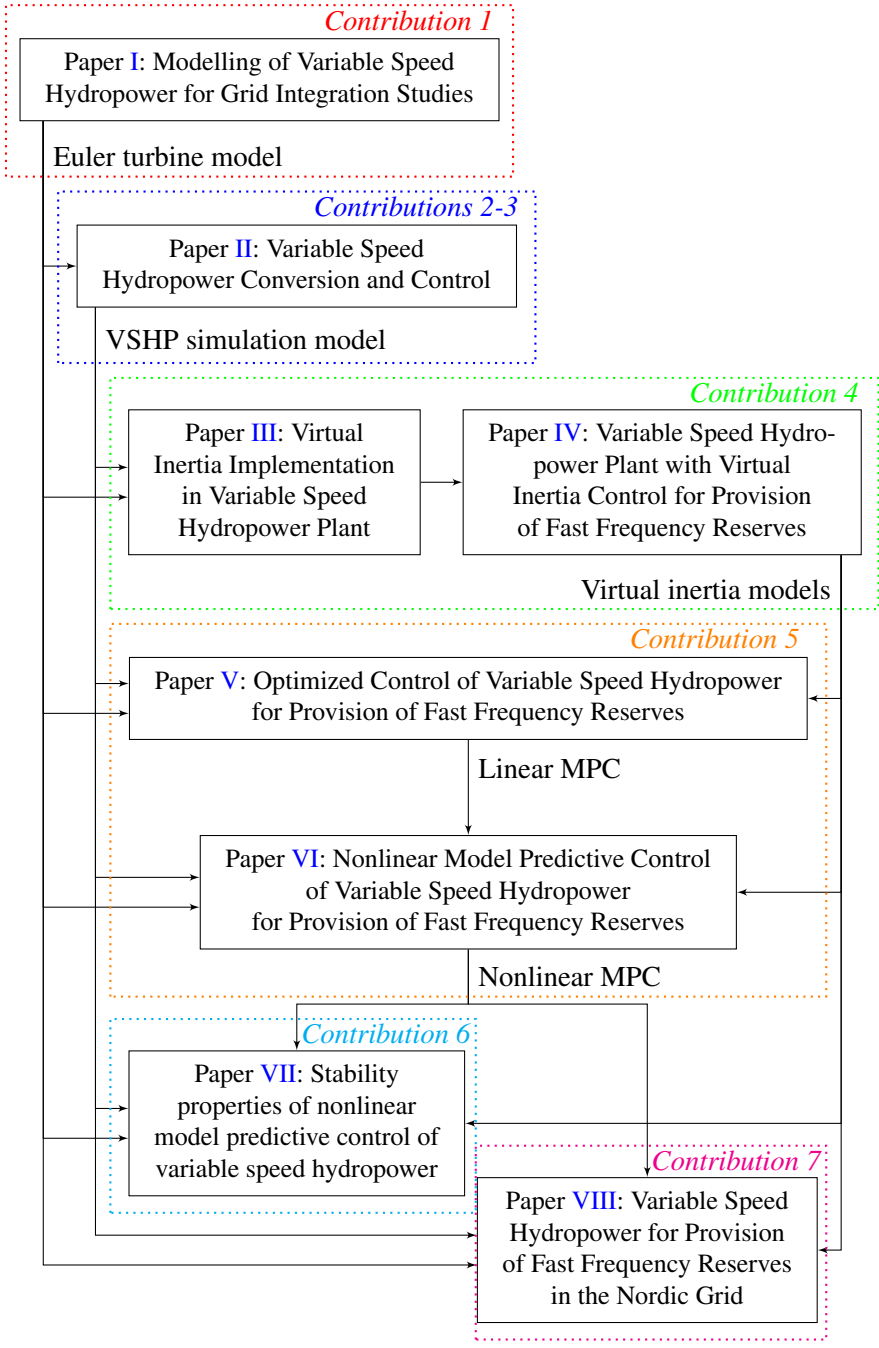

Figure 1.1: Relationship between the papers and the main contributions

Chapter 2

Power system stability

Power system stability is defined in [28] as the ability of a power system to:

- remain in an equilibrium state under normal operating conditions, and to
- regain an acceptable state of equilibrium after being subjected to a disturbance.

Another definition is provided by an IEEE/CIGRE Joint Task Force on Stability Terms and Definitions [29]: "Power system stability is the ability of an electric power system, for a given initial operating condition, to regain a state of operating equilibrium after being subjected to a physical disturbance, with most system variables bounded so that practically the entire system remains intact."

The power system is continuously exposed to perturbations such as changes in active and reactive power of both consumption and production units, tapping of transformers and static VAR compensators (SVCs) or even short-circuits. To maintain the stability, the oscillations caused by these disturbances must be damped. Deep knowledge about a variety of power system stability properties, for instance frequency stability and interarea oscillations is needed in order to design and operate the power system [30].

The power system stability properties may be divided into three main quantities, as shown in Figure 2.1; rotor angle stability, frequency stability and voltage stability [31]. Since the classification primarily focuses on one variable, respectively rotor angle, frequency and voltage, the approach is known as partial stability [32]. This thesis will mainly investigate how the short-term frequency stability, small-signal stability and transient stability can be improved by implementing VSHP.

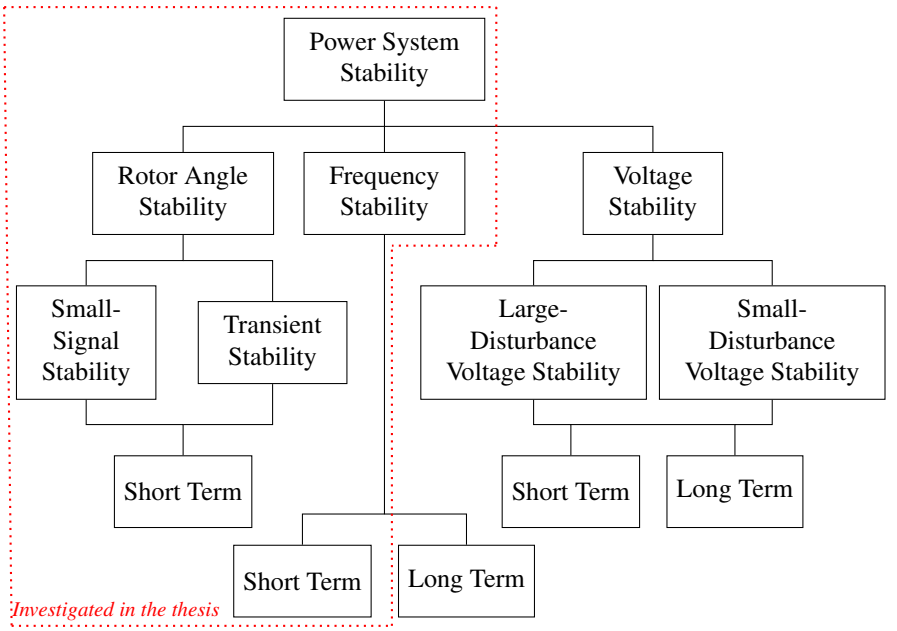

Figure 2.1: Classification of power system stability

2.1 Frequency stability and control

Frequency stability is the power system's ability to maintain steady frequency after a severe disturbance resulting in a significant imbalance between generation and load [29]. Sustained frequency swings may lead to tripping generation units and/or loads, causing frequency instability. The system is in equilibrium when the generated power P_{gen} in the system equals the sum of load and losses P_{load} [31].

2.1.1 Swing equation

The swing equation (2.1) is based on Newton's second law for rotation and is important for understanding the frequency stability of a power system. An imbalance between the mechanical torque τ_t and the electromagnetic torque τ_e causes an acceleration or deceleration of the rotor shaft velocity ω_m. The swing equation of a single generator is given as:

$$J\frac{d\omega_m}{dt} + D_d\omega_m = \tau_t - \tau_e \tag{2.1}$$

J is the total moment of inertia of the turbine and the generator rotor while D_d is the damping-torque coefficient.

The inertia constant H is defined as the kinetic energy stored in the rotating mass:

$$H = \frac{1}{2}\frac{J\omega_{0m}^2}{S_b} \tag{2.2}$$

Here, ω_{0m} is the rated angular velocity of the rotor and S_b is generator base rating. With this, the swing equation for a one-generator system can be reformulated to [30], [31]:

$$\frac{df}{dt} = f_n\frac{P_m - P_e - P_d}{2H}, \quad P_d = \frac{D_d\omega_{0m}}{f_n S_b}f \tag{2.3}$$

where f is the frequency, $df/dt = \dot{f}$ is the ROCOF, f_n is the nominal system frequency, P_m is the mechanical power, P_e is the electrical power, P_d is the damping power and H is the inertia constant.

2.1.2 Inertia

The inertia of a power system is defined as the ability of a system to oppose changes in frequency due to resistance provided by the kinetic energy of the rotating masses in turbines and generators. Due to this inertia, instantaneous power reserves are supplied by the physical stabilising effect of all the grid-connected synchronous machines. The total kinetic energy of the system is the energy stored in the rotating masses of all turbines and generators and usually quantifies the total system inertia.

The inertia of the power system H_g is the average of the inertia H_i for each generator i, weighed for the generator rated apparent power S_{ni}:

$$H_g = \frac{\sum_{i=1}^{N} S_{ni}H_i}{S_n} \tag{2.4}$$

where the total apparent power in the system is $S_n = \sum_{i=1}^{N} S_{ni}$. The total kinetic stored energy is then given as:

$$E_g = S_n H_g = \sum_{i=1}^{N} S_{ni}H_i \tag{2.5}$$

The average ROCOF $\dot{f}$ can thereby be found as:

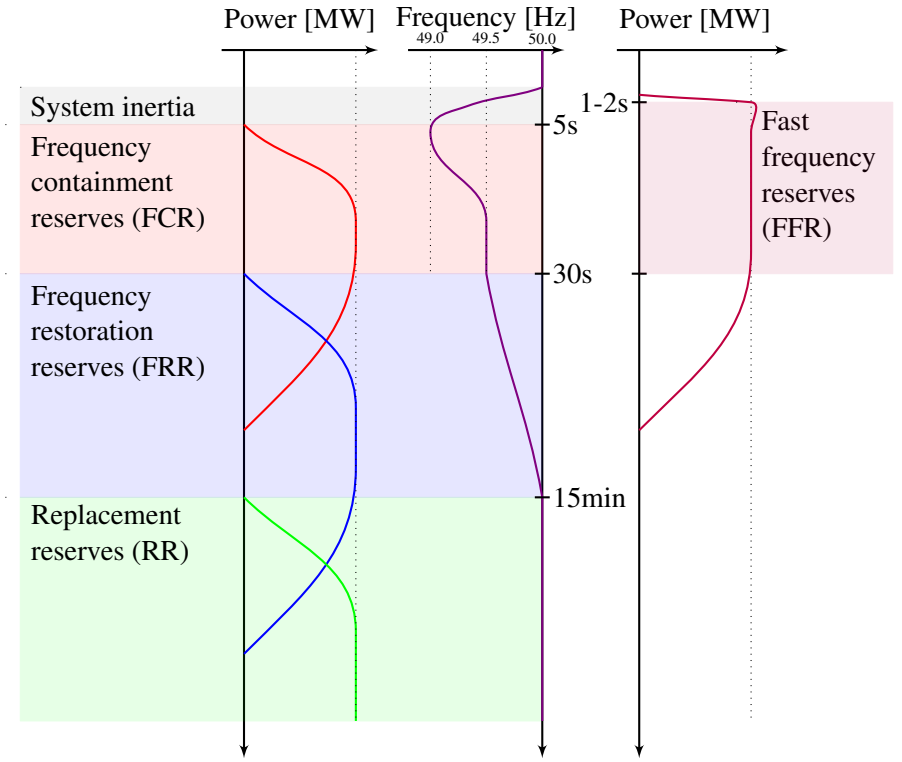

Figure 2.2: General frequency system response and controllers involved

$$\dot{f} = \frac{f_n}{2H_g S_n}\left(P_{gen} - P_{load} - D_m \Delta f\right), \quad \Delta f = f - f_n \tag{2.6}$$

where P_{gen} and P_{load} are, respectively, the total generation and load in the system and D_m is the damping.

2.1.3 Frequency control systems

Power reserves are needed to maintain the balance between power generation and power consumption and to control the grid frequency. Four different reserve levels are defined in [18], [33] as illustrated in Figure 2.2.

- **System inertia:** The instantaneous power reserves come from the physical stabilising effect of all grid-connected synchronous machines due to their inertia.

- **FCR**: Frequency deviations are contained by the primary reserves that are automatically and locally activated from within seconds to a few minutes to stabilise the frequency. In the Nordic grid, the FCR is divided into two parts:
  - FCR-N: activated at frequency deviations $\pm 0.1 Hz$.
  - FCR-D: activated at $49.9 Hz$ and fully activated at $49.5 Hz$. The required size of FCR-D is found such that the largest generator outage the system is dimensioned to handle, the dimensioning incident (DI), should not cause a steady-state frequency below 49.5 Hz.

  Both should be automatic and fully activated within 30 sec.
- **FRR**: Secondary reserves are activated to restore the grid frequency to the rated value, to release primary reserves and restore the power flow between control areas. In the Nordic grid, the frequency restoration reserve (FRR) is divided into an automatically controlled service (aFRR), usually controlled by automatic generation controls (AGCs), and the reserves activated through the balancing control market (mFRR). FRR must be activated within 15 minutes.
- **RR**: Tertiary reserves or reserve replacement (RR) can be used to free up secondary reserves. However, there is no market for RR in the Nordic system.

In addition, FFR is suggested as a complementary service with a faster response than FCR, as shown in Figure 2.2. FFR is defined as a system service that delivers a fast power change to mitigate the effect of reduced inertial response, so that frequency stability can be maintained. The motivation for introducing this service is low-inertia situations where FCR-D may not be sufficient to limit the frequency deviation after a disturbance. Increasing the level for FRC-D could be problematic since stability issues may arise due to the dynamic performance of the hydropower plants [14]. The Nordic TSOs have evaluated FFR as the most technical and economical solution in advance of increasing the inertia by virtual inertia control [15]. Technical requirements for the FFR are evaluated in [12] with a suggested activation level of $49.5 - 49.7 Hz$ and a maximum full activation time of $0.7 - 1.3 s$. The duration is minimum $5 s$ for the short support duration FFR and $30 s$ for the long support duration FFR. In addition, the FFR providing unit must be ready for a new FFR activation cycle within 15 minutes.

Primary control

The primary control is traditionally performed by the droop characteristic of the governors to maintain the balance between generation and demand and limit the

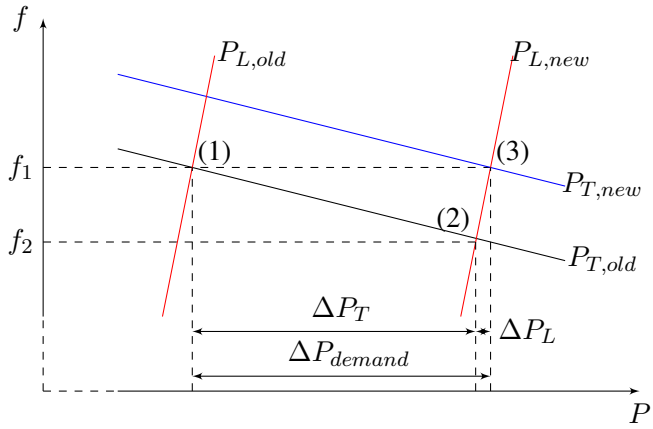

Figure 2.3: Equilibrium points for an increase in power demand. Reproduced from [31]

frequency deviation. Negative feedback of the frequency deviation Δf causes the power production to increase when the frequency reduces, and to reduce when the frequency increases. Since power plants have different power response times, their contributions to primary reserves are also different. However, it is the total primary control reserves in the power system that limit the frequency deviation.

Figure 2.3 shows the stationary behaviour of the primary control with a case where the power demand is increased by ΔP_{demand}. This causes the load characteristic curve to move from P_L^{old} to P_L^{new}, the generation to increase by ΔP_T, the system loads to reduce by ΔP_L and the equilibrium point to move from point 1 to point 2. Next, the FRR increases the power production to P_T^{new}, bringing the equilibrium point to point 3 and eliminating the frequency deviation.

Spinning reserves are the difference between the total power rating of all generation units in the system and their actual power. They are needed to ensure that enough power can be delivered to keep the system frequency within the given limits and ensure safe system operation. If some of the generators reach their power limits, they will not contribute with more frequency reserves and the deviation in frequency will increase.

The cost of primary control is low for hydropower compared to other generating units due to the small efficiency loss.

2.1.4 Frequency stability situation in the Nordic power system

The inertia of the rotating masses of the synchronous generators counteracts grid frequency deviations and is therefore essential for the frequency stability [34].

This reduction of inertia has raised concerns about the frequency stability in the Nordic power system [13], [14], [35], continental Europe [36] and other grids around the world [37]. Less inertia also causes less damping and faster and larger frequency drop [38] and may result in load-shedding if the frequency deviates too much before the frequency reserves have reacted sufficiently [35]. The frequency deviations may be caused by loss of generators or loads, line faults, system splits and variable production of renewable sources [39].

The inertia in the Nordic grid decreases because of the higher share of wind energy, out-phasing of nuclear power and higher import from Europe through HVDC connection, especially in low-load cases during summer [14]. As insufficient levels of inertia will threaten the system stability if a large generator trips, reduced inertia is considered to be one of the main challenges in the Nordic grid heading towards 2025 [35]. The frequency stability can be improved by limiting the power of the largest units, setting minimum requirements for kinetic energy in the system, running existing power plants at reduced productions, adding more frequency containment reserves (FRC), adding synchronous condensers or adding virtual inertia. To increase and optimise the supply of frequency control services, new and innovative control systems of both production and consumption units are needed. This thesis investigates how VSHP plants can contribute.

2.2 Rotor angle stability

Rotor angle stability is the ability of a synchronous machine to remain in synchronism with the rest of the power system after being subjected to a disturbance. Rotor angle instability occurs when large angular swing between generators causes one or more generators to lose its synchronism with the other generators. In steady-state conditions, the electromagnetic torque and the mechanical torque are equal, keeping the rotor speed and the rotor angle between the stator rotating magnetic field and the rotor magnetic field constant. A disturbance, either on the mechanical power or on the power system, will cause a transient behaviour of the rotor angle. For small positive deviations in the rotor angles, the electromagnetic torque reduces the acceleration of the rotor since it increases as the rotor angle increase. However, the electromagnetic torque reduces rapidly for large rotor angles. Thereby, the synchronous generator will lose the synchronism above a certain value of the rotor angle since the mechanical torque is larger than the electromagnetic torque.

The electromagnetic torque of a synchronous generator can be resolved into two components:

- The synchronising torque is in phase with the deviation in rotor angle and

help bring the rotor speed back to the synchronous speed. In this way, it keeps the machine in synchronisation with the help of the governor and the excitation system.

- The damping torque is in phase with the speed variation and is mainly provided by the damper winding of the synchronous machines.

The synchronising torque can be increased by faster control of the excitation system; however, this may cause instability because it weakens the damping torque [30]. A power system stabiliser can solve this problem by adding an additional signal to the excitation system to damp power oscillations.

The rotor angle stability is normally classified into two subcategories. Small-signal stability, also called small-disturbance rotor angle stability, considers small disturbances in order to be able to linearise the system and utilise linear control techniques. Transient stability considers the rotor angle stability at large disturbances.

2.2.1 Small-signal stability

A system is small-signal stable for a particular operating condition if it returns to a steady-state operation close to or identical to the initial operating point after a small disturbance [31]. The small-signal analysis is performed by linearising the system around a steady-state operation point. Since the linearised system may deviate from the original nonlinear system when moving away from the operating point, the method is only valid for small disturbances. If the disturbance is very small, the transient responses are the same for the two systems. Analytical methods developed in linear control theory, such as control tuning, can be utilised on the linear system to improve the performance of the control. Besides this, analysis of the locations of poles in the complex s-plane offers an easy understanding of the dynamic performance and stability of the system.

In this thesis, the small-signal analysis is used for tuning the controllers and the analysis of possible oscillations between the VSHP plant and other synchronous generators in the grid. The linearisation methods are also used for developing the linear MPC controller.

The nonlinear system equations are given as:

$$\begin{aligned} \dot{x} &= f(x, u, t) \\ y &= g(x, u) \end{aligned} \tag{2.7}$$

where x is the state vector, $\dot{x}$ is the time derivative of the state vector, u is the input

vector, t is the time and y is the output vector.

The nonlinear system is linearised in an equilibrium point, also called steady-state point, where the system variables and inputs are constant, respectively x_0 and u_0 and their derivatives are zero. An approximated linear model for small perturbation Δx, Δu is found by utilising Taylor's series expansion (2.8).

$$\begin{aligned}\dot{x}_i &= \dot{x}_0 + \Delta\dot{x}_i \\ &= f_i\left(\left(x_0 + \Delta x\right), \left(u_0 + \Delta u\right)\right) \\ &= f_i\left(x_0, u_0\right) + \frac{\delta f_i}{\delta x_1}\Delta x_1 + \cdots + \frac{\delta f_i}{\delta x_n}\Delta x_n + \frac{\delta f_i}{\delta u_1}\Delta u_1 + \cdots + \frac{\delta f_i}{\delta u_r}\Delta u_r\end{aligned} \tag{2.8}$$

By setting $\Delta x_0 = 0$ and $\Delta u_0 = 0$, we find that $x_{i0} = f_i(x_0, u_0)$ and can simplify (2.8):

$$\Delta\dot{x}_i = \frac{\delta f_i}{\delta x_1}\Delta x_1 + \cdots + \frac{\delta f_i}{\delta x_n}\Delta x_n + \frac{\delta f_i}{\delta u_1}\Delta u_1 + \cdots + \frac{\delta f_i}{\delta u_r}\Delta u_r \tag{2.9}$$

The output equation $g(x, u)$ is linearised with the same method, resulting in:

$$\Delta\dot{y}_j = \frac{\delta g_j}{\delta x_1}\Delta x_1 + \cdots + \frac{\delta g_j}{\delta x_n}\Delta x_n + \frac{\delta g_j}{\delta u_1}\Delta u_1 + \cdots + \frac{\delta g_j}{\delta u_r}\Delta u_r \tag{2.10}$$

By solving (2.9) for $i = 1, 2, \ldots, n$ and (2.10) for $j = 1, 2, \ldots, m$, the state matrix A, the input matrix B, the output matrix C and the feed-forward matrix D can be constructed such that:

$$\begin{aligned}\Delta\dot{x} &= A\Delta x + B\Delta u \\ \Delta y &= C\Delta x + D\Delta u\end{aligned} \tag{2.11}$$

Utilising Laplace transformation and rearranging (2.11), we find that the poles of the solution for Δx and Δy are the roots of the characteristic equation of A, given as [28]:

$$\det\left(sI - A\right) = 0 \tag{2.12}$$

These poles are called the eigenvalues of matrix A and determine whether the system is small-signal stable or not. The system is small-signal unstable if at least one of the eigenvalues $\lambda = \sigma + j\omega$ has a positive part. The frequency f of the oscillations corresponding to the eigenvalue is found from the imaginary part of the eigenvalues while the damping ratio ζ is found from both the real and imaginary part, as given in (2.13).

$$\begin{aligned} f &= \frac{\omega}{2\pi} \\ \zeta &= \frac{-\sigma}{\sqrt{\sigma^2 + \omega^2}} \end{aligned} \tag{2.13}$$

The right eigenvector Φ and left eigenvector Ψ corresponding to the eigenvalue λ_i are found as the solution of:

$$\begin{aligned} A\Phi_i &= \lambda_i \Phi \\ \Psi_i A &= \lambda_i \Psi \end{aligned} \tag{2.14}$$

By defining Φ and Ψ as $n \times n$-matrices where:

$$\begin{aligned} \Phi &= \begin{bmatrix} \Phi_1 & \Phi_2 & \dots & \Phi_n \end{bmatrix} \\ \Psi &= \begin{bmatrix} \Psi_1^T & \Psi_2^T & \dots & \Psi_n^T \end{bmatrix}^T \end{aligned} \tag{2.15}$$

(2.14) can be written as:

$$\begin{aligned} A\Phi &= \Phi\Lambda \\ \Psi A &= \Lambda\Psi \end{aligned} \tag{2.16}$$

The dot product of the left and right eigenvectors corresponding to different eigenvalues is zero since they are orthogonal. Normally, the dot product of the left and right eigenvectors corresponding to the same eigenvalue is normalised such that $\Psi_i \Phi_i = 1$. This is possible since (2.14) is homogeneous equations where any scalar product of the eigenvector are also a solution. Thereby,

$$\begin{aligned} \Phi^{-1} A\Phi &= \Lambda \\ \Psi A\Phi &= \Lambda \end{aligned} \tag{2.17}$$

where Λ is the diagonal matrix of the eigenvalues λ:

$$\Lambda = diag(\lambda_1, \lambda_2, \ldots, \lambda_n) \tag{2.18}$$

The rate of change of each state variable is a linear combination of all state variables. Therefore, a new state vector z, such that $\Delta x = \Phi z$ is defined to eliminate this cross-coupling. The free motion system with zero inputs is rearranged to:

$$\begin{aligned} \Delta\dot{x} &= A\Delta x \\ \Phi\dot{z} &= A\Phi z \\ \dot{z} &= \Phi^{-1}A\Phi z = \Lambda z \end{aligned} \tag{2.19}$$

The solution for z is n uncoupled first-order equations:

$$z_i(t) = z_i(0)e^{\lambda_i t} \tag{2.20}$$

Thereby, the solution of the primary equations of free motion is found as:

$$\Delta x(t) = \sum_{i=1}^{N} \Phi_i z_i(0) e^{\lambda_i t} \tag{2.21}$$

The relationship between the two state vectors x and z is given as:

$$\begin{aligned} \Delta x(t) = \Phi z(t) \quad &= \begin{bmatrix} \Phi_1 & \Phi_2 & \ldots & \Phi_n \end{bmatrix} z(t) \\ z(t) = \Psi \Delta x(t) &= \begin{bmatrix} \Psi_1^T & \Psi_2^T & \ldots & \Psi_n^T \end{bmatrix}^T \Delta x(t) \end{aligned} \tag{2.22}$$

The first equation with the right eigenvalue Φ defines the mode shape; the relative activity of the state variables x when a particular mode z_i is excited. The left eigenvector Ψ from the second equation identifies which combination of the original state variables x displays only mode z_i.

Participation Factor-Based Interaction Analysis

A participation factor-based interaction mode method proposed in [40] is utilised to investigate the interactions between the subsystems. An interaction mode is defined as a mode with participation from more than one subsystem and proves a dynamic interaction between the subsystems [41].

The participation factor p_{ki} of state variable x_k in mode i is defined in [28] as:

$$p_{ki} = \Phi_{ki}\Psi_{ki} \tag{2.23}$$

where ϕ and ψ are, respectively, the right and left eigenvector. The parameter $\eta_{\alpha i}$ is defined in [40] as a measure for the overall participation for each subsystem α in mode i.

$$\eta_{\alpha i} = \frac{||p_{\alpha i||}}{||p_i||} \tag{2.24}$$

where $||\cdot||$ denotes the L_1-norm. While the participation factor p_{ki} measures the participation of a state variable in a mode, $\eta_{\alpha i}$ calculates the degree of participation of a group for state variable, a subsystem, in a mode.

Small-signal stability for hydropower dominated systems

Four different types of power system oscillatory modes are particularly relevant for hydropower plants [28], [42], [43].

- Electromechanical local modes occur when units in a power plant are oscillating with the rest of the system, typically at 1-2 Hz. These modes are most common when the power plant is weakly connected with the rest of the grid, has a fast response excitation system and is heavily loaded. They are related to rotor angle oscillations.
- Electro-mechanical inter-area modes are usually associated with groups of machines oscillating with other groups of machines across a relatively weak transmission path and are also related to rotor angle oscillations. The typical frequency is 0.1-1 Hz.
- Torsional modes are characterised by resonance between series compensated high voltage transmission lines and the inter-mass mechanical modes of a steam-turbine-generator shaft in the area of 15-50 Hz.

- Control modes are usually caused by poorly tuned controllers in excitation systems, governors and power converters and have a wide range of frequencies.

In systems with high hydro penetration, other types of oscillations are also reported [43]. These can be related to the characteristics of the water column feeding the turbine. The effects of water inertia, water compressibility and pipe wall elasticity in the penstock cause travelling waves of pressure and flow in the pipe [28]. These rapid pressure oscillations, called "water hammer" can occur when flowing water at steady operation in a pipe is suddenly varied, for instance, fast control of the valve [43], [44]. For precise modelling of hydraulic turbines, the effects of elastic-walled pipe and compressible fluid must be included, especially for long penstocks [28].

Water hammer is characterised by a series of positive and negative pressure waves. The waves are travelling back and forth in the penstock until they are damped by friction. They are the result of pressure changes in the penstock. These pressure changes are caused by acceleration or deceleration of water due to the opening or closing of the guide vane or changing of the water velocity in some other manner [45].

2.2.2 Transient stability

Transient stability, or large-disturbance rotor angle stability, is the ability of the power system or a synchronous generator to maintain synchronism when subjected to a severe disturbance [30]. Severe disturbances, in this case, may include short-circuits on transmission lines or disconnection of power plants and loads with high production or consumption. In addition to the type and the severity of the disturbance, the stability also depends on the initial operating condition. In the case of a short circuit close to a generator, the following course of events is expected:

1. The terminal voltage of the synchronous generator drops, causing the excitation system to boost the terminal voltage and thereby contribute to maintaining the stability.
2. The short circuit is eliminated, for instance by line disconnection.
3. Oscillations caused by the short circuit and the change to a new operating point must be damped.

Because of the nonlinear nature of the power system and the large disturbance,

linear control system theory cannot be applied in this case. Instead, the system dynamics are normally simulated in the time-domain by integration numerical methods. The oscillations of the generators' relative angles provide information about the transient stability such that three different characteristic cases can be distinguished:

1. The stable case: The oscillations are damped and all rotor angles reach their post-disturbance steady-state value.
2. First-swing instability: One or more generators lose synchronism at the first swing after the disturbance and their rotor angle increases continuously.
3. First-swing stable; however, small-signal unstable at the post-disturbance steady-state: The oscillations will grow in magnitude until one or more generators lose synchronism since the system is not small-signal stable.

The critical fault clearing time is defined as the maximum duration of a fault that ensures the power system reaches a post-disturbance steady-state [30]. It can be found by the equal area criterion, the extended equal area criterion (EEAC) or time-domain simulations.

Chapter 3

Variable speed hydropower modelling

The hydraulic system, including the turbine and the waterways, will experience different operating conditions when running at variable speed. Thus, a sufficiently detailed model of the VSHP considering the effects of variable speed is required. It should both aid the design of VSHP controllers and investigations of the interactions between the VSHP plant and the grid. The model must also consider the dynamic constraints and limitations that need to be taken into account. This was the main motivation for the development of a non-linear time-domain simulation model that include tunnels, with physical constraints on water flows, turbine, governor, generator with the magnetising system, generator-side converter and grid-side converter, and a representative test grid.

The VSHP model utilised in Papers III-VIII is developed and presented in the two first papers. Paper I deals with the modelling of the hydraulic system; the waterway and the turbine while Paper II presents a full model of a VSHP, including the electrical system as illustrated in Figure 3.1.

3.1 Hydraulic system

In Paper I, four different hydropower plant models are compared for the purpose of grid integration studies of VSHP.

- The HYGOV model is frequently used for power system modelling; however, it does not consider the variable speed operation and has simple models of the waterway and turbine [28].

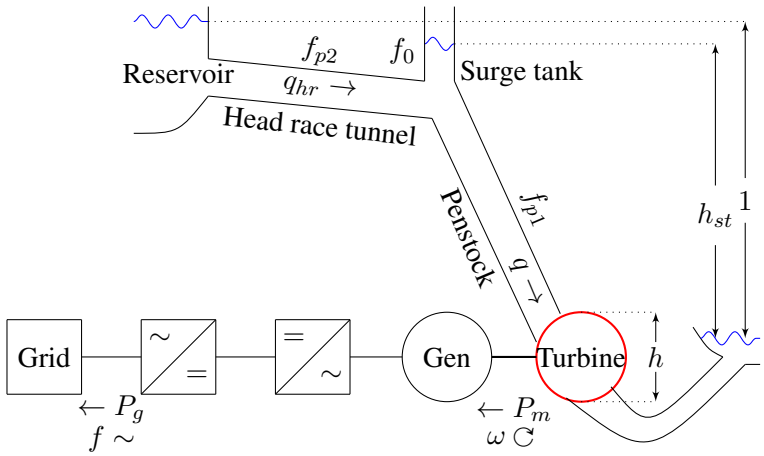

Figure 3.1: VSHP layout

- The Linearised model is a linearisation of the HYGOV model [28].
- The IEEE model [46] has similarities with the HYGOV model; however, it includes a more detailed model of the waterway. The modelling of the penstock is based on the 1D momentum and continuity balance for a water-filled elementary pipe allowing for water hammering modelling. Mass oscillations are also considered since the model includes a surge tank and a headrace tunnel.
- The Euler model is developed in Paper I. In essence, the waterway model from the IEEE model is combined with the Euler turbine equations [47]. With these equations, the calculation of the turbine mechanical torque, turbine flow and turbine efficiency becomes more accurate, primarily since the turbine rotational speed is considered.

More details about the models and results from the comparison are found in Paper I.

3.1.1 Hydraulic System Modelling with Electrical Equivalent

Another method for modelling the waterway, not presented in Paper I, is to utilise the analogy between the water flowing through a pipe and the electrical current flowing in a line [48]. The simulation program SIMSEN utilises this method for both the electric end hydraulic circuits. The 1D momentum and continuity balance for an water-filled elementary pipe of length dx are given as a partial differential equation in [49] and can be represented as (3.1) [43]:

$$\begin{aligned} \frac{\delta H}{\delta x} + \frac{1}{gA} \cdot \frac{\delta Q}{\delta t} + \frac{f}{2gDA^2} \cdot Q|Q| = 0 \\ \frac{\delta Q}{\delta x} + \frac{gA}{a^2} \cdot \frac{\delta H}{\delta t} = 0 \end{aligned} \tag{3.1}$$

where A is the cross-section, Q is the discharge, H is the head, g is the gravity, D is the pipe diameter, f is the local loss coefficient, and a is the wave speed. Equation (3.1) is per unitised to (3.3) by using the per unitised definitions of head and flow given in (3.2) [43].

$$\begin{aligned} h_{p.u.} &= \frac{H}{H_0} \\ q_{p.u.} &= \frac{Q}{Q_0} \end{aligned} \tag{3.2}$$

$$\begin{aligned} \frac{\delta h}{\delta x} + \frac{Q_0}{H_0 gA} \cdot \frac{\delta q}{\delta t} + \frac{fQ_0^2}{2gH_0DA^2} \cdot q|q| = 0 \\ \frac{\delta q}{\delta x} + \frac{gAH_0}{Q_0 a^2} \cdot \frac{\delta h}{\delta t} = 0 \end{aligned} \tag{3.3}$$

The lumped description (3.5) of (3.3) can be found for a small pipe segment δx by substituting (3.4) into (3.3).

$$\begin{aligned} \Delta h &= \frac{\delta h}{\delta x} \Delta x \\ \Delta q &= \frac{\delta q}{\delta x} \Delta x \end{aligned} \tag{3.4}$$

$$\begin{aligned} \Delta h &= -\frac{Q_0 \Delta x}{H_0 gA} \cdot \frac{\delta q}{\delta t} - \frac{fQ_0^2 \Delta x}{2gH_0DA^2} \cdot q|q| \\ \Delta q &= -\frac{gAH_0 \Delta x}{Q_0 a^2} \cdot \frac{\delta h}{\delta t} \end{aligned} \tag{3.5}$$

The equivalent electrical circuit parameter's RLC, given in (3.6) is found by representing the head h as voltage and discharge q as current.

$$\Delta L = \frac{Q_0 \Delta x}{g H_0 A}, \Delta R = \frac{f Q_0^2 \Delta x}{2 g D H_0 A^2}, \Delta C = \frac{g A H_0 \Delta x}{Q_0 a^2} \tag{3.6}$$

By substituting (3.6) into (3.5) and changing the direction of the positive water hammer gradient, the analogue representation of a RLC circuit is given as:

$$\begin{aligned} \Delta h &= \Delta L \cdot \frac{\delta q}{\delta t} + \Delta R \cdot q|q| \\ \Delta q &= \Delta C \cdot \frac{\delta h}{\delta t} \end{aligned} \tag{3.7}$$

If we assume that the pipe is not extensible and that the water is not compressible, the captive element can be eliminated since $\Delta q = 0$. The RL circuit element for a pipe of length l is then given as:

$$\begin{aligned} L &= \frac{Q_0 l}{g H_0 A} \\ R &= \frac{f Q_0^2 l}{2 g D H_0 A^2} \end{aligned} \tag{3.8}$$

The surge tank can be modelled as an analogue capacitor with capacitance C_s [43].

$$C_s = \frac{A_s H_0}{Q_0} \tag{3.9}$$

Since all flows are unidirectional except for the surge tank, the pressure losses in each pipe segment can be written as:

$$\begin{aligned} h_{losses} &= R \cdot q|q| = R \cdot q^2 \quad \forall q \geq 0 \\ R &= \frac{\lambda |\overline{Q}| dx}{2 g D A^2} \\ L &= \frac{dx}{gA} \\ C &= \frac{g A dx}{a^2} \end{aligned} \tag{3.10}$$

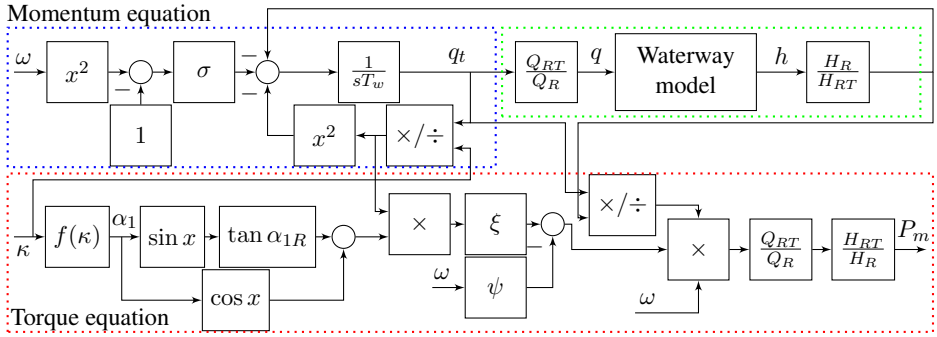

Figure 3.2: Turbine model based on the Euler Equations.

3.2 Corrigendum to Paper I

The Euler model of the hydraulic system is presented in Paper I. Some mistakes in this model were later discovered; however, these do not affect the results of either this paper or the following papers. The most important mistake is related to the different per-unit values of the turbine and the rest of the VSHP. This difference appears since the per-unit system of the Euler model from [47] is referred to the operation point of turbine flow and guide vane opening where the turbine efficiency is maximum. Thereby, the rated water flow of the turbine Q_{RT} is less than the rated water flow of the waterway Q_R. Moreover, there could be differences between the rated head of the turbine H_{RT} and waterway H_R; however, these are equal in this case. The two different per-unit systems are considered for the inputs to the Euler turbine mode, but not for the output; the mechanical power P_m. This has been corrected in (3.11) and Figure 3.2 by multiplying with Q_{RT}/Q_R and H_{RT}/H_R. The mechanical power P_m is then found as a function of the turbine flow q_t and turbine head h_t referred to the turbine, or the flow q and head h referred to the waterway (3.12).

$$\begin{aligned} T_w \frac{dq_t}{dt} &= h_t - \left(\frac{q_t}{\kappa}\right)^2 - \sigma\left(\omega^2 - 1\right) \\ T_a \frac{d\omega}{dt} &= \frac{Q_{RT}}{Q_R}\frac{H_{RT}}{H_R}\left(\frac{1}{h_t} q_t \left(m_s - \psi\omega\right)\right) - P_g/\omega \end{aligned} \tag{3.11}$$

$$\begin{aligned} P_m &= \frac{Q_{RT}}{Q_R}\frac{H_{RT}}{H_R}\left(\frac{1}{h_t} q_t \left(m_s - \psi\omega\right)\right)\omega \\ &= \left(\frac{H_{RT}}{H_R}\right)^2 \left(\frac{1}{h} q \left(m_s - \psi\omega\right)\right)\omega \end{aligned} \tag{3.12}$$

In Paper I, values of the turbine parameters ξ and ϕ have been found to match the efficiency curve of the turbine. Thereby, these values have been too low by a factor of $(Q_{RT}/Q_R) \times (H_{RT}/H_R)$ and the resulted mechanical power P_m has been correct. Since the per-unit factors (Q_{RT}/Q_R) and (H_{RT}/H_R) are included in ξ and ψ, the results of the following papers are also correct. The conclusion is that the model presented in Paper I is correct as long as the per-unit factors are included in ξ and ψ. However, if ξ and ψ are calculated from the turbine dimensions instead of estimated from the turbine efficiency curve, the per-unit factor must be included as in (3.11) and Figure 3.2. This is also necessary to obtain the correct efficiency from (3.13).

$$\eta_t = \frac{1}{h_t} \left(m_s - \psi\omega \right) \omega \tag{3.13}$$

Additionally, the torque equation of Figure 3.2 was incorrectly visualised Paper I.

3.3 Electrical system

A detailed model of the VSHP, including the Euler model from Paper I and an electrical system with converters and controllers, is presented in Paper II. The electrical system consists of a sixth-order synchronous generator model, and converters with control systems in dq-axis [50]. For simplicity, the automatic voltage regulator (AVR) supplies a constant field voltage $E_{f,d}$. Both the synchronous generator converter and the grid converter includes conventional inner controllers for current control, as elaborated in Paper II. As seen from Figure 3.3, the outer controller of the synchronous generator converter controls the DC voltage by providing the q-axis current reference to the current controller. The d-axis current is set to zero. The outer controllers of the grid converter control the active and reactive power output to the grid by controlling, respectively, the d-axis and q-axis currents. In addition, a phase-locked loop (PLL) is utilised to estimate the grid frequency and voltage phase at the connection point to the grid and thereby to synchronise the d-axis voltage of the converter with the grid voltage. More details, figures and equations for the converter modelling and control are found in Paper II.

The parameters of the converter controllers and the PLL are found by the modulus optimum (MO) and symmetrical optimum (SO) criterion, as explained in Paper II.

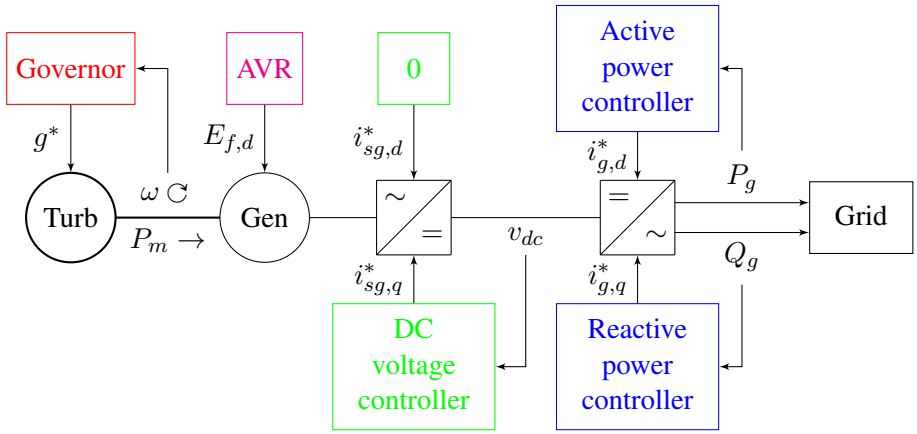

Figure 3.3: VSHP controller scheme

Chapter 4

Virtual inertia control

Traditionally, large thermal and hydropower plants have contributed with both enough inertia and power reserves for frequency control. However, the shift towards more renewable energy sources (RESs) reduces the share of production by large synchronous generators to the advantage of inverter-based generation. This compromises the frequency stability since the inverter-based generation does not provide any mechanical inertial response. The total system inertia will, therefore, be reduced, causing higher ROCOF after a disturbance. One possible solution will be to add virtual inertia through the converter control. Three main categories of different virtual inertia concepts developed over the last few years are reviewed in [16];

- The synchronous generator-based models intend to emulate a synchronous machine continuously with a machine model, including for instance inertia, damping and voltage control [51]–[56].
- The swing equation-based models use a simpler power-frequency swing equation instead of a fully detailed model of the synchronous generator to emulate inertia [57].
- The power versus frequency response-based models are controlled proportionally to frequency deviation (damping term) and/or proportionally to the derivative of the frequency deviation (inertia term) [58]–[62].

Virtual inertia from different sources has been investigated in the literature, for instance batteries [63], capacitors [64], HVDC [65], and wind power [18], [59], [66], [67]. In order to be able to deliver virtual inertia, the source must be able to

increase and decrease the power production more or less instantaneously. Alternatively, the virtual inertia control may utilise stored energy from batteries, capacitors or rotating masses. Solar energy cannot increase power production on demand and has almost no energy stored in its capacitors. It is therefore unsuited for virtual inertia control [34]. Wind power may increase its production temporarily by letting the virtual inertia controller obtain energy from its rotating masses; however, the production must subsequently be reduced even more to regain the optimal rotational speed [68].

Implementation of virtual inertia in VSHP is barely mentioned, although VSHP is highly suitable for this purpose. The grid-connected converter of the VSHP can obtain energy from the rotational masses in turbine and generator for the first inertia response and thereby adjust the turbine flow and mechanical power by governor action to return to the optimal rotational speed.

Papers III and IV present five different virtual inertia control schemes. The first two are known from the literature. The first is the power-frequency PD controller known as the VSG [69] and shown in Figure 4.1. The VSG is a frequency-power response based virtual inertia system, meaning that the output power is a function of the grid frequency. A PD controller calculates the current reference in the d-axis from the deviation in grid frequency, calculated by phase-looked-loop, a PLL. The VSG also compensates for voltage and reactive power when the d-axis current is calculated. Since it depends on frequency measurements from a PLL, it is grid-following and unable to operate in an islanded system. Over-current protection is easily implemented since the VSG outputs a current reference.

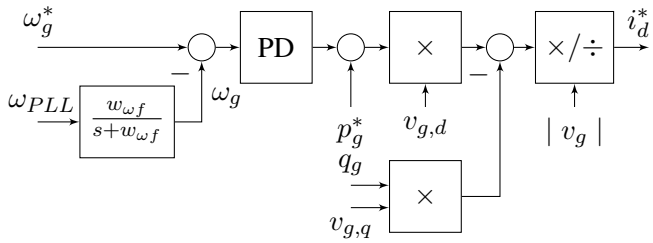

Figure 4.1: Virtual synchronous generator (VSG)

The second virtual inertia control scheme is the VSM, as presented in Figure 4.2 [52], [70]. It is a synchronous-generator based virtual inertia model which attempts to emulate a real synchronous generator. Since the VSM imitates a synchronous generator, it includes a voltage control model supplying the voltage reference to the electrical model. This model calculates the magnitude of the current reference to the grid-connected converter. The frequency control reacts to frequency deviations

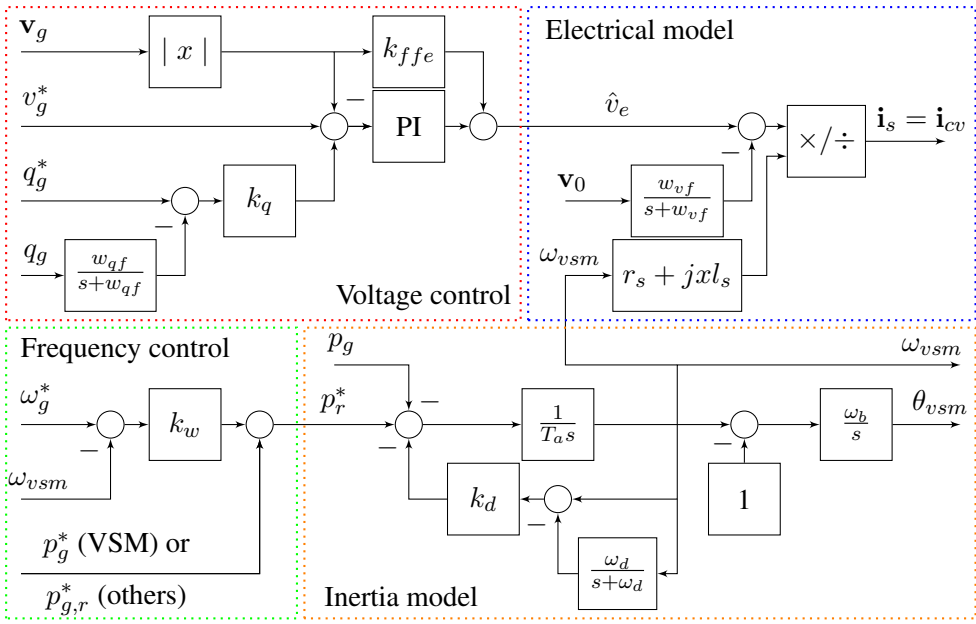

Figure 4.2: Virtual synchronous machine (VSM)

in the grid and supplies the power reference to the inertia model. Finally, the inertia model calculates emulated frequency and the current reference phase angle. Like a synchronous generator, the VSM is grid forming and able to work in islanded systems, without changing the control structure or any parameters.

The other three virtual inertia control schemes are extended versions of the VSG or the VSM, as proposed in Papers III and IV. Figure 4.3 shows the power-frequency PID controller with permanent droop (VSG-PID) based on the VSG; however, with a PID controller instead of a PD controller. PID controllers have the advantage of being slightly faster than PD controllers. Nonetheless, to supply FCR, a permanent droop has to be added to the output of the controller.

In order to improve the performance of the VSM, it is combined with the VSG to create the VSM with power-frequency PD controller (VSM-PD) as presented in Figure 4.4 and utilised in Paper VIII. In essence, a PD controller is added to the frequency control to obtain stationary frequency-droop control to the VSM. Similarly, a PID controller with permanent droop is added to the VSM (VSM-PID).

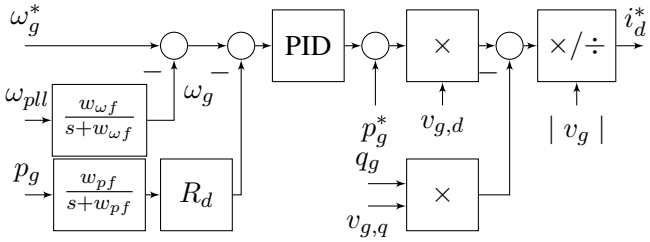

Figure 4.3: Power-frequency PID controller with permanent droop (VSG-PID)

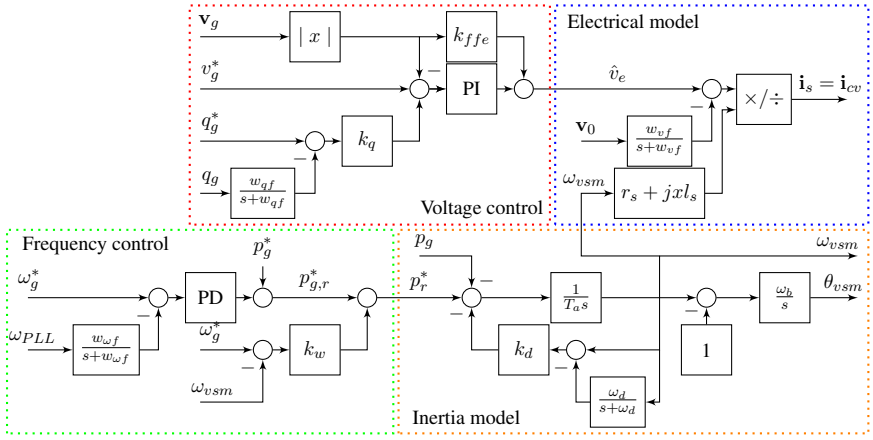

Figure 4.4: VSM with power-frequency PD controller (VSM-PD)

Chapter 5

Model predictive control

MPC is a closed-loop optimisation problem where a discrete-time model is optimised on a given time horizon. Only the inputs for the first time step are used and the optimisation problem is recalculated for the next time step, with the new initial state values. Although MPC is more complex, it offers significant advantages compared to traditional PID controllers for multiple reasons:

- MPC handles constraints, nonlinear systems such as power electronics and multiple-input, multiple-output (MIMO) systems.
- They are more robust and may offer a faster and smoother response and lower rising time, settling time and overshoots.
- The MPC optimises control by utilising dynamic models of the process to solve an optimisation problem.
- The control method is a well-developed and widely used in process control.

The principle of model predictive control (MPC) is formulated in [71]:

> Model predictive control is a form of control in which the current control action is obtained by solving, at each sampling instant, a finite horizon open-loop optimal control problem, using the current state of the plant as the initial state; the optimisation yields an optimal control sequence and the first control in this sequence is applied to the plant.

Nonlinear MPC is recently proposed for control of a variable-speed pumped-storage power plant in [72]. Its objective is to minimise the power loss of the VSHP. A static optimiser is utilised to find the optimal stationary point and an extended Kalman filter estimates the states. Moreover, the waterway is modelled by the spectral element method (SEM), and a detailed turbine model is obtained from [73] to increase the accuracy. A double-fed induction generator (DFIG) is utilised; however, this can be replaced by a synchronous generator with a full-converter. No VI control is implemented. Instead, the output power follows a power reference with rate limits.

MPC has also been suggested for control of conventional hydropower governors and/or excitation systems [74]–[77]. These works assume direct-connected connected generators where the turbine rotational speed follows the grid frequency. Thus, the corresponding hydraulic models do not consider deviation in turbine rotational speed and the MPC does not utilise the kinetic energy of the turbine and generator for provision of virtual inertia and FFR.

Other possible range of applications for MPC include the damping of power oscillations [78]–[82], power system frequency control [83]–[86] and voltage control [87]. MPC is also utilised together with virtual inertia control to optimise the control of a wind farm with battery storage system (BESS) [66].

In this thesis, MPC is utilised to coordinate and optimise the control of the hydraulic and electric system of a VSHP. The purpose of the controller is to maximise the delivery of FFR to the power system without exceeding the constraints given by the electric and hydraulic systems. Moreover, the control system should limit mass oscillations and water hammering that can damage the hydraulic system. For one of the proposed controllers, the MPC also damps power oscillations.

An MPC with linear system model, quadratic objective function and linear constraints called output feedback linear MPC is developed in Paper V. Since the system model is linearised at the steady-state operation point for each time step, the optimisation problem is a quadratic programming (QP) problem with linear equality constraints. In Paper VI, an MPC with a nonlinear system model is proposed to increase the accuracy of the solution. When comparing the MPC equations, we see that the equality constraint is now nonlinear, requiring more advanced solvers and more computational capacity.

Various versions of MPC controllers are found in Papers V-VIII. These papers include, respectively, MPC equations, parameters and deception of the MPC dynamic model. In Paper VIII, the number of states is reduced from six to five to reduce computational time. The grid frequency is removed as a state and is instead

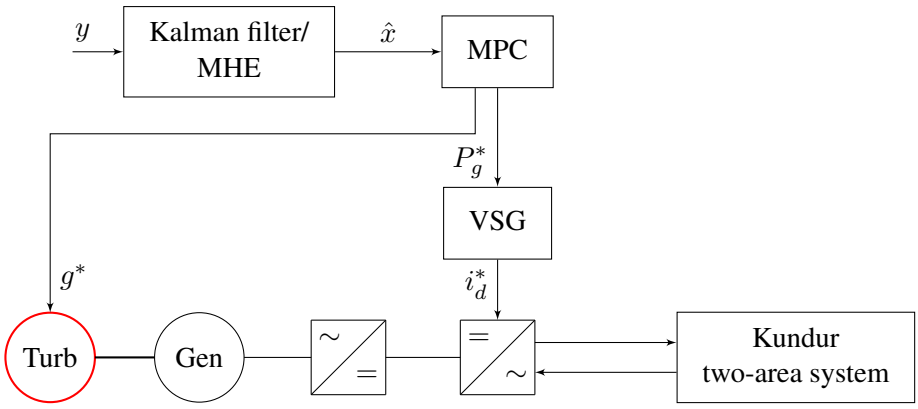

Figure 5.1: VSHP control structure

predicted from the measured frequency and ROCOF.

The unmeasured states need to be estimated as input to the MPC. A Kalman filter is utilised in Papers V and VII, while the states are estimated by a moving horizon estimator (MHE) in Papers VI and VIII. These methods are explained in the respective papers.

5.1 Objectives of the controller

The main objective of the MPC in this thesis is to coordinate the control of the hydraulic and electric system of the VSHP. The MPC solves the optimisation problem to find the optimal inputs u; the power reference P_g^* and the guide vane reference g^*, while handling all constraints defined in the MPC model. In this way, the VSHP contribution to frequency control and virtual inertia can be maximised without exceeding the limitations given by the hydraulic system. A traditional control system based on PID controllers would not be able to consider these constraints and the tuning of the system would, therefore, need to be conservative in order to avoid damage to the turbine and waterway.

The main tasks of the MPC in this thesis are defined below. Chapter 5.3 presents their arguments and the prioritisations between them.

- Primary frequency control:
  - Provide power reference P_g^* to the VSG.
  - Minimise deviation in grid frequency Δf.
  - Keep the converter power P_g within its limits.

  - Damp power oscillations (only implemented in Paper VI).

- Hydraulic system control:
  - Provide guide vane reference g^* to the governor.
  - Minimise the operation of the guide vane opening g to reduce wear and tear.
  - Optimise the control of the guide vane opening g to minimise water hammering and mass oscillation. (Only Paper VI considers water hammering.)
  - Keep the surge tank head h_{st} within its limits and close to the stationary value.
  - Keep the turbine flow q above its minimum level.
  - Optimise the rotational speed of the turbine ω.

- Turbine speed control:
  - Keep the rotational speed of the turbine ω within its limits and close to its optimal speed.
  - Make sure that the turbine rotational speed ω recovers after a disturbance.

The MPC prioritises the different control objectives by its objective function and thereby handles conflicts between the control objectives. An example is a case where the output power of the VSHP changes rapidly. The MPC will, in this case, increase the guide vane opening reference g^* as fast as possible in order to reduce the deviation in turbine rotational speed ω. However, this causes a reduction in the surge tank head h_{st} and increases mass oscillation and water hammering. If the surge tank head exceeds its limit, this will cause a high value of the cost function, in addition to the cost related to the mass oscillation and water hammering. The MPC will compare these costs with the cost of deviation in turbine rotational speed ω to optimise the control.

5.2 Constraints and slack variables

Two different types of constraints are utilised by the MPC. Hard constraints are absolute limits and the MPC will not find any solution outside these constraints. This may cause non-convergence of the MPC problem. To avoid this problem, slack variables are used instead of hard constraints. The slack variables allow the states to exceed its limit; however, an extra, and often high, cost is added to the

cost function. A very high cost of the slack variable will ensure that the solution of the MPC will exceed the constraint only if no possible solution can be found within the constraints.

The following constraints have been implemented in the MPC:

- Hard constraints
  - Maximum and minimum guide vane opening reference g^*.
  - Maximum and minimum rate of change of the guide vane opening reference g^*.
  - Maximum and minimum VSHP output power P_g.
- Constraints with slack variables
  - Maximum and minimum turbine flow q.
  - Maximum and minimum surge tank head h_{st}.
  - Maximum turbine head h.
  - Maximum and minimum turbine rotational speed ω

The constraints of the guide vane opening reference g^* are related to its physical limits, while the VSHP output power P_g is limited to avoid overload of the converters. These constraints can be absolute since they are directly related to the inputs u.

Slack variables are utilised for the other constraints in the hydraulic system. The limit on the turbine flow q ensures that the turbine functions properly. The surge tank head h_{st} should be kept below its maximum value to avoid blowouts, while the turbine head h should be less than the maximum pressure over the turbine, normally 1.1-1.15 p.u to avoid damage of the turbine blades. In addition, the surge tank head h_{st} should be above a certain level to avoid sand from rising from the sand trap between the surge shaft and pressure shaft. The sand will increase the wear and tear and reduce the lifetime of the turbine.

The maximum constraint of the turbine rotational speed ω should reduce the high consequence risk of the poles falling off. The minimum constraint should avoid a situation where the turbine could stop. When the turbine rotational speed ω reduces and the converter output power P_g is kept constant, the electrical torque will increase. The increase in mechanical torque will be less, and the MPC controller has to increase the guide vane opening g to regain the reference turbine speed ω^*. If ω decreases too much, the MPC controller will not be able to regain the reference turbine speed without reducing the converter output power P_g.

5.3 Costs

The relative values of the costs determine how the MPC prioritises between the objectives that are given in Section 5.1. A high cost related to an objective causes the MPC controller to prioritise this objective to reduce the cost function. We have chosen to prioritise the objectives that may cause damage to the system, like too high water pressure and too large deviation in the turbine speed. Next, we want to reduce oscillations in both the hydraulic system and the power system, as these also may cause damage. The next point on the list of prioritisation is keeping the VSHP output power reference P_g^* at its nominal value to ensure that the VI controller performs the frequency control as intended. This objective is regarded as more important than keeping the turbine rotational speed at its optimal value. The reason is that we want the turbine rotational speed to be controlled by the guide vane opening reference g^* and not by the VSHP output power reference P_g^* when possible. Though, the VSHP output power reference P_g^* can be controlled to avoid the water pressure or turbine rotational speed to exceed its constraints and to damp power oscillations.

The objectives are prioritised as follows:

1. Keep the surge tank head h_{st} within its constraints to avoid damage to the hydraulic system.
2. Keep the turbine rotational speed ω within its constraints to avoid undesirable operation conditions of the hydraulic system and damage to the generator.
3. Minimise water hammering (only implemented in Paper VI) and mass oscillations to avoid damages to the hydraulic system.
4. Minimise power oscillations to improve the stability of the power grid (only implemented in Paper VI).
5. Minimise the deviation in the VSHP power reference P_g^* to ensure that the VSHP is contributing to the frequency control as intended by the VSG/VSM.
6. Minimise the deviation of the turbine rotational speed ω from the best efficiency operating point and maximise the turbine efficiency to increase the efficiency of the system.
7. Keep the turbine flow q within its constraints to avoid undesired operational conditions of the hydraulic system.
8. Minimise the deviation in grid frequency Δf.

The details of how each of these objectives are implemented in the MPC function can be found in Papers V-VIII.

Chapter 6

Discussion and results

In this chapter, the main results of the papers are discussed in the elucidation of the objectives and contributions given in Chapter 1.1. The outline is similar to the classification of contributions in Figure 1.1, where the connections between the main contributions and the papers are explained.

6.1 Modelling of the hydraulic system - Paper I

The first step of this thesis was to develop an accurate model of the hydraulic system. The model should be able to recognise possible limitations in the hydraulic system, to model the turbine power and rotational speed correctly and thereby to be able to maximise power delivery for system control purposes. Four hydraulic turbine models are investigated to find a model with a suitable level of detail for analysis and control design of VSHP; the HYGOV model, a linearisation of the HYGOV model, the IEEE model that is similar to the HYGOV model but with improved waterway modelling and the Euler model based on the Euler turbine equations and the waterway model from the IEEE model. The detailed level of the Euler turbine model is considered necessary for multiple reasons:

- It includes models of the penstock, the headrace tunnel and the surge tank such that dynamics like mass oscillations and water hammering can be recognised.
- Since the turbine torque is a nonlinear function of both the turbine rotational speed ω and the turbine flow q, the turbine efficiency η_t is closer to the values given by the turbine hill curve. The efficiency is maximum at the rated speed while higher or lower speed causes less efficiency, as given in Figure 6.1.

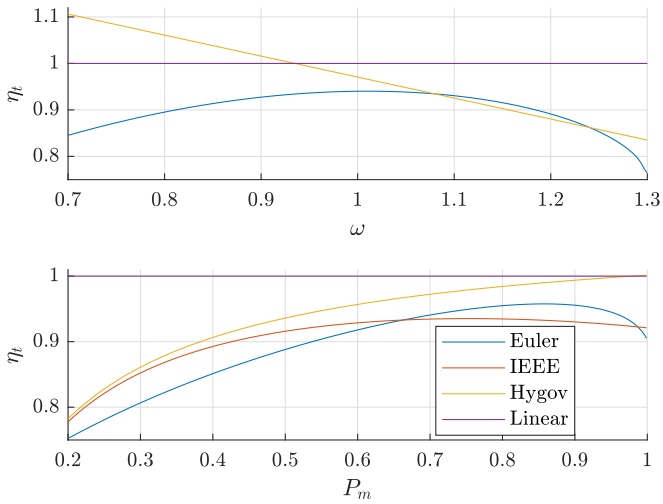

Figure 6.1: Hydraulic efficiency as a function of turbine rotational speed ω and turbine power P_m. The efficiencies of the *IEEE* and *Hygov* models as a function of ω are equal.

- The turbine flow q depends on the turbine rotational speed.
- The Euler model parameters can be found directly from the turbine dimensions.

Both dynamic simulations and eigenvalue analysis are performed to show the strength of the Euler model compared to conventional hydropower models. Since the Euler model considers variation in the turbine rotational speed, these equations are especially important when designing a VSHP control system.

6.2 Modelling and simple control of VSHP - Paper II

The second paper presents a VSHP model that can aid the design of controllers that can maximise the utilisation of power plants for the provision of ancillary services, considering the limitations given by the hydraulic system. A detailed model of a VSHP plant, including hydraulic system models, a synchronous generator and converter models with more or less conventional controllers, has been developed in this paper. The model is analysed to identify critical modes, adverse interactions or other limitations that must be taken into account in the future design of more advanced multivariable controllers for VSHP.

In order to fully utilise the potential of ancillary services from a VSHP, the power delivery to the grid needs to be as fast and flexible as possible. As seen from Figure 6.2, the VSHP power output P_g follows the step response of the power reference

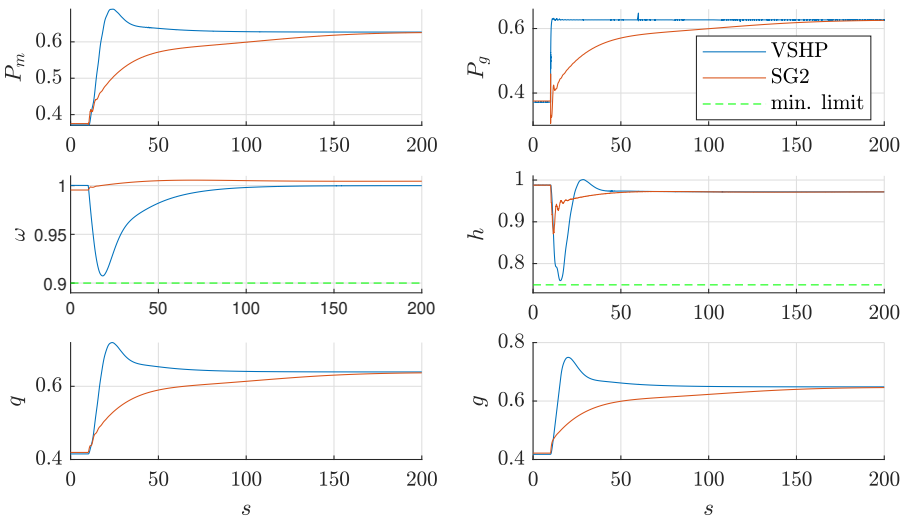

Figure 6.2: Power set point of respectively VSHP (blue) and conventional hydropower (red) is increased in a step at $t = 0$

almost perfectly with the proposed controllers. In contrast, the response of the conventional hydropower plant SG2 is significantly slower. However, the turbine power P_m will not be able to react as instantaneously, due to the governor and servo time constants. This will cause a deviation in the rotational speed ω and the governor will react to regain the reference rotational speed. As a result of the fast change in the VSHP output power, the peaks in the mechanical power P_m, rotational speed ω, turbine head h, turbine flow q and guide vane opening g will be larger compared to a conventional hydropower plant. The maximum extent of the grid converter power step is thereby limited by the maximum allowed turbine rotational speed, the minimum rotational speed to regain the reference rotational speed, as highlighted in Paper I, the minimum and maximum limits of the governor, the rate limit of the governor, the surge tank head limits and the current limits of the converters. Increased wear and tear on the guide vane servo due to additional operation and on the waterway due to more water hammering and mass oscillations must also be considered when designing the control system.

A participation factor-based interaction analysis shows that the VSHP system can be divided into two parts where there is no mode interacting in both parts. The turbine side of the DC-link will be affected by a perturbation on the grid side of the DC-link; however, there is no coupling the other way since the grid converter control is not influenced by the DC-link voltage. The result shows that there are no strong dynamic couplings between the hydraulic system of the VSHP and the rest

of the grid, and, from a small-signal perspective, that the modes of the hydraulic system will not need to be considered when tuning the grid converter. A similar analysis is performed for the MPC controller in Paper VII.

The proposed control system from Paper II is well suited for virtual inertia control of the grid converter, since the governor controls the turbine rotational speed and the converter connected to the synchronous generator controls the DC link voltage. Thus, the output power of the VSHP can be controlled directly by the grid converter with great flexibility without considering small-signal stability issues in the turbine side of the DC-link. The control system also makes it possible to take advantage of the rotational energy of the turbine and the generator as energy storage by allowing the turbine rotational speed to deviate from its nominal value. The virtual inertia control of the grid converter utilises this energy storage to deliver faster power response to the grid, as discussed in Papers III and IV. However, there are still limitations related to the maximum speed of the governor, the turbine rotational speed range, the turbine head and possible water hammering in the penstock that affect the VSHP output power control ability. As discussed in Papers V and VI, these constraints can be handled by an MPC to optimise the ancillary services given by the VSHP.

6.3 Virtual inertia implementation in VSHP - Papers III and IV

Papers III and IV investigate how a VSHP plant with VI control can utilise the rotational energy of the turbine and generator to deliver fast power reserves to the grid. These power reserves are necessary to compensate for variable production and reduced inertia of renewables and maintain the power system stability after disturbances. The advantage of the VSHP is that it can change the electric power output significantly within a few seconds and maintain it for a longer period. This is possible since the energy is obtained from the rotating masses of the generator and the turbine during the first seconds. Thereafter, the turbine flow and thereby the mechanical power are adjusted by governor action to return the turbine to its optimal speed.

Two main virtual inertia control structures, the VSG and the VSM, are further developed, implemented and tested on the VSHP plant simulation model from Paper II. The power-frequency PID controller with permanent droop (VSG-PID) is based on the VSG, while a PD and PID frequency controller is added to the VSM for, respectively, the VSM-PD and VSM-PID structures. The virtual inertia control structures are evaluated by two main criteria; their ability to deliver instantaneous power, or inertia, to reduce ROCOF and their contribution to the frequency containment control by reducing the steady-state frequency droop.

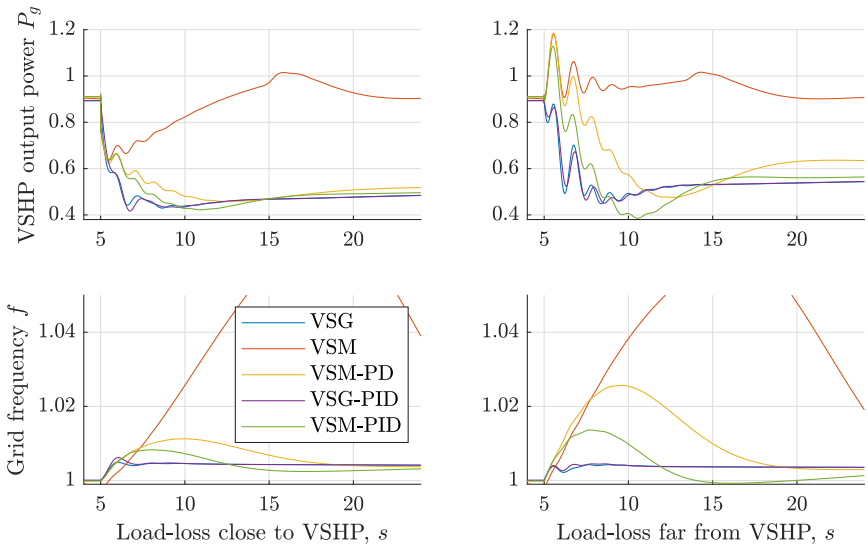

Figure 6.3: Response to sudden load reduction at respectively 50% on Bus 7 and 30% on Bus 9

Transient and eigenvalue analyses are performed to compare the control structures. Figure 6.3 presents the transients after a load loss close to the VSHP at $t = 5s$. The VSG-based control structures contribute the most FCR since the droop characteristic of the VSG controller will cause the output power to stabilise at a lower value after the disturbance. With the VSM controller, the output power returns to its reference value since it has zero steady-state feedback from the grid frequency. In Paper IV, the stationary performance of the VSM is improved by adding a frequency controller with droop characteristic to the VSHP power reference, for instance, a PD controller with feedback from grid frequency (VSM-PD) or a PID controller with permanent frequency droop (VSM-PID).

The output power of the VSM-based virtual inertia controllers shows the fastest response the first milliseconds after the disturbance when the load loss is close to the VSHP. Thereby, the VSM-based virtual inertia controllers deliver more inertia than the VSG-based virtual inertia controllers in this case. When the load loss is farther away from the VSHP, power oscillations are triggered by rapid changes in the power flow. Due to these power oscillations, there will be higher oscillations in both the output power of the VSG- and VSM-based virtual inertia controllers in this case. In particular, these power oscillations affect the VSM-based virtual inertia controllers since they are dependent on the voltage angle. The dependence on the voltage seems to be a major disadvantage by emulating a synchronous machine and the use of VSM might cause problems in a system with large power

oscillations. On the other hand, the VSM does not need a PLL since its controller is based on emulating the response of a synchronous generator. This makes the VSM able to work in islanded systems without changing parameters and control structure.

Although the VSM-based controllers show the fastest response during the first 200 ms after a disturbance, the VSG-based controllers provide better frequency control for the following seconds, thus reducing the maximum frequency deviation. With this in mind, the VSG seems to be the better alternative as long as the virtual inertia controller can be grid-following and does not need to be grid-forming, like the VSM.

The transient behaviour of the hydraulic system is more or less equal for the VSG, VSG-PID and VSM-PID. The VSHP output power response of the VSM-PD is marginally smaller, causing smaller deviations in the hydraulic system variables.

6.4 Model predictive control of VSHP - Papers V and VI

Paper V and Paper VI present the development of, respectively, linear and non-linear MPCs for controlling VSHP plants. The MPC coordinates the control of the turbine with the VSG control of the grid-connected converter to optimise the plant's performance. Its main objective is to maximise the delivery of FFR to the grid while keeping the electric and hydraulic variables within their constraints.

6.4.1 MPC compared to PID governor

Figure 6.4 compares the dynamic results of the linear MPC controller with Kalman filter for state estimation presented in Paper V, the nonlinear MPC with MHE from Paper VI and the PID governor from Paper II. After the generator loss at $t = 0$, the VSG increases the VSHP output power in all the three cases to reduce the grid frequency deviation.

The PID governor has to be tuned carefully in order to avoid exceeding the hydraulic constraints and is therefore relatively slow. Since the MPCs consider the limitations in surge tank head h_{st} and turbine head h, the guide vane opening g can be increased close to its maximal rate of change until its maximum value is reached or the minimum value of h_{st} is reached. This results in higher turbine mechanical power P_m and thereby a significant reduction of the turbine rotational speed ω deviation. Thus, the turbine losses will be reduced. The more aggressive control of the guide vane opening g causes higher deviation and more oscillations in the surge tank head h_{st}, however, this can be tolerated since the MPC controller handles the system constraints. Due to the increased performance of the turbine control and lower deviation in turbine rotational speed ω, it is possible to increase

the FFR delivery.

The linear MPC will keep the VSHP output power reference P_g^* almost constant as long as the turbine rotational speed ω does not exceed its limits. This is because the cost of deviation in the VSHP output power reference P_g^* is higher than the cost of deviation in the turbine rotational speed ω. Thereby, the VSHP output power P_g and grid frequency f will be almost equal for the cases with linear MPC and PID governor.

6.4.2 Nonlinear MPC compared to linear MPC

To minimise the deviation in turbine rotational speed ω, the MPC has to increase the turbine mechanical power P_m as quickly as possible. As seen from the result, the nonlinear MPC outperforms the linear MPC in this task because of its more accurate prediction of the turbine mechanical power P_m. Firstly, this allows a slightly faster response of the guide vane opening g after the disturbance. The linear MPC is slower, causing higher deviations in turbine rotational speed ω and thereby a self-energising effect due to reduced mechanical power P_m. Secondly, the linearisation of the turbine model for the linear MPC causes unnecessary overshoot in the guide vane opening from approximately $3-15s$ after the disturbance, as shown in Figure 6.4. In addition, this will also result in larger deviations in the turbine flow q and thereby the turbine speed ω, and larger deviations in the surge tank head h_{st} and turbine head h.

6.4.3 Power Oscillation Damper

The nonlinear MPC includes a function for damping of power oscillations in the grid. By adjusting the VSHP output power reference P_g^*, the MPC minimises the deviation between the local frequency at the VSHP and the average system frequency $\overline{f}$. From Figure 6.4, we see how this function affects the VSHP output power and the frequency deviation Δf when we compare the nonlinear MPC with the linear MPC. The results from Paper VI also shows a significant improvement of the damping of power oscillations between the two areas in the system.

6.4.4 Modelling of Water Hammering in the Penstock

Modelling of the water hammering in the penstock is also included in the nonlinear MPC. Without it, the turbine head h exceeds its limits when the guide vane is closing, as shown in Figure 7 in Paper VI. The guide vane closing speed is faster, resulting in less deviation in turbine rotational speed ω. The difference between the two cases with and without modelling of the water hammering is less when the guide vane is opening since the constraints of the turbine head h or surge tank head h_{st} are not active in this case.

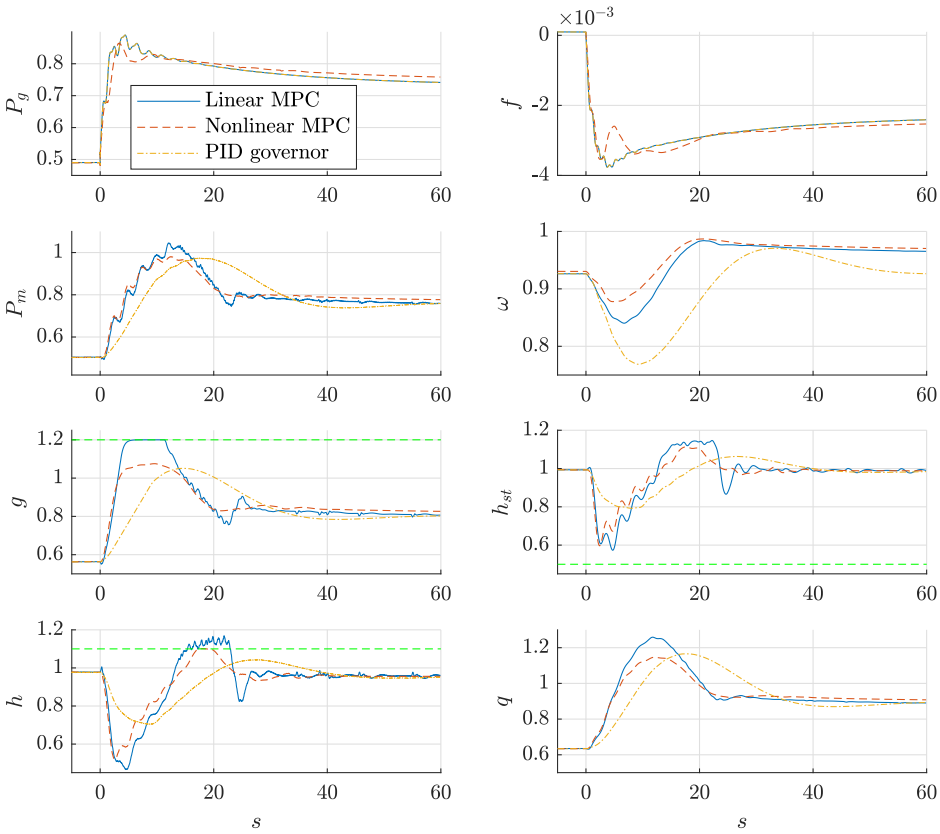

Figure 6.4: Comparison of the linear MPC as presented in Paper V (blue), the nonlinear MPC (red) as presented in Paper VI and the PID controller as presented in Papers II and IV (yellow): VSHP output power P_g, frequency deviation Δf, turbine mechanical power P_m, turbine rotational speed ω, guide vane opening g, penstock flow q, turbine head h and surge tank head h_{st}.

The drawback by modelling the water hammering waves is that it causes an increase of oscillations in certain cases. The reason for this is that the MPC tries to keep the turbine head h at its maximum value by counteracting the oscillations in the penstock. The guide vane opening is slightly adjusted to obtain this, causing more pressure oscillations in the penstock. Because of this effect, the model of the water hammering in the penstock is not included in the MPC system model of Paper VIII.

6.4.5 State Estimators

The performances of the Kalman filter in Paper V and the MHE in Paper VI are shown to be sufficient; however, both introduce a delay. The most noticeable difference is that the MHE has a more accurate estimation of the turbine flow q and the headrace tunnel flow q. However, the Kalman filter is best suited for small-signal analysis, as discussed in Paper VII.

6.5 Small-signal properties of MPC - Paper VII

A method for small-signal analysis of the proposed VSHP control system including the MPC and VSG is developed in Paper VII. This comprises the derivation of a state-space representation of the MPC. In order to utilise the state-space formulation of an MPC derived in [88] and [89], the system is assumed to be stable and in a steady-state operation point where the reference values of the MPC cost function are fulfilled. In addition, no constraints or slack variables of the MPC must be active, costs related to changes in states are neglected, the cost matrices are time-independent, the perturbation is small, and all modes are damped.

The MHE utilised in Paper VI is not suitable for state-space representation since it depends on previous measurements and a state-space model will, therefore, imply a very high number of states. Instead, the states are estimated by a Kalman filter, as utilised in Paper V.

The purpose of the small-signal analysis is to investigate how the MPC cost function should be parametrised to minimise oscillatory modes between the hydraulic system of the VSHP and the power system. If there is low or no interactions between these two parts of the system, the virtual inertia controller, a VSG in this case, can be tuned without considering small-signal stability issues with the hydraulic system of the VSHP.

A participation factor-based interaction analysis [40] is performed for two different sets of cost factors of the MPC, as shown in Figures 6.5 and 6.6. The first case is similar to the MPC from Paper VI where the cost of deviation of the VSHP output power reference P_g^* is high. The MPC will, therefore, prioritise controlling the guide vane opening reference g^* instead of P_g^* in order to minimise the deviation of the turbine rotational speed ω. A disturbance in the power system will cause the VSG to change the VSHP output power P_g due to the frequency deviation. This will lead to a deviation in the turbine rotational speed ω. However, it will not affect the VSHP output power reference P_g^* since the MPC changes the guide vane opening reference g^* to regain the turbine rotational speed ω. This explains why the system in Figure 6.5 is divided into two parts where there is almost no interaction between these parts in the frequency range of interest.

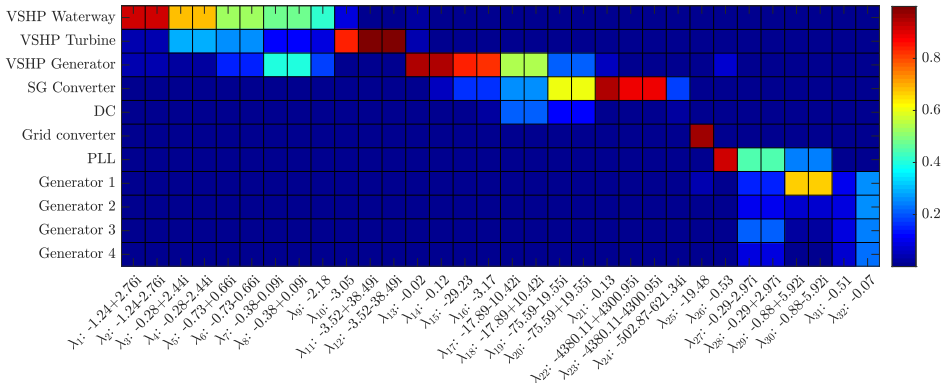

Figure 6.5: Case 1: Participation factor-based interaction analysis with high cost on deviation in the VSHP output power reference P_g^*

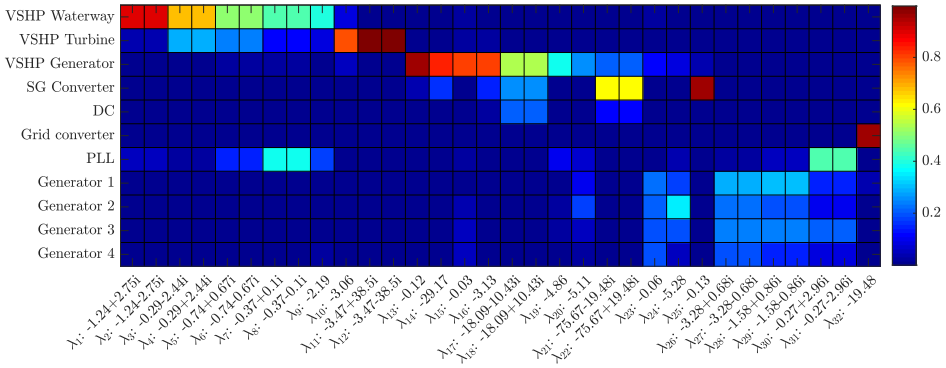

Figure 6.6: Case 2: Participation factor-based interaction analysis with no cost on deviation in the VSHP output power reference P_g^*

In the second case (Figure 6.6), the cost for deviation of the VSHP output power reference P_g^* is zero. Thereby, the MPC can adjust this input in addition to the guide vane opening reference g^* to regain the turbine rotational speed ω after a disturbance. The result is that the two parts of the system interact with each other such that there exist modes between the hydraulic system of the VSHP and the rest of the power system, as indicated in the figure.

A sensitivity analysis of the VSG parameters is performed to demonstrate how the virtual inertia controller can improve system stability. By proving that the VSG is equal to a phase lead controller, existing methods can be utilised to tune the VSG to damp power oscillations. The results show how the choice of the corner frequencies and gains of the VSG affect the damping. Although changing

a parameter may increase the damping of one mode, the damping of other modes can be decreased.

6.6 Stability improvements of the Nordic power system - Paper VIII

Paper VIII demonstrates the grid support capability of the VSHP by transient simulation on a Nordic 44-bus model. The VSHP is controlled by a simplified version of the MPC presented in Paper VI operating together with the VSG and VSM presented in Paper IV. For possible future real-time simulations, the model is developed to comply with Opal-RT tools. The VSHP with the virtual inertia control is simulated in MatLab/Simulink, CasAdi calculates the MHE and MPC problems and the PSS/E grid model is implemented in ePHASORSIM. Moreover, a new low-load case of the Nordic grid with high HVDC import is created to represent a low-inertia situation.

Two additional cases are created by replacing a large conventional hydropower plant located in southern Norway by VSHP plants with, respectively, VSG and VSM virtual inertia control. The transients of these three cases are compared after three different disturbances in the network:

- Disconnection of a nuclear power plant in Sweden (1450 MW).
- Disconnection of an HVDC-connection in southern Norway importing 1400 MW and located close to the VSHP.
- Three-phase line short circuit close to the VSHP.

With the introduction of the VSHP, the maximum frequency deviation after the two first disturbances is reduced by approximately 40%, even the VSHP rated power is less than 5% of the total system power. The grid frequency f and the VSHP output power P_g after the loss of the nuclear power plant are shown in Figure 6.7. There is, in the cases including VSHP, enough inertia and FFR in the Nordic grid to limit the maximal transient frequency deviation to $|\Delta f| \leq 0.9Hz$ and enough FCR to limit the maximal stationary frequency deviation to $|\Delta f| \leq 0.4Hz$. These are demands given by the Nordic TSOs for maximal frequency deviation after the loss of the dimensional unit (1450 MW).

The introduction of both the VSG and VSM controllers generally reduces oscillations after the disturbances; however, they also add new oscillation modes. The VSM control, that emulates a synchronous generator, introduces a new and slower oscillation mode at approximately $0.55Hz$. Primarily, the origin of this mode is

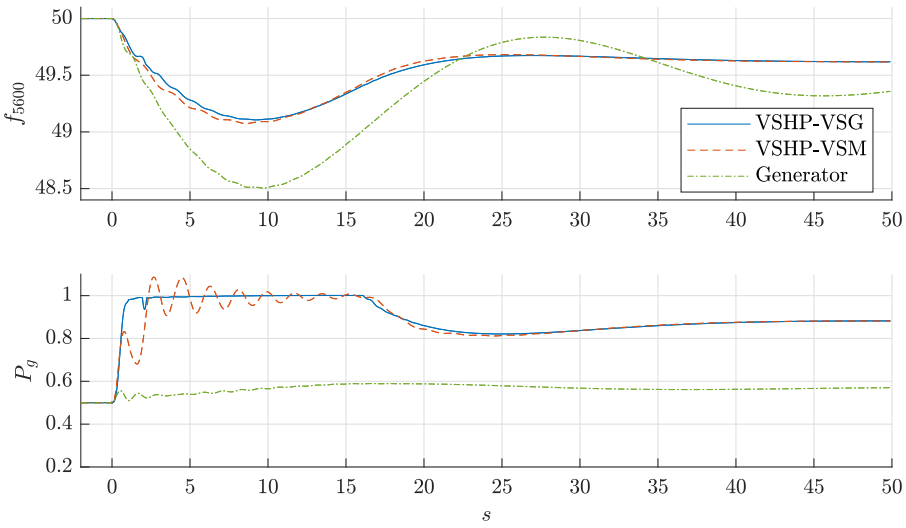

Figure 6.7: Dynamic performance of frequency f and hydropower plant power output P_g after generator loss for three different plants at bus 5600: VSHP with VSG (blue), VSHP with VSM (red) and conventional hydropower plant (green)

the virtual inertia of the VSM, oscillating with the other generators in the power system. It is recognised as the oscillations of the VSHP output power P_g the first $10s$ after the generator loss. This causes oscillations in grid frequency, rotor angles and voltages, both close to and far from the VSHP. However, the damping of this oscillation is fair. For the VSG, the oscillations in output power occur after the short circuit due to the combination of the derivation term of the VSG and the high ROCOF.

In most cases, the VSG and especially the VSM increase the critical fault clearing time, defined as the maximum duration of a fault that ensures the power system to reach a post-disturbance steady-state. Thereby, the virtual inertia controller increases the transient stability margin.

The performance of internal control of the VSHP by MPC and VSG is as expected; the turbine rotational speed is regained as fast as possible without any oscillations. At the same time, the constraints of the system are met. This is also the case for the VSM. However, the oscillations in VSHP output power cause oscillations in the hydraulic system.

The results of Paper VIII show that VSHP with the proposed control structure based on MPC and virtual inertia can increase the frequency stability and thereby reduce the demand for increasing the inertia of the power system. In addition, the

virtual inertia controller can damp power oscillations, and in this way, increase the stability margins.

Chapter 7

Conclusion and recommendations for further work

The green shift comprises new solutions for maintaining power system stability. Large thermal power plants with high-inertia generators are being replaced by renewable energy with low or no inertia. This reduction of the system inertia causes larger frequency deviations, and thereby reduced frequency stability. Moreover, it challenges the rotor angle stability due to less damping of power oscillations and thus might cause instability. Faster frequency containment resources and improved power oscillation damping are therefore needed to secure the system stability.

According to the results of this thesis, VSHP has a great potential for supplying virtual inertia and FFR. The frequency stability of a large power system, in this case, the Nordic power system, is improved significantly by implementing a rather small share of VSHP. With the introduction of virtual inertia control, the VSHP grid-connected converter can be controlled quickly to counteract frequency deviations and reduce the maximal frequency deviation. The results also show how appropriate tuning of the virtual inertia controllers increases the damping of oscillations and the rotor angle stability.

Two types of virtual inertia controllers are investigated. The grid-following VSG is essentially a PD controller on the grid frequency deviation, outputting current reference to the grid-connected converter of the VSHP. With a first-order low-pass filter on the derivation term, it is equal to the phase lead controller and can thereby be tuned to damp oscillations between the selected corner frequencies. The VSG

requires frequency measurements, for instance, a PLL, thus causing a low accuracy of the ROCOF measurement. This limits the gain of the VSG derivation term and thereby the quantity of virtual inertia supplied by the VSG.

The VSM is grid-forming, thus it is able to work in islanded systems without changing parameters and control structure. Moreover, it does not depend on measurements from a PLL. Since the VSM does not contribute with steady-state frequency droop response, a PD controller, equal to the VSG, is added to control the VSM power reference. In this way, the improved VSM contributes to frequency containment control.

Although the VSM responds to frequency deviations faster than the VSG immediately after a disturbance, the VSG outperforms the VSM with regards to damping oscillations. Moreover, its simpler control structure makes it more suitable for integration with an MPC controller.

By allowing the turbine rotational speed to temporarily deviate from its optimal value, the virtual inertia control can obtain the energy to balance the power system from the rotational energy of the turbine and generator. The internal control of the VSHP must then control the guide vane opening and thereby the turbine mechanical power to bring the rotational speed back to its reference value. This action must be as fast as possible in order to minimise the deviation in turbine rotational speed and maximise turbine efficiency. In addition, situations where the turbine rotational speed is too low to produce enough mechanical power to regain the optimal rotational speed must be avoided. At the same time, the speed of the guide vane control is limited by its maximal rate of change, maximum turbine head and maximum and minimum head of the surge tank. Limitations on turbine flow and VSHP output power must also be considered.

In this thesis, MPC is proposed to coordinate the control of the hydraulic and electric systems. Primarily, the MPC controls the guide vane opening to fulfil the internal control objectives of the VSHP; minimising deviation in turbine rotational speed, minimising mass oscillations and water hammering and fulfilling the constraints on surge tank head, turbine head, turbine flow and turbine rotational speed. Secondarily, the MPC controls the VSHP output power reference since the output power should normally be controlled by the virtual inertia controller. However, in situations where the constraints of the hydraulic and electric systems cannot be fulfilled with control of the guide vane opening, the MPC must adjust the VSHP output power reference to regain the turbine rotational speed.

These properties of the MPC are obtained by defining the MPC cost function such that the costs of deviations in the hydraulic system are low compared to the cost

of deviations in the VSHP output power reference. When this is fulfilled, small-signal analysis demonstrates negligible dynamic interaction between the hydraulic system and the power system. Thereby, small-signal stability issues within the VSHP do not need to be considered when tuning the virtual inertia controller. The same conclusion is found for a VSHP with conventional controllers, supposing the turbine rotational speed is controlled by the guide vane opening, the DC-link voltage by the generator-connected converter and the VSHP output power by the grid-connected converter.

Comparisons between the MPCs developed in this thesis show that the nonlinear MPC outperforms the linear MPC. Due to the nonlinear property of the hydraulic system, the estimation of the turbine power becomes inaccurate when the system is linearised. The nonlinear MPC increases the precision of the guide vane opening control and reduces the turbine rotational speed deviation. However, it also increases the computational demand for solving the optimisation problem.

The performance of the MPC depends on accurate models of the hydraulic system. This motivated the development of a nonlinear model based on the Euler turbine equations and the 1D momentum and continuity balance for a water-filled elementary pipe. The mechanical power of the turbine depends on both flow and its rotational speed as opposed to conventional hydraulic models for grid integration studies. However, the model is simple enough to be utilised in the MPC.

Development of VSHP plants with the proposed control system is dependent upon the marked solution for fast frequency resources. The increased profit of such markets may trigger new pump storage hydropower plant projects with the purpose of power balancing. Moreover, the system services and the corresponding improved system stability will benefit the system operator, allowing for further integration of renewable energy.

7.1 Future work

The results of this thesis are based on simulations. A natural next step will be to implement the proposed controller in a laboratory setup. The MPC controller and the Nordic grid model are already implemented in the Opal-RT software; however, some work remains to be conducted before they can be simulated in real-time. Real-time testing will investigate if the MPC is able to find solutions within a respectable time or if the MPC has to be simplified. Hardware-in-the-loop testing is possible by combining the MPC and the Nordic grid model implemented in the Opal-RT with the variable speed hydropower setup, including generator and converters, that is under development in the HydroCen project. This setup should include a more advanced and detailed hydraulic model. This model allows for

validation of the Euler turbine model utilised in this thesis and testing of the MPC controller on a more realistic hydraulic mode.

Other possible tasks will be to:

- Investigate the possibility of utilising a similar MPC on a conventional hydropower plant.
- Design a similar control system for wind power plants to maximise the contribution of FFR.
- Utilise the experience from this thesis to design a control system for an offshore grid with wind power based on MPC and virtual inertia.
- Develop and test an MPC control system for multiple turbines sharing the waterway.
- Test the proposed VSHP control system in pumping mode.

Bibliography

[1] IEA, 'Renewables 2019', IEA,Paris, Tech. Rep., 2019.

[2] E. Commission *et al.*, 'The european green deal', *Communication from the Commission to the European Parliament, the European Council, the Council, the European Economic and Social Committee and the Committee of the Regions. Brussels*, p. 24, 2019.

[3] ——, 'Clean energy for all europeans', p. 24, 2019.

[4] *Norway's role as a flexibility provider in a renewable europe*, https://www.ntnu.no/documents/7414984/1281984692/Norway%E2%80%99s+role+as+a+flexibility+provider+in+a+renewable+Europe.pdf/a055c776-f2a5-468f-bce2-c2cf1943f1fc, Accessed: 2020-09-03.

[5] M. Valavi and A. Nysveen, 'Variable-speed operation of hydropower plants: A look at the past, present, and future', *IEEE Industry Applications Magazine*, vol. 24, no. 5, pp. 18–27, 2018.

[6] N. H. Association *et al.*, 'Challenges and opportunities for new pumped storage development', *NHA Pumped Storage Development Council*, 2012.

[7] J. Liang and R. G. Harley, 'Pumped storage hydro-plant models for system transient and long-term dynamic studies', in *Power and Energy Society General Meeting, 2010 IEEE*, IEEE, 2010, pp. 1–8.

[8] D. Fayolle and S. Lafon, 'Variable speed applied to hydroelectric schemes: History of a technology and today's state of the art', *Hydro*, 2008.

[9] M. Basic, P. C. de Oliveira e Silva and D. Dujic, 'High power electronics innovation perspectives for pumped storage power plants', Tech. Rep., 2018.

[10] Statnett, 'Systemdrifts- og markedsutviklingsplan 2014-20. tiltaksplan for sikker og effektiv drift av kraftsystemet', 2014.

[11] ——, 'Vilkår for tilbud, aksept, rapportering og avregning i marked for fcr', 2016.

[12] N. Modig, R. Eriksson, L. Haarla, M. Kuivaniemi, K. S. Hornnes, P. A. Vada, S. A. Meybodi and D. Karlsson, 'Technical requirements for fast frequency reserve provision in the nordic synchronous area', *Online: https://www.statnett.no/globalassets/for-aktorer-i-kraftsystemet/utvikling-av-kraftsystemet/nordisk-frekvensstabilitet/technical-requirements-for-ffr-v.1.0.pdf*, 2019, Accessed: 2020-04-27.

[13] E. Ørum, M. Kuivaniemi, M. Laasonen, A. I. Bruseth, E. A. Jansson, A. Danell, K. Elkington and N. Modig, 'Future system inertia', *ENTSOE, Brussels, Tech. Rep*, 2015.

[14] E. Ørum, L. Haarla, M. Kuivaniemi, M. Laasonen, A. Jerkø, I. Stenkløv, F. Wik, K. Elkington, R. Eriksson, N. Modig and P. Schavemaker, 'Future system inertia 2', *ENTSOE, Brussels, Tech. Rep*, 2018.

[15] Statnett, 'Fast frequency reserves 2018 - pilot for raske frekvensreserver', Tech. Rep., 2018, Accessed: 2019-02-15.

[16] U. Tamrakar, D. Shrestha, M. Maharjan, B. P. Bhattarai, T. M. Hansen and R. Tonkoski, 'Virtual inertia: Current trends and future directions', *Applied Sciences*, vol. 7, no. 7, p. 654, 2017.

[17] S. Wang, J. Hu, X. Yuan, L. Sun *et al.*, 'On inertial dynamics of virtual-synchronous-controlled dfig-based wind turbines', *IEEE Trans. Energy Convers*, vol. 30, no. 4, pp. 1691–1702, 2015.

[18] F. Diaz-Gonzalez, M. Hau, A. Sumper and O. Gomis-Bellmunt, 'Participation of wind power plants in system frequency control: Review of grid code requirements and control methods', *Renewable and Sustainable Energy Reviews*, vol. 34, pp. 551–564, 2014.

[19] J. A. Andersson, J. Gillis, G. Horn, J. B. Rawlings and M. Diehl, 'Casadi: A software framework for nonlinear optimization and optimal control', *Mathematical Programming Computation*, vol. 11, no. 1, pp. 1–36, 2019.

[20] T. I. Reigstad and K. Uhlen, 'Modelling of variable speed hydropower for grid integration studies', *Presented at IFAC World Congress 2020, Germany, to be published in IFAC-PapersOnLine*,

[21] ——, 'Variable speed hydropower conversion and control', *IEEE Transactions on Energy Conversion*, vol. 35, no. 1, pp. 386–393, March 2020.

[22] ——, 'Virtual inertia implementation in variable speed hydropower plant', *Presented on the Modern Electric Power System conference (MEPS'19), September 9-12, 2019, Wroclaw, Poland*,

[23] ——, 'Variable speed hydropower plant with virtual inertia control for provision of fast frequency reserves', *International Journal of Power and Energy Systems*, vol. 35, no. Volume 41, issue 2, 2021.

[24] ——, 'Optimized control of variable speed hydropower for provision of fast frequency reserves', *Electric Power System Research, Special issue: Proceedings of the 21st Power Systems Computation Conference (PSCC 2020)*, vol. 189, 2020.

[25] ——, 'Nonlinear model predictive control of variable speed hydropower for provision of fast frequency reserves', *Electric Power Systems Research*, vol. 194, p. 107 067, 2021.

[26] ——, 'Stability properties of non-linear model predictive control of variable speed hydropower', *IET Renewable Power Generation*, 2020.

[27] ——, 'Variable speed hydropower for provision of fast frequency reserves in the nordic grid', *Submitted to IEEE Transaction on Power Systems*, 2020.

[28] P. Kundur, N. J. Balu and M. G. Lauby, *Power system stability and control*. McGraw-hill New York, 1994, vol. 7.

[29] P. Kundur, J. Paserba, V. Ajjarapu, G. Andersson, A. Bose, C. Canizares, N. Hatziargyriou, D. Hill, A. Stankovic, C. Taylor *et al.*, 'Ieee/cigre joint task force on stability terms and definitions,'definition and classification of power system stability'', *IEEE transactions on power systems*, vol. 19, no. 2, pp. 1387–1401, 2004.

[30] M. Eremia and M. Shahidehpour, *Handbook of electrical power system dynamics: modeling, stability, and control*. John Wiley & Sons, 2013, vol. 92.

[31] J. Machowski, J. Bialek and J. Bumby, *Power system dynamics: stability and control*. John Wiley & Sons, 2011.

[32] V. I. Vorotnikov, *Partial stability and control*. Springer Science & Business Media, 2012.

[33] ENTSO-E, Continental Europe Operation Handbook, *P1-policy 1: Load-frequency control and performance*, 2009.

[34] P. Tielens and D. Van Hertem, 'The relevance of inertia in power systems', *Renewable and Sustainable Energy Reviews*, vol. 55, pp. 999–1009, 2016.

[35] Svenska kraftnät, Statnett, Fingrid and Energinet.dk, 'Challenges and opportunities for the nordic power system', *Online:* https://www.fingrid.fi/globalassets/dokumentit/fi/yhtio/tki-toiminta/report-challenges-and-opportunities-for-the-nordic-power-system.pdf, 2016, Accessed: 2020-03-09.

[36] RG-CE System Protection & Dynamics Sub Group, 'Frequency stability evaluation criteria for the synchronous zone of continental europe', *Online:* https://docstore.entsoe.eu/Documents/SOC%20documents/RGCE_SPD-_frequency_stability_criteria_v10.pdf, 2016, Accessed: 2020-03-09.

[37] F. Milano, F. Dörfler, G. Hug, D. J. Hill and G. Verbič, 'Foundations and challenges of low-inertia systems', in *2018 Power Systems Computation Conference (PSCC)*, IEEE, 2018, pp. 1–25.

[38] A. Ulbig, T. S. Borsche and G. Andersson, 'Impact of low rotational inertia on power system stability and operation', *IFAC Proceedings Volumes*, vol. 47, no. 3, pp. 7290–7297, 2014.

[39] B. K. Poolla, D. Groß and F. Dörfler, 'Placement and implementation of grid-forming and grid-following virtual inertia and fast frequency response', *IEEE Transactions on Power Systems*, vol. 34, no. 4, pp. 3035–3046, 2019.

[40] J. Beerten, S. D'Arco and J. A. Suul, 'Identification and small-signal analysis of interaction modes in vsc mtdc systems', *IEEE Transactions on Power Delivery*, vol. 31, no. 2, pp. 888–897, 2016.

[41] A. G. Endegnanew, 'Stability analysis of high voltage hybrid ac/dc power systems', 2017.

[42] R. G. Farmer, 'Power system dynamics and stability', *The Electric Power Engineering Handbook*, 2001.

[43] H. V. Pico, J. D. McCalley, A. Angel, R. Leon and N. J. Castrillon, 'Analysis of very low frequency oscillations in hydro-dominant power systems using multi-unit modeling', *IEEE Transactions on Power Systems*, vol. 27, no. 4, pp. 1906–1915, 2012.

[44] J. Parmakian, *Water hammer analysis*, 1955.

[45] S. Mansoor, 'Behaviour and operation of pumped storage hydro plants', Ph.D. dissertation, University of Wales, Bangor, 2000.

[46] F. Demello, R. Koessler, J. Agee, P. Anderson, J. Doudna, J. Fish, P. Hamm, P. Kundur, D. Lee, G. Rogers *et al.*, 'Hydraulic-turbine and turbine control-models for system dynamic studies', *IEEE Transactions on Power Systems*, vol. 7, no. 1, pp. 167–179, 1992.

[47] T. K. Nielsen, 'Simulation model for francis and reversible pump turbines', *International Journal of Fluid Machinery and Systems*, vol. 8, no. 3, pp. 169–182, 2015.

[48] P. Anderson and A. Fouad, 'Power system control and stability', 2003.

[49] E. B. Wylie, V. L. Streeter and L. Suo, *Fluid transients in systems*. Prentice Hall Englewood Cliffs, NJ, 1993, vol. 1.

[50] J. Machowski, J. Bialek, J. R. Bumby and J. Bumby, *Power system dynamics and stability*. John Wiley & Sons, 1997.

[51] M. A. Torres L, L. A. Lopes, L. A. Moran T and J. R. Espinoza C, 'Self-tuning virtual synchronous machine: A control strategy for energy storage systems to support dynamic frequency control', *IEEE Transactions on Energy Conversion*, vol. 29, pp. 833–840, 2014.

[52] O. Mo, S. D'Arco and J. A. Suul, 'Evaluation of virtual synchronous machines with dynamic or quasi-stationary machine models', *IEEE Transactions on Industrial Electronics*, vol. 64, no. 7, pp. 5952–5962, 2017.

[53] S. D'Arco, J. A. Suul and O. B. Fosso, 'A virtual synchronous machine implementation for distributed control of power converters in smartgrids', *Electric Power Systems Research*, vol. 122, pp. 180–197, 2015.

[54] J. Alipoor, Y. Miura and T. Ise, 'Power system stabilization using virtual synchronous generator with alternating moment of inertia', *IEEE Journal of Emerging and Selected Topics in Power Electronics*, vol. 3, no. 2, pp. 451–458, 2015.

[55] I. Serban and C. P. Ion, 'Microgrid control based on a grid-forming inverter operating as virtual synchronous generator with enhanced dynamic response capability', *International Journal of Electrical Power & Energy Systems*, vol. 89, pp. 94–105, 2017.

[56] J. Liu, Y. Miura, T. Ise *et al.*, 'Comparison of dynamic characteristics between virtual synchronous generator and droop control in inverter-based distributed generators', *IEEE Trans. Power Electron*, vol. 31, no. 5, pp. 3600–3611, 2016.

[57] K. Sakimoto, Y. Miura and T. Ise, 'Stabilization of a power system with a distributed generator by a virtual synchronous generator function', in *Power Electronics and ECCE Asia (ICPE & ECCE), 2011 IEEE 8th International Conference on*, IEEE, 2011, pp. 1498–1505.

[58] N. R. Ullah, T. Thiringer and D. Karlsson, 'Temporary primary frequency control support by variable speed wind turbines—potential and applications', *IEEE Transactions on Power Systems*, vol. 23, no. 2, pp. 601–612, 2008.

[59] M. Wang-Hansen, R. Josefsson and H. Mehmedovic, 'Frequency controlling wind power modeling of control strategies', *IEEE Transactions on Sustainable Energy*, vol. 4, no. 4, pp. 954–959, 2013.

[60] Y. Wang, G. Delille, H. Bayem, X. Guillaud and B. Francois, 'High wind power penetration in isolated power systems—assessment of wind inertial and primary frequency responses', *IEEE Transactions on Power Systems*, vol. 28, no. 3, pp. 2412–2420, 2013.

[61] L. Wu and D. G. Infield, 'Towards an assessment of power system frequency support from wind plant—modeling aggregate inertial response', *IEEE Transactions on Power Systems*, vol. 28, no. 3, pp. 2283–2291, 2013.

[62] J. Brisebois and N. Aubut, 'Wind farm inertia emulation to fulfill hydroquébec's specific need', in *Power and Energy Society General Meeting, 2011 IEEE*, IEEE, 2011, pp. 1–7.

[63] N. Soni, S. Doolla and M. C. Chandorkar, 'Improvement of transient response in microgrids using virtual inertia', *IEEE transactions on power delivery*, vol. 28, no. 3, pp. 1830–1838, 2013.

[64] M. F. M. Arani and E. F. El-Saadany, 'Implementing virtual inertia in dfig-based wind power generation', *IEEE Transactions on Power Systems*, vol. 28, no. 2, pp. 1373–1384, 2013.

[65] J. Zhu, C. D. Booth, G. P. Adam, A. J. Roscoe and C. G. Bright, 'Inertia emulation control strategy for vsc-hvdc transmission systems', *IEEE Trans. Power Syst*, vol. 28, no. 2, pp. 1277–1287, 2013.

[66] W. Bao, Q. Wu, L. Ding, S. Huang, F. Teng and V. Terzija, 'Synthetic inertial control of wind farm with bess based on model predictive control', *IET Renewable Power Generation*, 2020.

[67] A. Gloe, C. Jauch, B. Craciun and J. Winkelmann, 'Continuous provision of synthetic inertia with wind turbines: Implications for the wind turbine and for the grid', *IET Renewable Power Generation*, vol. 13, no. 5, pp. 668–675, 2019.

[68] B. G. Rawn, M. Gibescu and W. L. Kling, 'A static analysis method to determine the availability of kinetic energy from wind turbines', in *IEEE PES General Meeting*, IEEE, 2010, pp. 1–8.

[69] M. Van Wesenbeeck, S. De Haan, P. Varela and K. Visscher, 'Grid tied converter with virtual kinetic storage', in *PowerTech, 2009 IEEE Bucharest*, IEEE, 2009, pp. 1–7.

[70] R. Hesse, D. Turschner and H.-P. Beck, 'Micro grid stabilization using the virtual synchronous machine (visma)', in *Proceedings of the International Conference on Renewable Energies and Power Quality (ICREPQ'09), Valencia, Spain*, 2009, pp. 15–17.

[71] D. Q. Mayne, J. B. Rawlings, C. V. Rao and P. O. Scokaert, 'Constrained model predictive control: Stability and optimality', *Automatica*, vol. 36, no. 6, pp. 789–814, 2000.

[72] J.-F. Mennemann, L. Marko, J. Schmidt, W. Kemmetmüller and A. Kugi, 'Nonlinear model predictive control of a variable-speed pumped-storage power plant', *IEEE Transactions on Control Systems Technology*, 2019.

[73] J. Schmidt, W. Kemmetmüller and A. Kugi, 'Modeling and static optimization of a variable speed pumped storage power plant', *Renewable Energy*, vol. 111, pp. 38–51, 2017.

[74] Y. Zheng, J. Zhou, W. Zhu, C. Zhang, C. Li and W. Fu, 'Design of a multimode intelligent model predictive control strategy for hydroelectric generating unit', *Neurocomputing*, vol. 207, pp. 287–299, 2016.

[75] N. Kishor and S. Singh, 'Nonlinear predictive control for a nnarx hydro plant model', *Neural computing and applications*, vol. 16, no. 2, pp. 101–108, 2007.

[76] H. Zhang, D. Chen, B. Xu and F. Wang, 'Nonlinear modeling and dynamic analysis of hydro-turbine governing system in the process of load rejection transient', *Energy Conversion and Management*, vol. 90, pp. 128–137, 2015.

[77] M. Beus and H. Pandžić, 'Application of model predictive control algorithm on a hydro turbine governor control', in *2018 Power Systems Computation Conference (PSCC)*, IEEE, 2018, pp. 1–7.

[78] A. Fuchs, M. Imhof, T. Demiray and M. Morari, 'Stabilization of large power systems using vsc–hvdc and model predictive control', *IEEE Transactions on Power Delivery*, vol. 29, no. 1, pp. 480–488, 2014.

[79] I. M. Sanz, P. Judge, C. Spallarossa, B. Chaudhuri, T. C. Green and G. Strbac, 'Effective damping support through vsc-hvdc links with short-term overload capability', in *2017 IEEE PES Innovative Smart Grid Technologies Conference Europe (ISGT-Europe)*, IEEE, 2017, pp. 1–6.

[80] S. P. Azad, R. Iravani and J. E. Tate, 'Damping inter-area oscillations based on a model predictive control (mpc) hvdc supplementary controller', *IEEE Transactions on Power Systems*, vol. 28, no. 3, pp. 3174–3183, 2013.

[81] A. Jain, E. Biyik and A. Chakrabortty, 'A model predictive control design for selective modal damping in power systems', in *American Control Conference (ACC), 2015*, IEEE, 2015, pp. 4314–4319.

[82] S. Koul and S. Tiwari, 'Model predictive control for improving small signal stability of a upfc equipped smib system', in *2011 Nirma University International Conference on Engineering*, IEEE, 2011, pp. 1–6.

[83] A. M. Ersdal, I. M. Cecilio, D. Fabozzi, L. Imsland and N. F. Thornhill, 'Applying model predictive control to power system frequency control', in *Innovative Smart Grid Technologies Europe (ISGT EUROPE), 2013 4th IEEE/PES*, IEEE, 2013, pp. 1–5.

[84] A. M. Ersdal, L. Imsland and K. Uhlen, 'Model predictive load-frequency control', *IEEE Transactions on Power Systems*, vol. 31, no. 1, pp. 777–785, 2016.

[85] A. M. Ersdal, L. Imsland, K. Uhlen, D. Fabozzi and N. F. Thornhill, 'Model predictive load–frequency control taking into account imbalance uncertainty', *Control Engineering Practice*, vol. 53, pp. 139–150, 2016.

[86] M. Elsisi, M. Soliman, M. Aboelela and W. Mansour, 'Improving the grid frequency by optimal design of model predictive control with energy storage devices', *Optimal Control Applications and Methods*, vol. 39, no. 1, pp. 263–280, 2018.

[87] M. Imhof, A. Fuchs, G. Andersson and M. Morari, 'Voltage stability control using vsc-hvdc links and model predictive control', in *XIII Symposium of Specialists in Electric Operational and Expension Planning, XIII SEPOPE, Foz do Iguassu, Brazil*, 2014.

[88] A. Faanes and S. Skogestad, 'State space realization of model predictive controllers without active constraints', *Modeling, identification and control*, vol. 24, no. 4, p. 231, 2003.

[89] K. R. Muske and J. B. Rawlings, 'Model predictive control with linear models', *AIChE Journal*, vol. 39, no. 2, pp. 262–287, 1993.

Papers

Paper I

Modelling of Variable Speed Hydropower for Grid Integration Studies

Modelling of Variable Speed Hydropower for Grid Integration Studies ⋆

T.I. Reigstad * **K. Uhlen** **

* *Norwegian University of Science and Technology (NTNU), NO-7491 Trondheim, Norway (email: tor.inge.reigstad@ntnu.no)*
** *Norwegian University of Science and Technology (NTNU), NO-7491 Trondheim, Norway (email: kjetil.uhlen@ntnu.no)*

Abstract: This paper proposes a hydraulic model based on the Euler turbine equations suitable for the purpose of grid integration studies of variable speed hydropower (VSHP). The work was motivated by the need to assess how the dynamic performance might change when a hydropower plant is operated at variable speed. The *Euler* model considers the water flow dependency on the turbine rotational speed and calculates the turbine power as a non-linear function of water flow, turbine rotational speed and guide vane opening. A waterway model is included, based on the 1-D momentum and continuity balance for a water-filled elementary pipe to simulate water hammer, mass oscillation and tunnel losses. These detailed and accurate models are necessary for recognising possible limitations in the hydraulic system, to model the turbine power and rotational speed correctly and thereby to be able to maximise power delivery for system control purposes. All *Euler* model parameters can be derived from the physical dimensions of the turbine and waterway, ensuring easy implementation. State-space representation of the *Euler* model is approximated by utilising a lumped-parameter equivalent of the penstock dynamics. Dynamic simulations and eigenvalue analysis show the strength of the *Euler* model compared to conventional hydropower models.

Keywords: Modelling and simulation of power systems, power systems stability, dynamic interaction of power plants, control system design, control of renewable energy resources, optimal operation and control of power systems

1. INTRODUCTION

Variable speed hydropower (VSHP) is a suitable source for delivering additional ancillary services to the grid by actively utilising the stored kinetic energy in the turbine and generator. By allowing the turbine rotational speed to deviate temporarily from its optimal speed, the VSHP can vary its output power quickly due to the converter technology, see Basic et al. (2018). In the first few seconds after a step response at the output power reference, the energy is delivered to or from the kinetic energy in the turbine and generator (Figure 1). Subsequently, the governor will react to the deviation in the turbine rotational speed and adjust the guide vane opening and thereby the mechanical power P_m to regain the optimal speed of the turbine. With that, the VSHP can contribute more effectively to primary frequency control and the maintaining of grid stability. The VSHP plants will be able to provide fast frequency reserves in both production and in pumping mode, and the efficiency and operating range will potentially be wider than for conventional hydropower and other variable renewable sources without storage, see Valavi and Nysveen (2018).

⋆ This work was supported by the Research council of Norway under Grant 257588 and by the Norwegian Research Centre for Hydropower Technology (HydroCen).

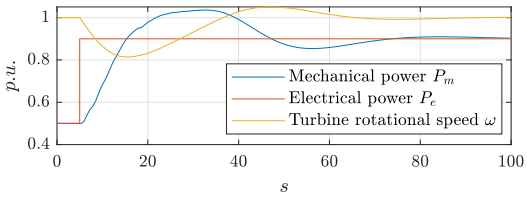

Fig. 1. Dynamic response when the VSHP output power is increased from 0.5 p.u. to 0.9 p.u. at $t = 5s$

The turbine and hydraulic system, including waterways, will experience new and different operating conditions when running at variable speed. When analysing the power system impacts and potential benefits of variable speed operation, we need to know which dynamic constraints and limitations concerning the technology need to be taken into account. Thus, in this context, there are several good reasons for revisiting the modelling and analysis of hydropower plants, which is the aim of this paper. A sufficiently detailed model of the system is needed to investigate the interactions between the VSHP plant and the grid: How can variable speed operation benefit the security and flexibility in power system operation? How can we explore the control possibilities from a system perspective while considering the limitations given by the water/turbine system? This requires the development of non-linear time-domain simulation models that include

tunnels, with physical constraints on water flows, turbine, governor, generator with the magnetising system, generator-side converter and grid-side converter, and a representative test grid. This paper will focus on the turbine side of the generator by comparing four different turbine models, two of them including a waterway model, to examine how accurate the models are when subjected to large variations in turbine rotational speed.

The hydraulic system is modelled in different ways, depending on application and performance requirements. For example, the conduits in the hydraulic system can be modelled as electrical equivalent circuits, as presented in Souza et al. (1999); Nicolet (2007) or as travelling waves, as suggested in Demello et al. (1992). These models can consider both penstock, surge tank and tunnel dynamics and losses. Hydroelectric turbine-governor simulation models for commercial simulation programs are reviewed in Koritarov et al. (2013). Except for the Hygovm model, most of the existing models only consider the water starting time when modelling the conducts.

The simplest turbine models assume that mechanical power equals the water flow in per unit, see Koritarov et al. (2013) and Kundur (1994). Hygov and similar models in Koritarov et al. (2013) do also consider variation in the head, the damping and the losses by subtracting the no-load water flow. These models are linearised at the operational point, as seen in Sarasúa et al. (2015) or a linearized model can be found from the turbine characteristic chart at the operational point, see Fang et al. (2008). Hill diagrams are used to include the turbine efficiency in Belhadji et al. (2011). Turbine characteristics are used in Pannatier et al. (2010) and Padoan et al. (2010) to find the torque and flow when rotational speed and guide vane opening are given. The Euler turbine equations of Nielsen (2015) also consider the rotational speed. A one-dimensional numerical model of a Francis turbine based on the Euler equations, which includes a waterway model is presented in Giosio et al. (2016). This model is tuned with test data and utilises look-up tables to find churning losses and is utilised in a VSHP model with a doubly-fed induction machine (DFIM) in Nag and Lee (2018).

Fang et al. (2008) present basic mathematical models for typical hydroelectric power plants and discuss how a turbine speed governor should be optimally tuned and how the physical dimensions of the waterway affect the dynamics. In Mohanpurkar et al. (2018), a transient stability analysis including VSHP with an elastic water column model, turbine model and DFIM is performed.

This paper is structured as follows: The models assessed for application to the analysis of variable speed hydropower models are described in Section 2. Section 3 presents the simulation result for four different hydraulic models and discusses the differences and strength of the models. The conclusions are summed up in Section 4.

2. VARIABLE SPEED HYDROPOWER MODELS

2.1 Waterway Model

To investigate how the hydraulic system and electrical system affect each other, the waterway model has to consider both water hammering and friction losses. Inelastic water column models are adequate for short penstocks; however, with longer penstocks, the effects of travelling waves and thereby the elasticity of the steel and the compressibility of the water must be considered. The derivation of the model starts with the 1-D momentum and continuity balance for a water-filled elementary pipe of length dx given as a partial differential equation in Wylie et al. (1993) which can be represented as (1), see Pico et al. (2012).

$$\begin{aligned} \frac{\delta H}{\delta x} + \frac{1}{g_r A} \cdot \frac{\delta Q}{\delta t} + \frac{f}{2 g_r D A^2} \cdot Q|Q| = 0 \\ \frac{\delta Q}{\delta x} + \frac{g_r A}{a^2} \cdot \frac{\delta H}{\delta t} = 0 \end{aligned} \tag{1}$$

The cross-section is A, Q is the discharge, H is the head, g_r is the gravity, D is the pipe diameter, f is the local loss coefficient, and a is the wave speed. Equation (1) can be per unitised to (3) by using the per unitised definitions of head and flow given in (2), see Pico et al. (2012).

$$h_{p.u.} = \frac{H}{H_R}, \quad q_{p.u.} = \frac{Q}{Q_R} \tag{2}$$

$$\begin{aligned} \frac{\delta q}{\delta x} + \frac{g_r A H_R}{Q_R a^2} \cdot \frac{\delta h}{\delta t} = 0 \\ \frac{\delta h}{\delta x} + \frac{Q_R}{H_R g_r A} \cdot \frac{\delta q}{\delta t} + \frac{f Q_R^2}{2 g_r H_R D A^2} \cdot q|q| = 0 \end{aligned} \tag{3}$$

By using Laplace transformation and neglecting the friction losses, (3) can be solved to find the transfer function of the flow rate q_U and the water pressure h_U of the upstream inlet as a function of the downstream outlet flow rate q_D and the water pressure h_D Nicolet (2007):

$$\begin{bmatrix} h_U(s) \\ q_U(s) \end{bmatrix} = \begin{bmatrix} \cosh(zT_e) & -Z_c \sinh(zT_e) \\ -\frac{1}{Z_c} \sinh(zT_e) & \cosh(zT_e) \end{bmatrix} \begin{bmatrix} h_D(s) \\ q_D(s) \end{bmatrix} \tag{4}$$

where the characteristic impedance is given as

$$Z_c = \frac{T_w}{T_e} \frac{z}{s}, \quad \text{where} \quad T_w = \frac{L}{g_r A} \frac{Q_R}{H_R}, \quad T_e = \frac{L}{a} \tag{5}$$

The water inertia time constant, also known as the water starting time, is given as T_w, T_e is the wave travel time and is the length of the waterway.

The classic wave solution given below considers both the elastic water hammer theory and the hydraulic losses as a hyperbolic tangent function. The derivation is shown in Brekke (1984).

$$\frac{h(s)}{q(s)} = -\frac{T_w}{T_e} \left(1 + \frac{f Q_R}{2 D A s}\right)^{1/2} \tanh\left(\left(s^2 + s \frac{f Q_R}{2 D A}\right)^{1/2} T_e\right) \tag{6}$$

If the hydraulic friction losses are neglected, (6) can be simplified to

$$\frac{h(s)}{q(s)} = -\frac{T_w}{T_e}\tanh\left(sT_e\right) = -Z_0\tanh\left(sT_e\right) \tag{7}$$

For small variations around the operating point, $\tanh\left(sT_e\right) \approx sT_e$ and (6) can be simplified to

$$\frac{h(s)}{q(s)} = -T_w s - H_f \tag{8}$$

where H_f is the hydraulic friction losses. Neglecting these, (8) becomes

$$\frac{h(s)}{q(s)} = -T_w s \tag{9}$$

For small-signal stability analysis, (7) can be approximated by a lumped-parameter equivalent for $\tanh\left(sT_e\right)$. With $n_{max} = 0$ and $T_e = 0.5s$ (inelastic water column), (10) is valid up to approximately 0.1 Hz, for $n_{max} = 1$ it is valid up to about 1.0 Hz. Kundur (1994)

$$\begin{aligned}\tanh\left(sT_e\right) &= \frac{1 - e^{-2T_e s}}{1 + e^{-2T_e s}} \\ &\approx \frac{sT_e \prod_{n=1}^{n_{max}} \left(1 + \left(\frac{sT_e}{n\pi}\right)^2\right)}{\prod_{n=1}^{n=\infty} \left(1 + \left(\frac{2sT_e}{(2n-1)\,\pi}\right)^2\right)}\end{aligned} \tag{10}$$

The transfer function for surge tanks and air accumulators is given in Xinxin (1988) and rewritten as

$$\frac{h(s)}{q(s)} = \frac{Q_R}{sH_R A_{eqv}} = \frac{1}{sT_s} \tag{11}$$

where the surge tank filling time T_s is defined as

$$T_s = \frac{A_{eqv} H_R}{Q_R} \tag{12}$$

The head loss h_f is the pressure drop over a length l of the penstock and can be expressed as Mansoor (2000)

$$h_f = f_r \frac{l}{d} \frac{v^2}{2g_a} \tag{13}$$

where f_r is the friction factor and d is the penstock diameter.

Figure 2 shows the non-linear model of the turbine including the surge tank and the travelling wave effects in the penstock, as presented in Demello et al. (1992). The model is based on (7), (8) and (11) and includes the losses in the penstock, the tunnel and the surge tank. It should be noted that the $e^{-2T_e s}$ term in (10) is a time delay in the time domain, ensuring a simple representation of the penstock dynamics.

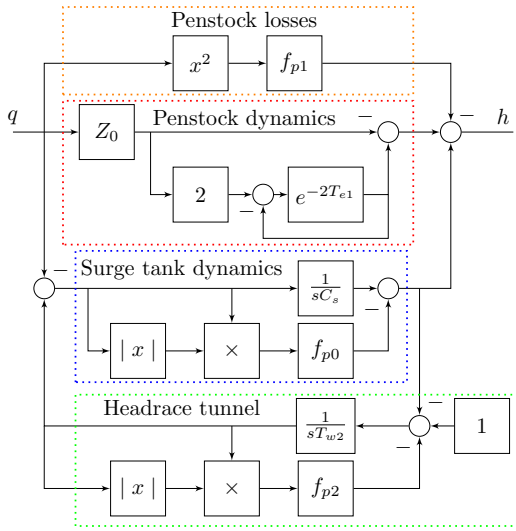

Fig. 2. Waterway dynamic model.

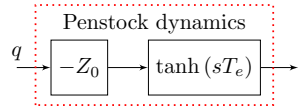

Fig. 3. Penstock model for small signal analysis.

For small signal stability analysis, the penstock dynamic is modelled as shown in Figure 3, using a 4th order approximation of tanh as given in (10).

2.2 Hydraulic Machine Simulation Models

Hydraulic turbine models have earlier been compared in, for instance, Koritarov et al. (2013). However, those models are relatively simple and do not consider variations in the turbine rotational speed. This paper presents a hydraulic turbine model based on the Euler turbine equations for grid integration studies of VSHP, and shows how three common hydraulic machine models are simplifications of the Euler equations.

The main part of the Euler turbine equations model is the Euler turbine equations (14) to (16) describing how the hydraulic power is transformed into mechanical rotational power. The model considers both guide vane opening, pressure, water flow and rotational speed and is used together with the waterway model (Figure 2) to also consider water hammer, mass oscillation and losses in the waterway, as shown in Figure 4. However, it does not consider the effect of acceleration on the flow through the runner and the angular acceleration of the water masses in the runner Nielsen (2015). The dimensionless turbine equations are derived in Nielsen (2015) where the dimensionless flow, head and angular speed of rotation are $q_t = Q/Q_{Rt}$, $h_t = H/H_{Rt}$ and $\omega = \Omega/\omega_R$. Since the turbine parameters can be derived from its physical dimensions, no detailed and restricted turbine data are needed. The momentum and torque equations are given as

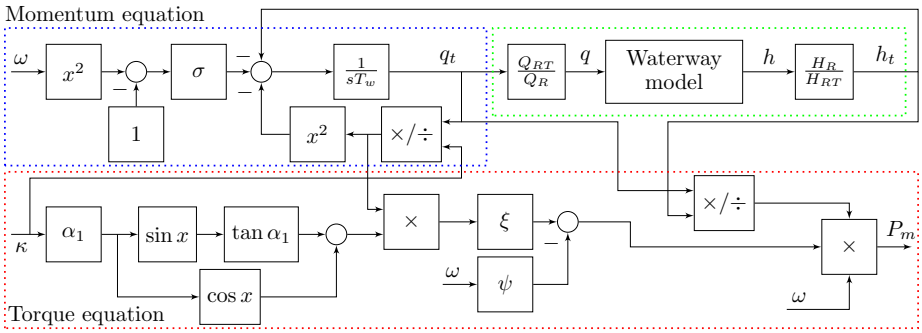

Fig. 4. Turbine model based on the Euler Equations.

$$\begin{aligned} T_w \frac{dq_t}{dt} &= h_t - \left(\frac{q_t}{\kappa}\right)^2 - \sigma\left(\omega^2 - 1\right) \\ T_a \frac{d\omega}{dt} &= \frac{1}{h_t} q_t \left(m_s - \psi\omega\right) - P_g \end{aligned} \tag{14}$$

$$\begin{aligned} m_s &= \xi \frac{q_t}{\kappa} \left(\cos\alpha_1 + \tan\alpha_{1R} \sin\alpha_1\right) \\ \kappa &= \frac{Q_R}{Q_{Rt}} g, \quad \alpha_1 = \sin^{-1}\left(\kappa \sin\alpha_{1R}\right) \end{aligned} \tag{15}$$

where P_g is the generator power, κ the opening degree of the turbine and the turbine parameters σ, ψ, ξ and α_{1R} is found in Appendix A. The turbine head h_t and the hydraulic efficiency η_h are given as

$$h_t = \left(\frac{q_t}{\kappa}\right)^2 - \sigma\left(\omega^2 - 1\right), \quad \eta_h = \frac{1}{h}\left(m_s - \psi\omega\right)\omega \tag{16}$$

The state-space representation of the *Euler* model is derived by utilising a lumped-parameter equivalent (10) of the penstock dynamics (Figure 3).

The *IEEE* model Demello et al. (1992) shown in Figure 5 utilises the same waterway model as the Euler turbine equations model but has a simpler turbine model. The mechanical power P_m and the water flow q are given by

$$\begin{aligned} P_m &= A_t h \left(q - q_{nl}\right) - D_t g \Delta\omega \\ q &= g\sqrt{h} \end{aligned} \tag{17}$$

In an ideal turbine, the mechanical power is proportional to the flow q times the head h. In this case, the no-load flow q_{nl} and the factor A_t are added to include a simple loss model. The equation includes the speed damping effect, depending on the guide vane opening g. The relationship between the flow q and the guide vane opening g is derived from (14) and (15) by assuming stationary conditions, $\omega = 1$, $Q_{Rt} = Q_R$ and thereby $q_t = q$.

The *Hygov* model presented in (18) and Figure 6 assumes an inelastic water column, does not consider water hammer, mass oscillation or deviation in the rotational speed, and has a simplified relationship between the guide vane opening and the torque. Kundur (1994). The flow q is found by integration of the turbine head. This equation

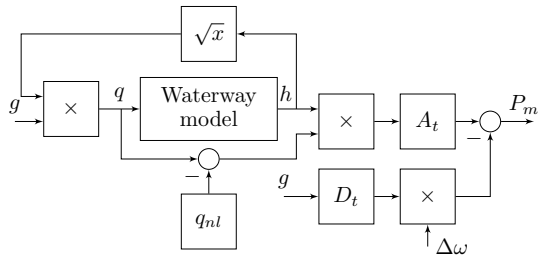

Fig. 5. *IEEE* model

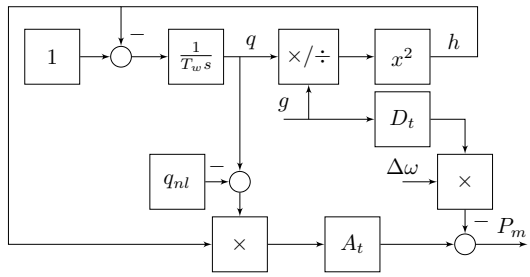

Fig. 6. *Hygov* model

can be derived from (14) by assuming $\omega = 1$, setting $h_t = 1$ and utilising that $q = g\sqrt{h}$ by assuming no turbine losses.

$$\begin{aligned} P_m &= A_t h \left(q - q_{nl}\right) - D_t g \Delta\omega \\ \frac{dq}{dt} &= \frac{1}{T_w}\left(1 - h\right), \quad h = \left(q/g\right)^2 \end{aligned} \tag{18}$$

The linearised hydraulic turbine model presented in (19) and Figure 7 only considers the water starting time T_w Kundur (1994). The model is a linearisation of the *Hygov* model around the nominal operating point but without the speed damping term.

$$\frac{P_m(s)}{g(s)} = \frac{1 - T_w s}{1 + \frac{1}{2} T_w s} \tag{19}$$

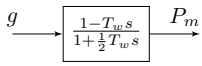

Fig. 7. *Linearised* hydraulic turbine model

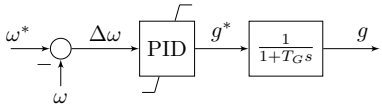

Fig. 8. Governor with PID control and without droop

2.3 Control Objectives and Design

The suggested main control objectives for the VSHP are:

- Control objectives for internal power plant control:
  - Optimise the rotational speed of the turbine with respect to the efficiency at part load
  - Minimise water hammering and mass oscillations
  - Minimise guide vane servo operation
  - Minimise hydraulic and electric losses
- Control objectives for the provision of power system support (ancillary services):
  - Contribute to primary frequency regulation
  - Increase the system inertia by virtual inertia control
  - Increase the voltage control speed

The achievement of the internal control objectives will to a great extent decide the constraints in reaching the power system support objectives. This paper will, therefore, primarily concentrate on modelling of the VSHP for achieving the internal control objectives.

2.4 Governor PID Controller without Permanent Droop

A governor with a PID controller and without permanent droop is presented in Figure 8 and (20). Droop control is not required since the grid converter performs power control. The PID controller output is saturated and rate limited.

$$\frac{g}{\Delta\omega} = \frac{g}{\omega^* - \omega} = \frac{k_{g,d}s^2 + k_{g,p}s + k_{g,i}}{s} \frac{1}{1+T_G s} \qquad (20)$$

3. COMPARISON OF TURBINE MODELS

The demand for modelling of the turbine is different for a VSHP compared to a conventional hydropower plant because of the large variance and dynamics in turbine rotational speed. Dynamic and eigenvalue analyses are performed on four different turbine models with different levels of detail to find a suitable turbine model for grid integration studies of VSHP. Figures 9 and 10 show the step response of the VSHP after a step in, respectively, reference power P^* and reference turbine rotational speed ω^* for the four different turbine models. The corresponding eigenvalue plots for different values of P^* and ω^* in the particular operational points are shown in Figures 11 and 12. Together with the participation matrices in Figures 13 and 14, they are the basis for explaining how the models handle a varying turbine rotational speed.

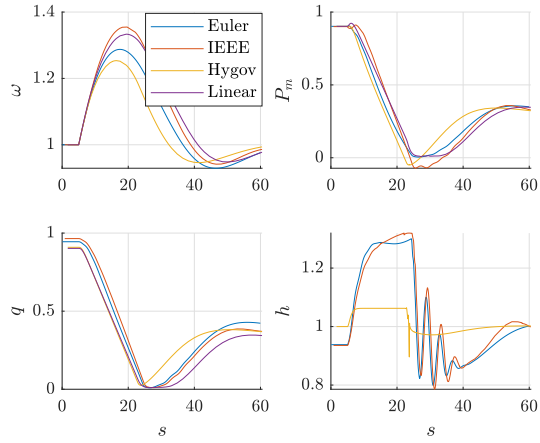

Fig. 9. Comparison of turbine dynamics - step on P^* from 0.9 to 0.3 p.u. at $t = 5s$.

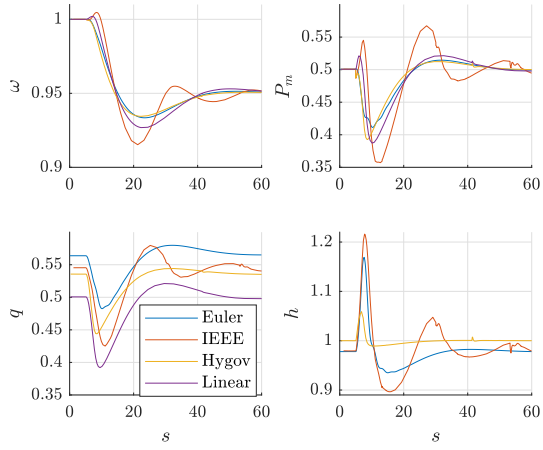

Fig. 10. Comparison of turbine dynamics - step on ω^* from 1.00 to 0.95 p.u. at $t = 5s$.

A selection of the most important modes related to the turbine models is provided in the participation factor matrices and the colour represents the absolute value of the relative participation of the state variables in the modes.

The *Euler* and *IEEE* models have a mode pair and a single-pole related to the governor control loop; $\lambda_{eul,7-8}$ and $\lambda_{eul,10}$ for the *Euler* model and $\lambda_{iee,5-6}$ and $\lambda_{iee,10}$ for the *IEEE* model. The frequency of the governor mode pair is approximately 0.02 Hz and is recognised in Figures 9 and 10 as the oscillations with the largest amplitude and as the only mode pair in Figures 11 and 12. For the *Euler* and *IEEE* models, the eigenvalue plots in Figure 11 show that the relative damping of these modes decreases with increasing power output P^*. This can be explained by the hydraulic efficiency, as shown in Figure 15; the relative losses are higher for cases with low power, and thereby the damping is better for these cases. Figure 12 shows that the damping of the *IEEE* modes related to governor control is less at low rotational speed ω. This

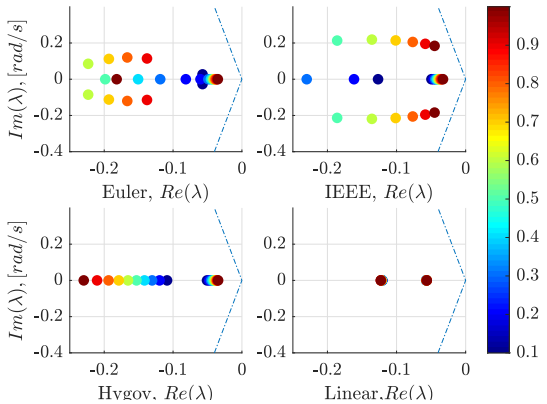

Fig. 11. Comparison of eigenvalues at different power references P^* and $\omega^* = 1.0$, where P^* is represented by the colour scheme.

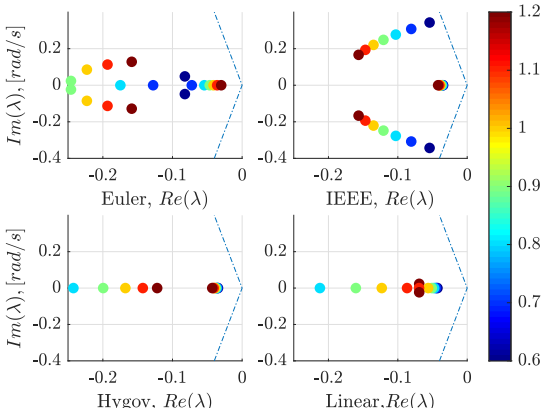

Fig. 12. Comparison of eigenvalues at different turbine rotational speed references ω^* and $P^* = 0.6$, where ω^* is represented by the colour scheme.

connection is more complex for the *Euler* modes related to governor control; the damping is less for high and low turbine rotational speed and higher for nominal rotational speed. The governor parameters must, therefore, be tuned for the worst-case operating points; the combinations of the minimum and maximum power and rotational speed.

The *Linearised* and *Hygov* models do not have any mode pair related to the governor control loop for most operating points. Generally, the lowest damping for these models is found for low power and high rotational speed.

The *Euler* and *IEEE* models include dynamics of the penstock, the headrace tunnel and the surge tank. The modes $\lambda_{eul,5-6}$ and $\lambda_{iee,7-8}$ primarily relate to the surge tank head h_{st}, the headrace tunnel flow q_{hr} and the penstock flow q (tanh-approximation for the *IEEE* model), as seen from Figures 13 and 14. These modes correspond to oscillations between the turbine and the surge tank and can be recognised as oscillations at approximately 0.4 Hz in the turbine head h in Figure 9.

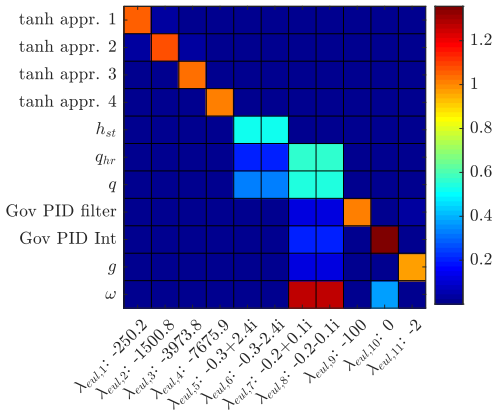

Fig. 13. Participation factor matrix for the *Euler* model with system inputs $\omega^* = 1.0$ and $P^* = 0.6$. The colour represents the absolute value of the relative participation of the state variables in the modes.

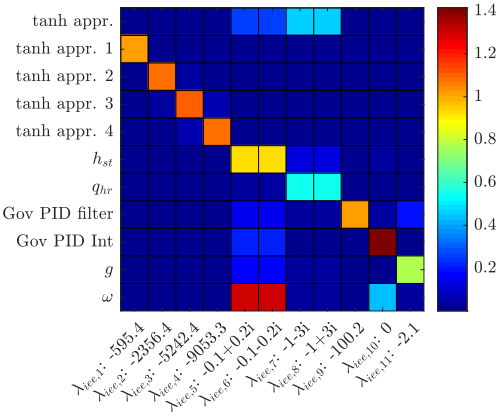

Fig. 14. Participation factor matrix for the *IEEE* model with system inputs $\omega^* = 1.0$ and $P^* = 0.6$. The colour represents the absolute value of the relative participation of the state variables in the modes.

The *Euler* and *IEEE* models allow elastic waterway and water hammering. The modes $\lambda_{eul,1-4}$ and $\lambda_{iee,1-4}$ are related to this phenomena, all of them related to the states in the lumped-parameter equivalent for $\tanh sT_e$ (10), as observed from Figures 13 and 14. The water hammering is well damped when the guide vane closing time is longer than twice the elastic water time constant for the penstock. This is the case in Figures 9 and 10 where no water hammering is observed. If the guide vane opening time is faster than the reflection time of the pressure wave in the penstock, water hammering may occur.

The total hydraulic efficiency is presented as functions of, respectively, the turbine rotational speed ω and the turbine power P_m in Figure 15. The efficiency of the *IEEE* model will, in contrast to the *Hygov* model, decrease for high turbine power since the waterway losses are included. As the rotational speed increases, the damping term of these two models will result in a decreasing efficiency.

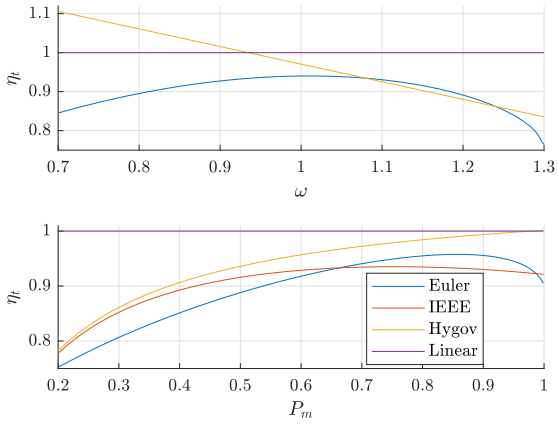

Fig. 15. Hydraulic efficiency as function of turbine rotational speed ω and turbine power P_m. The efficiencies of the *IEEE* and *Hygov* models as function of ω are equal.

The efficiency curve of the *Euler* model is closer to the reality since it has a maximum efficiency point near the nominal rotational speed, mainly due to the σ-parameter. However, the parameters of the *Euler* model must be tuned to represent the hill diagram of the turbine in the best way.

The most detailed model is the *Euler* model, considering many aspects of the turbine:

- The flow q is dependent on the rotational speed ω
- The torque and the efficiency are dependent on the rotational speed ω and they are nonlinear functions of the flow g.

Another advantage of the *Euler* model is that its parameters can be found directly from the turbine dimensions.

The torque calculated by the *Euler* equations will increase with decreasing rotational speed ω. However, as $P_m = T_m\omega$, the output power will reduce. This may cause problems in cases where the output power to the grid is high and the rotational speed is decreasing below a critical value. In this situation, the turbine will not be able to deliver enough power to regain the nominal rotational speed and the turbine will stop if the output power to the grid is not reduced quickly.

4. CONCLUSION

The analysis and design of hydropower conversion and control systems require accurate modelling of the turbine mechanical power and rotational speed. Precise models are needed when developing a control design aiming to maximise the utilisation of the rotational energy in the generator and the turbine for the provision of fast frequency reserves during power system disturbances. In this paper, four hydraulic turbine models are investigated to show that a detailed model is needed for grid integration studies of VSHP. A hydraulic model based on the Euler turbine equations including a one-dimensional waterway model is proposed for the purpose.

When linearised, all four models have a similar complex mode pair and a real pole related to the governor control loop. The relative damping of the complex mode pair reduces with higher power levels and lower rotational speeds. The *Euler* and the *IEEE* models add dynamics related to the penstock, the headrace tunnel and the surge tank, and mass oscillations are recognised in the head and mechanical power.

The *Linearised* model is independent of both the power level and the turbine rotational speed. The *Hygov* model has a very simplified model of the waterway and the head, and thereby the mechanical power during transients becomes inaccurate. A more detailed one-dimensional waterway model is included in the *IEEE* model; however, the simple turbine model does not consider that the turbine efficiency depends on the rotational speed and is a nonlinear function of the flow. For the *Euler* model, the Euler turbine equations are used directly to describe how the hydraulic power is transformed into mechanical power. This includes the dependency between the water flow and the rotational speed, and the representation of losses is more detailed. This is also the only model that considers that the turbine power will be reduced as the rotational speed reduces. The investigation of the turbine models shows that the variable speed operation of the hydropower plant causes the need for a detailed hydraulic model. Therefore, our conclusion is that the accuracy of the *Euler* model is needed for simulating the transients and variation in rotational speed that will take place in a VSHP. Further analysis will answer how this model interacts with the rest of the power system.

REFERENCES

Basic, M., de Oliveira e Silva, P.C., and Dujic, D. (2018). High power electronics innovation perspectives for pumped storage power plants. Technical report.

Belhadji, L., Bacha, S., and Roye, D. (2011). Modeling and control of variable-speed micro-hydropower plant based on axial-flow turbine and permanent magnet synchronous generator (mhpp-pmsg). In *IECON 2011-37th Annual Conference on IEEE Industrial Electronics Society*, 896–901. IEEE.

Brekke, H. (1984). *A stability study on hydro power plant governing including the influence from a quasi nonlinear damping of oscillatory flow and from the turbine characteristics*, volume 1. Kværner Brug.

Demello, F., Koessler, R., Agee, J., Anderson, P., Doudna, J., Fish, J., Hamm, P., Kundur, P., Lee, D., Rogers, G., et al. (1992). Hydraulic-turbine and turbine control-models for system dynamic studies. *IEEE Transactions on Power Systems*, 7(1), 167–179.

Fang, H., Chen, L., Dlakavu, N., and Shen, Z. (2008). Basic modeling and simulation tool for analysis of hydraulic transients in hydroelectric power plants. *IEEE Transactions on energy conversion*, 23(3), 834–841.

Giosio, D.R., Henderson, A.D., Walker, J.M., and Brandner, P.A. (2016). Physics-based hydraulic turbine model for system dynamic studies. *IEEE Transactions on Power Systems*, 32(2), 1161–1168.

Koritarov, V., Guzowski, L., Feltes, J., Kazachkov, Y., Baldwin, L., Grande-Moran, C., Thomann, G., Eng, L., Trouille, B., and Donalek, P. (2013). Review of existing hydroelectric turbine-governor simulation models.

Decision and Information services, Argonne National Laboratory.

Kundur, P. (1994). *Power system stability and control*. McGraw-hill New York.

Mansoor, S. (2000). *Behaviour and operation of pumped storage hydro plants*. Ph.D. thesis, University of Wales, Bangor.

Mohanpurkar, M., Ouroua, A., Hovsapian, R., Luo, Y., Singh, M., Muljadi, E., Gevorgian, V., and Donalek, P. (2018). Real-time co-simulation of adjustable-speed pumped storage hydro for transient stability analysis. *Electric Power Systems Research*, 154, 276–286.

Nag, S. and Lee, K.Y. (2018). Dfim-based variable speed operation of pump-turbines for efficiency improvement. *IFAC-PapersOnLine*, 51(28), 708–713.

Nicolet, C. (2007). Hydroacoustic modelling and numerical simulation of unsteady operation of hydroelectric systems.

Nielsen, T.K. (2015). Simulation model for francis and reversible pump turbines. *International Journal of Fluid Machinery and Systems*, 8(3), 169–182.

Padoan, A.C., Kawkabani, B., Schwery, A., Ramirez, C., Nicolet, C., Simond, J.J., and Avellan, F. (2010). Dynamical behavior comparison between variable speed and synchronous machines with pss. *IEEE Transactions on Power Systems*, 25(3), 1555–1565.

Pannatier, Y., Kawkabani, B., Nicolet, C., Simond, J.J., Schwery, A., and Allenbach, P. (2010). Investigation of control strategies for variable-speed pump-turbine units by using a simplified model of the converters. *IEEE Transactions on Industrial Electronics*, 57(9), 3039–3049.

Pico, H.V., McCalley, J.D., Angel, A., Leon, R., and Castrillon, N.J. (2012). Analysis of very low frequency oscillations in hydro-dominant power systems using multi-unit modeling. *IEEE Transactions on Power Systems*, 27(4), 1906–1915.

Sarasúa, J.I., Pérez-Díaz, J.I., Wilhelmi, J.R., and Sánchez-Fernández, J.Á. (2015). Dynamic response and governor tuning of a long penstock pumped-storage hydropower plant equipped with a pump-turbine and a doubly fed induction generator. *Energy conversion and management*, 106, 151–164.

Souza, O., Barbieri, N., and Santos, A. (1999). Study of hydraulic transients in hydropower plants through simulation of nonlinear model of penstock and hydraulic turbine model. *IEEE Transactions on Power Systems*, 14(4), 1269–1272.

Valavi, M. and Nysveen, A. (2018). Variable-speed operation of hydropower plants: A look at the past, present, and future. *IEEE Industry Applications Magazine*, 24(5), 18–27.

Wylie, E.B., Streeter, V.L., and Suo, L. (1993). *Fluid transients in systems*, volume 1. Prentice Hall Englewood Cliffs, NJ.

Xinxin, L. (1988). Hydropower system modelling by the structure matrix method.

Appendix A. PARAMETERS, SET-POINTS AND VARIABLES

Table A.1. Parameters and set-points

Parameter	Symbol	Value
Waterway		
Rated water flow	Q_R $[m^3/s]$	170
Rated height	H_R $[m]$	425
Penstock:		
Water starting time	T_w $[s]$	1.211
Water traveling time	T_e $[s]$	0.126
Characteristic impedance	Z_0 $[pu]$	9.61
Friction factor	f_{p1} $[pu]$	0.049
Surge tank:		
Friction factor	f_{p0} $[pu]$	0.036
Storage constant	C_s $[pu]$	0.099
Head race tunnel:		
Water starting time	T_{w2} $[s]$	4.34
Friction factor	f_{p2} $[pu]$	0.020
Hydraulic Machine		
Turbine gain	A_t $[pu]$	1.075
No-load water flow	q_{nl} $[pu]$	0.07
Turbine mechanical damping	D_t $[pu]$	0.5
Turbine constant	ψ $[pu]$	0.376
Turbine constant	ξ $[pu]$	0.906
Turbine constant	α_{1R} $[pu]$	0.738
Turbine constant	σ $[pu]$	0.369
Rated speed	Ω $[rpm]$	750
Rated water flow	Q_{Rt} $[m^3/s]$	153
Rated height	H_{Rt} $[m]$	425
Governor		
Rotational speed reference	ω^* $[pu]$	1.00
Governor proportional gain	$k_{g,p}$ $[pu]$	1.80
Governor integration gain	$k_{g,i}$ $[pu]$	0.172
Governor derivation gain	$k_{g,d}$ $[pu]$	0.696
Rate limit	$[pu/s]$	+/-0.05
Servo time constant	T_G $[s]$	0.500

Table A.2. Variables

Variable	Symbol
Waterway	
Surge tank head	h_{st}
Head race tunnel flow	q_{hr}
Hydraulic Machine	
Turbine head	h
Turbine water flow	q
Mechanical torque	T_m
Mechanical power	P_m
Turbine efficiency	η_h
Turbine head	h_t
Turbine flow	q_t
Opening degree of turbine	κ
Governor	
Guide vane opening reference	g^*
Guide vane opening	g

Paper II

Variable Speed Hydropower Conversion and Control

Variable Speed Hydropower Conversion and Control

Tor Inge Reigstad, Kjetil Uhlen, *Member, IEEE*

***Abstract*—The objective of this paper is to develop and analyse a variable speed hydropower (VSHP) model that can aid the design of controllers that maximize the utilization of power plant for the provision of ancillary services, considering the limitations given by the hydraulic system. The model is tested and analysed with more or less conventional controllers to identify critical modes, adverse interactions or other limitations that must be taken into account in the future design of potentially multivariable or more advanced controllers for VSHP. Dynamic tests are performed by simulating step responses in power demand and by comparing responses of the model with the VSHP and with a conventional hydropower plant. A participation factor-based interaction analysis shows that there are no strong dynamic couplings between the hydraulic system of the VSHP and the rest of the grid. This simplifies the tuning of the control system. However, the analysis concludes that some oscillatory modes associated with the hydraulic system become significantly more excited when operating at variable speed; which is due to the larger deviation in turbine rotational speed. Extra awareness when designing the control system is therefore needed to keep the hydraulic system variables within their limits.**

***Index Terms*—AC-AC power conversion, eigenvalues and eigenfunctions, frequency control, hydraulic systems, hydraulic turbines, hydroelectric power generation, power generation control, power system modeling, power system simulation, stability.**

I. Introduction

MORE flexible resources are required to control the balance of the grid and to maintain the power system security as the share of electricity generation from variable renewables increases. Variable speed hydropower (VSHP) plants represent one solution that has the potential to contribute effectively to the required flexibility. The hypothesis is that VSHP plants can offer additional ancillary services by contributing more effectively to frequency control and this maintaining of grid stability, thus allowing for higher penetration of variable renewables in the grid. The advantage compared to conventional pumped-storage hydropower with constant rotational speed is more effective utilization of the kinetic energy in the turbine and generator and improved power control in pumping mode. The efficiency and operating range of VSHP will also be higher and they can contribute to frequency control both in the generation and in the pumping mode. [1] The converter technology offers faster control of reactive power and potentially higher reactive power capability, which benefits the voltage regulation. Compared with conventional hydropower plants, the VSHP enables a further degree of freedom to control power and speed. This opens new possibilities, but also necessitates proper co-ordination of the controls - and there will be new constraints that must be taken into account.

A detailed model of the VSHP system is needed to investigate the interactions between the VSHP plant and the grid, how variable speed operation can benefit the security and flexibility of the power system operation and to explore the control possibilities from a system perspective while considering the limitations given by the water/turbine system. This comprises the development of non-linear time-domain simulation models with limitations for water flows in the tunnel, turbine, governor, generator with a magnetizing system, generator-side converter and grid-side converter, and a representative test grid. This paper will focus on the converter models and the interaction between the hydraulic system in the VSHP and the grid.

A number of different dynamic models of VSHP including converter models have been presented in the last decade, most of which make use of doubly-fed induction generators (DFIG). There are large differences in the levels of detail in the models, especially in regard to hydraulic modelling. Reference [2] presents the modelling, simulation, and analysis of a VSHP with an electric equivalent hydraulic system, DFIG configuration and converter control system. In [3], a dynamic VSHP model including an elastic water column model, turbine model and DFIG is derived. An autonomous variable speed micro hydropower station with a simple Kaplan-model, DFIG configuration and converters is presented in [4]. Experimental results on a small VSHP with DFIG-configuration are shown in [5]. Dynamic modelling of adjustable-speed pumped storage hydropower plant with DFIG is performed in [6]. Reference [7] reviews technical considerations related to VSHP for the provision of frequency containment reserves (FCRs), and modelling and control for power system studies are discussed. Power regulation of VSHP for mitigating wind power variation is investigated in [8]. Reference [9] explores the improvement of power step performance for a VSHP compared to a conventional pumped storage power plant by using a numerical simulation model in SIMSEN. It is found that the maximum power step to the grid is strongly dependent on the hydro-mechanical characteristics of the power plant. In [10], four different hydraulic turbine models are compared to select a model that is best suited for use in grid integration studies of VSHP plants.

VSHP with a synchronous generator and full-power converters are found more rarely in the literature. A small VSHP with diode rectifier, DC-DC boost converter, optimal rotational speed control and converter control is presented in [11]. Reference [12] presents the dynamic modelling, simulation and control design of a small VSHP with diode rectifier, DC-DC boost converter, voltage source inverter and control

This work was supported by the Research Council of Norway under Grant 257588 and by the Norwegian Research Centre for Hydropower Technology (HydroCen).

T.I. Reigstad and K. Uhlen are with Department for Electric Power Engineering, Norwegian University of Science and Technology (NTNU), NO-7491 Trondheim, Norway (email: tor.inge.reigstad@ntnu.no, kjetil.uhlen@ntnu.no)

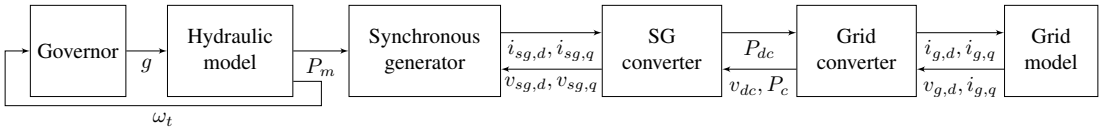

Fig. 1: Overview of VSHP model

system.

The main purpose of this paper is to present a complete model of a VSHP plant that can serve as a reference and basis for further development and choice of control systems. The paper is organized as follows: The variable speed hydropower models and the power system model are presented in Section II and III respectively. The dynamic analysis results and discussion are given in Section IV. Section V presents the theory, results and discussion from the participation factor analysis. Finally, in Section VI, the conclusions are given .

II. Variable Speed Hydropower Models

A. Control Objectives

A set of control objectives for a VSHP can be formulated as follows:

- Objectives for internal control of the plant:
  - Optimize the rotational speed of the turbine with respect to efficiency at part load.
  - Minimize water hammering and mass oscillations.
  - Minimize the guide vane servo operation.
  - Minimize the hydraulic and electric losses.
- Objectives for grid support control:
  - Contribute to the frequency containment reserves by faster and more precise frequency droop control.
  - Contribute to increasing the effective system inertia by virtual inertia (VI) control.
  - Improve the voltage control response time.

This paper will primarily concentrate on the internal control objectives. An overview of the VSHP with the variables connecting the subsystem is presented in Figure 1.

B. Hydraulic System Models

The hydraulic system is modelled with the Euler turbine equations model presented in [10]. The Euler turbine equations are used to describe how the hydraulic power is transformed into mechanical rotational power. The model presented in Figure 2 considers guide vane opening, pressure, water flow and rational speed. It is used together with a non-linear waterway model [13] to also consider travelling wave effects in the penstock (water hammer), headrace tunnel dynamics (mass oscillation), surge tank dynamics and head loss in the waterway. However, the model does not consider the effect of acceleration of the flow through the runner and the angular acceleration of the water masses in the runner [14]. The dimensionless turbine equations are derived in [14] where the dimensionless flow, head and angular speed of rotation are $q = Q/Q_R$, $h = H/H_R$ and $\tilde{\omega} = \omega/\omega_R$. Figure 3 shows the layout of the VSHP waterway and turbine.

C. Governor PID Controller without Permanent Droop

A governor with a PID controller and without permanent droop is chosen (1) for the VSHP. Droop control is not required since the shaft speed is decoupled from the grid and primary power-frequency control is performed by the grid converter. The PID controller output is saturated and rate limited.

$$\frac{g}{\Delta\omega} = \frac{g}{\omega^* - \omega} = \frac{k_{g,d}s^2 + k_{g,p}s + k_{g,i}}{s}\frac{1}{1 + T_G s} \tag{1}$$

III. Power System Model

A. Grid Model

The chosen basis for the grid model is the Two-Area Kundur grid model (Figure 4) as presented in Example 12.6b (iv) in [15], with the following changes:

- A *Hygov* governor is added to all generators in order to be able to compare the VSHP to conventional power plants.
- A 640 MW VSHP, as described below, is added at Bus5.

B. Grid Converter

The inner controller (4) of the grid converter, Figure 5, controls the d- and q-axis currents, while the outer controls the active power to the grid in the d-axis (2) and the reactive power to the grid in the q-axis (3). Alternatively, VI control can be implemented instead of standard active power control. The converter model, filter model and power calculation are given in (5) - (7) while the dc-link model is given in (8) and Figure 6. The parameters of the PI inner and outer controller are obtained by the Modulus Optimum (MO) and Symmetrical Optimum (SO) criterion, respectively, according to the approach explained in [16], [17], assuming a switching frequency of 1 kHz. The MO criterion is a simple and fast response tuning method for low order control plants without time delay and is used for tuning the inner loop. The method cancels the largest time constant, the filter constant, and ensures that the closed-loop gain is larger than one for as high frequencies as possible. The SO criterion is used to achieve maximum phase margin at the crossover frequency of the simplified outer loop, open-loop transfer function. A design parameter a is tuned to ensure that the bandwidth of the outer controller is approximately one decade below the bandwidth of the inner controller. The utilization of these methods ensures equivalent tuning of converters with different parameters and avoids the use of " trial and error" methods.

1) Outer Controller - Active Power Control:

$$\begin{aligned} \frac{d}{dt}N_{c,d} &= k_{Pi}\left(P_g^* - P_g\right) \\ i_{g,d}^* &= k_{Pp}\left(P_g^* - P_g\right) + N_{c,d} \end{aligned} \tag{2}$$

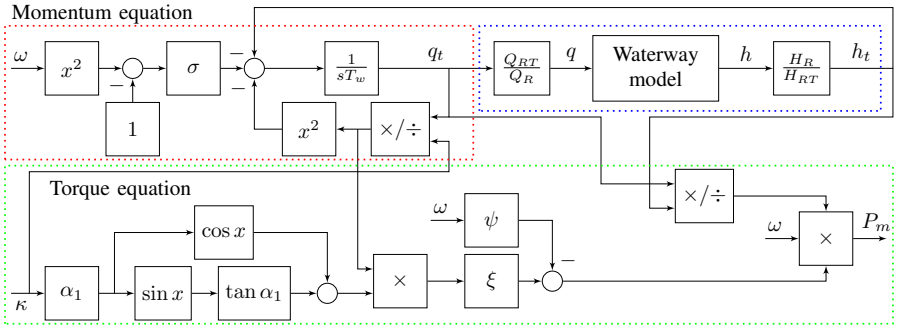

Fig. 2: Turbine model based on the Euler Equations

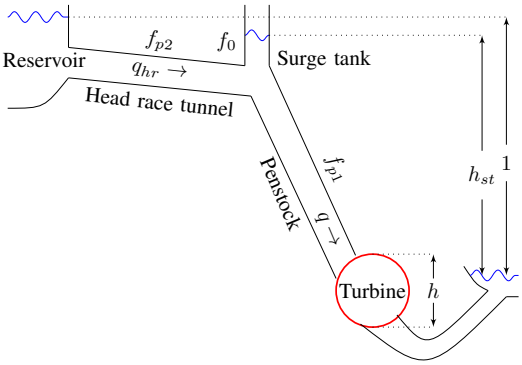

Fig. 3: Waterway layout

2) Outer Controller - Reactive Power Control:

$$\begin{aligned}\frac{d}{dt}N_{c,q} &= k_{Qi}\left(Q_g^* - Q_g\right)\\ i_{g,q}^* &= k_{Qp}\left(Q_g^* - Q_g\right) + N_{c,q}\end{aligned} \tag{3}$$

3) Inner Controller:

$$\begin{aligned}\frac{d}{dt}M_{c,d} &= k_{ii,c}\left(i_{g,d}^* - i_{g,d}\right)\\ v_{c,d}^* &= v_{g,d} - \omega_g l_f i_{g,q} + k_{ip,c}\left(i_{g,d}^* - i_{g,d}\right) + M_{c,d}\\ \frac{d}{dt}M_{c,q} &= k_{ii,c}\left(i_{g,q}^* - i_{g,q}\right)\\ v_{c,q}^* &= v_{g,q} + \omega_g l_f i_{g,d} + k_{ip,c}\left(i_{g,q}^* - i_{g,q}\right) + M_{c,q}\end{aligned} \tag{4}$$

4) Converter Model:

$$\begin{aligned}\frac{d}{dt}v_{c,d} &= \frac{1}{T_{r,c}}\left(v_{c,d}^* - v_{c,d}\right)\\ \frac{d}{dt}v_{c,q} &= \frac{1}{T_{r,c}}\left(v_{c,q}^* - v_{c,q}\right)\end{aligned} \tag{5}$$

5) Filter:

$$\begin{aligned}\frac{d}{dt}i_{g,d} &= \frac{\omega_0}{l_f}\left(v_{c,d} - v_{g,d} - r_f i_{g,d} + \omega_{pll} l_f i_{g,q}\right)\\ \frac{d}{dt}i_{g,q} &= \frac{\omega_0}{l_f}\left(v_{c,q} - v_{g,q} - r_f i_{g,q} - \omega_{pll} l_f i_{g,d}\right)\end{aligned} \tag{6}$$

6) Power Calculation:

$$\begin{aligned}P_g &= v_{g,d} i_{g,d} + v_{g,q} i_{g,q}\\ Q_g &= -v_{g,d} i_{g,q} + v_{g,q} i_{g,d}\end{aligned} \tag{7}$$

7) Dc-link Capacitor Voltage:

$$\begin{aligned}\frac{d}{dt}v_{dc} &= \frac{1}{c}\left(i_{dc,sg} - i_{dc,c}\right)\\ &= \frac{1}{c v_{dc}}\left(P_{sg} - \left(v_{c,d} i_{g,d} + v_{c,q} i_{g,q}\right)\right)\end{aligned} \tag{8}$$

C. Phase-Locked Loop

The phase-locked loop (PLL) in Figure 7 attempts to align the d-axis voltage of the converter $v_{g,d}$ with the voltage at PCC by estimating the PCC voltage phase angle and grid frequency. The PLL model (9) uses a PI controller to control $v_{g,q}$ to zero to achieve this. The SO criteria are obtained to find the PLL controller parameters. The relationship between the converter dq-reference frame and the synchronous reference frame of the grid is given in (10) [18].

$$\begin{aligned}\frac{d}{dt}\theta_{p,pll} &= k_{p,pll}\left(-v_{gRe}\sin\theta_{p,pll} + v_{gIm}\cos\theta_{p,pll}\right)\\ &\quad + x_{pll}\\ \frac{d}{dt}x_{pll} &= k_{i,pll}\left(-v_{gRe}\sin\theta_{p,pll} + v_{gIm}\cos\theta_{p,pll}\right)\\ \omega_{pll} &= \frac{\Delta\omega_{pll}}{\omega_0} + \omega_s\end{aligned} \tag{9}$$

$$\begin{bmatrix}d\\ q\end{bmatrix} = \begin{bmatrix}\cos\theta_{p,pll} & \sin\theta_{p,pll}\\ -\sin\theta_{p,pll} & \cos\theta_{p,pll}\end{bmatrix}\begin{bmatrix}Re\\ Im\end{bmatrix} \tag{10}$$

D. Synchronous Generator

The VSHP-model utilize a sixth-order synchronous generator model as presented in [19]. Since the reactances are dependent on the rotational speed, they cannot be assumed to be constant in a VSHP. The reactances are therefore assumed to be proportional to the rotational speed ω such that $X_x = (\omega_s + \Delta\omega)\, L_x$.

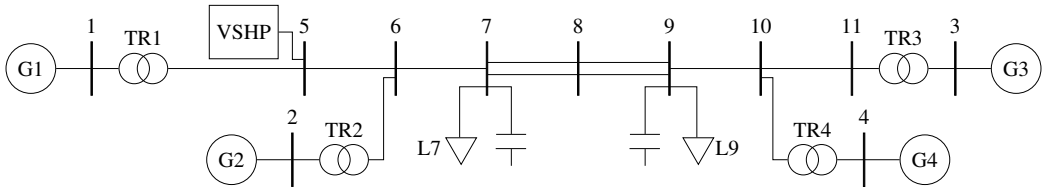

Fig. 4: Kundur Two-area system

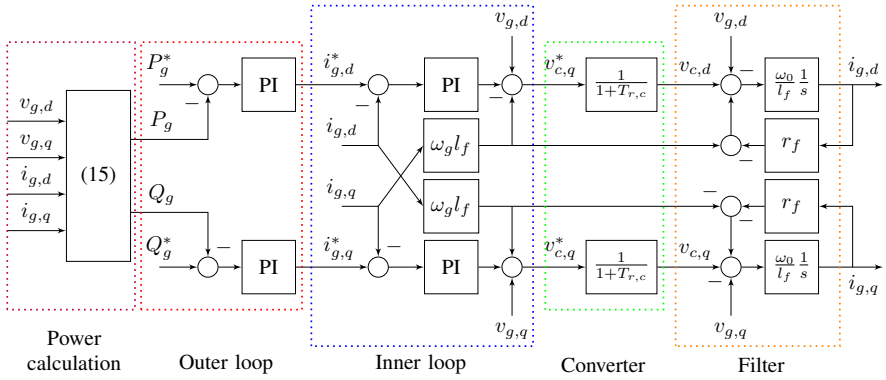

Fig. 5: Grid converter

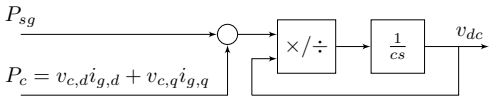

Fig. 6: DC-circuit

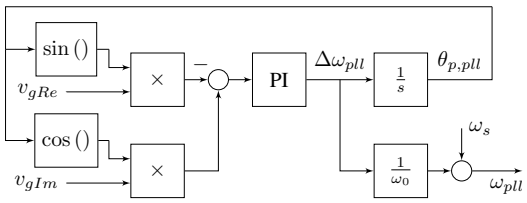

Fig. 7: PLL

The generator current is obtained from the voltage difference between the internal sub-transient generator voltage and converter voltage over the generator impedance:

$$
\begin{aligned}
i_{sg,d} &= \mathrm{Im}\left(\frac{\left(E_q^{''}-v_{c,q}\right)+j\left(E_d^{''}-v_{c,d}\right)}{R_a+j\omega X_d^{''}}\right)\\
i_{sg,q} &= \mathrm{Re}\left(\frac{\left(E_q^{''}-v_{c,q}\right)+j\left(E_d^{''}-v_{c,d}\right)}{R_a+j\omega X_d^{''}}\right)
\end{aligned}
\tag{11}
$$

E. Synchronous Generator Converter

The synchronous generator converter, Figure 8, controls the dc-link voltage v_{dc} by controlling the q-axis current $i_{sg,q}$ in the outer controller (12). In addition to a PI-controller on the dc-voltage error $v_{dc}^{*}-v_{dc}$, there is a forward coupling on the grid converter output power P_g to increase the precision and speed of the controller. The d-axis current reference $i_{sg,d}$ is set to zero.

The inner controller (13) consist of two PI current controllers with deviation in respectively d-axis current $i_{sg,d}^{*}-i_{sg,d}$ and q-axix current $i_{sg,q}^{*}-i_{sg,q}$ as input.

The PI inner and outer controller parameters are calculated by respectively the MO and SO criterion, assuming a switching frequency of 4 kHz.

1) Outer controller:

$$
\begin{aligned}
\frac{d}{dt}N_{sg,q} &= k_{dc,p}\left(v_{dc}^{*}-v_{dc}\right)\\
i_{sg,q}^{*} &= k_{dc,i}\left(v_{dc}^{*}-v_{dc}\right)+N_{sg,q}+P_g\\
i_{sg,d}^{*} &= 0
\end{aligned}
\tag{12}
$$

2) Inner Controller:

$$
\begin{aligned}
\frac{d}{dt}M_{sg,d} &= k_{ii,sg}\left(i_{sg,d}^{*}-i_{sg,d}\right)\\
v_{sg,d}^{*} &= k_{ip,sg}\left(i_{sg,d}^{*}-i_{sg,d}\right)-\omega L_q^{''}i_{sg,q}+M_d\\
\frac{d}{dt}M_{sg,q} &= k_{ii,sg}\left(i_{sg,q}^{*}-i_{sg,q}\right)\\
v_{sg,q}^{*} &= k_{ip,sg}\left(i_{sg,q}^{*}-i_{sg,q}\right)+\omega L_d^{''}i_{sg,d}+M_q
\end{aligned}
\tag{13}
$$

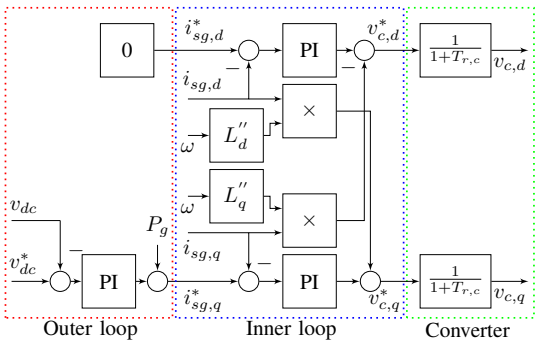

Fig. 8: SG converter

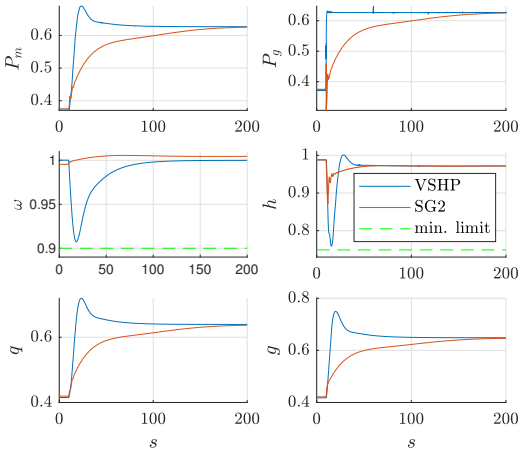

Fig. 9: Step response when power is increased

3) Converter Model:

$$\begin{aligned}\frac{d}{dt}v_{sg,d} &= \frac{1}{T_{r,sg}}\left(v^*_{sg,d} - v_{sg,d}\right)\\ \frac{d}{dt}v_{sg,q} &= \frac{1}{T_{r,sg}}\left(v^*_{sg,q} - v_{sg,q}\right)\end{aligned} \tag{14}$$

4) Power Calculation:

$$\begin{aligned}P_{sg} &= v_{sg,d}i_{sg,d} + v_{sg,q}i_{sg,q}\\ Q_{sg} &= -v_{sg,d}i_{sg,q} + v_{sg,q}i_{sg,d}\\ P_{dc} &= v_{dc}i_{dc,sg} = P_{sg}\end{aligned} \tag{15}$$

IV. Dynamic Analysis

The step responses of a VSHP and a conventional hydropower plant are compared in Figures 9 and 10, for, respectively, increase and reduction in power. The Euler turbine model is used for both types of hydropower plants, however, the governor differs; the VSHP utilizes a PID-controller without permanent droop, the conventional utilizes a droop controller. For the conventional hydropower plant, the step response is applied by a step in reference speed at the governor

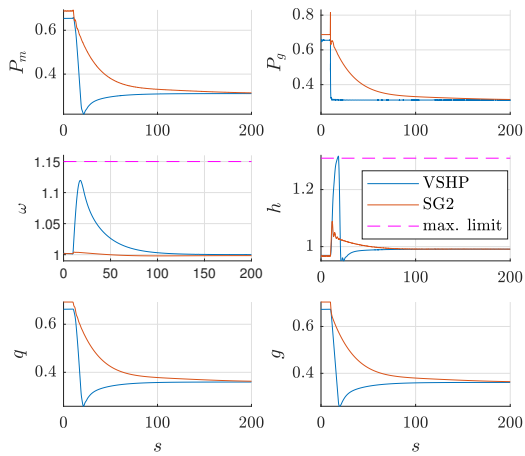

Fig. 10: Step response when power is decreased

input. The VSHP has one more degree of freedom since both the governor reference speed and the grid converter power reference affect the power produced by the turbine. However, a change in the governor reference speed will not cause the output power to the grid to change, only the rotational speed of the turbine. Therefore, the step response of the VSHP is applied to the grid converter power reference.

For fully utilizing the potential of ancillary services from a VSHP, the power delivery to the grid needs to be as flexible and quickly as possible. The power control of the VSHP grid converter allows the power output to the grid P_g to follow the step response in power reference almost perfectly.

However, the turbine power P_m will not be able to react as quickly, due to the governor and servo time constants. The deviation between the grid converter power P_g and the turbine power P_m will cause a deviation in rotational speed ω, approximately equal to the integration of the difference $P_m - P_g$. Next, the governor reacts to regain the reference rotational speed, causing the guide vane opening g and turbine water flow q to change. This causes changes in surge tank head h_{st}, headrace tunnel flow q_{hr}, turbine head h and turbine power P_m. The maximum size of the grid converter power step is thereby limited by the limits of the variables in the waterway, governor, turbine, SG and SG converter:

- maximum allowed rotational speed of the turbine/SG
- minimum rotational speed to regain the reference rotational speed, as pointed out in [10]
- minimum and maximum limits of the governor
- rate limit of the governor
- surge tank head limits
- current limits of the SG converter and the SG

As Figures 9 and 10 show, the fast change in output power of the VSHP causes larger peaks in mechanical power P_m, rotational speed ω, pressure (head) high h, flow q and guide vane opening g compared to a conventional hydropower plant. These variables must be within the limits given above. Increased wear and tear on the guide vane servo due to

additional operation and on the waterway due to more water hammering and mass oscillations must also be considered when designing the control system.

Although the power reference step in the two figures is the same, larger deviations in h, g, q and ω are observed when the power is reduced, compared to the case with an increase in power. From the Euler turbine equations, we see that the turbine mechanical power P_m decreases slower from an initial high power operational point when ω is increasing than P_m increases for an initial low operation point when ω increases. This causes a larger deviation in ω, faster operation of the guide vane opening g and hence larger overshoot in the head h and the flow q.

V. Participation Factor Based Interaction Analysis

A participation factor-based interaction mode method proposed in [20] is used to investigate the interactions between the subsystems. An interaction mode is defined as a mode with participation from more than one subsystem and proves a dynamic interaction between the subsystems [18].

The participation factor p_{ki} of state variable x_k in mode i is defined in [15] as

$$p_{ki} = \phi_{ki}\psi_{ki} \tag{16}$$

where ϕ and ψ are respectively the right and left eigenvector. The parameter $\eta_{\alpha i}$ is defined in [20] as a measure for the overall participation for each subsystem α in mode i.

$$\eta_{\alpha i} = \frac{||p_{\alpha i}||}{||p_i||} \tag{17}$$

where $||\cdot||$ denotes the L_1-norm. While the participation factor p_{ki} measures the participation of a state variable in a mode, $\eta_{\alpha i}$ calculates the degree of participation of a group for state variable, a subsystem, in a mode.

The VSHP system is divided into 12 subsystems, as presented on the y-axis in Figure 11. The modes on the x-axis are sorted according to the participation in each subsystem. The colours show the magnitude of $\eta_{\alpha i}$ for each subsystem and mode. The modes only participating in generators G1-G4 are not presented in the figure.

The participation factor-based interaction analysis presented in Figure 11 shows that the system can be divided into two parts, where no modes are interacting in both these parts. The division is between the two converters in the VSHP. The turbine side of the DC-link includes VSHP waterway, VSHP turbine, VSHP governor, VSHP generator, SG converter and DC-link while the grid side of the DC-link includes the subsystems that are interfering with the other generators in the grid; the grid converter and the PLL.

The reason why there are no modes between the two parts can be found by investigating the variables between the subsystems in Figure 1. The turbine side of the DC-link will be affected by a perturbation on the grid side of the turbine since this will cause the DC-voltage and thereby the power of the SG converter to change. A perturbation on the turbine side of the DC-link will also cause the DC-link voltage to change; however, the grid converter control is not influenced by the DC-link voltage, see Figure 5. Since the two parts do not influence each other, there will be no modes between the two parts.

A more detailed model of the grid converter may consider the DC-link voltage, for instance when calculating the PWM modulation. However, this is only compensating for a deviation in DC-voltage such that the converter output voltage follows the reference voltage. Therefore, this will, in practice, not result in any new coupling between the two parts.

We believe that the proposed control system in this paper is perfectly suited for VI control of the grid converter for two reasons. Firstly, the control system has very good performance from a grid perspective since no modes are interacting between the VSHP turbine, waterway and generator and the rest of the grid. The output power of the VSHP can, therefore, be controlled directly by the grid converter with great flexibility without considering small signal stability issues in the turbine side of the DC-link. This makes the design of the VI controller easier than alternative control layouts; i.e. if the governor is controlled by the grid frequency as in a conventional hydropower plant or if the SG converter is controlled by the grid frequency and the governor controls the turbine rotational speed. Secondly, the control system makes it possible to use the rotational energy of the turbine and the generator as energy storage by allowing the turbine rotational speed to deviate from its nominal value. The VI control of the grid converter utilizes this energy storage to deliver faster power response to the grid. However, there are still limitations due to the maximum speed of the governor, the limits of the turbine rotational speed range and turbine head and water hammering in the penstock that affect the VSHP output power control ability. VI will be implemented and tested in further works to verify this assumption.

VI. Conclusion

A detailed model of a VSHP plant, including hydraulic system models and converter models, has been developed and presented in this paper. The model is tested for the purpose of utilizing the VSHP for ancillary services and to explore the limitations given by the hydraulic system. The results are compared with a conventional hydropower plant. A key finding is that in variable speed operation the gradients and peaks in guide vane opening, flow and head tend to become more excited due to the larger deviations in turbine rotational speed.

Extra awareness when designing the control system is therefore needed to keep the hydraulic system variables, such as the surge tank head, within their limits.

The participation factor-based interaction analysis shows that the VSHP-system can be divided into two parts where there is no mode interacting in both parts. The turbine side of the DC-link will be affected by a perturbation on the grid side of the DC-link; however, there is no coupling the other way since the grid converter control is not influenced by the DC-link voltage. The result is that there will be no modes

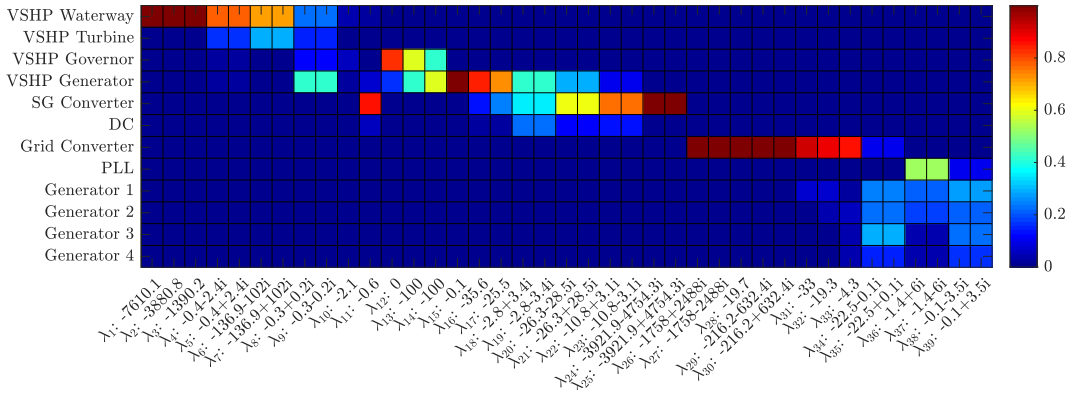

Fig. 11: Participation factor-based interaction analysis

between the hydraulic system of the VSHP and the rest of the grid, and, from a small signal perspective, that the modes of the hydraulic system will not need to be considered when tuning the grid converter.

The possibility for utilizing the rotational energy in the turbine and generator and controlling the output power without causing small-signal instability in the hydraulic system makes VSHP very suitable for VI control. However, the limitations in the hydraulic system must be fulfilled. For this reason, more advanced control systems considering such limits, such as model predictive control, might be favourable to optimize the ancillary services given by the VSHP.

Appendix A
Parameters, Set-points and Variables

The model parameters and set-points are given in Table I while the variables are given in Table II.

References

[1] M. Valavi and A. Nysveen, "Variable-speed operation of hydropower plants: Past, present, and future," in *Electrical Machines (ICEM), 2016 XXII International Conference on*. IEEE, 2016, pp. 640–646.

[2] Y. Pannatier, B. Kawkabani, C. Nicolet, J.-J. Simond, A. Schwery, and P. Allenbach, "Investigation of control strategies for variable-speed pump-turbine units by using a simplified model of the converters," *IEEE Transactions on Industrial Electronics*, vol. 57, no. 9, pp. 3039–3049, 2010.

[3] M. Mohanpurkar, A. Ouroua, R. Hovsapian, Y. Luo, M. Singh, E. Muljadi, V. Gevorgian, and P. Donalek, "Real-time co-simulation of adjustable-speed pumped storage hydro for transient stability analysis," *Electric Power Systems Research*, vol. 154, pp. 276–286, 2018.

[4] A. Ansel and B. Robyns, "Modelling and simulation of an autonomous variable speed micro hydropower station," *Mathematics and computers in simulation*, vol. 71, no. 4-6, pp. 320–332, 2006.

[5] S. Breban, A. Ansel, M. Nasser, B. Robyns, and M. M. Radulescu, "Experimental results on a variable-speed small hydro power station feeding isolated loads or connected to power grid," in *Electrical Machines and Power Electronics, 2007. ACEMP'07. International Aegean Conference on*. IEEE, 2007, pp. 760–765.

[6] E. Muljadi, M. Singh, V. Gevorgian, M. Mohanpurkar, R. Hovsapian, and V. Koritarov, "Dynamic modeling of adjustable-speed pumped storage hydropower plant," in *Power & Energy Society General Meeting, 2015 IEEE*. IEEE, 2015, pp. 1–5.

[7] T. Mercier, M. Olivier, and E. Dejaeger, "Operation ranges and dynamic capabilities of variable-speed pumped-storage hydropower," in *Journal of Physics: Conference Series*, vol. 813, no. 1. IOP Publishing, 2017, p. 012004.

[8] W. Yang and J. Yang, "Advantage of variable-speed pumped storage plants for mitigating wind power variations: Integrated modelling and performance assessment," *Applied Energy*, vol. 237, pp. 720–732, 2019.

[9] A. Béguin, C. Nicolet, J. Hell, and C. Moreira, "Assessment of power step performances of variable speed pump-turbine unit by means of hydro-electrical system simulation," in *Journal of Physics: Conference Series*, vol. 813, no. 1. IOP Publishing, 2017, p. 012001.

[10] T. I. Reigstad and K. Uhlen, "Modelling of variable speed hydro power for grid integration studies," *Manuscript submitted for publication*.

[11] D. Borkowski and T. Wegiel, "Small hydropower plant with integrated turbine-generators working at variable speed," *IEEE Transactions on Energy Conversion*, vol. 28, no. 2, pp. 452–459, 2013.

[12] J. Marquez, M. Molina, and J. Pacas, "Dynamic modeling, simulation and control design of an advanced micro-hydro power plant for distributed generation applications," *International journal of hydrogen energy*, vol. 35, no. 11, pp. 5772–5777, 2010.

[13] F. Demello, R. Koessler, J. Agee, P. Anderson, J. Doudna, J. Fish, P. Hamm, P. Kundur, D. Lee, G. Rogers *et al.*, "Hydraulic-turbine and turbine control-models for system dynamic studies," *IEEE Transactions on Power Systems*, vol. 7, no. 1, pp. 167–179, 1992.

[14] T. K. Nielsen, "Simulation model for francis and reversible pump turbines," *International Journal of Fluid Machinery and Systems*, vol. 8, no. 3, pp. 169–182, 2015.

[15] P. Kundur, N. J. Balu, and M. G. Lauby, *Power system stability and control*. McGraw-hill New York, 1994, vol. 7.

[16] C. Bajracharya, M. Molinas, J. A. Suul, T. M. Undeland *et al.*, "Understanding of tuning techniques of converter controllers for vsc-hvdc," in *Nordic Workshop on Power and Industrial Electronics (NORPIE/2008), June 9-11, 2008, Espoo, Finland*. Helsinki University of Technology, 2008.

[17] S. D'Arco, J. A. Suul, and O. B. Fosso, "Control system tuning and stability analysis of virtual synchronous machines," in *2013 IEEE Energy Conversion Congress and Exposition*. IEEE, 2013, pp. 2664–2671.

[18] A. G. Endegnanew, "Stability analysis of high voltage hybrid ac/dc power systems," 2017.

[19] J. Machowski, J. Bialek, J. R. Bumby, and J. Bumby, *Power system dynamics and stability*. John Wiley & Sons, 1997.

[20] J. Beerten, S. D'Arco, and J. A. Suul, "Identification and small-signal analysis of interaction modes in vsc mtdc systems," *IEEE Transactions on Power Delivery*, vol. 31, no. 2, pp. 888–897, 2016.

TABLE I: Parameters and set-points

Parameter	Value
Waterway	
Rated water flow Q_R, $[m^3/s]$	170
Rated height H_R, $[m]$	425
Penstock:	
Water starting time T_w, $[s]$	1.211
Water traveling time T_e, $[s]$	0.126
Characteristic impedance Z_0	9.61
Friction factor f_{p1}, $[s^4/m^5]$	0.049
Surge tank:	
Friction factor f_{p0}, $[s^4/m^5]$	0.036
Storage constant C_s	0.099
Head race tunnel:	
Water starting time T_{w2}, $[s]$	4.34
Friction factor f_{p2}, $[s^4/m^5]$	0.020
Hydraulic Machine	
Turbine constant ψ	0.404
Turbine constant ξ	0.918
Turbine constant α	0.745
Turbine constant σ	0.015
Rated water flow Q_{Rt}, $[m^3/s]$	144
Rated height H_{Rt}, $[m]$	425
Governor conventional hydropower	
Governor time constant T_r, $[s]$	4.00
Servo time constant T_g, $[s]$	0.50
Temporary droop r	0.40
Permanent droop R	0.05

Parameter	Value
Governor VSHP	
Rotational speed reference ω^*, pu	1.00
Governor proportional gain $k_{g,p}$	3.00
Governor integration gain $k_{g,i}$	0.100
Governor derivation gain $k_{g,d}$	1.000
Rate limit	+/-0.05
Servo time constant T_G, $[s]$	0.500
Synchronous generator	
Inertia constant H, $[s]$	6.5
Damping constant D	0
Stator resistance R_a, pu	2.5e-3
Transient time constants:	
$T^{'}_{d0}$, $[s]$	8
$T^{'}_{q0}$, $[s]$	0.4
Sub-transient time constants:	
$T^{''}_{d0}$, $[s]$	0.03
$T^{''}_{q0}$, $[s]$	0.05
Synchronous reactances:	
X_d, pu	1.8
X_q, pu	1.7
Transient reactances:	
$X^{'}_{d}$, pu	0.3
$X^{'}_{q}$, pu	0.55
Sub-transient reactances:	
$X^{''}_{d}$, pu	0.25
$X^{''}_{q}$, pu	0.25

Parameter	Value
SG converter	
Switching time delay $T_{r,sg}$, $[ms]$	0.25
Inner controller:	
Proportional gain $k_{ip,sg}$	0.3
Integral gain $k_{ii,sg}$	20
Outer controller:	
Dc-voltage reference v^*_{dc}	1.00
Proportional gain $k_{dc,p}$	0.64
Integral gain $k_{dc,i}$	0.082
Grid converter	
Inner controller:	
Proportional gain $k_{ip,c}$	0.509
Integral gain $k_{ii,c}$	10
Outer controller:	
Proportional gain k_{Pp},k_{Qp}	21.2
Integral gain k_{Pi},,k_{Qi}	94.3
Converter and filter:	
Switching time delay $T_{r,c}$, $[ms]$	1.00
Filter resistance r_f, pu	0.01
Filter impedance l_f, pu	0.16
PLL:	
Proportional gain $k_{p,pll}$	2.26
Integral gain $k_{i,pll}$	34.3
Base grid frequency ω_0, rad/s	$2\pi f$
Dc-link:	
Capacitance c, pu	0.02

TABLE II: Variables

Variable	Symbol
Waterway	
Surge tank head	h_{st}
Head race tunnel flow	q_{hr}
Hydraulic Machine	
Turbine head	h
Turbine water flow	q
Mechanical torque	T_m
Mechanical power	P_m
Turbine efficiency	η_h
Turbine head	h_t
Turbine flow	q_t
Opening degree of turbine	κ
Governor	
Guide vane opening reference	g^*
Guide vane opening	g

Variable	Symbol
Synchronous generator	
Rotor angle	δ
Rotor speed deviation	$\Delta\omega$
Transient voltages	$E^{'}_{d}$, $E^{'}_{q}$
Sub-transient voltages	$E^{''}_{d}$, $E^{''}_{q}$
Field excitation voltage	E_{fd}
Stator currents	$i_{sg,d}$, $i_{sg,q}$
Stator voltage	$v_{sg,d}$, $v_{sg,q}$
Electrical power	P_e
SG converter	
Stator current references	$i^*_{sg,d}$, $i^*_{sg,q}$
Stator voltage references	$v^*_{sg,d}$, $v^*_{sg,q}$
Active/reactive power	P_{sg}, Q_{sg}
Dc-link power	P_{dc}
Dc-link voltage	v_{dc}

Variable	Symbol
Grid converter	
Grid currents	$i_{g,d}$, $i_{g,q}$
Grid current references	$i^*_{g,d}$, $i^*_{g,q}$
Converter voltages	$v_{c,d}$, $v_{c,q}$
Converter voltage references	$v^*_{c,d}$, $v^*_{c,q}$
Grid voltage	$v_{g,d}$, $v_{g,q}$
Active/reactive power	P_g, Q_g
Active/reactive power ref.	P^*_g, Q^*_g
PLL	
Estimated PCC voltage angle	$\theta_{p,pll}$
Speed deviation of converter control	$\Delta\omega_{pll}$
Reference machine speed	ω_s
Real part of PCC voltage	v_{gRe}
Imaginary part of PCC voltage	v_{gIm}

Tor Inge Reigstad received his M.Sc degree from Department of Electric Power Engineering at the Norwegian University of Science and Technology (NTNU), Trondheim, Norway, in 2007. He previously work with Siemens AS and SINTEF Energy Research, both Trondheim, until he started his PhD studies within grid integration of variable speed hydropower in 2018. His current research interests are principally related to the analysis and control of power electronic converters in onshore and offshore grids.

Kjetil Uhlen is a professor in Power Systems at the Norwegian University of Science and Technology (NTNU), Trondheim, and a Special Adviser at STATNETT (the Norwegian TSO). He has a Master's degree (1986) and PhD degree (1994) in control engineering. His main areas of work include research and education within control and operation of power systems, grid integration of renewable energy and power system dynamics.

Paper III

Virtual Inertia Implementation in Variable Speed Hydropower Plant

Virtual Inertia Implementation in Variable Speed Hydropower Plant

1st Tor Inge Reigstad
Department for Electric Power Engineering
Norwegian University of Science and Technology (NTNU)
Trondheim, Norway
tor.inge.reigstad@ntnu.no

2nd Kjetil Uhlen
Department for Electric Power Engineering
Norwegian University of Science and Technology (NTNU)
Trondheim, Norway
kjetil.uhlen@ntnu.no

***Abstract*—This paper investigates how a variable speed hydropower (VSHP) plant with virtual inertia (VI) control can deliver fast power reserves to compensate for variable production of renewables and maintain grid stability after disturbances. The advantage of the VSHP is that it is able to change the electric power output significantly within a few seconds and maintaining it for a longer period. During the first seconds, the energy is taken from the rotating masses in the generator and the turbine. Thereafter, the water flow and thereby the mechanical power are adjusted by governor action to return the turbine to its optimal speed.**

Two VI control structures are implemented and tested on a VSHP plant simulation model. The virtual synchronous generator (VSG) and the virtual synchronous machine (VSM) are further developed to fulfil the main objective of the control; to maximize the grid support from the VSHP by utilizing the turbine and generator rotational energy. At the same time, the impact on the hydraulic system must be considered in order to fulfil the objectives for internal control of the plant; i.e. to optimize the turbine rotational speed, minimize water hammering and mass oscillations, minimize guide vane servo operation and minimize hydraulic and electric losses.

Dynamic analyses are performed to compare the control structures; the power-frequency PID controller with permanent droop (VSG-PID) based on the VSG and the VSM with power-frequency PID controller and permanent droop (VSM-PID). They are evaluated by two main criteria; their ability to deliver instantaneous power (inertia) to reduce the rate of change of frequency (ROCOF) and their contribution to frequency containment control (steady state frequency droop response).

Keywords - Virtual inertia, synthetic inertia, virtual synchronous generator, virtual synchronous machine, variable speed hydropower, hydropower, grid integration study

I. Introduction

As the share of wind and solar energy production increases, more flexible production and loads are required to control the balance of the grid in order to maintain power system security. A potential use of VSHP plants is to provide this flexibility and compensate the production of variable renewables, for instance by use of virtual inertia control. The hypothesis is that VSHP can offer additional ancillary services, contributing to improving the frequency control and maintaining the grid stability, allowing for higher penetration of variable renewables in the grid. The advantages compared to conventional pumped-storage hydropower with constant rotational speed are better utilization of the rotational energy in the turbine and the generator and improved power control in pumping mode. The efficiency and operating range of the VSHP will also be higher and it can contribute to frequency control both in generation and pumping mode [1]. The converter technology offers faster control of reactive power and potentially higher reactive power capability, which benefits the voltage regulation. However, the converter short circuit current is limited, which challenges the established practice for implementing generator and grid protection.

This work was supported by the Research council of Norway under Grant 257588 and by the Norwegian Research Centre for Hydropower Technology (HydroCen).

Power reserves are needed to maintain the balance between power generation and power consumption and to control the grid frequency. Four different reserve levels are defined in [2], [3].

- The instantaneous power reserves are supplied by the physical stabilizing effect of all the grid-connected synchronous machines due to their inertia.
- Frequency deviations are contained by the primary reserves that are automatically or locally activated within seconds to a few minutes. In the Nordic grid, the frequency containment reserves (FCR) are divided into two parts:
  - FCR-N: activated at frequency deviations $\pm 0.1 Hz$
  - FCR-D: activated at $49.9 Hz$ and fully activated at $49.5 Hz$

  Both should be automatic and fully activated within 30 sec.
- Secondary reserves are activated to restore the grid frequency to the rated value, to release primary reserves and restore the power flow between control areas. In the Nordic grid, the frequency restoration reserves (FRR) are divided into automatically controlled services (aFRR) and the reserves activated through the balancing control market (mFRR). FRR must be activated within 15 minutes.
- Tertiary reserves or reserve replacement (RR) can be used to free up secondary reserves. There is no market for RR in the Nordic system.

The Nordic TSOs have analyzed potential actions in situ-

ations with low grid inertia [4], [5]. Fast frequency reserves (FFR) have been evaluated as the most technical and economical solution in advance of increasing the inertia by virtual inertia control [6]. According to the suggestion, a power response should be activated at $49.60Hz$ and reaches its full value within 2 sec. The duration should be at least 30 sec and a new power response may be activated after 15 min. A pilot project shows promising results, however, neither the tested hydropower Pelton or Francies turbines were able to deliver the power step within time.

Traditionally, large hydro and thermal power plants are used for frequency control. However, the share of inverter-based generation is increasing in the modern grid as more renewable energy sources (RESs) are implemented. This compromises the frequency stability since the inverter-based generation does not provide any mechanical inertial response, causing less inertia and faster change in frequency in the power system. One solution will be to add virtual inertia through the converter control. The different typologies of virtual inertia concepts developed over the last years are reviewed in [7], and classified in three main categories;

- The synchronous generator (SG) based models intend to emulate a synchronous machine (SM) continuously with a machine model, including for instance inertia, damping and voltage control [8]–[13].
- The swing equation based models use a simpler power-frequency swing equation instead of a full detailed model of the SG to emulate inertia [14].
- The power versus frequency response-based models are controlled proportionally to frequency deviation (damping term) and/or proportionally to the derivative of the frequency deviation (inertia term) [15]–[19].

In literature, virtual inertia from different sources are investigated, like batteries [20], capacitors [21], HVDC [22], and wind power [2], [16], [23], [24]. Implementation of virtual inertia in VSHP is barely mentioned, although VSHP is very suitable for the purpose. Photovoltaic (PV) systems are less suitable since the energy storage is very small unless connected to battery storage. Wind turbines must be returned to its optimal rotational speed and pitch quickly and are therefore best fitted for frequency-power response based control with temporary grid support [25]. VSHP, however, is better suited for continuously active SG based models since it can obtain energy from the rotational masses in turbine and generator for the first inertia response and thereby adjust the water flow and mechanical power by governor action to return to the optimal rotational speed.

This paper investigates the instantaneous and primary power reserves of a VSHP and aims to find the best-suited control scheme for VSHP considering the defined control objectives.

The paper is outlined as follows: The virtual inertia models and the VSHP and grid models are presented in respectively Section II and III. The dynamic analysis results and discussion are given in Section IV. The conclusions are summed up in Section V.

II. Virtual Inertia Models

A. Control Objectives

The VSHP control objectives can be divided into objectives for internal control and for grid support:

- Objectives for internal control of the plant:
  - To optimize the rotational speed of the turbine with respect to the efficiency at part load,
  - to minimize water hammering and mass oscillations,
  - to minimize the guide vane servo operation,
  - and to minimize the hydraulic and electric losses.
- Objectives for grid support control:
  - Contribute to FCR by faster and more precise frequency droop control,
  - contribute to increasing the effective system inertia by virtual inertia control,
  - improve the voltage control response time,
  - and increase the damping in the system.

This paper will focus on the grid support where the main control objective is to maximize the grid support from the VSHP by utilizing the turbine and generator rotational energy. The virtual inertia control has to deliver both instantaneous power (inertia) to reduce the rate of change of frequency (ROCOF) and contribute as much as possible to frequency control to regain the grid frequency as fast as possible after a disturbance.

This section presents two different virtual inertia typologies; the power-frequency PID controller with permanent droop (VSG-PID) based on the VSG, and the VSM [9], [26] with power-frequency PID controller and permanent droop (VSM-PID).

B. VSM with Power-Frequency PID controller and Permanent Droop

The VSM is a SG based virtual inertia model based on control strategies for voltage source converters (VSC). In addition to providing virtual inertia to the grid, VSMs are also able to work in islanded systems without changing parameters and control structure [26]–[31]. The VSM is able to deliver virtual inertia to support the grid, however, its output power is returning to the reference power relatively fast when the VSM speed has returned to its rated value.

The frequency support is improved by combining the VSM with a PID controller with permanent droop as presented in Figure 1. The output of this controller $P^*_{g,r}$ is added to the frequency droop of the VSM to find the virtual power p^*_r. This control layout will be very similar to a conventional hydropower plant with the representation of both SG and governor control, however, it offers significantly faster primary frequency control.

The VSM model used in this thesis is presented in [9] and Figure 1, where the inertia model is given as

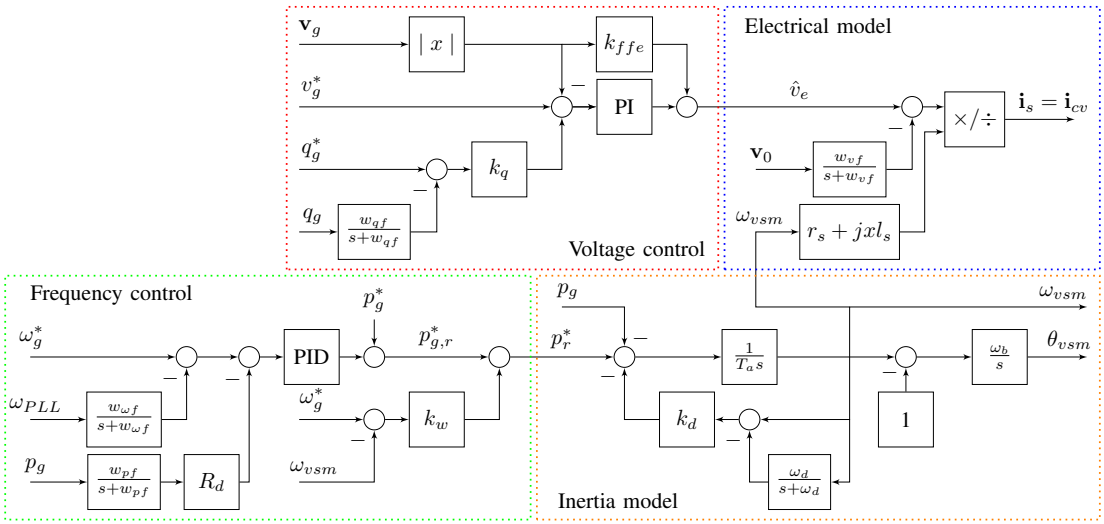

Fig. 1: Virtual synchronous machine (VSM)

$$\begin{aligned}\frac{d\omega_{vsm}}{dt} &= \frac{p_r^*}{T_a} - \frac{p_g}{T_a} - \frac{k_d\left(\omega_{vsm} - \kappa\right)}{T_a} \\ \frac{d\kappa}{dt} &= \omega_d\omega_{vsm} - \omega_d\kappa \\ \frac{d\theta_{vsm}}{dt} &= \omega_{vsm}\omega_b\end{aligned} \tag{1}$$

p_r^* is the virtual power driving the inertia, p_g is the measured power to the grid and T_a is the mechanical time constant.

An outer frequency droop controller generates the power reference for the ideal prime mover as

$$p_r^* = p_g^* + k_\omega\left(\omega_{vsm}^* - \omega_{vsm}\right) \tag{2}$$

where p_g^* is the external power reference, ω_{vsm}^* is the VSM speed reference and k_ω is the frequency droop gain.

The voltage controller is defined as

$$\begin{aligned}\hat{v}_e &= k_{pv}\left(\hat{v}^* - \hat{v}_0\right) + k_{pv}k_q\left(q_g^* - q_f\right) \\ &\quad + k_{iv}\zeta + k_{ffe}\hat{v}_0 \\ \hat{v}_0 &= \sqrt{v_{0,d}^2 + v_{0,q}^2} \\ \frac{dq_f}{dt} &= \omega_{qf}\left(q_g - q_f\right) \\ \frac{d\zeta}{dt} &= \left(\hat{v}^* - \hat{v}_0\right) + k_q\left(q_g^* - q_f\right)\end{aligned} \tag{3}$$

q_f is the low-pass filtered reactive power and ζ is the integrator state of the PI controller.

The synchronous machine (SM) is represented by a Quasi-stationary electrical SM model (QSEM) and assumes a phasor-based representation of the SM stator impedance. The current reference $\mathbf{i}_{cv}$ to the current control loop equals the virtual SM stator current $\mathbf{i}_s^{QSEM}$, expressed as

$$\begin{aligned}\mathbf{i}_s^{QSEM} &= \frac{\mathbf{v}_e - \mathbf{v}_m}{r_s + j\omega_{vsm}l_s} \\ &= \frac{r_s\left(\mathbf{v}_e - \mathbf{v}_m\right)}{r_s^2 + \left(\omega_{vsm}l_s\right)^2} - j\frac{\omega_{vsm}l_s\left(\mathbf{v}_e - \mathbf{v}_m\right)}{r_s^2 + \left(\omega_{vsm}l_s\right)^2} \\ \mathbf{v}_e &= \hat{v}_e \\ \frac{\mathbf{v}_m}{dt} &= \omega_{vf}\left(\mathbf{v}_0 - \mathbf{v}_m\right)\end{aligned} \tag{4}$$

Since active damping is included in the VSM model, the forward couplings of the grid voltage in the current control loop, $v_{g,d}$ and $v_{g,q}$ are replace by the voltage output from the active damping filter $v_{g,d,ad}$ and $v_{g,q,ad}$, given as

$$\begin{aligned}v_{g,d,ad} &= k_{ad,vsm}\left(1 - \frac{\omega_{ad,vsm}}{s + \omega_{ad,vsm}}\right)v_{g,d} \\ v_{g,q,ad} &= k_{ad,vsm}\left(1 - \frac{\omega_{ad,vsm}}{s + \omega_{ad,vsm}}\right)v_{g,q}\end{aligned} \tag{5}$$

C. Power-Frequency PID controller with Permanent Droop

The VSG-PID controller is based on the VSG, which is a power-frequency response based virtual inertia system [7], [17]. The VSG tries to emulate the inertial response characteristics of a synchronous generator in a simple way, without incorporating all the detailed equations involved in an SG. While the VSG uses a PD controller to calculate the current reference in the d-axis, $i_{g,d}^*$, from the deviation in grid frequency $\Delta\omega_g$, the VSG-PID controller utilizes a PID controller and permanent droop instead, as shown in Figure 2 and (6). The PID controller allows for faster control and less deviation in frequency while the permanent droop allows

for power sharing between generators as with conventional power plants. The power reference p_g^* is added to achieve the wanted power at zero frequency deviation and the controller compensates for deviations in voltage and for reactive power delivery. p_f is the low-pass filtered active output power p_g.

$$\begin{aligned} p_{vsg-pid} &= k_{vsg-pid,p}\epsilon + \frac{k_{vsg-pid,d}\omega_{vsg-pid}s}{s+\omega_{vsg-pid}}\epsilon \\ &+ \frac{k_{vsg-pid,i}}{s}\epsilon + p_g^* \\ \epsilon &= \omega_g^* - \omega_g - Rp_f \\ i_{g,d}^* &= \frac{v_{c,d}p_{vsg-pid} - v_{c,q}q_g}{v_{c,d}^2 + v_{c,q}^2} \end{aligned} \tag{6}$$

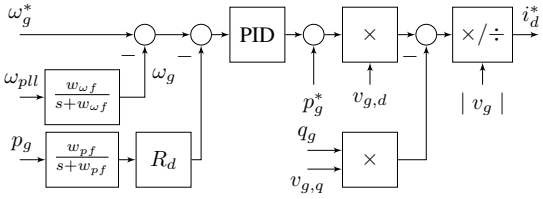

Fig. 2: Power-frequency PID controller with permanent droop (VSG-PID)

III. Variable Speed Hydropower and Grid Models

The VSHP model and the two-area power system used for the simulations in this paper are presented in [32] and the hydraulic system is modelled by the Euler turbine equation model presented in [33]. The grid converter outer control loop is replaced by the virtual inertia models given in this paper. For the VSG-PID, only the outer controller in d-axis is changed by inserting a new controller for $i_{g,d}^*$. In the case of a VSM-PID, the inner current control is kept, however, the outer control loops are replaced with the VSM model.

IV. Dynamic Analysis

The performance of the two different control schemes is analyzed by time-domain simulations, comparing responses to step changes in loads and controller set-points. Figure 3 shows the responses to a sudden loss of load at Bus 7.

The droop characteristics of the VSG-PID and VSM-PID controllers causes the VSHP output power p_g to stabilize at a lower value after the disturbance and in that way contribute to frequency containment. Both controllers show fast responses and provide the best frequency containment during the first 10-15 seconds after the loss of load. The difference between the VSG-PID and VSM-PID controllers - that is most clearly seen in grid frequency f deviations - can be explained by the way the two controllers react differently to changes in voltage angles. The result of this can be observed in the slightly different converter power outputs p_g between approximately 1 and 4 seconds after the disturbance. Some higher amplitudes of the oscillations are observed in the VSHP output power p_g

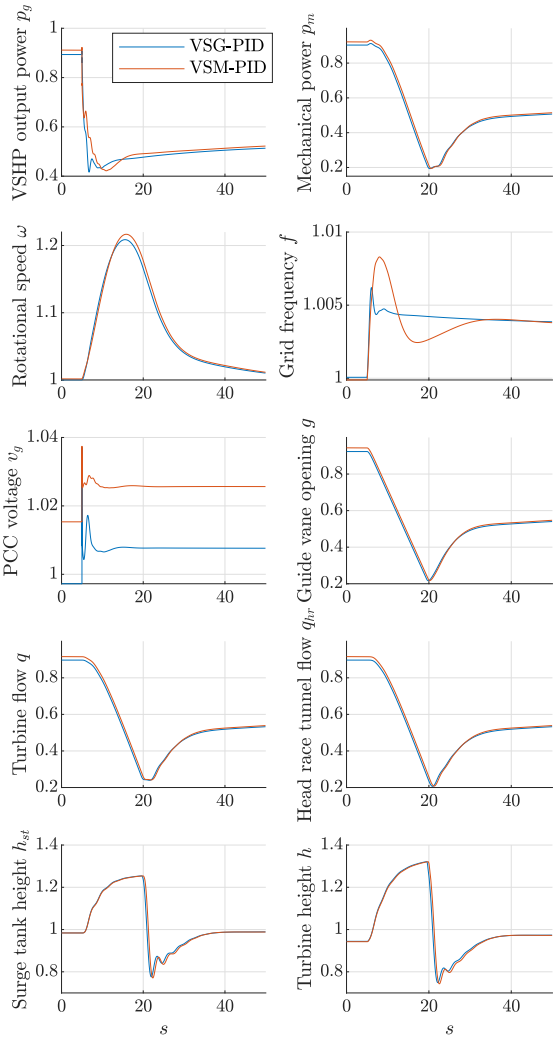

Fig. 3: Comparison of load step responses on Bus 7 for different VSHP control schemes

power for the VSG-PID control compared to the VSM-PID control, however, the oscillations are small and well damped. The hydraulic variables are very little affected by the type of control schemes.

A basic idea behind the VSM-PID controller is to make the converter respond similarly as a synchronous machine. Thus, due to the controllers' dependence of the voltage angle, their responses will be different depending on where the grid disturbance appears. To illustrate that, the results from two cases are compared in Figure 4; a load loss of 50% on Bus 7, near the VSHP, and a load loss of 30% on Bus 9, far from the VSHP. When the load loss is close to the VSHP, the VSM-

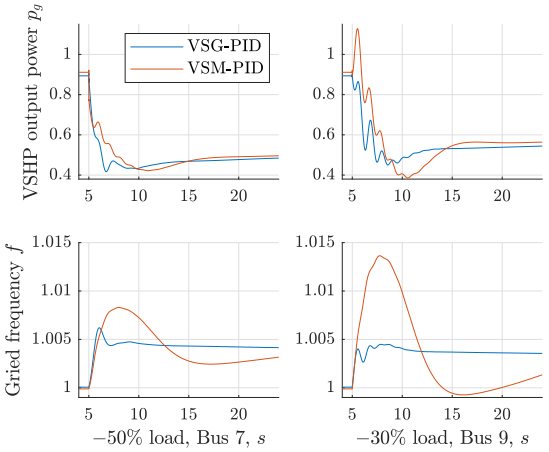

Fig. 4: Step response with load reduction at respectively 50% on Bus 7 and 30% on Bus 9

PID controller delivers most inertia the first half second and thereby oscillating to its reference power. However, when the load loss is far away from the VSHP, the output power of the VSM-PID controller is actually increasing the first second. This phenomenon is related to the inter-area power oscillations in the grid since the same behaviour is observed of the nearby generators, SG1 and SG2.

The inertial response of the VSG-PID is some slower compared to a VSM-PID when the load loss is close to the VSHP. After 10 ms, the output power of the VSG-PID is reduced by 0.04 pu. The same number for the VSM is 0.13 pu. However, the performance of the VSG-PID is better when the load loss is far away. In addition, the VSG-PID will reduce the output power until the frequency has recovered and therefore deliver much more primary reserves, thus reducing the maximum grid frequency deviation.

The inter-area power oscillations are larger when the load reduction is far away from the VSHP. This is due to the fact that most of the primary reserves are delivered by the VSHP. When the load disturbance occurs on the other side of the connection between the two areas, the power flow through this connection is changed, causing inter-area oscillations.

V. Conclusion

Two virtual inertia typologies are investigated and compared in this paper with the objective of maximizing the grid support from the VSHP by utilizing the turbine and generator rotational energy. They are evaluated by two main criteria; the property of delivering instantaneous power (inertia) to reduce the rate of change of frequency (ROCOF) and the property of contributing to frequency control to regain the grid frequency as fast as possible after a disturbance.

The results show clearly that the choice of virtual inertia typology has an insignificant impact on the hydraulic system. The VSM-PID controller shows the fastest response during the first 200 ms after a disturbance, however, the VSG-PID controller provides better frequency regulation for the next 5 seconds. In cases where the disturbance is far away from the VSHP, the performance of the VSM-PID controller is reduced and the VSG-PID perform better regarding the instantaneous response (synthetic inertia) and permanent frequency droop control.

The dynamic analysis clearly shows that the VSG-PID has the best performance from a grid-integration point of view. However, since the VSM-PID controller is based on emulating the response of a synchronous generator, the PLL is not needed. This makes the VSM-PID able to work in islanded systems without changing parameters and control structure.

TABLE I: Parameters and set-points

Parameter	Value
VSG-PID	
Proportional gain $k_{vsg-pid,p}$	100 p.u.
Integral gain $k_{vsg-pid,i}$	286 p.u.
Derivative gain $k_{vsg-pid,d}$	33.6 p.u.
Derivative filter constant ω_{vsg-pd}	0.01 s
VSM-PID	
Voltage controller proportional gain	0.29 p.u.
Voltage controller integral gain	92 p.u.
Voltage feedforward in voltage controller k_{ffe}	0 p.u.
Reactive power filter ω_{qf}	200 rad/s
Reactive power droop gain k_q	0.1 p.u.
Voltage low pass filter ω_{vf}	200 rad/s
SM inductance l_s	0.25 p.u.
SM resistance r_s	0.01 p.u.
Frequency controller gain k_ω	20 p.u.
Inertia constant T_a	4 s
Damping coefficient k_d	40 p.u.
Damping filter ω_d	5 rad/s
Rated angular frequency ω_b	50 rad/s
Active damping gain k_{AD}	0.3 p.u.
Active damping ω_{AD}	50 rad/s
Proportional gain $k_{vsm-pid,p}$	3000 p.u.
Integral gain $k_{vsm-pid,i}$	476 p.u.
Derivative gain $k_{vsm-pid,d}$	12600 p.u.
Derivative filter constant $\omega_{vsm-pid}$	1 s
Frequency controller gain $k_{vsm-pid}$	2000 p.u.
Common parameters	
Droop R_d	0.01 p.u.
PLL frequency filter constant	0.001 s

Appendix A
Parameters, set-points and variable

The VI model parameters are given in Table I.

References

[1] M. Valavi and A. Nysveen, "Variable-speed operation of hydropower plants: Past, present, and future," in Electrical Machines (ICEM), 2016 XXII International Conference on. IEEE, 2016, pp. 640-646.

[2] F. Diaz-Gonzalez, M. Hau, A. Sumper, and O. Gomis-Bellmunt, "Partcipation of wind power plants in system frequency control: Review of grid code requirements and control methods, "Renewable and Sustainable Energy Reviews, vol. 34, pp. 551-564, 2014.

[3] C. E. O. H. ENTSO-E, "P1-policy 1: Load-frequency control and performance," 2009.

[4] E. Orum, M. Kuivaniemi, M. Laasonen, A. I. Bruseth, E. A. Jansson, A. Danell, K. Elkington, and N. Modig, "Future system inertia," ENTSOE, Brussels, Tech. Rep, 2015.

[5] E. Orum, L. Haarla, M. Kuivaniemi, M. Laasonen, A. Jerk, I. Stenklv, F. Wik, K. Elkington, R. Eriksson, N. Modig, and P. Schavemaker, "Future system inertia 2, "ENTSOE, Brussels, Tech. Rep, 2018.

[6] Statnett, "Fast frequency reserves 2018 - pilot for raske frekvensreserver, https://www.statnett.no, Tech. Rep., 2018, accessed: 2019-02-15.

[7] U. Tamrakar, D. Shrestha, M. Maharjan, B. P. Bhattarai, T. M. Hansen, and R. Tonkoski, "Virtual inertia: Current trends and future directions," Applied Sciences, vol. 7, no. 7, p. 654, 2017.

[8] M. A. Torres L, L. A. Lopes, L. A. Moran T, and J. R. Espinoza C, "Self-tuning virtual synchronous machine: a control strategy for energy storage systems to support dynamic frequency control," IEEE Transactions on Energy Conversion, vol. 29, pp. 833-840, 2014.

[9] O. Mo, S. DArco, and J. A. Suul, "Evaluation of virtual synchronous machines with dynamic or quasi-stationary machine models," IEEE Transactions on Industrial Electronics, vol. 64, no. 7, pp. 5952-5962, 2017.

[10] S. DArco, J. A. Suul, and O. B. Fosso, "A virtual synchronous machine implementation for distributed control of power converters in smartgrids," Electric Power Systems Research, vol. 122, pp. 180-197, 2015.

[11] J. Alipoor, Y. Miura, and T. Ise, "Power system stabilization using virtual synchronous generator with alternating moment of inertia," IEEE Journal of Emerging and Selected Topics in Power Electronics, vol. 3, no. 2, pp. 451-458, 2015.

[12] I. Serban and C. P. Ion, "Microgrid control based on a grid-forming inverter operating as virtual synchronous generator with enhanced dynamic response capability," International Journal of Electrical Power & Energy Systems, vol. 89, pp. 94-105, 2017.

[13] J. Liu, Y. Miura, T. Iseet al., "Comparison of dynamic characteristics between virtual synchronous generator and droop control in inverter-based distributed generators," IEEE Trans. Power Electron, vol. 31, no. 5, pp. 3600-3611, 2016.

[14] K. Sakimoto, Y. Miura, and T. Ise, "Stabilization of a power system with a distributed generator by a virtual synchronous generator function," in Power Electronics and ECCE Asia (ICPE & ECCE), 2011 IEEE 8th International Conference on. IEEE, 2011, pp. 1498-1505.

[15] N. R. Ullah, T. Thiringer, and D. Karlsson, "Temporary primary frequency control support by variable speed wind turbines potential and applications," IEEE Transactions on Power Systems, vol. 23, no. 2, pp.601-612, 2008.

[16] M. Wang-Hansen, R. Josefsson, and H. Mehmedovic, "Frequency controlling wind power modeling of control strategies," IEEE Transactions on Sustainable Energy, vol. 4, no. 4, pp. 954-959, 2013.

[17] Y. Wang, G. Delille, H. Bayem, X. Guillaud, and B. Francois, "High wind power penetration in isolated power systems assessment of wind inertial and primary frequency responses," IEEE Transactions on Power Systems, vol. 28, no. 3, pp. 2412-2420, 2013.

[18] L. Wu and D. G. Infield, "Towards an assessment of power system frequency support from wind plant modeling aggregate inertial response," IEEE Transactions on Power Systems, vol. 28, no. 3, pp. 2283-2291,2013.

[19] J. Brisebois and N. Aubut, "Wind farm inertia emulation to fulfill hydro-Quebecs specific need," in Power and Energy Society General Meeting, 2011 IEEE. IEEE, 2011, pp. 1-7.

[20] N. Soni, S. Doolla, and M. C. Chandorkar, "Improvement of transient response in microgrids using virtual inertia," IEEE transactions on power delivery, vol. 28, no. 3, pp. 1830-1838, 2013.

[21] M. F. M. Arani and E. F. El-Saadany, "Implementing virtual inertia in dfig-based wind power generation," IEEE Transactions on Power Systems, vol. 28, no. 2, pp. 1373-1384, 2013.

[22] J. Zhu, C. D. Booth, G. P. Adam, A. J. Roscoe, and C. G. Bright, "Inertia emulation control strategy for vsc-hvdc transmission systems," IEEE Trans. Power Syst, vol. 28, no. 2, pp. 1277-1287, 2013.

[23] L. Zeni, A. J. Rudolph, J. Munster-Swendsen, I. Margaris, A. D. Hansen, and P. Sorensen, "Virtual inertia for variable speed wind turbines," Wind Energy, vol. 16, no. 8, pp. 1225-1239, 2013.

[24] S. Wang, J. Hu, X. Yuan, L. Sunet al., "On inertial dynamics of virtual-synchronous-controlled dfig-based wind turbines," IEEE Trans. Energy Convers, vol. 30, no. 4, pp. 1691-1702, 2015.

[25] L. Saarinen, P. Norrlund, W. Yang, and U. Lundin, "Linear synthetic inertia for improved frequency quality and reduced hydropower wear and tear," International Journal of Electrical Power & Energy Systems, vol. 98, pp. 488-495, 2018.

[26] R. Hesse, D. Turschner, and H.-P. Beck, "Micro grid stabilization using the virtual synchronous machine (visma)," in Proceedings of the International Conference on Renewable Energies and Power Quality (ICREPQ09), Valencia, Spain, 2009, pp. 15-17.

[27] H.-P. Beck and R. Hesse, "Virtual synchronous machine," in Electrical Power Quality and Utilisation, 2007. EPQU 2007. 9th International Conference on. IEEE, 2007, pp. 1-6.

[28] J. Driesen and K. Visscher, "Virtual synchronous generators, 2008," in Proceedings of the IEEE PES Meeting, pp. 20-24.

[29] K. Visscher and S. W. H. De Haan, "Virtual synchronous machines (vsgs) for frequency stabilisation in future grids with a significant share of decentralized generation," in SmartGrids for Distribution, 2008. IET-CIRED. CIRED Seminar. IET, 2008, pp. 1-4.

[30] Y. Chen, R. Hesse, D. Turschner, and H.-P. Beck, "Investigation of the virtual synchronous machine in the island mode," in Innovative Smart Grid Technologies (ISGT Europe), 2012 3rd IEEE PES International Conference and Exhibition on. IEEE, 2012, pp. 1-6.

[31] S. DArco and J. A. Suul, "Virtual synchronous machines classification of implementations and analysis of equivalence to droop controllers for microgrids," in PowerTech (POWERTECH), 2013 IEEE Grenoble. IEEE, 2013, pp. 1-7.

[32] T. I. Reigstad and K. Uhlen, "Variable speed hydropower conversion and control, "Manuscript submitted for publication.

[33] T. I. Reigstad and K. Uhlen, "Modelling of variable speed hydro power for grid integration studies, " Manuscript submitted for publication.

Paper IV

Variable Speed Hydropower Plant with Virtual Inertia Control for Provision of Fast Frequency Reserves

VARIABLE SPEED HYDROPOWER PLANT WITH VIRTUAL INERTIA CONTROL FOR PROVISION OF FAST FREQUENCY RESERVES

Abstract

Variable Speed Hydropower (VSHP) is well suited for Virtual Inertia (VI) control since it can utilise the kinetic energy of the turbine and generator to provide a fast power response to a frequency deviation. Moreover, governor control of the turbine can effectively regain the optimal turbine rotational speed. Despite this advantage, no investigation into different VI control structures for VSHP has previously been performed. In this paper, the results of dynamic simulations and eigenvalue analysis show that all five tested control structures deliver fast power reserves to maintain grid stability. The VI controllers based on the Virtual Synchronous Machine (VSM) algorithm provide the best response in terms of inertia; however, a proportional controller must be added to also provide Frequency Containment Reserves (FCR). The Virtual Synchronous Generator (VSG) is concluded to be the overall best alternative. It is better at reducing frequency deviations, it provides Fast Frequency Reserves (FFR) and contributes more effectively to power oscillation damping in the two-area power system. The behaviour of the hydraulic system is similar for all VI control structures. However, a more advanced control system is needed to optimise the internal control of the VSHP plant while considering the constraints of the hydraulic system.

Keywords

Virtual Inertia, Synthetic Inertia, Virtual Synchronous Generator, Virtual Synchronous Machine, Variable Speed Hydropower

1. Introduction

The increasing share of variable and less controllable renewable energy demands the introduction of new flexible producers and consumers to ensure the balance of the power grids. In the Nordic power system, large hydro and thermal power plants have until recently supplied inertia and power-frequency control. The introduction of wind, solar and HVDC connections to Europe creates new production scenarios where the inertia in the grid is very low. This compromises the frequency stability as the inverter-based generation does not provide any response to frequency deviations unless it is implemented in the controls, e.g. as Virtual Inertia (VI) control. The goal of VI is to control the converters to increase the effective inertia in the grid.

In this paper, we investigate the use of Variable Speed Hydropower (VSHP) to provide Fast Frequency Reserves (FFR) and VI to the grid. These are ancillary services that are or will be demanded to improve balancing control and frequency stability. One of the challenges is that these services require very fast controlled responses to frequency deviations - with the typical activation time of within $1s$. Since the system inertia reduces as the share of converter-interfaced generation increases, the utilisation of VI may be essential for the green shift.

The ancillary services related to power balancing control and reserves are often divided into four levels as in [1], each of them necessary for maintaining the balance between power generation and power consumption and thereby ensuring that the frequency is kept within the limits given by the grid codes. The fastest power reserves are the instantaneous power reserves, also called inertia. These are generated by the physical stabilising effect of all the grid-connected synchronous machines due to the energy in the rotating masses in turbines and generators. The Frequency Containment Reserves (FCR) or primary control should be fully activated within $30s$ in the Nordic grid. The FCR is locally activated and implemented as part of the governor control of turbines with a frequency droop characteristic. There are two levels of FCR in the Nordic grid; FCR-N is activated at frequency deviations $\pm 0.1Hz$ while FCR-D is activated at $49.9Hz$ and fully activated at $49.5Hz$. The two slowest levels of power reserves, secondary and tertiary reserves, are not considered in this paper.

A report from the Nordic Transmission System Operators (TSOs) [2] states that Fast Frequency Reserves (FFR) is the best technical and economical solution to improve frequency stability [3].

This assumes the FFR is activated at $49.60Hz$, reaches the full value within $2s$, and holds this value for at least $30s$. A market for offering FFR has been tested in a pilot project in Norway; however, offers from hydropower plants with Pelton and Francis turbines were found to be too slow to deliver the power step within $2s$.

The use of VSHP plants is attractive because of their higher efficiency at lower production levels than conventional hydropower plants and their ability to control power in pumping modes while keeping the efficiency at an acceptable level [4]. Moreover, the converter technology of the VSHP can improve the speed of the voltage control and potentially increase the reactive power capability. The drawbacks are the power losses of the converters, increased costs and the reduced reliability if bypassing the converters is impossible. The limited short circuit current of the converters may also cause challenges for the generator and grid protection.

VSHP plants are particularly well suited for VI control since the rotational energy of the turbine and generator can be utilised by allowing the rotational speed to vary. Following an activation of VI, the guide vane opening, water flow and, consequently, the mechanical power, can be effectively controlled to regain the rotational speed to the optimal setpoint. Although VSHP has better qualifications than other sources of VI, the research on VSHP with VI is limited. Alternative solutions, such as from Photovoltaic systems (PV) and wind power plants have their limitations. PV systems lacks energy storage if not integrated with batteries. The kinetic energy of wind turbine rotors can be utilized but the rotational speed [5,6] must be regained by reducing the power output, which may cause a second drop in the frequency. Wind turbines are therefore best suited for power-frequency response-based control with temporary grid support [7]. Other possibilities investigated in the literature are to provide VI from battery energy storages [8] and through HVDC-links [9].

Different VI controllers are reviewed in [10] and divided into three categories. The simplest type is the frequency-response based models where the power is controlled proportionally to the frequency deviation and/or the rate of change of frequency [11]. Other models emulate a synchronous machine by use of a machine model and are therefore referred to as synchronous generator-based models. They might contain models of inertia, damping and voltage [12]. The swing-equation models are similar to the synchronous generator-based models; however, they are based on a simpler power-frequency swing equation [13].

This paper investigates the instantaneous and primary power reserves of a VSHP and aims

to find the best-suited control scheme for VSHP considering the defined control objectives. The implementation of known VI control structures on VSHP is investigated, and these are further developed in order to improve their contribution of FFR. Eigenvalue analysis shows the impact of the VI control on the power oscillation modes while the dynamic analysis shows the reduction for the maximum frequency deviation and the effect on the hydraulic system of the VSHP.

The paper is outlined as follows: The VI models and the VSHP and grid models are presented in, respectively, Sections 2 and 3. The dynamic analysis results and discussion are given in Section 4. Section 5 presents the results and discussion from the eigenvalue analysis. Finally, some conclusions are offered in Section 6.

2. Virtual Inertia Models

2.1. Control Objectives

The control objectives for a VSHP are divided into objectives for internal control and grid support:

- Objectives for internal control of the plant:
  - To optimise the rotational speed of the turbine with respect to the efficiency;
  - to minimise water hammering and mass oscillations;
  - to minimise guide vane servo operation;
  - and to minimise the hydraulic and electric losses.
- Objectives for grid support control:
  - Contribute to FCR by faster and more precise frequency droop control;
  - contribute to increasing the effective system inertia by VI control;
  - improve the voltage control response time;
  - and increase the damping in the system.

The main focus of this paper is to maximise the grid support from the VSHP by utilising the turbine and generator rotational energy. The VI controllers should deliver VI by changing the power instantaneously to reduce the Rate of Change of Frequency (ROCOF). Moreover, the

Table 1: Parameters

Parameter	**Value**	**Parameter**	**Value**
CPC		**VSM-PD**	
Proportional gain k_{Pp}	0.045 p.u.	Proportional gain $k_{vsm-pd,p}$	100 p.u.
Integral gain k_{Pi}	0.023 p.u.	Derivative gain $k_{vsm-pd,d}$	500 p.u.
VSG		Derivative filter constant ω_{vsm-pd}	1 s
Proportional gain $k_{vsg,p}$	100 p.u.	Frequency controller gain k_{vsm-pd}	200 p.u.
Derivative gain $k_{vsg,d}$	33.6 p.u.	**VSG-PID**	
Derivative filter constant ω_{vsg}	0.01 p.u.	Proportional gain $k_{vsg-pid,p}$	100 p.u.
VSM-PID		Integral gain $k_{vsg-pid,i}$	286 p.u.
Proportional gain $k_{vsm-pid,p}$	3000 p.u.	Derivative gain $k_{vsg-pid,d}$	33.6 p.u.
Integral gain $k_{vsm-pid,i}$	476 p.u.	Derivative filter cons. ω_{vsg-pd}	0.01 s
Derivative gain $k_{vsm-pid,d}$	12600 p.u.	**Common parameters**	
Derivative filter const. $\omega_{vsm-pid}$	1 s	Droop R_d	0.01 p.u.
Frequency contr. gain $k_{vsm-pid}$	2000 p.u.	PLL frequency filter constant	0.001 s

VI controller will contribute with primary reserves/FCR to regain the grid frequency as fast as possible after a disturbance.

This section presents five different VI control structures. The power-frequency PD controller known as Virtual Synchronous Generator (VSG) [14] and the Virtual Synchronous Machine (VSM) [15, 16] are known from the literature. The other three structures are extended versions of the ones presented in this paper; Power-frequency PID controller with permanent droop (VSG-PID), VSM with power-frequency PD controller (VSM-PD), and VSM with power-frequency PID controller and permanent droop (VSM-PID). The parameters are given in Table 1.

2.2. Virtual Synchronous Generator

The VSG is a power-frequency response based VI system. It tries to emulate the inertial response characteristics of a synchronous generator simply, without incorporating all the detailed equations involved in a synchronous generator. A PD controller calculates the current reference in the d-axis, $i^*_{g,d}$ from the deviation in grid frequency $\Delta\omega_g$ as shown in (1). The power reference p^*_g is added to achieve the desired VSG output power P_{vsg} at zero frequency deviation and the controller compensates for deviations in voltage ($v_{c,d}$, $v_{c,q}$ and for reactive power q delivery [10].

$$\begin{aligned} p_{vsg} &= k_{vsg,p}\Delta\omega_g + \frac{k_{vsg,d}\omega_{vsg}s}{s+\omega_{vsg}}\Delta\omega_g + p^*_g \\ \Delta\omega_g &= \omega^*_g - \omega_g \\ i^*_{g,d} &= \frac{v_{c,d}p_{vsg} - v_{c,q}q_g}{v^2_{c,d} + v^2_{c,q}} \end{aligned} \tag{1}$$

The VSG is current-controlled and unable to operate in an islanded system. Over-current protection is easily implemented; however, multiple units as current sources and the use of Phase-Locked Loop (PLL) may result in instability.

2.3. Power-Frequency PID Controller with Permanent Droop

An alternative control layout for the VSG with PID controller and permanent droop R (VSG-PID) is shown in (2) to calculate the VSG-PID output power $P_{vsg-pid}$. The benefit of the PID controller is that it can be tuned to be somewhat faster than the PD controller. Due to the integration part, the permanent droop is needed to ensure power-sharing between generators as seen with conventional power plants.

$$\begin{aligned} p_{vsg-pid} &= k_{vsg-pid,p}\epsilon + \frac{k_{vsg-pid,d}\omega_{vsg-pid}s}{s+\omega_{vsg-pid}}\epsilon + \frac{k_{vsg-pid,i}}{s}\epsilon + p^*_g \\ \epsilon &= \omega^*_g - \omega_g - Rp_f \\ i^*_{g,d} &= \frac{v_{c,d}p_{vsg-pid} - v_{c,q}q_g}{v^2_{c,d} + v^2_{c,q}} \end{aligned} \tag{2}$$

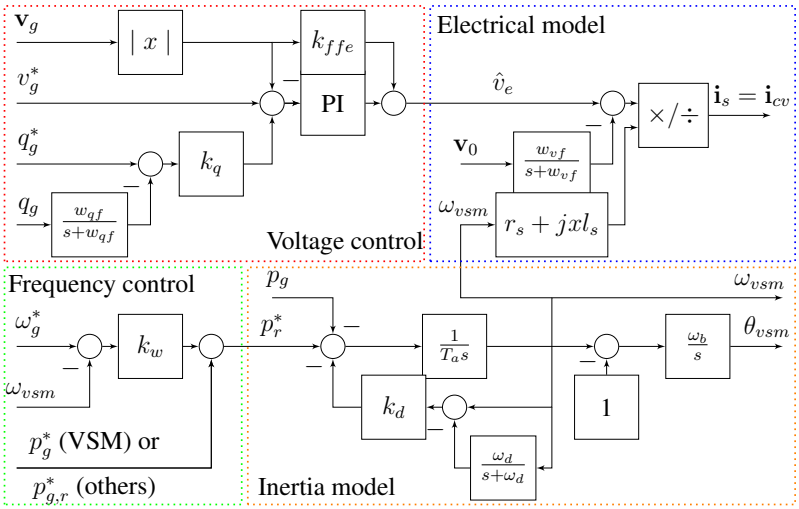

Figure 1: Virtual synchronous machine (VSM)

2.4. Virtual Synchronous Machines

The VSM is a synchronous generator-based VI model. In this paper, the model presented in [16], with equal variables and parameters, is utilised. It includes models for voltage control, frequency control and a model for inertia and the electrical system, as shown in Fig. 1. The main benefit of the VSM is that it can work in islanded systems without changing parameters and control structure [17, 18].

2.5. VSM with Power-Frequency PD Controller

The main drawback with the VSM is that its output power does return relatively quickly to the reference power, even if there are still deviations in the grid frequency. It does not, therefore, contribute to primary control/FRC. This problem can be solved by combining the VSM with other frequency-regulation schemes. The first option to be tested is to add the output power reference from a power-frequency PD controller to the VSM power reference $p_{g,r}^*$, as presented in (3). Both a deviation and a change in grid frequency will adjust the output to the VSM p_{vsm-pd}. A PLL is used to measure the grid frequency ω_g.

$$
\begin{aligned}
p_r^* &= p_g^* + k_\omega \left(\omega_{vsm}^* - \omega_{vsm}\right) + p_{vsm-pd} \\
p_{vsm-pd} &= k_{vsm-pd,p}\Delta\omega_g + \frac{k_{vsm-pd,d}\omega_{vsm-pd}s}{s+\omega_{vsm-pd}}\Delta\omega_g \\
\Delta\omega_g &= \omega_g^* - \omega_g
\end{aligned}
\tag{3}
$$

2.6. VSM with Power-Frequency PID Controller and Permanent Droop

Frequency control can alternatively be added to the VSM by including a PID controller with permanent droop, as presented in (4). The output of this controller p_{vsm-pd} is added to the VSM power reference $p_{g,r}^*$. The function of the PID controller will be similar to the function of the governor of a conventional hydropower plant. However, since the speed of the governor servo is not limiting, the frequency response of the VSM-PID will be significantly faster primary frequency control.

$$
\begin{aligned}
p_r^* &= p_g^* + k_\omega \left(\omega_{vsm}^* - \omega_{vsm}\right) + p_{vsm-pid} \\
p_{vsm-pid} &= k_{vsm-pid,p}\epsilon + \frac{k_{vsm-pid,d}\omega_{vsm-pid}s}{s+\omega_{vsm-pid}}\epsilon + \frac{k_{vsm-pid,i}}{s}\epsilon \\
\epsilon &= \omega_g^* - \omega_g - Rp_f
\end{aligned}
\tag{4}
$$

p_f is the low-pass filtered active output power p_g.

3. Variable Speed Hydropower and Grid Models

The VI controllers are tested on the VSHP model provided in [19, 20] connected to the Kundur two-area power system [21], as shown in Fig. 2. The VI is implemented as the outer control loop of the grid converter. For the VSG controllers, the VSG supplies the current reference in the d-axis $i_{g,d}^*$ to the current controller to control active power, while the reactive power is controlled by a conventional voltage controller. For the VSM controllers, both the active and reactive power is controlled by the VSM model.

4. Dynamic Analysis

The performance of the different control schemes is first analysed by dynamic simulations, both in cases with overproduction and underproduction in the grid. In Fig. 3, the responses to step load

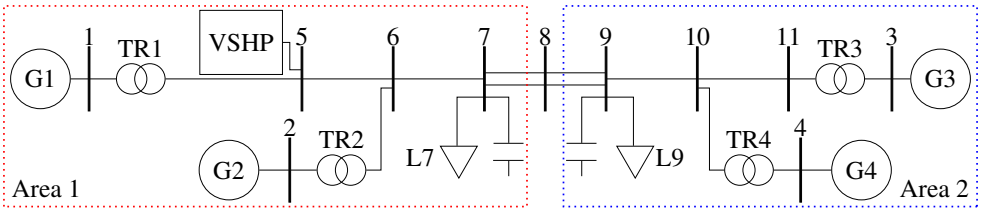

Figure 2: Kundur two-area system

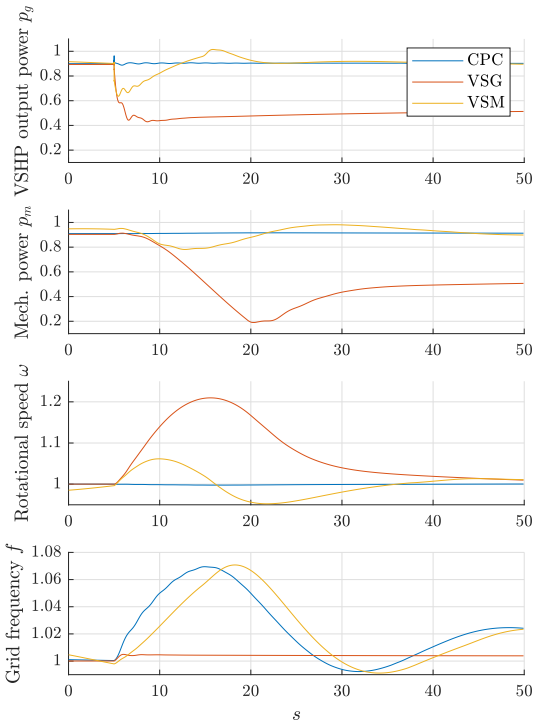

Figure 3: Responses to a load step change on Bus 7 for different VSHP control schemes

loss at Bus 7 are shown. The responses illustrate the difference between three different control schemes for power control of the grid-connected converter; the Constant Power Controller (CPC) that do not provide any frequency droop control, the VSM that provides an inertial response, and the VSG, providing both inertial response and frequency containment.

The VSG contributes with FCR since the droop characteristic of the VSG controller will cause the output power to stabilise at a lower value after the disturbance. With the VSM controller,

the output power returns to its reference value since it has zero steady-state feedback from grid frequency. The maximal frequency deviation will be similar, or even higher, than with the CPC. The performance of the VSM can be improved by controlling the power reference to the VSM with a PD controller with feedback from grid frequency (VSM-PD) or a PID controller with permanent frequency droop (VSM-PID).

Fig. 4 shows the results for both the electric and hydraulic variables of the four most promising controllers, the VSG, VSG-PID, VSM-PD and VSM-PID. The main observation is that the VSG and the VSG-PID have the shortest response time and can reduce the maximum deviation in grid frequency f. This is due to a larger power reduction of the VSHP output power p_g with VSG-based inertia controllers compared to the VSM-based inertia controllers from $1 - 10s$ after the disturbance.

The oscillation in VSHP output power p_g is somewhat larger for the VSG-based inertia; however, they are small and well-damped. As seen in Fig. 4, the variables of the hydraulic system are mostly unaffected by the choice of VI controllers. The VSM-PC controller stands out because of its slower reaction to grid frequency deviations. The reduction in VSHP output power p_g is less, causing less deviations in turbine rotational speed ω, turbine power p_m, guide vane opening g and thereby turbine flow q and surge tank head h_{st}.

Two cases with load loss at different locations are compared in Fig. 5, showing the first $25s$ after the load loss and Fig. 6 is focused upon for the first $2s$ to show the difference in inertia response. The sizes of the load losses are similar and they are located, respectively, close to the VSHP (Bus 7 in Area 1) and far away from the VSHP (Bus 9 in Area 2).

From Fig. 6, we observe that the output power of the VSM-based VI controllers has the fastest response in the first milliseconds after the disturbance when the load loss is close to the VSHP. They, therefore, deliver more inertia than the VSG controllers. However, when the load loss appears at Bus 9 farther away from the VSHP, the situation is totally different, as discussed below.

Since most of the FRC is delivered by the VSHP, the power from Area 1 to Area 2 will decrease in the case of load loss in Area 2 and trigger power oscillations between the two areas. Due to these power oscillations, there will be higher oscillations in both the output power of the VSG- and VSM-based VI controllers when the load loss is far away from the VSHP. This is related to inter-area power oscillation between the two areas of the system, as also observed in the nearby

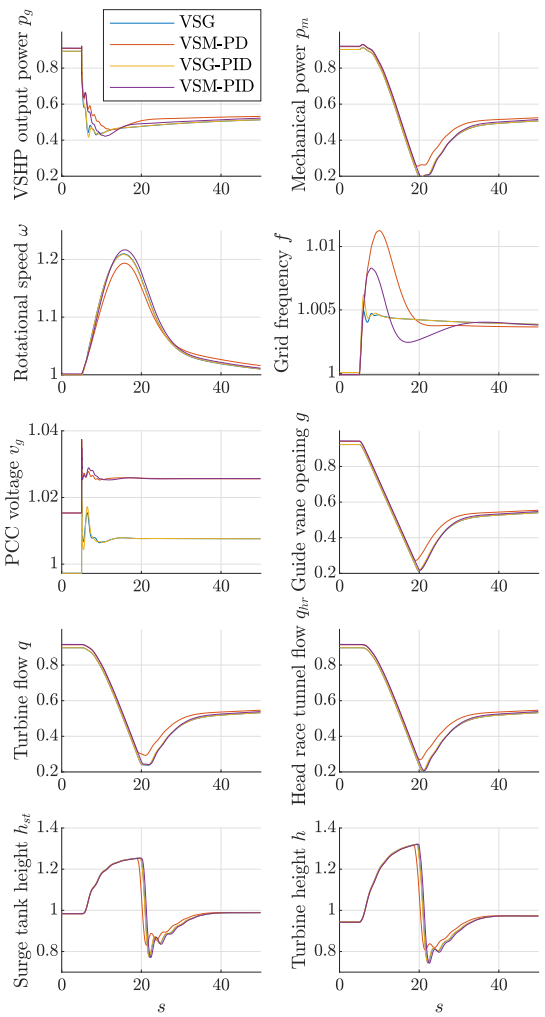

Figure 4: Responses to a load step change on Bus 7 for different VSHP control schemes

generators. In particular, these power oscillations affect the VSM-based VI controllers since they are dependent on the voltage angle. In the case of load loss at Bus 9, the power output of the VSM-based VI controllers actually increases immediately after the load loss, causing a higher deviation in grid frequency f. The dependence on the voltage seems to be a major disadvantage by emulating a synchronous machine, and the use of VSM might cause problems in a system with large power oscillations.

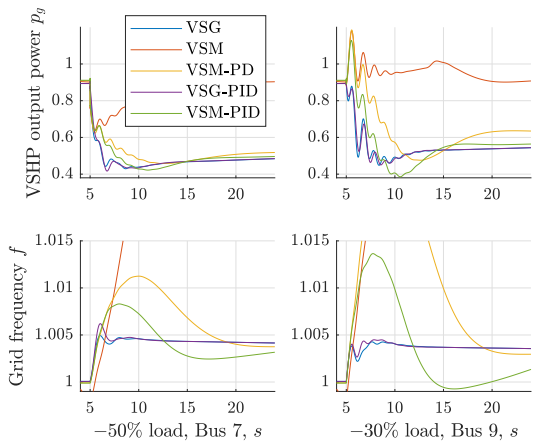

Figure 5: Responses to a load step change at, respectively, 50% on Bus 7 and 30% on Bus 9

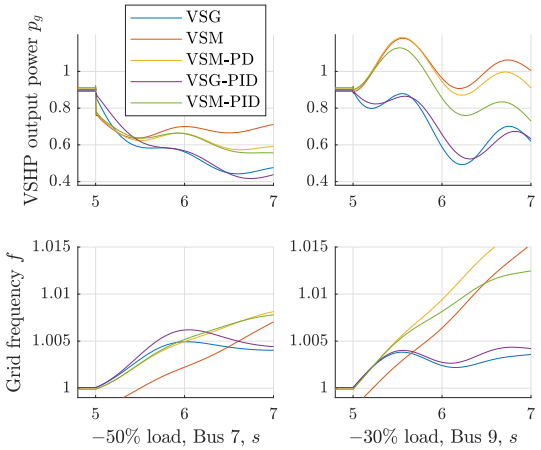

Figure 6: Responses to a load step change at, respectively, 50% on Bus 7 and 30% on Bus 9

The VSG-based VI controllers only consider the frequency, and not the angle, when controlling the VSHP output power. Therefore, the power oscillation will have less impact, and the response to a load loss in Area 2 will be almost as fast as if the load loss occurred in Area 1, albeit with more oscillations. Moreover, the VSG-based VI controllers reduce the frequency deviation by a larger reduction in VSHP output power between $1 - 3s$ after the load loss.

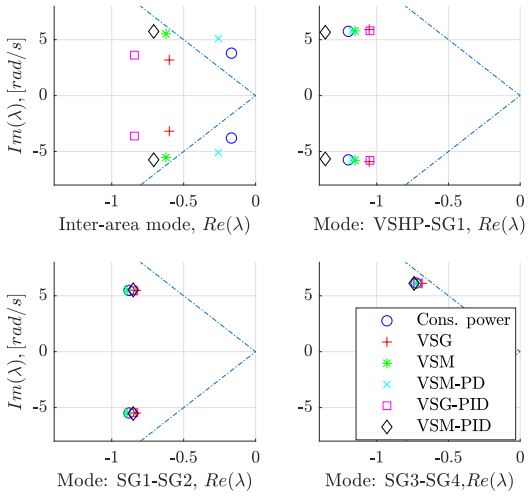

Figure 7: Power oscillation modes for different VSHP control schemes

5. Eigenvalue Analysis

In this chapter, the most important results from the eigenvalue analysis are presented. In the Kundur Two-Area system, an interarea mode exists between Area 1 and Area 2 and a local mode in each area, between, respectively, SG1-SG2 and SG3-SG4. As the VSHP is connected on Bus 5, close to SG1, a new local mode appears between the VSHP and SG1. Fig. 7 shows these four modes for the different control schemes of the VSHP.

The inter-area mode is the mode most dependent on the VSHP control scheme. Compared to the case with constant power control, the modes of the VSM and its variants have a higher frequency and higher relative damping. The damping of this mode for the VSM-PD is still poor. The relative damping of the inter-area mode is doubled when the VSG control of the VSHP is introduced. In addition, the frequency of the oscillation is reduced. The relative damping is slightly better for the VSG-PID than for the VSG.

The relative damping of the mode between the VSHP and SG1 is slightly better for the VSM-based control schemes than the VSG-based control schemes. The local modes between the generators are more or less independent of the VSHP control scheme.

6. Conclusion

Two VI controllers, the VSG and the VSM, have been further developed in this paper to increase the contribution of instantaneous and primarily frequency resources, which are the main objectives for grid support control. At the same time, the objectives of internal control of the VSHP have to be considered in order to limit water hammering, mass oscillations and guide vane operation and to ensure that the turbine rotational speed is regained within an acceptable time.

The VSM topology shows the fastest response when simulating a disturbance and thus delivers the best inertial response. However, since it has zero steady-state feedback from grid frequency, the output power returns to its reference value, and the VSM is not contributing to the frequency control. Frequency control is added by controlling the power reference to the VSM with a PD controller with feedback from grid frequency (VSM-PD) or a PID controller with permanent frequency droop (VSM-PID).

The VSG-based control structures do not have an instantaneous response to the load loss; however, the power response is larger from $200ms$ to $5s$ after the disturbance. In addition, the VSG-based controllers damp oscillations against other generators more effectively, resulting in lower frequency deviation.

Although the VSM controller shows the fastest response during the first $200ms$ after a disturbance, the VSG controller provides better frequency regulation for the next $5s$. In cases where the disturbance is far away from the VSHP, the performance of the VSM controller is reduced, and the VSG performs more effectively regarding the instantaneous power response and permanent frequency droop control.

The dynamic analysis clearly shows that the VSG has the best performance from a grid-integration point of view. However, since the VSM controller is based on emulating the response of a synchronous generator, the PLL is not needed. This makes the VSM capable of working in islanded systems without changing parameters and control structure.

The transient behaviour of the hydraulic system is more or less equal for the VSG, VSG-PID and VSM-PID. The VSHP output power response of the VSM-PD is marginally smaller, causing smaller deviations in the hydraulic system variables.

References

[1] C. E. O. H. ENTSO-E, "P1-policy 1: Load-frequency control and performance," 2009.

[2] E. Ørum, L. Haarla, M. Kuivaniemi, M. Laasonen, A. Jerkø, I. Stenkløv, F. Wik, K. Elkington, R. Eriksson, N. Modig, and P. Schavemaker, "Future system inertia 2," *ENTSOE, Brussels, Tech. Rep*, 2018.

[3] Statnett, "Fast frequency reserves 2018," https://www.statnett.no/globalassets/for-aktorer-i-kraftsystemet/utvikling-av-kraftsystemet/nordisk-frekvensstabilitet/fast-frequency-reserves-pilot-2018.pdf, Tech. Rep., 2018, accessed: 2020-08-19.

[4] M. Valavi and A. Nysveen, "Variable-speed operation of hydropower plants: Past, present, and future," in *Electrical Machines (ICEM), 2016 XXII International Conference on*. IEEE, 2016, pp. 640–646.

[5] W. Bao, Q. Wu, L. Ding, S. Huang, F. Teng, and V. Terzija, "Synthetic inertial control of wind farm with bess based on model predictive control," *IET Renewable Power Generation*, 2020.

[6] A. Gloe, C. Jauch, B. Craciun, and J. Winkelmann, "Continuous provision of synthetic inertia with wind turbines: implications for the wind turbine and for the grid," *IET Renewable Power Generation*, vol. 13, no. 5, pp. 668–675, 2019.

[7] L. Saarinen, P. Norrlund, W. Yang, and U. Lundin, "Linear synthetic inertia for improved frequency quality and reduced hydropower wear and tear," *International Journal of Electrical Power & Energy Systems*, vol. 98, pp. 488–495, 2018.

[8] L. Toma, M. Sanduleac, S. A. Baltac, F. Arrigo, A. Mazza, E. Bompard, A. Musa, and A. Monti, "On the virtual inertia provision by bess in low inertia power systems," in *2018 IEEE International Energy Conference (ENERGYCON)*. IEEE, 2018, pp. 1–6.

[9] S. D'Arco, T. T. Nguyen, and J. A. Suul, "Evaluation of virtual inertia control strategies for mmc-based hvdc terminals by p-hil experiments," in *IECON 2019-45th Annual Conference of the IEEE Industrial Electronics Society*, vol. 1. IEEE, 2019, pp. 4811–4818.

[10] U. Tamrakar, D. Shrestha, M. Maharjan, B. P. Bhattarai, T. M. Hansen, and R. Tonkoski, "Virtual inertia: Current trends and future directions," *Applied Sciences*, vol. 7, no. 7, p. 654, 2017.

[11] N. R. Ullah, T. Thiringer, and D. Karlsson, "Temporary primary frequency control support by variable speed wind turbines—potential and applications," *IEEE Transactions on Power Systems*, vol. 23, no. 2, pp. 601–612, 2008.

[12] M. A. Torres L, L. A. Lopes, L. A. Moran T, and J. R. Espinoza C, "Self-tuning virtual synchronous machine: a control strategy for energy storage systems to support dynamic frequency control," *IEEE Transactions on Energy Conversion*, vol. 29, pp. 833–840, 2014.

[13] K. Sakimoto, Y. Miura, and T. Ise, "Stabilization of a power system with a distributed generator by a virtual synchronous generator function," in *Power Electronics and ECCE Asia (ICPE & ECCE), 2011 IEEE 8th International Conference on*. IEEE, 2011, pp. 1498–1505.

[14] M. Van Wesenbeeck, S. De Haan, P. Varela, and K. Visscher, "Grid tied converter with virtual kinetic storage," in *PowerTech, 2009 IEEE Bucharest*. IEEE, 2009, pp. 1–7.

[15] R. Hesse, D. Turschner, and H.-P. Beck, "Micro grid stabilization using the virtual synchronous machine (visma)," in *Proceedings of the International Conference on Renewable Energies and Power Quality (ICREPQ'09), Valencia, Spain*, 2009, pp. 15–17.

[16] O. Mo, S. D'Arco, and J. A. Suul, "Evaluation of virtual synchronous machines with dynamic or quasi-stationary machine models," *IEEE Transactions on Industrial Electronics*, vol. 64, no. 7, pp. 5952–5962, 2017.

[17] H.-P. Beck and R. Hesse, "Virtual synchronous machine," in *Electrical Power Quality and Utilisation, 2007. EPQU 2007. 9th International Conference on*. IEEE, 2007, pp. 1–6.

[18] J. Driesen and K. Visscher, "Virtual synchronous generators, 2008," in *Proceedings of the IEEE PES Meeting*, pp. 20–24.

[19] T. I. Reigstad and K. Uhlen, "Variable speed hydropower conversion and control," *IEEE Transactions on Energy Conversion*, vol. 35, no. 1, pp. 386–393, March 2020.

[20] T. I. Reigstad and K. Uhlen, "Modelling of Variable Speed Hydropower for Grid Integration Studies," *arXiv e-prints*, p. arXiv:2003.06298, Mar. 2020.

[21] P. Kundur, N. J. Balu, and M. G. Lauby, *Power system stability and control*. McGraw-hill New York, 1994, vol. 7.

Paper V

Optimized Control of Variable Speed Hydropower for Provision of Fast Frequency Reserves

Optimized Control of Variable Speed Hydropower for Provision of Fast Frequency Reserves

Tor Inge Reigstad
Kjetil Uhlen
Department for Electric Power Engineering
Norwegian University of Science and Technology (NTNU)
Trondheim, Norway
{tor.inge.reigstad, kjetil.uhlen}@ntnu.no

***Abstract*—This paper deals with the design of controllers for variable speed hydropower (VSHP) plants with the objective of optimize the plants' performance. The control objectives imply enabling fast responses to frequency deviations while keeping the electric and hydraulic variables within their constraints. A model predictive controller (MPC) was developed to coordinate the turbine controller with the virtual synchronous generator (VSG) control of the power electronics converter. The simulation results show that the VSG is able to deliver fast power responses by utilizing the rotational energy of the turbine and the generator. The MPC controls the guide vane opening of the turbine to regain the nominal turbine rotational speed. If this is not possible due to the constraints of the hydraulic system, the MPC adjusts the power output of the VSHP by changing the VSG power reference. The proposed control system allows the VSHP to provide fast frequency reserves (FFR).**

***Index Terms*—Fast frequency response, frequency control, model predictive control, variable speed hydropower, virtual synchronous generator**

I. Introduction

Variable speed operation of hydropower plants is currently being investigated, and is motivated by several factors. One key factor is the potential for providing ancillary services, such as fast frequency reserves (FFR). More renewables like wind and solar energy increase the need for flexible production and loads to balance the grid and maintain the power system security. Variable speed hydropower (VSHP) may provide this flexibility with virtual inertia (VI) control by utilizing the rotational energy of the turbine and the generator, both in production and in pumping mode. Challenges and opportunities for VSHP are further explained in [1]. The hypothesis is that the VSHP can offer additional ancillary services, contributing to improving frequency control and maintaining grid stability, thus allowing for higher penetration of variable renewables in the grid. Complete utilization of this potential comprises the development of an advanced control system optimizing the operation of the power plant while considering the constraints in the electric and the hydraulic systems. This can be achieved by combining VI control for improving the power response to frequency deviations with model predictive control (MPC) for handling the internal control of the VSHP.

Research on the use of MPC for control of hydropower plants and frequency control is limited, however, both locally and centralized based MPCs are used for this purpose. In [2], a local MPC controller is used for hydro turbine governor control in a conventional power plant. The Francis turbine is represented by a linearized hygov-model, the guide vane opening speed is limited and generalized predictive control is used to solve the optimization problem. MPC is also used for frequency control as in [3]. A bat-inspired algorithm is utilized to optimize the MPC design for load frequency control of superconducting magnetic storage and capacitive energy storage.

A centralized MPC considering limitations on tie-line power flow, generation capacity, and generation rate of change is studied for load frequency control in [4]–[6], applying both linear and nonlinear MPC. MPC can also be used to damp oscillations in the AC system by minimizing the generators' frequency deviation from the average system frequency by a global MPC-based grid control [7]–[10]. This control layout can be modified to also control voltage and ensure voltage stability [11].

A PID controller is utilized to control the guide vane opening of a VSHP in [12] while virtual inertia control methods for VSHP are investigated in [13]. The internal control of the VSHP and the virtual inertia control is not coordinated and a more advanced controls system is needed to ensure that the power response of the virtual control will not cause problems for the internal control of the power plant. In this paper, the VSHP control is improved by proposing a new control scheme: MPC and virtual synchronous generator (VSG) control are combined to optimize the frequency response of the power plant while keeping the electric and hydraulic variables within their limits. While a conventional hydropower plant has a direct relation between guide vane opening reference g^*, guide vane opening g, mechanical power P_m, electrical power P_e, frequency f and turbine rotational speed ω as shown in Figure 1, the VSHP enables one more degree of freedom to control power and speed. The proposed control scheme utilizes the VSHP output power P_g to control the frequency f while

This work was supported by the Research Council of Norway under Grant 257588 and by the Norwegian Research Centre for Hydropower Technology (HydroCen).

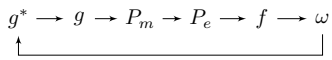

Fig. 1: Control layout of conventional hydropower plant

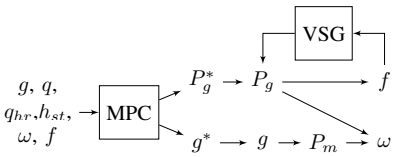

Fig. 2: Control layout of VSHP plant with MPC control

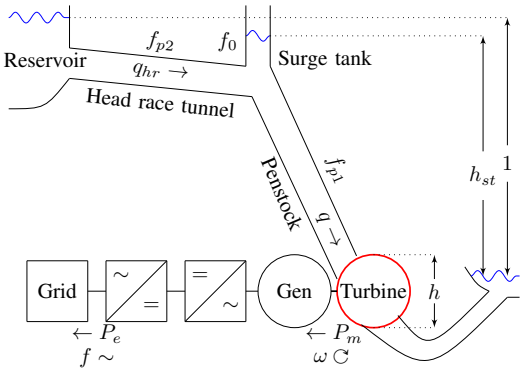

Fig. 3: Waterway layout

the guide vane opening reference g^* and the VSHP output power reference P_g^* control the turbine rotational speed ω, as indicated in Figure 2. There is still a direct relationship between the VSHP output power P_g and the frequency since the VSG controls P_g with the frequency as input. However, the turbine rotational speed and the frequency are disengaged in this case. This allows for quicker changes of the VSHP output power by utilizing the rotational energy of the turbine and generator compared to a conventional power plant where the slow governor will limit the ancillary service capabilities. With that, new possibilities emerges as faster frequency control and other grid ancillary service, but it also necessitates proper coordination of the controls - and there will be new constraints that must be taken into account.

This paper is organized as follows: The MPC theory and the control objectives for the MPC controller are presented in Section II while the development of the MPC model and Kalman filter are presented in, respectively, Sections III and IV. The results and discussions are given in Section V and the conclusion in Section VI.

II. Model Predictive Control

MPC controllers offer great advantages compared to transitionally PID controllers, although they are more complex. They are multiple-input, multiple-output (MIMO) controllers, they offer a faster and smoother response and lower rising time, settling time and overshoots compared to PID controllers and they are more robust. While the PID controller is a linear controller, MPC can handle non-linear systems as power electronics. However, a proper system model is needed for the design of the MPC controller.

MPC is a closed-loop optimization problem where a discrete-time model is optimized on a time horizon from $t = 0$ to $t = N$. Only the inputs for the first time step are used and the optimization problem is recalculated for the next time step, with the new initial state values.

A linear MPC model with quadratic objective function and linear constraints called an output feedback linear MPC [14], is used in this paper. The model (1)-(3) includes cost for the error of state/variables values, changes in state values, the error of input values, changes in input values and cost for exceeding the constraints on the states with the use of slack variables.

$$\begin{aligned}\min_{x\in\mathbb{R}^n, u\in\mathbb{R}^m} f(x,u) = \sum_{t=0}^{N-1} &\frac{1}{2}x_{t+1}^{\mathrm{T}} Q_{t+1} x_{t+1} \\ &+ d_{xt+1}x_{t+1} + \frac{1}{2}\Delta x_{t+1}^{\mathrm{T}} Q_{\Delta t}\Delta x_{t+1} + \frac{1}{2}u_t^{\mathrm{T}} R_t u_t \\ &+ d_{ut}u_t + \frac{1}{2}\Delta u_t^{\mathrm{T}} R_{\Delta t}\Delta u_t + \rho^{\mathrm{T}}\epsilon + \frac{1}{2}\epsilon^{\mathrm{T}} S\epsilon \end{aligned} \quad (1)$$

subjected to

$$\begin{aligned} x_{t+1} &= A_t x_t + B_t u_t && t = 0,\dots,N-1 \\ x_0, u_{-1} &= \text{given} \\ x^{\text{low}} - \epsilon &\le x_t \le x^{\text{high}} + \epsilon && t = 1,\dots,N \\ -\Delta x^{\text{high}} &\le \Delta x_t \le \Delta x^{\text{high}} && t = 1,\dots,N \\ A_{ineq}x_t + B_{ineq}u_t &\le b_{ineq} && t = 1,\dots,N \\ u^{\text{low}} &\le u_t \le u^{\text{high}} && t = 0,\dots,N-1 \\ -\Delta u^{\text{high}} &\le \Delta u_t \le \Delta u^{\text{high}} && t = 0,\dots,N-1 \end{aligned} \quad (2)$$

where

$$\begin{aligned} Q_t &\succeq 0 && t = 1,\dots,N \\ Q_{\Delta t} &\succeq 0 && t = 1,\dots,N \\ R_t &\succeq 0 && t = 0,\dots,N-1 \\ R_{\Delta t} &\succeq 0 && t = 0,\dots,N-1 \\ \Delta x_t &= x_t - x_{t-1} && t = 1,\dots,N \\ \Delta u_t &= u_t - u_{t-1} && t = 0,\dots,N-1 \\ z^{\mathrm{T}} &= \left(x_1^{\mathrm{T}},\dots,x_N^{\mathrm{T}},u_0^{\mathrm{T}},\dots,u_{N-1}^{\mathrm{T}}\right) \\ \epsilon &\in \mathbb{R}_x^n \ge 0 \\ \rho &\in \mathbb{R}_x^n \ge 0 \\ S &\in \text{diag}\left\{s_1,\dots,s_{n_x}\right\}, s_i \ge 0, \quad i = \{1,\dots,n_x\} \end{aligned} \quad (3)$$

The optimization problem is solved by the `quadprog` function in MATLAB.

A. Control Objectives for the MPC Controller

The MPC controller solves the optimization problem to find the optimal inputs u; the power reference P_g^* and the guide vane reference g^*, while handling all constraints defined in the MPC model. The main tasks of the MPC in this paper are:

- Primary frequency control:
  - Provide power reference P_g^* to the VSG.
  - Minimize deviation in grid frequency Δf.
  - Keep the converter power P_g within its limits.
- Hydraulic system control:
  - Provide guide vane reference g^* to the turbine.
  - Minimize the operation of guide vane opening g to reduce wear and tear.
  - Minimize the rate of change of g to reduce water hammering and mass oscillation.
  - Keep the surge tank level h_{st} within its limit and close to the stationary value.
  - Keep the water flow q above its minimum level.
  - Optimize the rotational speed of the turbine ω.
- Turbine speed control:
  - Keep the rotational speed of the turbine ω within the limits and close to its optimal speed.
  - Make sure that ω will recover after a disturbance.

Other possible tasks for the MPC, not implemented in this paper, will be:

- Power oscillation damper (POD).
- Optimize the control of guide vane opening g to minimize water hammering and mass oscillation.
- Voltage control.

Some of these control objectives are conflicting. For instance, fast regulation of the guide vane opening g reduces the deviation in turbine rotational speed ω, however, this will increase the deviation in the surge tank level h_{st} and increase mass oscillation and water hammering. The cost of changing g^*, of deviations in h_{st} and of exceeding the limits of h_{st} will reduce the rate of change of g. Similarly, the cost of deviation in ω will increase the rate of change of g.

III. MPC Dynamic Model

This section presents the MPC model with its costs and constraints. Finally, linearization and discretization of the model are shown.

The step length of the MPC model is set to $\Delta t = 0.2s$ to cover the low frequency ($< 0.5Hz$) dynamics of the waterway system. An appropriate number of time steps is found to be $N = 41$, resulting in a prediction horizon of $8.2s$. Based on simulation studies, we have found that the prediction horizon is long enough to ensure the performance and stability of the control system. Control input blocking is used to reduce the number of control input decision variables. The block sizes are equal to the step sizes for the first 10 steps, thereafter the sizes of the blocks gradually increase such that the total number of blocks becomes $m = 21$.

The MPC model is based on the models presented in [15] and [12], and is combined with the VSG presented in [13]. These papers present all parameters and variables that are not explained in this paper. Sections III-A to III-F presents the differential-algebraic equations (DAE) (4)-(9) of the MPC model. These are necessary to construct the matrices A_t and B_t in the equality constraints in (2) [14] as presented in Section III-J. The inequality constraints of (2) and the cost function (1) are constructed from the information given in respectively Sections III-G and III-H.

A. Governor

The governor can either set the rotational speed reference ω^* or the governor control can be performed by the MPC, setting the guide vane opening reference g^*. Although the open-loop system without a governor control is unstable, the latter alternative is chosen in this paper since the MPC will manage the governor control. The guide vane opening g is found as

$$\dot{g} = \frac{1}{T_G}\left(g^* - g\right) \tag{4}$$

B. Waterway

The hydraulic system is modelled by the Euler turbine equation model presented in [15]. To reduce the number of states, the penstock water column is assumed to be inelastic, and the differential equations for the waterway are thereby given as:

$$\begin{aligned} \dot{h}_{st} &= \frac{1}{C_s}\left(q_{\mathrm{hr}} - q\right) \\ \dot{q}_{hr} &= \frac{1}{T_{\mathrm{w2}}}\left(1 - h_{\mathrm{st}} + f_0(q_{\mathrm{hr}} - q)^2 - f_{\mathrm{p2}}{q_{\mathrm{hr}}}^2\right) \\ h &= h_{st} - f_0\left(q_{\mathrm{hr}} - q\right)^2 - f_{\mathrm{p1}}q^2 \end{aligned} \tag{5}$$

C. Turbine

The turbine model is based on the Euler turbine equation, as presented in [15], [16].

$$\begin{aligned} P_m &= \frac{H_{\mathrm{Rt}}}{H_{\mathrm{R}}}\frac{Q_R}{Q_{Rt}} \\ &\quad \left(\left(\frac{\xi q}{g}\left(\tan\alpha_{1R}\sin\alpha_1 + \cos\alpha_1\right)\right) - \psi\omega\right)\frac{q\omega}{h} \\ \alpha_1 &= \sin^{-1}\left(\frac{Q_{\mathrm{R}}}{Q_{\mathrm{Rt}}}g\sin\alpha_{1R}\right) \\ \dot{q} &= \frac{1}{T_{\mathrm{w1}}}\left(h\frac{H_{\mathrm{R}}}{H_{\mathrm{Rt}}} - \sigma\left(\omega^2 - 1\right) - \left(\frac{q}{g}\right)^2\right)\frac{Q_{Rt}}{Q_R} \end{aligned} \tag{6}$$

D. Synchronous Generator

To save simulation time, a simple first-order synchronous generator model (7) is used in the MPC model. The torque must be used in the swing equation instead of the power since the rotational speed is not constant. Since the converter controller time constants are significantly smaller than the

sampling time of the MPC, the electrical power of the synchronous generator is assumed to be equal to the output power of the VSHP P_g.

$$\begin{aligned}\dot{\omega} &= \frac{1}{2H}\left(T_m - P_g/\omega - D\left(\omega^* - \omega\right)\right)\\ \dot{\omega} &= \frac{1}{2H\omega}\left(P_m - P_g - D\left(\omega^* - \omega\right)\omega\right)\end{aligned} \tag{7}$$

E. Grid Converter

To simplify the model, only the outer d-axis loop control of the grid converter, the active power control, is considered. This simplification is satisfactory since the inner controller is faster than the step length of the MPC and since the voltage control is not considered. The active power is controlled by a VSG, which is found to be more suitable for the purpose than the virtual synchronous machine (VSM) [13].

It is assumed that the converter output power P_g equals the d-axis current $i_{g,d}$ such that

$$\begin{aligned}P_g &= i_{g,d} = k_{vsg,p}\Delta f + k_{vsg,d}\Delta\dot{f} + P_g^*\\ \Delta f &= f^* - f\end{aligned} \tag{8}$$

F. Grid Model

The grid frequency is derived from the swing equation [17].

$$\Delta\dot{f} = \frac{\omega_s}{2H_g S_n}\left(P_g + P_{pb} - D_m\Delta f\right) \tag{9}$$

where P_{pb} is the power balance of the grid without the VSHP; $P_{pb} = P_{generation} - P_{loads} - P_{losses}$. The initial value of the mean grid inertia is $H_g = 25.35p.u.$, the total rated power of all connected power producers is $S_n = 1p.u.$ and the damping of the grid is $D_m = 0$. These values could either be estimated locally by system identification techniques or as in this case continuously supplied from the TSO. We have chosen to use a conservatively low value of the system inertia parameter since analysis shows that the results are not very sensitive to this parameter.

The electrical power in the grid is estimated from the measured grid frequency f and rate-of-change-of-frequency (ROCOF) $\dot{f}$ by the PLL.

$$P_{pb} = -P_g + \frac{2H_g S_n}{\omega_s}\frac{\omega_{\dot{f}}}{s+\omega_{\dot{f}}}\Delta\dot{f} + D_m\frac{\omega_f}{s+\omega_f}\Delta f \tag{10}$$

f and $\dot{f}$ are filtered by first order filters with filter constants at respectively $\omega_f = 0.625rad/s$ and $\omega_{\dot{f}} = 0.25rad/s$.

G. Constraints and Slack Variables

The constraints on the inputs and variables u are given in Table I. The guide vane opening reference g^* is limited by the minimum and maximum values during normal operation and the converter power P_g is limited by its maximal nominal power. Power transfer from the grid to the generator is blocked by setting the lower constraint of P_g to zero. In addition, the change in g^* from one step to the next is limited to $\Delta g^*_{max} = 0.2\Delta t = 0.04$, which correspond to the maximum operational speed of the guide vane.

TABLE I: Constraints on inputs and variables

Input	Min. value	Max. value
Guide vane opening reference g^*	0.1	1.3
Converter power P_g	0	1

TABLE II: Slack variables

Slack variable	Min. limit	Max. limit	Cost factor $S(i,i)$
Water flow q	0.3	1.3	1
Surge tank level h_{st}	0.5	1.1	1e6
Turbine rot. speed ω	0.7	2	1e5

TABLE III: Cost on deviations in states and inputs

State/input	Reference value	Cost factor $Q(i,i)$
Grid frequency Δf	0	0.01
Turbine rotational speed ω	$f(P_{pb})$, (11)	100
VSHP power reference P_g^*	0.8	1000

To avoid non-convergence, slack variables are used instead of constraints on the state variables, as given in Table II. The turbine needs a minimum and maximum water flow q to function properly, and a slack variable is used to add costs to the cost function if q is outside its constraints. The next slack variable ensures that the surge tank level h_{st} will be limited to the maximum pressure over the turbine, normally 1.1-1.15 p.u., or the maximum head of the surge tank. Exceeding these values may cause damage to the turbine blades or water to blow out of the surge shaft. This slack variable also avoids the surge tank level from becoming too low. Normally a sand trap is located between the surge shaft and pressure shaft. Too low surge tank level will cause sand to raise here and to be sent through the turbine, causing increased wear and tear and reduced lifetime of the turbine.

The third slack variable is related to the turbine rotational speed ω, which is limited by the maximal rated speed of the generator. If this speed is exceeded, there is a high consequence risk of the poles to falling off.

When ω is reduced and the converter output power P_g is kept constant, the electrical torque will increase. The increase in mechanical torque will be less, and the MPC controller has to increase the guide vane opening g to regain the reference turbine speed ω^*. If ω decreases too much, the MPC controller will not be able to regain the reference turbine speed without reducing the converter output power P_g. A lower limit slack variable is therefore used on ω to prevent this situation.

H. Costs in MPC Cost Function

The cost function includes costs for deviation in the grid frequency Δf, turbine rotational speed ω and the VSHP power reference P_g^* from their reference value, as given in Table III. The costs for exceeding the constraints of the slack variables, given in Table II, are also included in the cost function.

The relative values of the costs determine how the MPC priorities between its objectives given in Section II-A. A

high cost related to an objective causes the MPC controller to prioritize this objective to reduce the cost function. The objectives are prioritized as follows:

1) Keep the surge tank level h_{st} within its constraints to avoid damage of the hydraulic system.
2) Keep the turbine rotational speed ω within its constraints to avoid undesired operation conditions of the hydraulic system and damage of the generator.
3) Minimize the deviation in the VSHP power reference P_g^* to assure that the VSHP is contributing to the frequency regulation as intended by the VSG.
4) Minimize the deviation of the turbine rotational speed ω from the best efficiency operating point to increase the efficiency of the system.
5) Keep the water flow q within its constraints to avoid undesired operation conditions of the hydraulic system.
6) Minimize the deviation in grid frequency Δf.

The cost of deviation in Δf is low and the cost of deviation in P_g^* is high since the grid frequency control should primarily be performed by the VSG. The VSHP power reference P_g^* is not supposed to compensate for deviations in the turbine rotational speed ω unless ω is predicted to go outside its constraints. The cost of deviations in P_g^* is, therefore, higher than the cost of deviation in ω. The deviations in ω will, when possible, be compensated only by adjusting the guide vane opening reference g^* and thereby the mechanical power. However, if constraints on the surge tank level h_{st}, the water flow q or the rate of change of the guide vane opening reference Δg^* block the turbine rotational speed ω from being recovered within its limit, the VSHP power reference P_g^* will be adjusted. In this way, situations, where the turbine rotational speed is reduced too much to be able to produce enough torque to increase again will be avoided.

I. Reference Turbine Rotational Speed

The optimal turbine rotational speed ω depends on the flow q and thereby by the produced power. This is implemented in the MPC by letting the turbine rotational speed reference ω^* be a function of the VSHP output power P_g, as given in (11). The curve is based on the measured optimal speed of a reversible pump-turbine presented in [18].

$$\begin{aligned} 0.85 < P_g \quad & \omega^* = 1 + 0.6(P_g - 0.85) \\ 0.73 < P_g < 0.85 \quad & \omega^* = 1 + 0.3(P_g - 0.85) \\ P_g < 0.73 \quad & \omega^* = 0.964 + 0.15(P_g - 0.73) \end{aligned} \tag{11}$$

J. Linearization and Discretization of the Model

The system DAEs are given from (4), (5), (7), (8) and (9) where

$$\begin{aligned} \dot{x} &= f(x,u) = [\Delta\dot{f} \quad \dot{g} \quad \dot{q} \quad \dot{q_{hr}} \quad \dot{h_{st}} \quad \dot{\omega}]^T \\ x &= [\Delta f \quad g \quad q \quad q_{hr} \quad h_{st} \quad \omega]^T \\ u &= [P_g^* \quad P_{pb} \quad g^*]^T \end{aligned} \tag{12}$$

The stationary operation point x_s is found from the previous estimation of the grid power balance P_{pb} and the previous value of the VSHP power reference P_g^* by solving the equation $\dot{x}_s = 0$ for $g^* = g$. The system is linearized around this point as given by (13).

$$\begin{aligned} \Delta\dot{x} &= A_c\Delta x + B_c\Delta u \\ \Delta\dot{y} &= C_c\Delta x + D_c\Delta u \\ A_c = \left.\frac{\delta f}{\delta x}\right|_{(x_s,u_s)} &= \begin{bmatrix} \left.\frac{\delta f_1}{\delta x_1}\right|_{(x_s,u_s)} & \cdots & \left.\frac{\delta f_1}{\delta x_n}\right|_{(x_s,u_s)} \\ \vdots & \ddots & \vdots \\ \left.\frac{\delta f_n}{\delta x_1}\right|_{(x_s,u_s)} & \cdots & \left.\frac{\delta f_n}{\delta x_n}\right|_{(x_s,u_s)} \end{bmatrix} \\ B_c = \left.\frac{\delta f}{\delta u}\right|_{(x_s,u_s)} &= \begin{bmatrix} \left.\frac{\delta f_1}{\delta u_1}\right|_{(x_s,u_s)} & \cdots & \left.\frac{\delta f_1}{\delta u_n}\right|_{(x_s,u_s)} \\ \vdots & \ddots & \vdots \\ \left.\frac{\delta f_n}{\delta u_1}\right|_{(x_s,u_s)} & \cdots & \left.\frac{\delta f_n}{\delta u_n}\right|_{(x_s,u_s)} \end{bmatrix} \end{aligned} \tag{13}$$

where $\Delta x = x - x_s$ and $\Delta u = u - u_s$ are the errors from the linearization point.

Next, the model is discretized as shown in (14), where Δt is the step time length.

$$\begin{aligned} A_t &= A_c\Delta t + I \\ B_t &= B_c\Delta t \end{aligned} \tag{14}$$

For each time step, a new stationary operation point based on the previous inputs and a new linearized function are found, and the equality constraints are updated with the new state system matrices. Cost matrices and inequality constraints must also be updated according to the new linearization point.

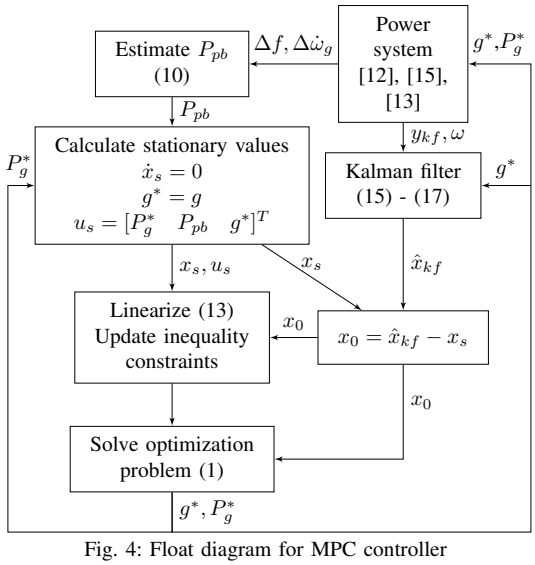

Fig. 4: Float diagram for MPC controller

The steps of the MPC are explained in Figure 4. The VSHP inputs g^* and P_g^* from the previous solution of the optimization problem are applied to the power system. At the next time step, the grid power balance P_{pb} is estimated to calculate the stationary state values by setting $\dot{x}_s = 0$. In parallel, the Kalman filter, explained in the next section, estimates the state values and the deviations from the stationary values are found. The system DAEs are then linearized based on the stationary values and cost matrices, and the inequality constraints are updated. Finally, the optimization problem is solved and the first inputs to the power system are found and applied.

IV. Kalman Filter

A Continuous-Time Kalman filter is used to estimate the unmeasured variables in the hydraulic system. The guide vane opening g, the surge tank height h_{st}, the height over the turbine h and the mechanical power P_m are measured. The Kalman filter is designed to filter g and h_{st} and estimate values of the pressure tunnel flow q and the headrace tunnel flow q_{hr}. The estimated values will be used as input to the MPC. The dynamical system model is:

$$\begin{aligned} \dot{x}_{kf} &= A_{kf}x_{kf} + B_{kf}u_{kf} + G_{kf}w \\ y_{kf} &= C_{kf}x_{kf} + D_{kf}u_{kf} + H_{kf}w + v \end{aligned} \tag{15}$$

where

$$\begin{aligned} x_{kf} &= [g \quad q \quad q_{hr} \quad h_{st}]^T \\ y_{kf} &= [g \quad h_{st} \quad h \quad P_m]^T \\ u_{kf} &= [g^* \quad \omega]^T \end{aligned} \tag{16}$$

The matrices A_{kf}, B_{kf}, C_{kf} and D_{kf} are found by linearizing the hydraulic system model (4) - (6) at the initial stationary operation point. w and v are, respectively, white process noise and measurement noise.

The Kalman filter equations are given as:

$$\begin{aligned} \dot{\hat{x}}_{kf} &= A_{kf}\hat{x}_{kf} + B_{kf}u_{kf} \\ &\quad + L_{kf}\left(y_{kf} - C_{kf}\hat{x}_{kf} - D_{kf}u_{kf}\right) \\ \begin{bmatrix}\hat{y}_{kf} \\ \hat{x}_{kf}\end{bmatrix} &= \begin{bmatrix}C_{kf} \\ I\end{bmatrix}\hat{x}_{kf} + \begin{bmatrix}D_{kf} \\ 0\end{bmatrix}u_{kf} \end{aligned} \tag{17}$$

where the filter gain L_{kf} is solved by an algebraic Riccati equation in MatLab [19], [20].

V. Results and Discussion

The dynamic performance of the MPC controller is tested on the grid presented in [12]. Cases with both overproduction and underproduction are investigated by first reducing the load by 160 MVA at Bus 7 at time $t = 0s$ and thereby increasing the load back to the initial value at $t = 60s$.

Figure 5 compares the real values of four states with the values estimated by the Kalman filter. The estimation of the guide vane opening g is almost perfect since the reference value (g^*) is known. A small delay is observed for the other states; the turbine flow q, the headrace tunnel flow q_{hr} and the surge tank head h_{st}.

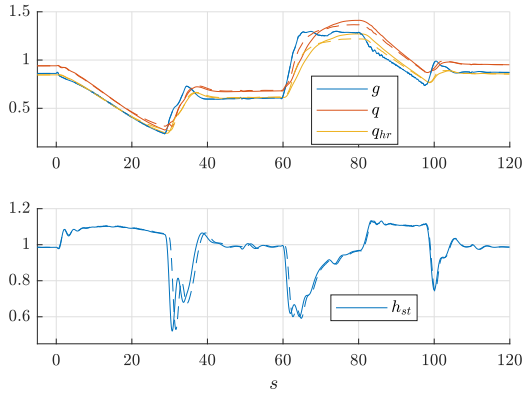

Fig. 5: Performance of Kalman filter: Real values (solid) and estimations by the Kalman filter (dashed)

Three different scenarios are investigated to show how the parameters of the MPC and VSG affect the grid and the hydraulic system:

1) MPC: Initial settings, VSG: 1% droop
2) MPC: Initial settings, VSG: 4% droop
3) MPC: Turbine speed constraints reduced to $0.85 - 1.10 p.u.$, VSG: 1% droop

Figure 6 shows the reference and the measured VSHP power P_g^*, P_g, the grid frequency f, the turbine rotational speed ω, the guide vane opening reference g^*, the turbine mechanical power P_m and the surge tank head h_{st}. When the grid load is reduced at $t = 0s$, the grid frequency f immediately starts increasing because of overproduction in the system. The VSG reduces the VSHP output power P_g depending on the droop; if the droop is low (1%), P_g is reduced by approximately 0.4 p.u. within 2 sec, and the peak frequency is limited to 0.4%. In this case, most of the loss reduction is actually compensated by the VSHP. With 4% droop, the decrease in P_g is less, causing a three times higher frequency deviation.

The MPC minimizes its cost given in Section III-H while fulfilling the constraints in Section III-G. To reduce the cost of deviation in turbine rotational speed ω, the MPC reduces the guide vane opening reference g^* immediately to regain ω as fast as possible. However, the maximal g^* step size is limited to the maximal operational speed of the governor. This constraint is active for the first time steps after the load reduction. The fast reduction in guide vane opening g causes the surge tank head h_{st} to increase close to its maximal value. To avoid h_{st} from exceeding its maximal value, the MPC reduces the rate of change of g^* and g after 0.6 sec.

The guide vane opening g is reduced as fast as possible until the turbine rotational speed ω is almost regained to its optimal value. Subsequently, g increases. Since there is a larger deviation between the stationary value and the lower constraint

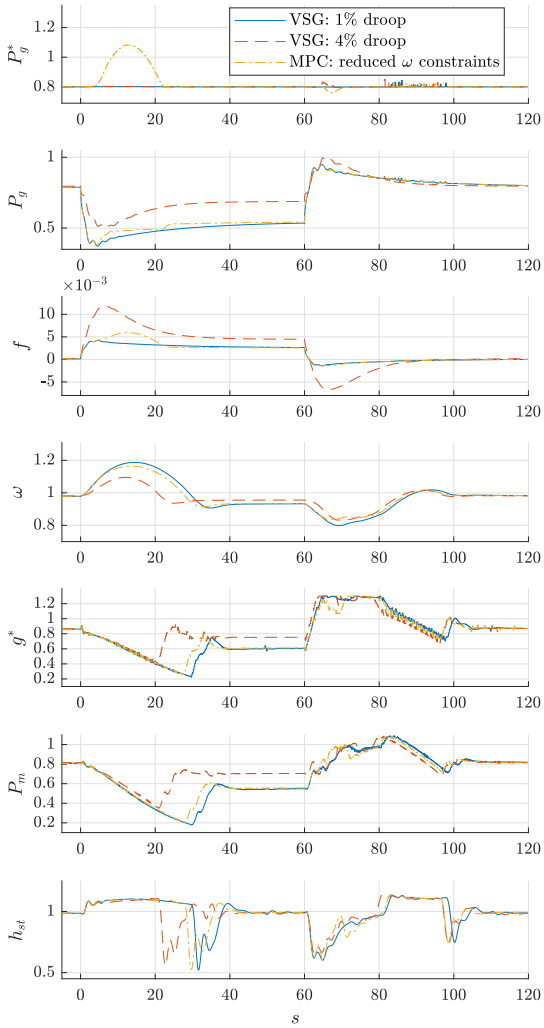

Fig. 6: Dynamic performance at 1% droop, 4% droop and reduced limits on turbine rotational speed

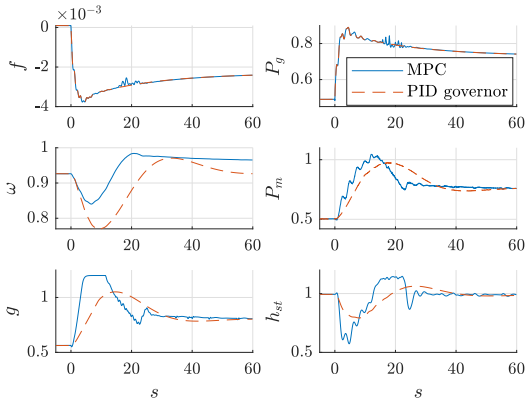

Fig. 7: Dynamic performance after generator loss; with MPC (blue) and PID governor from [12] (red). VSG with 1% droop is utilized in both cases.

of h_{st} than of the stationary value and the higher constraint of h_{st}, g^* and g are allowed to increase faster than it decreases. Partly, the rate of change of the guide vane opening is limited by the maximum step size of g^*.

After 60 sec, the grid load increases by 160 MW, back to its initial value. This causes the grid frequency f to drop. The guide vane opening reference g^* increases with its maximal rate of change until it almost reaches its maximum value. The maximal deviation in turbine rotational speed ω is less for the case of load increase compared to the case of load decrease. The rate of change of the guide vane is faster since the lower constraint of the surge tank head h_{st} is not active for most of the time. Thereby, the turbine mechanical power P_m changes faster to recover ω. This is a very important quality of the proposed MPC control since too low rotational speed must be avoided. In cases with high VSHP output power P_g and low turbine rotational speed ω, the turbine might not be able to deliver enough power to regain ω without reducing P_g. If P_g is not reduced in this case, the turbine stops. While a conventional governor control increases and decreases the guide vane opening g at the same speed, the MPC controller makes it possible to increase the opening speed of g. This reduces the minimum rotational speed, and thereby avoid situations where P_g has to be reduced to regain ω.

The third case in Figure 6 shows how the MPC handles situations where both surge tank height h_{st} and the turbine rotational speed ω exceed its constraints. In this case, the constraints of ω are reduced to $0.85-1.10 p.u.$. At $t = 10s$, h_{st} has reached its maximal value and limits the rate of change of guide vane reference g^*. It is therefore not possible to close g faster to reduce ω, which is simultaneously getting close to its maximal value. Since the cost of the h_{st} and ω slack variables are higher than the cost of deviations in VSHP output power reference P_g^*, the MPC increases P_g^* to avoid h_{st} and ω from exceeding its constraints. This causes a temporary increase in VSHP output power P_g and grid frequency Δf.

The performance of the controller system after disconnection of half of the generators at G2 at $t = 0$ is shown in Figure 7. To illustrate its benefits, the MPC controller is compared to the governor control presented in [12], however, the VSG with 1 % droop controls the grid converter output power. Since the MPC considers the limitations in surge tank level h_{st}, the guide vane opening g can be increased faster until its maximum value is reached or the minimum value of h_{st} is reached. This results in higher turbine mechanical power P_m and thereby less deviation in turbine rotational speed ω and higher efficiency of the turbine. The more aggressive control

of the guide vane opening g causes higher deviation and more oscillations in the surge thank level h_{st}, however, this can be tolerated since the MPC controller handles the system constraints. Due to the increased performance of the turbine control and lower deviation in turbine rotational speed ω, it is possible to increase the FFR delivery.

The step responses in Figures 5, 6 and 7 show that the linearized MPC model is not a perfect model of the system. For instance, the surge tank head h_{st} should be closer to its maximum constraint between $0 - 30s$ and the overshoots in turbine rotational speed ω and guide vane opening g should be less. The use of a nonlinear MPC will improve the calculation of the turbine torque and thereby increase the precision of the control and reduce or eliminate these problems.

VI. Conclusion

As the share of wind and solar energy production increases, more flexible production and loads are required to control the balance of the grid in order to maintain the power system security. By utilizing the rotational energy of the turbine and the generator, VSHPs are able to deliver both VI and FFR. However, an advanced MIMO control system is needed to optimize the control and to ensure that the hydraulic and electric variables are within their constraints. A control system with an overall MPC and VSG control of the grid-connected converter is developed to fulfil the control objectives. When a grid frequency deviation occurs, the VSG controls the output power of the converter to reduce the frequency deviation. Thereby, the MPC will primarily control the turbine guide vane opening to regain the nominal turbine rotational speed. The speed of the control will be faster than for a conventional governor control since the MPC maximizes the rate of change of the guide vane opening while considering the surge tank head guide vane speed constraints. In cases where the turbine rotational speed could not be kept within its limits due to these constraints, the MPC will adjust the VSG power reference and thereby change the VSHP output power to regain the turbine rotational speed. The linearization of the MPC model causes inaccurate prediction and overshoots that may be improved by the use of nonlinear MPC.

References

[1] M. Valavi and A. Nysveen, "Variable-speed operation of hydropower plants: Past, present, and future," in *Electrical Machines (ICEM), 2016 XXII International Conference on*. IEEE, 2016, pp. 640–646.

[2] M. Beus and H. Pandžić, "Application of model predictive control algorithm on a hydro turbine governor control," in *2018 Power Systems Computation Conference (PSCC)*. IEEE, 2018, pp. 1–7.

[3] M. Elsisi, M. Soliman, M. Aboelela, and W. Mansour, "Improving the grid frequency by optimal design of model predictive control with energy storage devices," *Optimal Control Applications and Methods*, vol. 39, no. 1, pp. 263–280, 2018.

[4] A. M. Ersdal, I. M. Cecilio, D. Fabozzi, L. Imsland, and N. F. Thornhill, "Applying model predictive control to power system frequency control," in *Innovative Smart Grid Technologies Europe (ISGT EUROPE), 2013 4th IEEE/PES*. IEEE, 2013, pp. 1–5.

[5] A. M. Ersdal, L. Imsland, and K. Uhlen, "Model predictive load-frequency control," *IEEE Transactions on Power Systems*, vol. 31, no. 1, pp. 777–785, 2016.

[6] A. M. Ersdal, L. Imsland, K. Uhlen, D. Fabozzi, and N. F. Thornhill, "Model predictive load–frequency control taking into account imbalance uncertainty," *Control Engineering Practice*, vol. 53, pp. 139–150, 2016.

[7] A. Fuchs, M. Imhof, T. Demiray, and M. Morari, "Stabilization of large power systems using vsc–hvdc and model predictive control," *IEEE Transactions on Power Delivery*, vol. 29, no. 1, pp. 480–488, 2014.

[8] I. M. Sanz, P. Judge, C. Spallarossa, B. Chaudhuri, T. C. Green, and G. Strbac, "Effective damping support through vsc-hvdc links with short-term overload capability," in *2017 IEEE PES Innovative Smart Grid Technologies Conference Europe (ISGT-Europe)*. IEEE, 2017, pp. 1–6.

[9] S. P. Azad, R. Iravani, and J. E. Tate, "Damping inter-area oscillations based on a model predictive control (mpc) hvdc supplementary controller," *IEEE Transactions on Power Systems*, vol. 28, no. 3, pp. 3174–3183, 2013.

[10] A. Jain, E. Biyik, and A. Chakrabortty, "A model predictive control design for selective modal damping in power systems," in *American Control Conference (ACC), 2015*. IEEE, 2015, pp. 4314–4319.

[11] M. Imhof, A. Fuchs, G. Andersson, and M. Morari, "Voltage stability control using vsc-hvdc links and model predictive control," in *XIII Symposium of Specialists in Electric Operational and Expension Planning, XIII SEPOPE, Foz do Iguassu, Brazil*, 2014.

[12] T. I. Reigstad and K. Uhlen, "Variable speed hydropower conversion and control," *IEEE Transactions on Energy Conversion*, vol. 35, no. 1, pp. 386–393, March 2020.

[13] T. I. Reigstad and K. Uhlen, "Variable speed hydropower plant with virtual inertia control for provision of fast frequency reserves," *arXiv e-prints*, p. arXiv:2003.07062, Mar. 2020.

[14] B. Foss and T. A. N. Heirung, "Merging optimization and control," *Lecture Notes*, 2013.

[15] T. I. Reigstad and K. Uhlen, "Modelling of Variable Speed Hydropower for Grid Integration Studies," *arXiv e-prints*, p. arXiv:2003.06298, Mar. 2020.

[16] T. K. Nielsen, "Simulation model for francis and reversible pump turbines," *International Journal of Fluid Machinery and Systems*, vol. 8, no. 3, pp. 169–182, 2015.

[17] P. Kundur, N. J. Balu, and M. G. Lauby, *Power system stability and control*. McGraw-hill New York, 1994, vol. 7.

[18] I. Iliev, C. Trivedi, E. Agnalt, and O. G. Dahlhaug, "Variable-speed operation and pressure pulsations in a francis turbine and a pump-turbine," in *IOP Conference Series: Earth and Environmental Science*, vol. 240, no. 7. IOP Publishing, 2019, p. 072034.

[19] F. L. Lewis, L. Xie, and D. Popa, *Optimal and robust estimation: with an introduction to stochastic control theory*. CRC press, 2017.

[20] MATLAB, *version 9.5.0 (R2010a)*. Natick, Massachusetts: The MathWorks Inc., 2018.

Paper VI

Nonlinear Model Predictive Control of Variable Speed Hydropower for Provision of Fast Frequency Reserves

Nonlinear Model Predictive Control of Variable Speed Hydropower for Provision of Fast Frequency Reserves

Tor Inge Reigstad[1], Kjetil Uhlen[1]

[a]*Department for Electric Power Engineering, Norwegian University of Science and Technology (NTNU), NO-7491 Trondheim, Norway*

Abstract

This paper presents the development of a nonlinear model predictive controller (MPC) for controlling variable speed hydropower (VSHP) plants. The MPC coordinates the turbine controller with the virtual synchronous generator (VSG) control of the power electronics converter to optimize the plant's performance. The main objective is to deliver a fast power response to frequency deviations by utilizing the kinetic energy of the turbine and generator. This is made possible by allowing the turbine rotational speed to deviate temporarily from its optimal speed. In addition, the efficiency should be maximized while keeping the electric and hydraulic variables within their constraints. The simulation results show that the proposed MPC is also able to damp power oscillations in the grid, reduce water hammering in the penstock and improve the estimation of turbine head, turbine power and turbine flow. This ensures that the turbine head does not exceed its limits and that the overshoot in the turbine speed after a disturbance is reduced. Besides, the VSG converter control enables a fast power response by utilizing the rotational energy of the turbine and generator. Thereby, the VSHP can provide a significant amount of fast frequency reserves (FFR) to the grid.

Keywords:
Fast frequency response, frequency control, model predictive control, variable speed hydropower, virtual synchronous generator

1. Introduction

1.1. Motivation

Hydropower is an important contributor in providing power system flexibility and will remain a significant source of large-scale energy storage in the

future. The share of variable renewable energy, such as wind and solar power, is increasing. Thus, more flexible generation and demand are required to control the balance of the grid and to maintain power system security. Variable speed operation of hydropower plants has the potential to provide faster control of active and reactive power than conventional hydropower plants. This is achieved by applying frequency converter technology and implementation of virtual inertia (VI) control by utilizing the kinetic energy stored in the turbine and generator rotor. The hypothesis is that the variable speed hydropower (VSHP) can offer additional ancillary services, contributing to improved frequency control and maintaining the grid stability, allowing for higher penetration of variable renewables in the grid. A robust and well-functioning control system needs to be developed to coordinate the control of the hydraulic system and the converter control. The control system must optimize the operation of the power plant while considering the constraints in the electric and the hydraulic systems to maximize the potential of the kinetic energy. In this paper, a nonlinear model predictive control (MPC) scheme is proposed for this task.

1.2. Literature Review

MPC control systems for control of hydropower plants have previously been investigated; however, the research is limited. The most relevant work is the nonlinear model predictive control strategy for a variable-speed pumped-storage power plant proposed in [1]. In addition to the MPC, it utilizes a static optimizer and an extended Kalman filter to minimize the power loss of the VSHP plant. The MPC system model differs significantly from the model proposed in this paper. Firstly, it has a different waterway layout as it does not consider a surge tank. Secondly, the penstock is divided into pipe-elements and utilizes the spectral element method (SEM) to increase the accuracy of the model instead of considering reflecting pressure waves directly as proposed in this paper. The models of the turbine do also differ. Moreover, a double-fed induction generator (DFIG) is used instead of a synchronous generator with a full-converter. Lastly, [1] assumes that the VSHP follows a power reference with rate limits as distinct from the VI control utilized in this paper.

Most other works assume direct-connected generators, such that the turbine rotational speed is following the grid frequency. Therefore, the hydraulic models do not consider varying turbine rotational speed. Moreover, they do

not optimize control with regards to the provision of frequency control services. A local MPC controller is developed in [2] for turbine governor control. This work uses a simple MPC dynamic model of the system, including a governor with limits on the speed of the guide vane opening and a linearized (HYGOV) model for representing a Francis turbine. A more detailed model of the hydraulic system is utilized in [3], where a nonlinear predictive control system is presented. The control system includes a terminal penalty function that proves Lyapunov stability for the discrete system. In [4], the guide vane opening is controlled by a neural network-based nonlinear predictive controller to optimize the control of the turbine power. A multi-mode MPC scheme is proposed in [5] for excitation control and load scheduling of a hydropower plant. Experimental results indicate both increased performance of voltage regulating, damping and control of the turbine governor.

Another possible area of application is wind energy. An MPC based virtual inertia control system is proposed in [6] to optimize the control of a wind farm, consisting of several wind turbines and a battery storage energy system (BESS). The introduction of the MPC is shown to reduce the minimum rotor speed and loss of captured wind energy when providing inertia support. Additionally, the degeneration of the BESS is significantly reduced.

MPC has also been utilized for improving primary frequency control, as presented in [7]. Here, the MPC design optimizes the control of superconducting magnetic storage. Load frequency control by MPC is studied in [8], where both linear and nonlinear centralized MPC solutions take into account limitations on tie-line power flow, generation capacity, and generation rate of change. Another possibility is to utilize MPC for damping of low damped electromechanical modes by minimizing the generator's frequency deviation from the average system frequency with the use of a global MPC-based grid controller [9, 10, 11, 12]. Looking beyond frequency control, similar control layouts can be applied to control voltage and ensure voltage stability [13].

Although MPC based control systems have been proposed for both conventional hydropower plant, frequency control and damping of power oscillations, limited work embrace VSHP and optimization of frequency support capabilities by utilizing the kinetic energy of the turbine and generator. However, a linear MPC is proposed in [14] to optimize the frequency support capabilities of the power plant while keeping the electric and hydraulic variables within their limits. The MPC is based on the VSHP models presented in [15] and [16], and is combined with the virtual synchronous generator (VSG) control approach presented in [17]. The VSG controls the VSHP

output power to reduce frequency deviation while the MPC coordinates the VSG control and the control of the turbine. By utilizing the kinetic energy of the turbine and generator, the VSHP can provide fast frequency reserves (FFR) to stabilize the grid. Simulation results show that the VSHP output power can be changed permanently by $0.4p.u.$ within $2s$. The proposed control system is also shown to be faster than a conventional control system with PID-controllers since the PID-controllers have to be tuned cautiously to avoid exceeding these constraints and thereby causing damage to the system. However, the linearization of the MPC dynamic model causes inaccurate predictions, especially of the turbine mechanical power, and thereby larger deviation in the turbine rotational speed. Nonlinear MPC might be a possible solution for these issues.

1.3. Contribution and Paper Structure

This paper contributes to further development of the concept from [14] by utilizing nonlinear MPC instead of linear MPC. It also offers a different MPC compared to [1] with more functions, like VI and damping of oscillations in both the waterway and the grid. Moreover, the Kalman filter is replaced by a moving horizon estimator (MHE) to increase the precision of the state estimator. The nonlinear dynamic model of the nonlinear MPC implies improved estimation of the turbine power and control of the guide vane opening of the turbine, reduced deviation in turbine rotational speed after a disturbance and, thereby, increased efficiency. Further, a function for damping power oscillation in the grid is added to benefit the system stability. The MPC dynamic model includes modelling of water hammering in the penstock. This allows for improved accuracy of the MPCs estimation of the turbine head, thus reducing the risk of exceeding the maximum pressure above the turbine and damaging the turbine blades. Also, the elaboration of the MPC design is considered as a significant contribution, as this makes reproducing and improving the control system possible.

The paper is organized as follows: The MPC theory, the control objectives for the MPC controller and the development of the MPC model are presented in Section 2 while the MHE is presented in Section 3. The results and discussions are given in Section 4 and the conclusion in Section 5.

2. Model Predictive Control

MPC is a well-developed and widely used method in process control, offering great advantages compared to traditional PID-controllers. By utilizing dynamic models of the process to solve an optimization problem, the MPCs handle both constraints, nonlinear systems and multiple-input, multiple-output (MIMO) systems. MPCs are more robust and may offer a faster and smoother response and lower rising time, settling time and overshoots compared to PID-controllers [18]. This is obtained by solving a closed-loop optimization problem where a discrete-time model is optimized from $t = 0$ to $t = N$.

A nonlinear MPC model with a quadratic objective function (1), nonlinear equality constraints (two first lines of (2)) and linear inequality constraints (2)-(3) is used in this paper. The cost function (1) includes the cost for the error of state/variables values x, changes in state values Δx, the error of input values u, changes in input values Δu and the cost for exceeding the limitations on the states with the use of slack variables ϵ.

$$\begin{aligned}\min_{x\in\mathbb{R}^n, u\in\mathbb{R}^m} f(x,u) = \sum_{t=0}^{N-1} &\frac{1}{2}x_{t+1}^{\mathrm{T}} Q_{t+1} x_{t+1} + d_{xt+1} x_{t+1} + \frac{1}{2}\Delta x_{t+1}^{\mathrm{T}} Q_{\Delta t} \Delta x_{t+1} \\ &+ \frac{1}{2}u_t^{\mathrm{T}} R_t u_t + d_{ut} u_t + \frac{1}{2}\Delta u_t^{\mathrm{T}} R_{\Delta t} \Delta u_t + \rho^{\mathrm{T}} \epsilon_t + \frac{1}{2}\epsilon_t^{\mathrm{T}} S \epsilon_t \end{aligned} \quad (1)$$

subjected to

$$\begin{aligned} x_{t+1} &= g\left(x_t, u_t\right) && t = 0, \ldots, N-1 \\ x_0, u_{-1} &= \text{given} \\ x^{\text{low}} - \epsilon \leq x_t &\leq x^{\text{high}} + \epsilon && t = 1, \ldots, N \\ -\Delta x^{\text{high}} \leq \Delta x_t &\leq \Delta x^{\text{high}} && t = 1, \ldots, N \\ A_{ineq} x_t + B_{ineq} u_t &\leq b_{ineq} && t = 1, \ldots, N \\ u^{\text{low}} \leq u_t &\leq u^{\text{high}} && t = 0, \ldots, N-1 \\ -\Delta u^{\text{high}} \leq \Delta u_t &\leq \Delta u^{\text{high}} && t = 0, \ldots, N-1 \end{aligned} \quad (2)$$

where

$$
\begin{aligned}
Q_t &\succeq 0 && t = 1, \ldots, N \\
Q_{\Delta t} &\succeq 0 && t = 1, \ldots, N \\
R_t &\succeq 0 && t = 0, \ldots, N-1 \\
R_{\Delta t} &\succeq 0 && t = 0, \ldots, N-1 \\
\Delta x_t &= x_t - x_{t-1} && t = 1, \ldots, N \\
\Delta u_t &= u_t - u_{t-1} && t = 0, \ldots, N-1 \\
\epsilon &\in \mathbb{R}_x^n \geq 0 \\
\rho &\in \mathbb{R}_x^n \geq 0 \\
S &\in \operatorname{diag}\left\{s_1, \ldots, s_{n_x}\right\}, s_i \geq 0, i = \{1, \ldots, n_x\}
\end{aligned}
\tag{3}
$$

The parameters of the MPC functions (1)-(3) are derived from the MPC dynamic model given in Section 2.2, the costs defined in Section 2.3 and the constraints and slack variables presented in Section 2.4. Solution of the nonlinear optimization problem for each time step is found by CasAdi [19] in MATLAB, using the direct multiple shooting method and the IPOPT solver [20].

2.1. Control Objectives of the MPC Controller

The main goal of the nonlinear MPC is to optimize the frequency support capabilities of the power plant while keeping the electric and hydraulic variables within their limits. To achieve this, the MPC calculates and supplies the optimal VSHP output power reference P_g^* to the VSG and guide vane opening reference g^* to the turbine, as indicated in Figure 1. As the VSG controls the VSHP output power P_g with the frequency f as input, there is a direct relationship between these variables, as in a conventional hydropower plant. However, due to the converter technology, the turbine rotational speed does not need to follow the frequency. Thereby, the VSHP output power can be controlled quicker by utilizing the rotational energy of the turbine and generator. The ancillary service capabilities are therefore no longer limited by the slow governor, as in a conventional hydropower plant. This opens new possibilities such as faster frequency control and other grid ancillary services, but it also necessitates proper co-ordination of the controls.

The control objectives of the MPC are an extended version of those presented in [14] and prioritized as follows:

1. Keep the surge tank head h_{st} within its constraints to avoid damage to the hydraulic system.

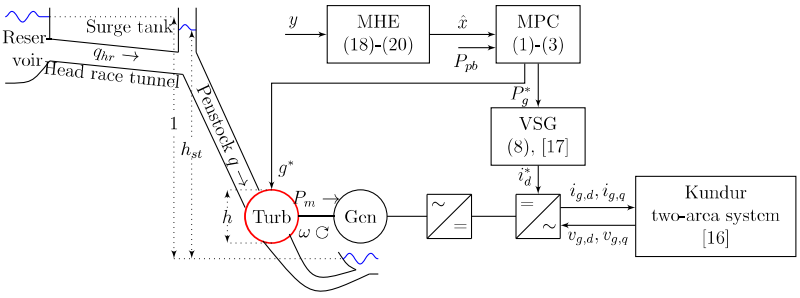

Figure 1: VSHP plant layout with equations for modelling and control structure

2. Keep the turbine rotational speed ω within its constraints to avoid undesirable operation conditions of the hydraulic system and damage of the generator.
3. Minimize water hammering and waterway oscillations.
4. Minimize power oscillations.
5. Minimize the deviation in the VSHP power reference P_g^* to ensure that the VSHP is contributing to the frequency regulation as intended by the VSG.
6. Minimize the deviation of the turbine rotational speed ω from the best efficiency operating point and maximize the turbine efficiency to increase the efficiency of the system.
7. Keep the turbine flow q within its constraints to avoid undesired operation conditions of the hydraulic system.

The MPC objective function handles conflicts between the control objectives. For instance, in cases where the output power of the VSHP changes rapidly, fast control of the guide vane opening g is needed to reduce the deviation in turbine rotational speed ω. This will increase the deviation in surge tank head h_{st}, increasing waterway oscillation and water hammering and thereby increase the cost of the objective function. The MPC compares these costs with the costs of deviation in turbine rotational speed ω to find the optimal solution.

2.2. Model Predictive Controller Dynamic Model

The nonlinear MPC dynamic model with its costs and limitations is presented in this section. Except for the modelling of the pressure waves in the

penstock h_p, it is identical to the model presented in [14]. Thus, the model is summarized in this section. All equations, variables and parameters are earlier presented in [15, 16, 17]. The differential equations for the waterway are thereby given as:

$$\begin{aligned}
\dot{h}_{st} &= \frac{1}{C_s}\left(q_{\mathrm{hr}} - q\right) \\
\dot{q}_{hr} &= \frac{1}{T_{\mathrm{w2}}}\left(1 - h_{\mathrm{st}} + f_0(q_{\mathrm{hr}} - q)^2 - f_{\mathrm{p2}}{q_{\mathrm{hr}}}^2\right) \\
h &= h_{st} - f_0\left(q_{\mathrm{hr}} - q\right)^2 - f_{\mathrm{p1}}q^2 + h_p \\
h_p &= -Z_0 \tanh\left(sT_e\right)q = -Z_0\left(\frac{1 - e^{-2T_e s}}{1 + e^{-2T_e s}}\right)q
\end{aligned} \tag{4}$$

where q_{hr} is the head race tunnel flow, q is the turbine flow, h_{st} is the surge tank head, h is the turbine head (pressure difference over the turbine) and $e^{-2T_e s}$ is a time delay of $2T_e$.

The turbine mechanical power P_m is derived from the Euler turbine equations, as presented in [21, 15]:

$$\begin{aligned}
P_m &= \frac{H_{\mathrm{Rt}}}{H_{\mathrm{R}}}\frac{Q_R}{Q_{Rt}}\left(\left(\frac{\xi q}{g}\left(\tan\alpha_{1R}\sin\alpha_1 + \cos\alpha_1\right)\right) - \psi\omega\right)\frac{q\omega}{h} \\
\alpha_1 &= \sin^{-1}\left(\frac{Q_{\mathrm{R}}}{Q_{\mathrm{Rt}}}g\sin\alpha_{1R}\right) \\
\dot{q} &= \frac{1}{T_{\mathrm{w1}}}\left(h\frac{H_{\mathrm{R}}}{H_{\mathrm{Rt}}} - \sigma\left(\omega^2 - 1\right) - \left(\frac{q}{g}\right)^2\right)\frac{Q_{Rt}}{Q_R}
\end{aligned} \tag{5}$$

The guide vane opening g is found as a first order model of the governor system [15]:

$$\dot{g} = \frac{1}{T_G}\left(g^* - g\right) \tag{6}$$

Moreover, the synchronous generator is modelled by a first order model [14]:

$$\dot{\omega} = \frac{1}{2H}\left(T_m - P_g/\omega - D\left(\omega^* - \omega\right)\right) \tag{7}$$

The virtual synchronous generator (VSG) of the VSHP grid-connected converter controls the output power P_g [17]:

$$P_g = i_{g,d} = k_{vsg,p}\Delta f + k_{vsg,d}\Delta\dot{f} + P_g^*, \quad \Delta f = f - f^* \tag{8}$$

Here, the grid frequency f is found at the VSHP connection point, f^* is the nominal frequency ($1p.u. = 50Hz$) and the deviation of the grid frequency Δf is modelled by the swing equation:

$$\Delta\dot{f} = \frac{\omega_s}{2H_g S_n}\left(P_g + P_{pb} - D_m\Delta f\right) \tag{9}$$

The power balance P_{pb} of the grid without the VSHP is $P_{pb} = P_{generation} - P_{loads} - P_{losses}$. This variable is estimated from the measured grid frequency f and ROCOF $\dot{f}$, where the frequency and ROCOF are calculated by the same phase-locked loop (PLL) utilized for control of the grid converter [16].

$$P_{pb} = -P_g + \frac{2H_g S_n}{\omega_s}\frac{\omega_{\dot{f}}}{s+\omega_{\dot{f}}}\Delta\dot{f} + D_m\frac{\omega_f}{s+\omega_f}\Delta f \tag{10}$$

The resulting MPC dynamic model DAEs are given in (4)-(9) where the states x and inputs u are [14]:

$$\begin{aligned} x &= [\Delta f \quad g \quad q \quad q_{hr} \quad h_{st} \quad \omega]^T \\ \dot{x} &= [\Delta\dot{f} \quad \dot{g} \quad \dot{q} \quad \dot{q}_{hr} \quad \dot{h}_{st} \quad \dot{\omega}]^T \\ u &= [P_g^* \quad g^*]^T \end{aligned} \tag{11}$$

To optimize the control of guide vane opening g to minimize water hammering, the elastic penstock water column has to be included in the model. One solution is to approximate the classical wave solution by a lumped-parameter equivalent for $\tanh(sT_e)$ as given in [15]. However, since the elastic water time constant T_e is low (126 ms), this would require a very short time step of the MPC controller to capture the dynamics of the water hammering.

Another solution is to utilize that $e^{2T_e s}$ is a time delay of $2T_e$; the time for the pressure wave to move up and down again in the penstock. By setting

the time step $\Delta t = 2T_e$, the future pressure waves h_p can be estimated based on the previous pressure waves and flow q. From (4), we get:

$$h_{p,n+1} = -Z_0 \left(q_{n+1} - q_n\right) - h_{p,n} \tag{12}$$

The pressure waves in the penstock h_p affect the turbine head h (4) and thereby the flow q. The term h_p is added to the next value of q during the Runge-Kutta method (RK4), such that

$$q_{n+1} = q_n + \frac{1}{6}\left(k_{1,q} + 2k_{2,q} + 2k_{3,q} + k_{4,q}\right) + \frac{H_R \Delta t}{H_{Rt} T_{w1}} h_{p,n+1} \tag{13}$$

The pressure waves also affect the turbine mechanical power P_m (5) and thereby the turbine rotational speed ω. However, the large inertia H of the turbine and generator will filter the oscillations, and the effect of h_p on P_m is therefore neglected.

2.3. Costs in MPC Cost Function

As the relative values of the cost factors determine how the MPC prioritizes between the objectives, their values are chosen to fulfil the order of objectives given in Section 2.1. A high cost related to an objective causes the MPC controller to prioritize this objective to reduce the cost function. Additionally, the relative difference between two cost factors is chosen to be higher if one of the corresponding objectives is much more important than the other. The costs are divided into three categories:

2.3.1. Cost on Deviations in States and Inputs

The MPC tries to keep the turbine rotational speed ω, the VSHP power reference P_g^* and the VSHP frequency f close to its reference value by considering the cost for deviations in these variables, as given in Table 1. The variables with the highest corresponding costs will be prioritized. For instance, the cost of deviations in P_g^* is higher than for deviations in turbine rotational speed ω since P_g^* is not supposed to compensate for deviations in ω unless ω is out outside its limits.

The MPC may contribute to the damping of power oscillations by minimizing the VSHP frequency deviation from the average system frequency, as suggested for HVDC converters in [9]. Since the MPC controls the VSHP

Table 1: Cost on deviations in states and inputs

State	Reference value	Cost factor $Q(i,i)/R(i,i)$
Turbine rotational speed ω	$f(P_g)$	100
Turbine rotational speed $\omega(N)$	$f(P_g)$	10000
VSHP power reference P_g^*	0.8	1000
VSHP frequency f	$\overline{f}$	1e7

power reference P_g^* to achieve this, the cost of deviations in VSHP frequency f is higher than the cost of deviations in VSHP power reference P_g^*. The average system frequency $\overline{f}$ found as

$$\overline{f}\,(t) = \frac{\sum_{i=1}^{n_{gen}} H_i f_i\,(t)}{\sum_i H_i} \tag{14}$$

where H_i and f_i are, respectively, the generator inertial constant and frequency of the i^{th} generator. A cost for the deviation between the VSHP frequency f and the average system frequency $\overline{f}$ is included in the MPC cost function, as stated in Table 1. Frequency measurements f_i from PMUs for all large generators are needed to calculate the average system frequency $\overline{f}$.

The time constant of the turbine speed dynamics is larger than the time horizon of the MPC. This means that the MPC's estimated values of the turbine speed do not reach the reference value after a large disturbance. To make sure the MPC tries to minimize the turbine speed deviation, a cost of not reaching the turbine reference speed at the end of the time horizon of the MPC is added. This is included by an extra cost for deviation in $\omega(N)$, which is larger than the cost of deviation in turbine speed ω for each time step.

2.3.2. Cost on Changes in States and Inputs

Costs for changes in the pressure waves in the penstock h_p and in guide vane opening reference g^* and g^*_{-5}, as given in Table 2, are introduced to reduce water hammering and oscillations in the waterway. The latter cost also reduces guide vane wear and tear. Increasing the cost of change of the guide vane opening reference Δg^* will reduce oscillations due to reduced

Table 2: Cost on changes in states and inputs

State	Cost factor $Q_{\Delta t}(i,i)/R_{\Delta t}(i,i)$
Δg^*	1000
Δg^*_{-5}	1000
Δh_p	1e10

speed of changes of the guide vane opening reference Δg^*. However, this will also cause increased deviation in turbine rotational speed ω. The solution is to instead damp the oscillations in the waterway by adding cost for changes in the guide vane opening reference over a period corresponding to half of the oscillation period, in this case, five time steps, such that $\Delta g^*_{-5} = g^*_t - g^*_{t-5}$.

Since the deviation in h_p is small, the cost factor of Δh_p must be very high to have an effect.

2.3.3. Cost on reduced efficiency in turbine

An additional cost for turbine speed deviation from its optimal value can be added by maximizing the efficiency η of the turbine [21, 15], as given in (15). This term in the cost function can be used instead of - or in addition to - the cost of deviation from the optimal turbine speed.

$$\eta = \omega\xi\sqrt{\sigma\left(\omega^2 - 1\right)}\left(\cos\left(\sin^{-1}\kappa\sin\alpha_1\right) + \kappa\tan\alpha_1\sin\alpha_1\right) - \psi\omega \tag{15}$$

$$\kappa = \frac{Q_R}{Q_{Rt}}g \tag{16}$$

The cost-efficiency factor is set to 10 in this case.

2.4. Constraints and Slack Variables

The MPC utilizes slack variables to allow the variables to exceed the constraints with a high additional cost. This is necessary for obtaining convergence of the optimization problem in some cases.

Absolute constraints are given in Table 3. The guide vane opening reference g^* is limited by the minimum and maximum values of the guide vane opening g. The limitation of VSHP output power P_g is set between $0 - 1p.u.$

Table 3: Limits on inputs and variables

Input	Min. value	Max. value
Guide vane opening reference g^*	0.1	1.2
Converter power P_g	0	1

Table 4: Slack variables

Slack variable	Min. limit	Max. limit	Cost factor $S(i,i)$
Turbine flow q	0.3	1.3	1
Surge tank head h_{st}	0.5	-	1e5
Turbine head h	-	1.1	1e5
Turbine rot. speed ω	0.7	2	1e4

such that the power is delivered to the grid. If the reactive power and the grid voltage are known at the point of common coupling (PCC), the constraints of P_g may be a function of these values to consider the current limit of the converter.

Table 4 presents the slack variable. The turbine flow q slack variable has a low cost factor since the consequences of exceeding the constraints are low. In contrast, the cost factor of the surge tank head h_{st} slack variable is higher since the consequences of exceeding the constraints are large. Too low surge tank head will cause sand to raise from the sand trap near the surge tank and send it through the turbine, causing increased wear and tear and reduced lifetime of the turbine. The maximum surge tank head is limited by the maximum level of the surge tank to avoid blowout of the surge shaft. However, the maximum constraint on the turbine head h is usually lower, normally 1.1-1.15 p.u., to avoid damage on the turbine blades. In this case, the maximum pressure is limited by the turbine. Moreover, the maximum constraint of h is set to 1.1 p.u.

The cost factor related to the turbine rotational speed ω slack variable is very high since the consequence of exceeding the maximal value is high; generator poles may physically fall off and destroy the generator. The lower limit of ω prevents cases where the turbine produces too low power because of low turbine speed. At low rotational speed and high VSHP output power P_g, the electrical torque will be very high. In such cases, the guide vane opening

g and turbine flow q must be increased to produce enough mechanical torque to increase ω. If the hydraulic variables reach their limits, the MPC controller might not be able to regain the reference turbine speed by only controlling the guide vane opening reference g^*. Thus, the MPC will reduce the VSHP power reference P_g^* since the cost factor for the VSHP power reference deviations is lower than the cost of the slack variables.

2.5. Reference Turbine Rotational Speed

For a given turbine flow q, and thereby a corresponding stationary VSHP output power P_g, there exists an optimal turbine rotational speed. Therefore, the turbine rotational speed reference ω^* is given as a function of the VSHP output power P_g (17) to maximize the power production. The function is derived from the hill chart of a reversible pump-turbine presented in [22]. It is provided as a reference value for turbine rotational speed ω in the MPC cost function, as stated in Table 1.

$$\begin{aligned} 0.85 < P_g \quad & \omega^* = 1 + 0.6(P_g - 0.85) \\ 0.73 < P_g < 0.85 \quad & \omega^* = 1 + 0.3(P_g - 0.85) \\ P_g < 0.73 \quad & \omega^* = 0.964 + 0.15(P_g - 0.73) \end{aligned} \tag{17}$$

3. Moving Horizon Estimation

MHE is a multivariable estimation algorithm that utilizes a series of measurements and an internal dynamic model of the process to estimate the current states. A major benefit compared to the Kalman filter from [14] is the possibility of representation of water hammering in the penstock. This is included in the internal dynamic model presented in Section 2.2, which is the basis for the MHE. The limits and slack variables from Section 2.4 are not included and the cost function is given as:

$$J_{N_{mhe}}(x, u) = \sum_{i=k-N_{mhe}}^{k} \|\tilde{y}(i) - y(i)\|_V^2 + \sum_{i=k-N_{mhe}}^{k-1} \|\tilde{u}(i) - u(i)\|_W^2 \tag{18}$$

subjected to

$$\begin{aligned} x_{t+1} &= g(x_t, u_t) \\ x_0, u_{-1} &= \text{given} \end{aligned} \tag{19}$$

where

$$\begin{aligned} y &= [\Delta f \quad g \quad h_{st} \quad \omega \quad h \quad P_m \quad P_g]^T \\ u &= [P_g^* \quad P_{pb} \quad g^*]^T \end{aligned} \tag{20}$$

The variables y and u are, respectively, the system outputs and inputs while $\tilde{y}$ and $\tilde{u}$ are the system output and inputs of the estimated model. The relative cost of deviation between the estimated and measured system outputs and system inputs are found from the standard deviation in Gaussian noise such that:

$$V = \begin{bmatrix} \sigma_{y(1)} & 0 & 0 \\ 0 & \ddots & 0 \\ 0 & 0 & \sigma_{y(n_y)} \end{bmatrix}^{-1} = \text{diag}(50, 100, 100, 1000, 100, 1, 1) \tag{21}$$

$$W = \begin{bmatrix} \sigma_{u(1)} & 0 & 0 \\ 0 & \ddots & 0 \\ 0 & 0 & \sigma_{u(m)} \end{bmatrix}^{-1} = \text{diag}(100, 1000, 10) \tag{22}$$

The initial and previous values for the states and for the pressure waves h_p are found by the MHE. The initial value of h_p is therefore based on the previous measurements, primarily of h and h_{st}.

4. Results and Discussion

This section presents the results of the dynamic simulation with the nonlinear MPC controller and compares it with the linear MPC controller developed in [14]. The dynamic performances of both the linear and nonlinear MPC controllers are tested on the same nonlinear model. The grid model, based on the Kundur two-area system, the hydraulic system, the synchronous generator and the converters are modelled as presented in [16] with some modifications: Firstly, the active power control of the grid-connected converter is replaced by a VSG, as presented in [17]. Secondly, the VSG power reference is provided by the MPC and lastly, the governor control is replaced by the guide vane reference from the MPC. An overall scheme of the system is shown in Figure 1.

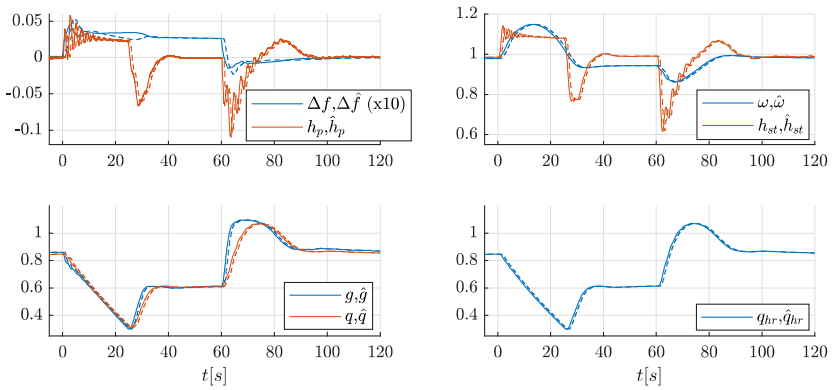

Figure 2: Comparison of real states (solid) and estimated states by the MHE (dashed): Frequency deviation Δf, penstock pressure waves h_p, turbine rotational speed ω, surge tank head h_{st}, guide vane opening g, penstock flow q and head race tunnel flow q_{hr}.

Cases with both overproduction and underproduction are investigated by first reducing the load by 160 MW at Bus 7 at time $t = 0s$ and thereby increasing the load back to the initial value at $t = 60s$.

4.1. Performance of Moving Horizon Estimation

The MPC controller needs reliable estimations of the states to find an optimal solution to the control problem. The MHE utilizes the same dynamic model as the MPC and the 10 previous measurements of the model inputs and outputs to estimate the current state. The deviation between the real values of the states (solid) and the estimated states (dashed) are shown in Figure 2.

For most of the states, the estimated values are following the real values with a time delay of approximately 1 second. This time delay causes the estimations of the surge tank head h_{st} and the penstock pressure waves h_p to be in anti-phase with the real values. The consequences are discussed in Section 4.4.

4.2. Nonlinear MPC compared to linear MPC

Figure 3 compares the dynamic results from the nonlinear MPC controller presented in this paper (solid) with the linear MPC controller presented in [14] (dashed). The nonlinear MPC outperforms the linear MPC controller

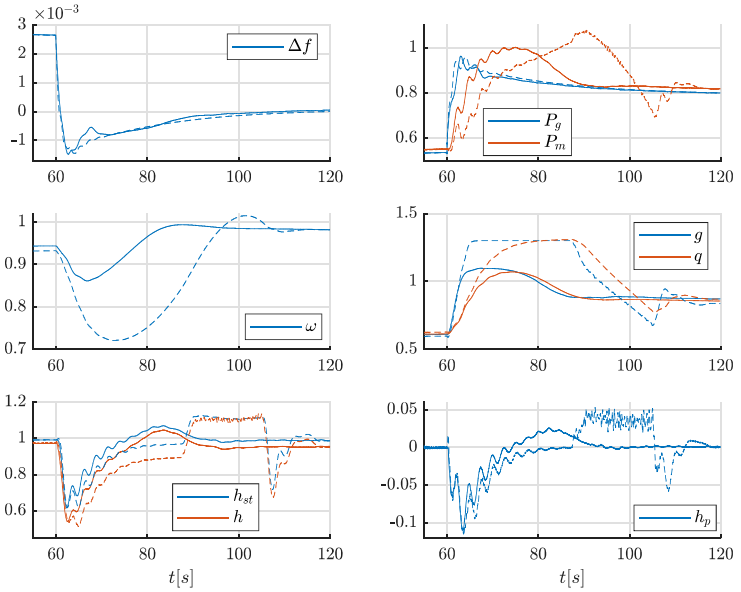

Figure 3: Comparison of nonlinear MPC (solid) as presented in this paper and linear MPC as presented in [14] (dashed): Frequency deviation Δf, grid converter power P_g, turbine mechanical power P_m, turbine rotational speed ω, guide vane opening g and penstock flow q, surge tank head h_{st}, turbine head h, penstock pressure waves h_p.

in most regards. The most recognizable and important improvement is the reduction of the deviation in turbine rotational speed ω. The nonlinear MPC responds slightly faster by increasing the guide vane opening g after the disturbance. The linear MPC is slower, causing higher deviations in turbine rotational speed ω and thereby a self-energizing effect due to reduced mechanical power P_m. Besides, the guide vane opening is increased too much because the linearization of the turbine model causes an inaccurate prediction of the mechanical power of the turbine. The prediction of the mechanical power P_m for the nonlinear MPC is better, reducing the overshoots in turbine rotational speed ω, gate opening g and penstock flow q after a disturbance.

4.3. Effect of the Power Oscillation Damper

The nonlinear MPC includes the damping of power oscillations, as explained in Section 2.3. Figure 4 shows how this function affects the frequency

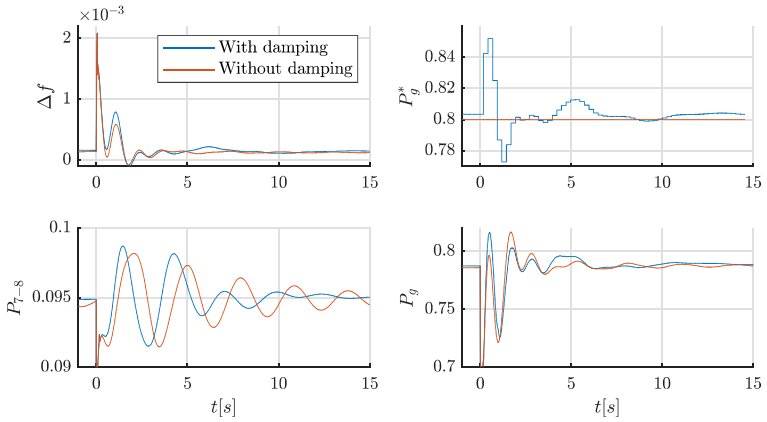

Figure 4: Effect of power oscillation damping by the MPC.

deviation Δf, the grid converter power reference P_g^*, the grid converter power P_g and the active power between the two areas of the grid P_{7-8} after a three-phase short-circuit at Bus 8 that is cleared after $50ms$. The peaks right after the short circuit are not shown. The damping function is deactivated by reducing the cost factor related to the deviation between the VSHP frequency f and its reference $\overline{f}$ from $1e7$ to zero. When the damping function is activated, the MPC adjusts the VSHP output power reference P_g^* to minimize the deviation between the local frequency at the VSHP and the average system frequency $\overline{f}$ and thereby damp the power oscillations. The VSHP output power reference P_g^* is first increased to increase the local frequency before it is reduced. The effect is seen in power between the two areas P_{7-8}. The magnitudes of the oscillations are similar with and without the damping function for the first 5 seconds. Subsequently, the damping of the dominated mode is improved by the damping function, as observed from the figure.

4.4. Effect of Modelling Water Hammering in the Penstock

The nonlinear MPC also includes modelling of the water hammering in the penstock. The effect of this is shown in Figure 5. Here, the presented nonlinear MPC is compared with a version of the nonlinear MPC that do not include the modelling of the water hammering in the MPC dynamic model, i.e. the pressure waves in the penstock h_p are removed from (4). However; the water hammering is still included in the simulation model. If the water

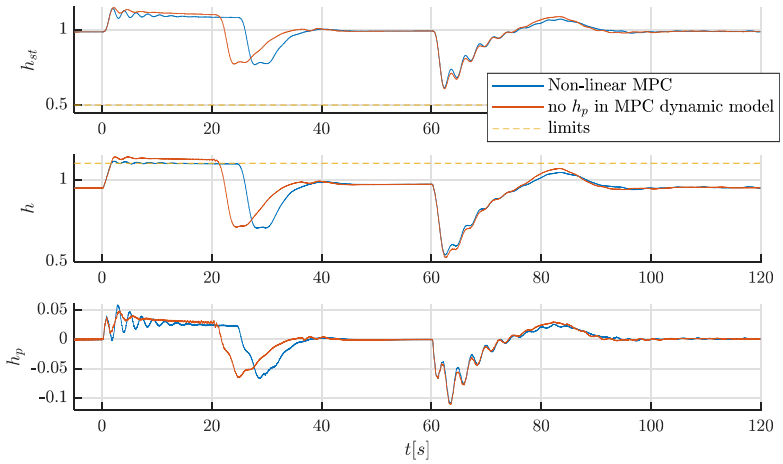

Figure 5: Effect of modelling water hammering in the penstock: Surge tank head h_{st}, turbine head h and penstock pressure waves h_p.

hammering is not modelled, the turbine head h will exceed its limits when the gate is closing at maximal speed, as seen from $t = 2s$ to $t = 20s$. Thereby, the gate closing speed will be faster in this period, resulting in less deviation in turbine rotational speed. The difference between the two cases will be less when the gate is opening since neither the turbine head h nor surge tank head h_{st} is not a constraint in this case.

The oscillations in the penstock pressure waves are larger from 0-20 seconds if they are included in the MPC dynamic model than if they are not. When the pressure waves are considered, the MPC tries to keep the turbine head h at its maximum value by counteracting oscillations in the penstock. The guide vane opening is slightly adjusted to obtain this. However, since the estimations of the penstock pressure waves h_p are delayed by approximately 1 second, the MPC will increase the oscillations in the penstock.

5. Conclusion

With the increased share of variable energy production, such as wind and solar, the demand for flexible generation and consumption is increasing. Most producers have limited energy storage and are not able to increase production quickly. Besides, a fast reduction in power will normally cause increased

energy losses. The advantage of a variable speed hydropower (VSHP) plant is the possibility to utilize the energy storage in the rotation masses, making it able to both increase and decrease its output power almost instantaneously. It is, therefore, suitable for delivering both virtual inertia and fast frequency regulation. This paper has described the development of a model predictive controller (MPC) to coordinate the control of the hydro turbine and the VSHP frequency converter, and at the same time considering the constraints in the electric and the hydraulic systems. A moving horizon estimator (MHE) is applied for the estimation of the state variables.

The nonlinear MPC presented in this paper shows improved performance compared to an earlier investigated linear MPC. The improvement is primarily due to a more accurate calculation of turbine power, causing less overshoot in the turbine speed after a disturbance. Furthermore, the proposed modelling of water hammering in the penstock improves the calculation of turbine pressure and thereby ensures that maximum pressure is not exceeded. The results do also show that the MPC can contribute to damping power oscillations by adding a cost for the deviation between the local and average frequency to the optimization function.

With the promising simulation results, the controllers need to be implemented and tested in a laboratory for further verification of performance. Future work will include real-time hardware-in-the-loop, the time delay of the controller and signal processing and a more realistic model of the hydraulic system.

References

[1] J.-F. Mennemann, L. Marko, J. Schmidt, W. Kemmetmüller, A. Kugi, Nonlinear model predictive control of a variable-speed pumped-storage power plant, IEEE Transactions on Control Systems Technology (2019).

[2] M. Beus, H. Pandžić, Application of model predictive control algorithm on a hydro turbine governor control, in: 2018 Power Systems Computation Conference (PSCC), IEEE, 2018, pp. 1–7.

[3] H. Zhang, D. Chen, B. Xu, F. Wang, Nonlinear modeling and dynamic analysis of hydro-turbine governing system in the process of load rejection transient, Energy Conversion and Management 90 (2015) 128–137.

[4] N. Kishor, S. Singh, Nonlinear predictive control for a nnarx hydro plant model, Neural computing and applications 16 (2) (2007) 101–108.

[5] Y. Zheng, J. Zhou, W. Zhu, C. Zhang, C. Li, W. Fu, Design of a multi-mode intelligent model predictive control strategy for hydroelectric generating unit, Neurocomputing 207 (2016) 287–299.

[6] W. Bao, Q. Wu, L. Ding, S. Huang, F. Teng, V. Terzija, Synthetic inertial control of wind farm with bess based on model predictive control, IET Renewable Power Generation (2020).

[7] M. Elsisi, M. Soliman, M. Aboelela, W. Mansour, Improving the grid frequency by optimal design of model predictive control with energy storage devices, Optimal Control Applications and Methods 39 (1) (2018) 263–280.

[8] A. M. Ersdal, L. Imsland, K. Uhlen, Model predictive load-frequency control, IEEE Transactions on Power Systems 31 (1) (2016) 777–785.

[9] A. Fuchs, M. Imhof, T. Demiray, M. Morari, Stabilization of large power systems using vsc–hvdc and model predictive control, IEEE Transactions on Power Delivery 29 (1) (2014) 480–488.

[10] I. M. Sanz, P. Judge, C. Spallarossa, B. Chaudhuri, T. C. Green, G. Strbac, Effective damping support through vsc-hvdc links with short-term overload capability, in: 2017 IEEE PES Innovative Smart Grid Technologies Conference Europe (ISGT-Europe), IEEE, 2017, pp. 1–6.

[11] S. P. Azad, R. Iravani, J. E. Tate, Damping inter-area oscillations based on a model predictive control (mpc) hvdc supplementary controller, IEEE Transactions on Power Systems 28 (3) (2013) 3174–3183.

[12] A. Jain, E. Biyik, A. Chakrabortty, A model predictive control design for selective modal damping in power systems, in: American Control Conference (ACC), 2015, IEEE, 2015, pp. 4314–4319.

[13] M. Imhof, A. Fuchs, G. Andersson, M. Morari, Voltage stability control using vsc-hvdc links and model predictive control, in: XIII Symposium of Specialists in Electric Operational and Expension Planning, XIII SEPOPE, Foz do Iguassu, Brazil, 2014.

[14] T. I. Reigstad, K. Uhlen, Optimized Control of Variable Speed Hydropower for Provision of Fast Frequency Reserves, Electric Power Systems Research 189 (2020).

[15] T. I. Reigstad, K. Uhlen, Modelling of Variable Speed Hydropower for Grid Integration Studies, arXiv e-prints (2020) arXiv:2003.06298arXiv:2003.06298.

[16] T. I. Reigstad, K. Uhlen, Variable speed hydropower conversion and control, IEEE Transactions on Energy Conversion 35 (1) (March 2020) 386–393.

[17] T. I. Reigstad, K. Uhlen, Variable speed hydropower plant with virtual inertia control for provision of fast frequency reserves, arXiv e-prints (2020) arXiv:2003.07062arXiv:2003.07062.

[18] F. M. Salem, M. I. Mosaad, M. A. Awadallah, A comparative study of mpc and optimised pid control, International Journal of Industrial Electronics and Drives 2 (4) (2015) 242–250.

[19] J. A. Andersson, J. Gillis, G. Horn, J. B. Rawlings, M. Diehl, Casadi: a software framework for nonlinear optimization and optimal control, Mathematical Programming Computation 11 (1) (2019) 1–36.

[20] A. Wächter, L. T. Biegler, On the implementation of an interior-point filter line-search algorithm for large-scale nonlinear programming, Mathematical programming 106 (1) (2006) 25–57.

[21] T. K. Nielsen, Simulation model for francis and reversible pump turbines, International Journal of Fluid Machinery and Systems 8 (3) (2015) 169–182.

[22] I. Iliev, C. Trivedi, E. Agnalt, O. G. Dahlhaug, Variable-speed operation and pressure pulsations in a francis turbine and a pump-turbine, in: IOP Conference Series: Earth and Environmental Science, Vol. 240, IOP Publishing, 2019, p. 072034.

Paper VII

Stability Properties of Nonlinear Model Predictive Control of Variable Speed Hydropower

IET Research Journals

Regular Paper

IET Journals
The Institution of Engineering and Technology

ISSN 1751-8644
doi: 0000000000
www.ietdl.org

Stability properties of nonlinear model predictive control of variable speed hydropower

Tor Inge Reigstad[1]*, *Kjetil Uhlen*[1]

[1] *Department for Electric Power Engineering, Norwegian University of Science and Technology (NTNU), NO-7491, Trondheim, Norway*
* *E-mail: tor.inge.reigstad@ntnu.no*

Abstract: This paper presents a method for small-signal analysis of an advanced, multi-variable control system for variable speed hydropower (VSHP) plants. A model predictive controller (MPC) optimises the power plant performance. In parallel, a virtual synchronous generator-type (VSG) converter control ensures that the VSHP contributes to virtual inertia and frequency control of the power system. The aim of the small-signal analysis is to parametrise the cost function of the MPC to minimise oscillatory modes between the VSHP hydraulic system and the power system. A state-space representation of the MPC is developed by assuming a stable steady-state operating point equal to the reference values of the MPC cost function, and that no constraints are active. This state-space representation allows for small-signal analysis of the power system, including the MPC. The results show that the modes between the hydraulic system and the power system are well-damped and negligible when the costs of deviations in the hydraulic system are low compared to the cost of deviations in the VSG power reference. Thus, these modes do not constrain the tuning of the VSG. The VSHP power output can, therefore, be optimised independently through the VSG controller to damp power oscillations and reduce frequency deviations.

1 Introduction

1.1 Motivation and Incitement

Integration of variable renewable energy resources (RES) challenges the established operation and control of power systems. Converter-interfaced wind and solar energy, contributing with no inertia, are replacing large thermal power plants with high inertia, causing a major reduction in the total system inertia. The inertia of the thermal energy and hydropower synchronous generators counteracts frequency deviations by absorbing or releasing kinetic energy and in that way aiding the short-term balance of power generation and demand in the grid. Less system inertia causes higher frequency deviations and reduced frequency stability, which is defined as is the ability of a system to maintain a steady frequency after a severe disturbance resulting in a significant imbalance between generation and load in the power system [1].

The reduction of system inertia has motivated the development of virtual inertia (VI) - also called synthetic inertia. By implementing VI in HVDC converters, energy storage systems (ESS) or converter-based generation and loads, their power output can change more or less instantaneously and thereby reduce the power imbalance by fast-acting power reserves. However, this assumes that the source of VI can adjust its production, consumption or power transfer quickly and/or utilising energy stored, in for instance, batteries or rotating masses. Depending on the properties of the source of VI, it may deliver both instantaneous power reserves (inertia), fast frequency reserves (FFR) with a response time of approximately one second and frequency containment reserves (FCR).

Most RESs cannot increase power production on demand and have limited stored energy. For instance, the power production of a PV-plant is in most cases already maximised, and unless battery storage is added, there is almost no energy stored in the plant. Wind turbines with variable speed will be able to utilise the energy stored in the rotating masses; however, the power delivery has to be reduced to regain the rotational speed of the turbine. Thus, their capability of delivering VI, FFR and FCR is limited.

Variable speed hydropower (VSHP) is potentially better suited for VI control since it can obtain energy from the rotational masses of the turbine and generator for the first inertia response and thereby adjust the water flow and the mechanical power by governor action to return to the optimal rotational speed. Utilising a model predictive control (MPC) system together with the VI control, as developed in [2, 3], VSHP plants are shown to be able to deliver both VI, FFR and FRC. Moreover, the MPC both optimises the efficiency of the system and assures that the constraints are fulfilled. In this paper, the small-signal properties of this control system are further investigated to fully benefit from the advantages of VSHP. The main research questions to be answered is how a small-signal stability analysis of the proposed MPC and VI control system can be executed, which assumptions are needed and how the MPC cost function must be parametrised to minimise undesirable interaction between the hydraulic system of the VSHP and the grid. The development of a small-signal model of the proposed MPC and VI control system also allows for using linear methods for analysis and tuning of the system.

1.2 Literature Review

This section starts by presenting different applications of MPC for power system and hydropower plant control to show how MPC can increase the power system stability. Next, a short review on VI control of RES and its possible contribution to power system auxiliary services is given. Although different types of VI controls are thoroughly investigated in the literature, little work has been performed on utilising VSHP for VI support. We will, therefore, review the newly proposed VSHP control system with both VI and MPC control for optimising fast frequency reserves and power oscillation damping.

Various MPC control systems for control of conventional hydropower governors and/or excitation control have previously been developed [4–7]. In these papers, conventional plants with synchronous generators are investigated. Thus, the turbine rotational speed follows the grid frequency and the control is not optimised with regards to the provision of frequency services. Moreover, the hydraulic models assume constant turbine rotational speed when calculating turbine mechanical power and water flow. These factors demand the development of new MPC schemes for optimising the

control of VSHP and methods for analysing their impact on grid stability. The control schemes presented in [2, 3] maximise the utilisation of the turbine and generator rotational energy for the provision of FFR to the power system.

MPC is utilised for a wide range of other applications in the power system. The damping of power oscillations [8–12] by minimising the frequency deviation between the local generator and the average system frequency is one example. Voltage stability [13], grid frequency control [14–17] and hydro turbine governor control [7] can also be improved by MPC.

Proper utilisation of VI control of the RES converters also increases the power system stability by damping the frequency oscillations and reducing the frequency deviation [18–22]. Many VI control structures with different properties are developed. They are classified into three main categories based on their basis equations [23]:

- Synchronous generator emulation models: These control structures try to emulate the behaviour of a synchronous machine by an internal dynamic model that may represent inertia, damping and synchronising torques and voltage control. [19, 24–28]
- Swing equation-based models: Instead of a full detailed model of a synchronous generator, these utilise a simpler power-frequency swing equation. [29]
- Power versus frequency response-based models: These control structures input frequency measurements, for instance from a PLL. They consist of a damping term proportionally to the frequency deviation and/or ad inertia term proportionally to the derivative of the frequency deviation. [30–34]

A virtual synchronous generator (VSG), which is a power versus frequency response-based model, is utilised in this paper. It is, in essence, a PD controller that inputs the frequency deviation and outputs the current reference in the d-axis to the convert [18].

VI from different sources are investigated in literature; batteries [35], capacitors [36], HVDC [37], and wind power [31, 38–42]. An MPC based VI control system for a wind farm (WF) with a battery energy storage system (BESS) is proposed in [42]. The control system is able to increase the efficiency of the WF, increasing the lifetime of the BESS and increasing the minimum speed of the wind turbine rotors.

VSHP plants are particularly suited for delivering VI and FFR compared to other RES because of the energy stored in the rotating masses and the possibility to adjust power production without major power loss [18, 43]. For full utilisation of this potential, an advanced control system is developed to maximise the contribution to system inertia and frequency control [2, 3]. The MPC coordinates the control of the hydraulic and electrical systems while considering the constraints in the system and optimising both the VSHP power output, the guide vane opening and the turbine rotational speed. At the same time, the MPC tries to reduce pressure oscillations in the hydraulic system and power oscillations in the electric system. The MPC dispatches the power reference to the VI controller, which is responsible for the frequency control and power oscillation damping. Small-signal stability analysis is performed for two types of VI controllers; the grid-following VSG [18] and the grid-forming virtual synchronous machine (VSM) [18, 24]. However, the MPC is not included in these works.

1.3 Contribution and Paper Structure

This paper investigates the small-signal properties of a VSHP controller structure with MPC and VSG controllers, as shown in Figure 1 and presented in [3]. The last-mentioned paper only presents dynamic results. Small-signal stability has not previously been investigated on this control system, nor has any methods for the small-signal analysis of the proposed MPC been proposed. Thus, the methods and results presented in this paper are important contributions to understand the stability properties of the given VSHP control scheme.

The stability analysis is based on the linearization of the nonlinear models, relevant for the analysis of small disturbances. The control structure is similar to the control structure presented in [3]; however, the moving horizon estimator (MHE) utilised in [3] is replaced by a Kalman filter since the small-signal analysis of the MHE would imply a high number of states and modes.

The purpose of the small-signal analysis is to understand how the MPC controller must be parametrised to avoid adverse interactions and oscillations between the hydraulic system of the VSHP and the grid. If these two systems are decoupled, the tuning of the VSG does not need to consider the dynamics of the hydraulic system. Consequently, the parameters of the VSG can be optimised to reduce the frequency deviation by delivering FFR and damp power oscillations.

The main contributions of this paper:

- Presents a method for small-signal properties of a VSHP controller structure with MPC and VSG controllers.
- Defines the assumptions for utilising this method.
- Investigates how the parametrisation of the MPC cost function affects interactions and oscillations between the hydraulic system of the VSHP and the grid.
- Concludes that the cost of the deviations in the hydraulic system must be low compared to the cost of deviations in the VSG power reference to avoid such oscillations.
- Propose to utilised power oscillation damper (POD) tuning method from [44] to parametrise the VSG.
- Investigates how the VSG parameters affect the damping of power oscillation modes.

The paper is arranged as follows: The theory of state-space representation of MPC is presented in Section 2. This theory is the basis for the development of a state-space representation of the VSHP control system with the MPC presented in Section 3. Sections 4 and 5 present the results and discussion of, respectively, the participation factor-based interaction analysis and the sensitivity analysis of the VSG parameters. Section 6 investigates the consequences of the necessary assumptions to derive the state-space representation of the MPC by transient simulation in the time-domain. Finally, in Section 7, the conclusions are given.

2 State-Space Representation of Model Predictive Controller

To enable the use of small-signal analysis of the VSHP with the proposed MPC controller and VSG, a state-space representation of the MPC is needed. We will utilise the state-space formulation of an MPC controller derived in [45] and [46]. This formulation includes a state estimator and assumes no active constraints. Therefore, the proposed MPC controller in [3] must be simplified in order to be able to make use of this method. We therefore chose to only consider operation points where no MPC constraints are active. As we will discuss later, this assumption applies to most stationary operation points.

The MPC controller from [3] is given as:

$$\begin{aligned}\min_{x\in\mathbb{R}^n, u\in\mathbb{R}^m} f(x,u) = \sum_{t=0}^{N-1} &\frac{1}{2}x_{t+1}^{\mathrm{T}} Q_{t+1} x_{t+1} \\ &+ d_{xt+1}x_{t+1} + \frac{1}{2}\Delta x_{t+1}^{\mathrm{T}} Q_{\Delta t}\Delta x_{t+1} + \frac{1}{2}u_t^{\mathrm{T}} R_t u_t \\ &+ d_{ut}u_t + \frac{1}{2}\Delta u_t^{\mathrm{T}} R_{\Delta t}\Delta u_t + \rho^{\mathrm{T}}\epsilon + \frac{1}{2}\epsilon^{\mathrm{T}} S\epsilon \quad (1)\end{aligned}$$

subjected to

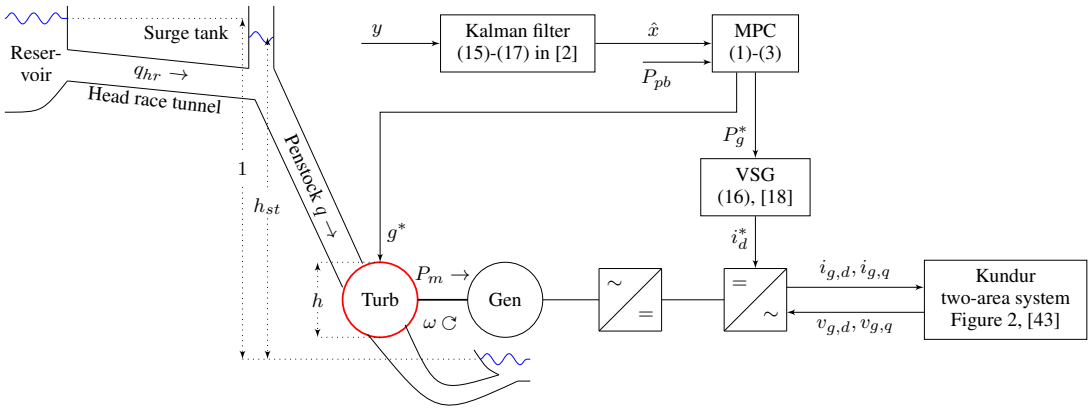

Fig. 1: VSHP plant layout with equations for modelling and control structure

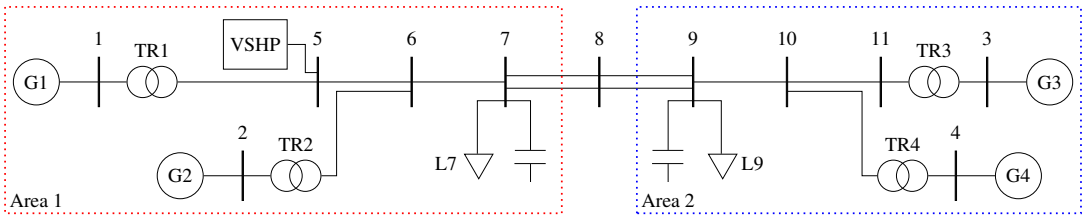

Fig. 2: Kundur two-area system

$$
\begin{aligned}
x_{t+1} &= g\left(x_t, u_t\right) && t = 0, \ldots, N-1 \\
x_0, u_{-1} &= \text{given} \\
x^{\text{low}} - \epsilon \leq x_t &\leq x^{\text{high}} + \epsilon && t = 1, \ldots, N \\
-\Delta x^{\text{high}} \leq \Delta x_t &\leq \Delta x^{\text{high}} && t = 1, \ldots, N \\
A_{ineq} x_t + B_{ineq} u_t &\leq b_{ineq} && t = 1, \ldots, N \\
u^{\text{low}} \leq u_t &\leq u^{\text{high}} && t = 0, \ldots, N-1 \\
-\Delta u^{\text{high}} \leq \Delta u_t &\leq \Delta u^{\text{high}} && t = 0, \ldots, N-1
\end{aligned} \tag{2}
$$

where

$$
\begin{aligned}
Q_t &\succeq 0 && t = 1, \ldots, N \\
Q_{\Delta t} &\succeq 0 && t = 1, \ldots, N \\
R_t &\succeq 0 && t = 0, \ldots, N-1 \\
R_{\Delta t} &\succeq 0 && t = 0, \ldots, N-1 \\
\Delta x_t &= x_t - x_{t-1} && t = 1, \ldots, N \\
\Delta u_t &= u_t - u_{t-1} && t = 0, \ldots, N-1 \\
\epsilon &\in \mathbb{R}_x^n \geq 0 \\
\rho &\in \mathbb{R}_x^n \geq 0 \\
S &\in \text{diag}\left\{s_1, \ldots, s_{n_x}\right\}, s_i \geq 0, i = \{1, \ldots, n_x\}
\end{aligned} \tag{3}
$$

Since small-signal analysis is performed in steady-state and at an equilibrium point where all the derivatives of the state variables are simultaneously zero, we only need to assume the constraints and slack variables ϵ to be inactive in the steady-state operation point. For the proposed MPC controller [2, 3], none of the MPC constraints or slack variables are active as long as the system is in steady-state, the water flow is higher than its minimum value 0.3, corresponding to $P_g \approx 0.2$ $p.u.$ and the VSHP output power P_g is less or equal its maximum value, 1 p.u. Accordingly, the slack variables for the surge tank head h_{st}, the turbine head h, the turbine rotational speed ω and the turbine flow q will not be activated in this case, neither will the constraints for the guide vane opening g or the VSHP output power P_g. The slack variables ϵ can, therefore, be eliminated from (1) and the inequality constraints can be eliminated from (2). Since only a small perturbation is applied when performing small-signal analysis, we can also disregard the constraints on changes in states (Δx) and inputs (Δu).

Before performing the small-signal analysis, the MPC and the system are linearised at the stationary values equal to the reference values of the MPC objective function such that $d_{xt+1} = 0$ and $d_{ut} = 0$ for the linearised system. The equality constraints are linearised to $x_{t+1} = Ax_t + Bu_t$. While final costs are added in [2, 3] to increase the robustness of the MPC and reduce the number of time steps N, these must be neglected to find the state-space representation of the MPC. Thereby, the cost matrices are equal for each time step, such that $Q_t = Q$, $R_t = R$ and $R_{\Delta t} = R_\Delta$ for all t. In addition, the costs related to changes in the states are disregarded, such that $Q_{\Delta t} = Q_\Delta = 0$.

With these assumptions, we get the following objective function without any constraints:

$$
\begin{aligned}
\min_{x \in \mathbb{R}^n, u \in \mathbb{R}^m} f(x, u) = \sum_{t=0}^{N-1} & \frac{1}{2} x_{t+1}^{\mathrm{T}} Q x_{t+1} \\
& + \frac{1}{2} u_t^{\mathrm{T}} R u_t + \frac{1}{2} \Delta u_t^{\mathrm{T}} R_\Delta \Delta u_t
\end{aligned} \tag{4}
$$

subjected to

$$
\begin{aligned}
x_{t+1} &= Ax_t + Bu_t \quad t = 0, \ldots, N-1 \\
x_0, u_{-1} &= \text{given}
\end{aligned} \tag{5}
$$

The derivation of an equivalent controller without active constraints is based on the MPC algorithm presented in [46]. By assuming that the output vector y_k equals the state vector x_k and the disturbance $d_k = 0$, the state-space model for the MPC control algorithm (6) presented in [46] equals (5).

$$\begin{aligned} x_{k+1} &= Ax_k + Bu_k + E_d d_k, \quad k = 0, 1, 2, \dots \\ y_k &= Cx_k \end{aligned} \tag{6}$$

The cost function in [46] is given as an infinite horizon criterion where the control input u_{k+j} is zero for all $j \geq N$ and $u_k^N = [u_k \quad u_{k+1} \dots u_{k+N-1}]$ is a vector of the N next moves of the control input:

$$\min_{u_k^N} \sum_{j=0}^{\infty} \left(x_{k+j}^T Q x_{k+j} + u_{k+j}^T R u_{k+j} + \Delta u_{k+j}^T R_\Delta \Delta u_{k+j} \right) \tag{7}$$

By assuming that $x_k = 0$ for $j \geq N$, (7) equals (4). As long as the perturbation is small, the system is stable and the modes damped, x_k is negligible for $j > N$.

In order to be able to use the method from [45] to find a state-space representation of the MPC, the following assumptions must be made:

- The system is stable and in steady-state.
- There are no active constraints or slack variables.
- Final costs are neglected such that the cost matrices are equal for all time steps.
- Costs related to changes in the states are disregarded.
- At the steady-state operation point, the solution of the linearised cost function is zero. This implies that the reference values of the objective function must equal the steady-state operation point.
- The perturbation is small and the modes are damped.

With these assumptions, we can simplify the MPC problem to (8) [45].

$$\begin{aligned} \min_{u_k^N} \Phi_k &= \left(u_k^N\right)^T H u_k^N + 2\left(u_k^N\right)^T (Gx_k - Fu_{k-1}) \\ \nabla\Phi\left(u_k^N\right) &= 2Hu_k^N + 2\left(Gx_k - Fu_{k-1}\right) = 0 \\ u_k^N &= -H^{-1}Gx_k + H^{-1}Fu_{k-1} \\ u_k &= K_x x_k + K_u u_{k-1} \end{aligned} \tag{8}$$

The state feedback K_x is the first r rows of $-H^{-1}G$, where r is the number of control inputs. Similarly, the feedback from the previous control input K_u is found as the first r rows of $H^{-1}F$. The matrices H, G and F are given in (9) [46].

$$H = \begin{bmatrix} a_{1,1} & a_{1,2} & \cdots & a_{1,n} \\ a_{2,1} & a_{2,2} & \cdots & a_{2,n} \\ \vdots & \vdots & \ddots & \vdots \\ a_{n,1} & a_{n,2} & \cdots & a_{n,n} \end{bmatrix}$$

$$\begin{aligned} a_{1,1} &= B^T\overline{Q}B + R + 2R_\Delta \\ a_{1,2} &= B^TA^T\overline{Q}B - R_\Delta \\ a_{1,n} &= B^TA^{T^{N-1}}\overline{Q}B \\ a_{2,1} &= B^T\overline{Q}AB - R_\Delta \\ a_{2,2} &= B^T\overline{Q}B + R + 2R_\Delta \\ a_{2,n} &= B^TA^{T^{N-2}}\overline{Q}B \\ a_{n,1} &= B^T\overline{Q}A^{N-1}B \\ a_{n,2} &= B^T\overline{Q}A^{N-2}B \\ a_{n,n} &= B^T\overline{Q}B + R + 2R_\Delta \end{aligned} \tag{9}$$

$$G = \begin{bmatrix} B^T\overline{Q}A^1 \\ B^T\overline{Q}A^2 \\ \vdots \\ B^T\overline{Q}A^N \end{bmatrix}, \quad F = \begin{bmatrix} R_\Delta \\ 0 \\ \vdots \\ 0 \end{bmatrix}$$

$$\overline{Q} = C^TQC + A^T\overline{Q}A$$

Since we have assumed a stable system, the terminal state penalty matrix, $\overline{Q}$, is found as given in (10) by solving the discrete Lyapunov equation (11) [46] where $C = I$ in this case.

$$\overline{Q} = \sum_{i=0}^{\infty} A^{T^i} C^T Q C A^i \tag{10}$$

$$\overline{Q} = C^TQC + A^T\overline{Q}A \tag{11}$$

A continuous version of (8) is found by assuming that the previous input u_{k-1} is a first-order lag of the input, as indicated in Figure 3:

$$u = K_x x + K_u u \frac{1}{1 + \Delta t s} \tag{12}$$

3 Model Predictive Controller

The method for deriving the state-space representation of an MPC controller for controlling a VSHP is tested on the nonlinear MPC presented in [3]. The MPC is derived from the system equations (13) presented in [43]. These equations include models of the grid, the VSG power control of the converters, the turbine and the waterway, as shown in Figure 1. The model contains six states (14): the local grid frequency Δf, the guide vane opening of the turbine g, the turbine flow q, the headrace tunnel flow q_{hr}, the surge tank head h_{st} and the turbine rotational speed ω. The inputs (15) are the power reference to the VSG P_g^* and the guide vane opening reference g^*. The derivation of the model and explanation of the parameters are found in [43]. The variables and parameters of the VSHP is given in, respectively, Table 1 and Table 2.

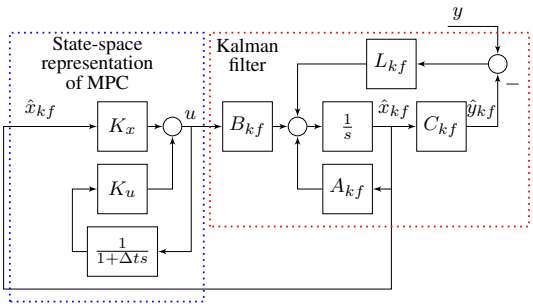

Fig. 3: Control layout of VSHP plant with MPC and Kalman filter

$$
\begin{aligned}
\Delta\dot{f} &= \frac{\omega_s}{2H_g S_n}\left(P_g + P_{pb} - D_m\Delta f\right)\\
\dot{g} &= \frac{1}{T_G}\left(g^* - g\right)\\
\dot{q} &= \frac{1}{T_{\mathrm{w1}}}\left(h\frac{H_{\mathrm{R}}}{H_{\mathrm{Rt}}} - \sigma\left(\omega^2 - 1\right) - \left(\frac{q}{g}\right)^2\right)\frac{Q_{Rt}}{Q_R}\\
\dot{q}_{hr} &= \frac{1}{T_{\mathrm{w2}}}\left(1 - h_{\mathrm{st}} + f_0(q_{\mathrm{hr}} - q)^2 - f_{\mathrm{p2}}{q_{\mathrm{hr}}}^2\right)\\
\dot{h}_{st} &= \frac{1}{C_s}\left(q_{\mathrm{hr}} - q\right)\\
\dot{\omega} &= \frac{1}{2H}\left(T_m - P_g/\omega - D\left(\omega^* - \omega\right)\right)
\end{aligned}
\tag{13}
$$

$$
\begin{aligned}
\dot{x} &= [\Delta\dot{f} \quad \dot{g} \quad \dot{q} \quad \dot{q}_{hr} \quad \dot{h}_{st} \quad \dot{\omega}]^T\\
x &= [\Delta f \quad g \quad q \quad q_{hr} \quad h_{st} \quad \omega]^T
\end{aligned}
\tag{14}
$$

$$
u = [P_g^* \quad g^*]^T \tag{15}
$$

The VSHP output power P_g controlled by the VSG is found in (16) while the turbine Power P_m is found in (17).

Table 1 Variables

Variable	Symbol
Waterway	
Surge tank head	h_{st}
Head race tunnel flow	q_{hr}
Hydraulic Machine	
Turbine head	h
Turbine water flow	q
Mechanical torque	T_m
Mechanical power	P_m
Turbine efficiency	η_h
Turbine head	h_t
Turbine flow	q_t
Opening degree of turbine	κ
Governor	
Guide vane opening reference	g^*
Guide vane opening	g
Synchronous generator	
Rotor speed	ω
Grid converter	
Active power	P_g
Grid	
Grid frequency	f

$$
P_g = i_{g,d} = -k_{vsg,p}\Delta f - k_{vsg,d}\Delta\dot{f} + P_g^* \tag{16}
$$

$$
\begin{aligned}
P_m = {} & \frac{H_{\mathrm{Rt}}}{H_{\mathrm{R}}}\frac{Q_R}{Q_{Rt}}\\
& \left(\left(\frac{\xi q}{g}\left(\tan\alpha_{1R}\sin\alpha_1 + \cos\alpha_1\right)\right) - \psi\omega\right)\frac{q\omega}{h}\\
\alpha_1 = {} & \sin^{-1}\left(\frac{Q_{\mathrm{R}}}{Q_{\mathrm{Rt}}}g\sin\alpha_{1R}\right)
\end{aligned}
\tag{17}
$$

The turbine head h is the difference in water pressure above and below the turbine and is given by (18), where h_p is the pressure waves in the penstock, called water hammering. For the linearised model, a fourth-order approximation of h_p is utilised ($n_{max} = 4$).

$$
\begin{aligned}
h &= h_{st} - f_0\left(q_{\mathrm{hr}} - q\right)^2 - f_{\mathrm{p1}}q^2 + h_p\\
h_p &= -Z_0\tanh\left(sT_e\right)q = -Z_0\left(\frac{1 - e^{-2T_e s}}{1 + e^{-2T_e s}}\right)q\\
&\approx -Z_0\frac{sT_e\prod_{n=1}^{n_{max}}\left(1 + \left(\frac{sT_e}{n\pi}\right)^2\right)}{\prod_{n=1}^{n_{max}}\left(1 + \left(\frac{2sT_e}{(2n-1)\,\pi}\right)^2\right)}
\end{aligned}
\tag{18}
$$

The parameters of the MPC functions (1)-(3) are derived from the MPC dynamic model given in (13)-(15) and the costs given in Tables 4 and 5. Constraints and slack variables are not included since they are assumed to be inactive. Next, the MPC is linearised at the operation point to find the MPC with linear equality constraints (4)-(5) and the feedback matrices K_x and K_u are found from (8) and (9).

The MHE is utilised to estimate the states in [3]. However, the MHE is not suited for state-space representation since it depends on previous measurements. Therefore, a linear continuous-time Kalman filter is used to estimate the states in this paper.

Table 2 Parameters

Parameter	Symbol	Unit	Value
Waterway			
Rated water flow	Q_R	$[m^3/s]$	170
Rated height	H_R	$[m]$	425
Penstock:			
Water starting time	T_w	$[s]$	1.211
Water traveling time	T_e	$[s]$	0.126
Characteristic impedance	Z_0		9.61
Friction factor	f_{p1}	$[s^4/m^5]$	0.049
Surge tank:			
Friction factor	f_{p0}	$[s^4/m^5]$	0.036
Storage constant	C_s		0.099
Head race tunnel:			
Water starting time	T_{w2}	$[s]$	4.34
Friction factor	f_{p2}	$[s^4/m^5]$	0.020
Hydraulic Machine			
Turbine constant	ψ		0.404
Turbine constant	ξ		0.918
Turbine constant	α		0.745
Turbine constant	σ		0.015
Rated water flow	Q_{Rt}	$[m^3/s]$	144
Rated height	H_{Rt}	$[m]$	425
Governor			
Servo time constant	T_G	$[s]$	0.50
Synchronous generator			
Inertia constant	H	$[s]$	6.5
Damping constant	D		0

The Kalman filter inputs the measurements y: the grid frequency deviation Δf, guide vane opening g, turbine rotational speed ω, turbine head h and turbine mechanical power P_m. The estimated states are found by the continuous-time Kalman filter equations (19), as explained in Figure 3.

$$\begin{aligned}\dot{\hat{x}}_{kf} &= A_{kf}\hat{x}_{kf} + B_{kf}u_{kf} \\ &\quad + L_{kf}\left(y_{kf} - C_{kf}\hat{x}_{kf} - D_{kf}u_{kf}\right)\end{aligned} \tag{19}$$

where

$$\begin{aligned}\hat{x}_{kf} &= [\Delta\hat{f} \quad \hat{g} \quad \hat{q} \quad \hat{q}_{hr} \quad \hat{h}_{st} \quad \hat{\omega}]^T \\ \hat{y}_{kf} &= [\Delta\hat{f} \quad \hat{g} \quad \hat{\omega} \quad \hat{h} \quad \hat{P}_m]^T \\ y &= [\Delta f \quad g \quad \omega \quad h \quad P_m]^T\end{aligned} \tag{20}$$

The matrices A_{kf}, B_{kf}, C_{kf} and D_{kf} are found by linearising the system model differential algebraic equations (DAE) (13) at the initial stationary operation point. In this case, $D_{kf} = 0$ and is therefore not included in Figure 3.

The algebraic Riccati equation (21) is solved to find the Kalman gain L_{kf} by the MatLab-function `kalman` [47, 48].

$$\begin{aligned}L &= \left(PC^T + \overline{N}\right)\overline{R}^{-1} \\ \overline{R} &= R + HN + N^T H^T + HQH^T \\ \overline{R} &= G\left(QH^T + N\right)\end{aligned} \tag{21}$$

Q_N (23) and R_N (23) are, respectively, the covariance matrices for the process noise w and the measurement noise v as given by the continuous system equations:

$$\begin{aligned}\dot{\hat{x}}_{kf} &= A_{kf}\hat{x}_{kf} + B_{kf}u + G_{kf}w \\ \hat{y}_{kf} &= C_{kf}\hat{x}_{kf} + H_{kf}w + v\end{aligned} \tag{22}$$

$$Q_N = \begin{bmatrix}0.01 & 0 \\ 0 & 0.01\end{bmatrix} \tag{23}$$

$$R_N = \begin{bmatrix}0.01 & 0 & 0 & 0 & 0 \\ 0 & 0.01 & 0 & 0 & 0 \\ 0 & 0 & 0.1 & 0 & 0 \\ 0 & 0 & 0 & 0.1 & 0 \\ 0 & 0 & 0 & 0 & 0.01\end{bmatrix} \tag{24}$$

4 Participation Factor-Based Interaction Analysis

The next sections present the results of the small-signal analysis of the VSHP with the MPC from Section 3. The grid model is presented in [43] and Figure 2 and is based on the Kundur two-area system. The VSHP is modelled as presented in [43] with some modifications:

- The guide vane reference is provided by the MPC instead of the governor control.
- A VSG replaces the active power control of the grid-connected converter, as presented in [18]. Its values are given in Table 3.
- The MPC provides the VSG power reference.

The main purpose of the small-signal analysis is to investigate possible modes between the grid and the hydraulic system of the VSHP. In [43], the small-signal analysis shows that no modes are interacting between two parts of the VSHP since the VSHP plant dynamic is effectively decoupled by the fast control of the voltage on the DC-link between the converters. Thus, the hydraulic system, generator and SG converter do not interact with the rest of the VSHP and the grid in the frequency range of interest. The guide vane opening g and the VSHP output power P_g are controlled individually and a perturbation on the hydraulic side of the DC-link will not affect the VSHP output power, thus explaining the lack of modes between the two parts of the VSHP.

In this paper, a VSHP with MPC control is investigated. The MPC coordinates the control of the guide vane opening reference g^* and the VSHP output power reference P_g^* to optimise the system performance. The degree of dynamic coupling between the hydraulic system of the VSHP and the grid therefore depends on the parameters of the MPC objective function. Two cases with different values of these parameters, as shown in Table 4 and 5, are compared to show how the MPC must be configured to avoid oscillations between the VSHP hydraulic system (Figure 1) and the grid (Figure 2).

Participation factors measure the interaction between the modes and the state variables of a linear system. More precisely, it measures the relative participation of a specific state variable of a specific mode, and vice versa [1]. The participation factor-based interaction analysis presented in [49] groups the states into subsystems, to show the relative interaction between each mode and all states of a subsystem. If there are high interactions between a mode and the states in several subsystems, this shows that these subsystems interact. An interaction mode is defined as a mode with participation from more than one subsystem and proves a dynamic interaction between the subsystems. When this is the case for a mode pair, the factor-based interaction analysis proves an oscillation mode between the two subsystems, with the frequency and damping given by the mode pair.

Case 1 is similar to the case presented in [3]; however, the simplifications from Section 2 are introduced. Figure 4 shows the participation factor-based interaction analysis. The colours represent the magnitude of the participation factor $\eta_{\alpha i}$ for the modes on the x-axis and for each subsystem on the y-axis. The modes are sorted by the participation in each of the 11 subsystems and modes that are only participating in generators G1-G4 and only in the VSHP water way model are not shown.

The system can be divided into two parts where no modes are interacting in both these parts, according to Figure 4. This was also the conclusion from [43]. The first part is the turbine side of the

Table 3 VSG parameters

Parameter	Value
ω_1	0.55
ω_2	0.77
T_1	1.81
T_2	1.30
ω_m	0.65
ω_{vsg}	0.77
$k_{vsg,p}$	50
$k_{vsg,d}$	25.4

Table 4 Cost of deviations in states and inputs

State/input	Reference value	Cost matrix	Cost factor Case 1	Cost factor Case 2
Turbine rotational speed ω	1	$Q(6,6)$	1000	1000
VSHP power reference P_g^*	0.8	$R(1,1)$	1000	0

Table 5 Cost of changes in states and inputs

State/input	Cost matrix	Cost factor Case 1	Cost factor Case 2
Guide vane opening Δg^*	$R_{\Delta t}(2,2)$	1000	1000

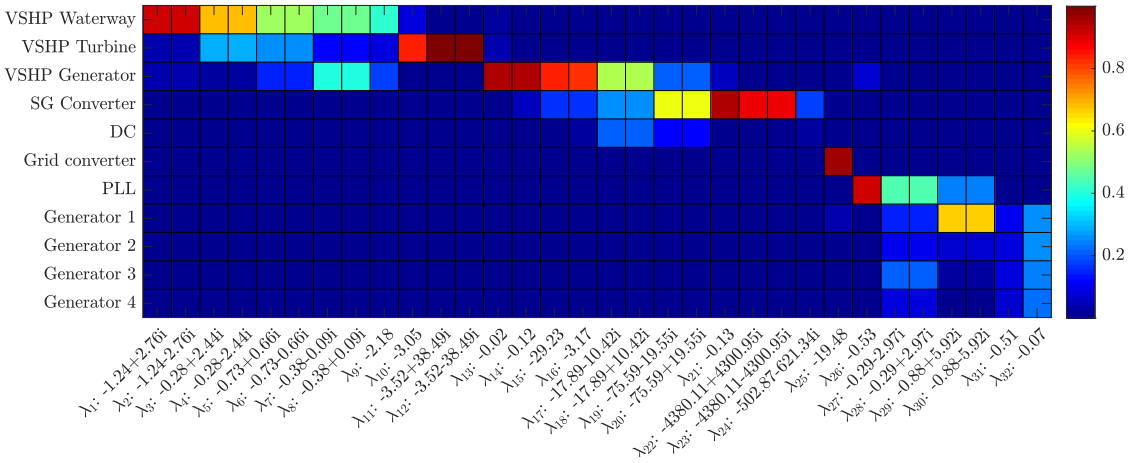

Fig. 4: Case 1: Participation factor-based interaction analysis

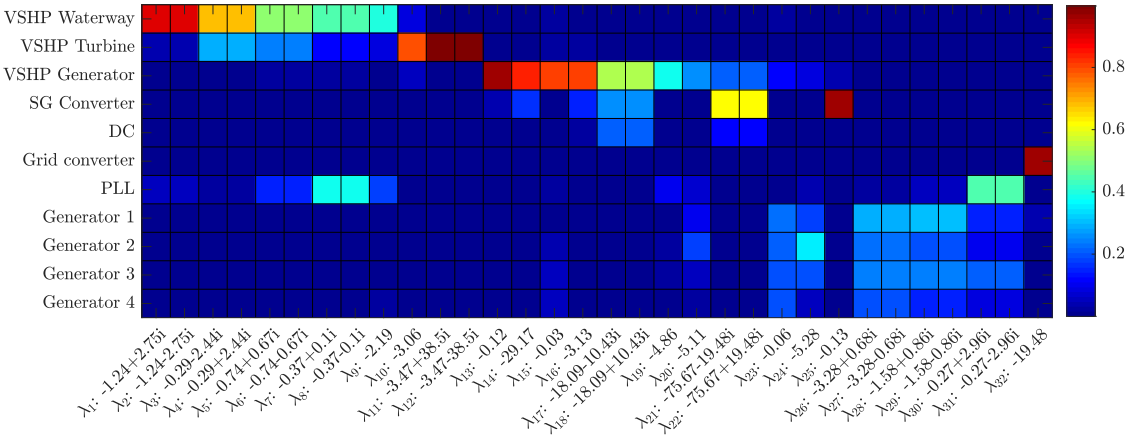

Fig. 5: Case 2: Participation factor-based interaction analysis with no cost on deviation in P_g^*

DC-link including the VSHP waterway, VSHP turbine, VSHP governor, VSHP generator, SG converter and DC-link. The second part is the grid side of the DC-link including the grid converter, the phase-locked loop (PLL) and the other generators in the grid. The two parts are decoupled since the cost for deviations in VSHP output power reference P_g^* is high while there is no cost on deviation in guide vane opening reference g^*. A deviation in the turbine rotational speed caused by a perturbation will therefore primarily be corrected by the MPC by controlling the guide vane opening reference g^*. Since the change in the VSHP output power reference P_g^* from the MPC will be negligible, a deviation on the turbine side of the DC-link will not affect the rest of the system and there will be no modes between the waterway, turbine and generator and the rest of the system.

Figure 5 presents Case 2, where the cost of deviations in VSHP output power reference P_g^* from its setpoint is reduced to zero. In Case 1, where the cost of deviation in P_g^* was high, the MPC only adjusted P_g^* in extreme cases when control of the guide vane opening reference g^* was not sufficient to bring the turbine rotational speed ω back to reference speed while keeping the system within its constraints. When there is no cost on deviation in the VSHP output power reference P_g^*, the MPC controller adjusts both g^* and P_g^* to return the turbine rotational speed ω to its reference. A perturbation in one of the two parts of the system will, therefore, affect the other part and there will be modes between the two parts, as seen for instance for λ_{13} and λ_{14} in Figure 5.

The modes with the highest interaction between the VSHP plant and the other generators in the grid are shown in Figure 6. Most of these modes are recognised in the estimated frequency f_{kf} by the Kalman filter. Modes λ_5 to λ_8 between the states in the Kalman filter and the hydraulic variables show oscillations between the estimated frequency and the turbine flow q, the headrace tunnel flow q_{hr} and the guide vane opening g. The next two modes, $\lambda_1 5$ and $\lambda_2 5$, show a relationship between the turbine rotational speed ω and the guide vane openings of all the four generators in the grid (c_1-c_4). The figure also shows some well-damped modes affecting the turbine rotational speed ω_{kf}, the d-axis voltage of the synchronous generator connected converter, $V_{cd,sg}$ and the transient voltage in the d-axis of the four generators in the power system, $E_{dd,1}$ to $E_{dd,4}$.

5 Sensitivity Analysis of VSG Parameters

The VSG with a first-order filter on its differentiation term (25) is equivalent to the POD [44] (26) and will, therefore, affect the damping of power oscillations in the grid. Consequently, the VSHP with the proposed control system can reduce power oscillation by proper tuning of the VSG. The POD tuning method from [44] can be utilised

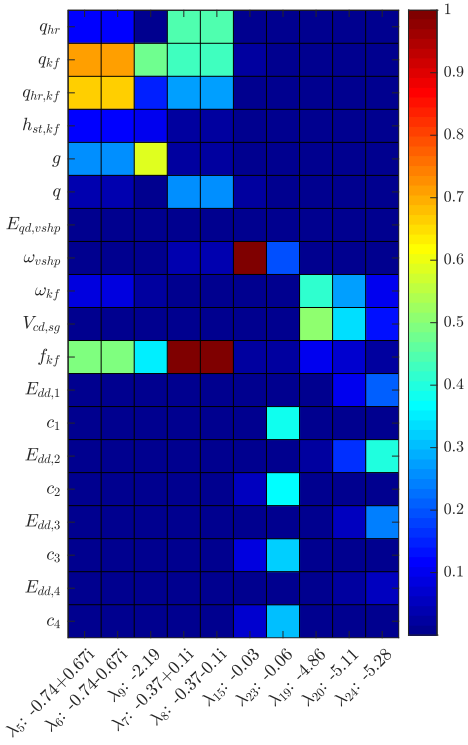

Fig. 6: Case 2: Participation factor analysis with no cost on deviation in P_g^*

for the VSG since the two controllers are equal. The corner frequencies $\omega_1 = 1/T_1$ and $\omega_2 = 1/T_2$ are chosen to provide a positive phase to the system between these values. The centre frequency ω_m (27) is the geometric mean of these two frequencies and should ideally correspond to the main oscillation to be damped.

$$C(s) = k_{vsg,p} + k_{vsg,d}\frac{\omega_{vsg}s}{s+\omega_{vsg}} \tag{25}$$

$$C(s) = K\left(\frac{1+T_1 s}{1+T_2 s}\right) \tag{26}$$

$$\omega_m = \frac{1}{T_2\sqrt{T_1/T_2}} \tag{27}$$

Figure 7 shows how the damping of the power oscillations is affected by the corner frequencies ω_1 and ω_2. The modes are plotted as a function of $k \in [0.5, 2]$, illustrated by the colours, where $\omega_1 = k\omega_{1-2}$, $\omega_2 = 2\omega_{1-2}/k$ and $\omega_{1-2} = 0.46rad/s$ is the frequency of the oscillations between Area 1 and Area 2, as indicated in Figure 2. As seen from (27), the centre frequency ω_m is thereby kept constant at $0.65rad/s$, close to the mean value of the power oscillation frequencies.

As k increases, the range of frequencies damped by the VSG becomes wider, and the damping of the power oscillations is increased for most cases. However, the added phase decreases. This effect causes the damping of the power oscillations between Area 1 and Area 2 to decrease when k increases above 1.2. We have therefore chosen to use the VSG parameters corresponding to $k = 1.2$ in this paper, as given in Table 3.

A high gain of the VSG reduced the grid frequency deviation after a disturbance; however, it also affects the damping of power oscillations in the grid. This phenomenon is investigated in Figure 8, where the colours illustrate how the interarea mode (Area 1-Area 2) and the

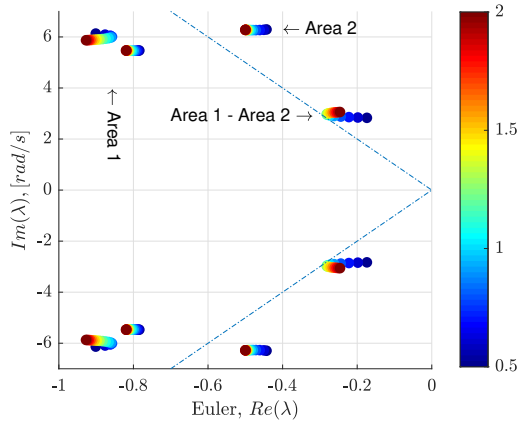

Fig. 7: Power oscillation modes plotted for different corner frequencies: $k \in [0.5, 2]$, $\omega_1 = k\omega_{1-2}$ and $\omega_2 = 2\omega_{1-2}/k$

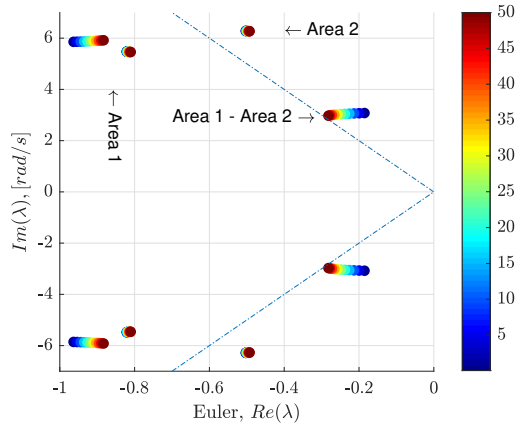

Fig. 8: Power oscillation modes plotted for increasing gains of the VSG, $k_{vsg,p} \in [0, 50]$ and $k_{vsg,d} \in [0, 25.4]$

local modes (Area 1 and Area 2) are influenced by the proportional gains of the VSG, $k_{vsg,p} \in [0, 50]$. The gain of the VSG derivation term $k_{vsg,d} \in [0, 25.4]$ is increased proportionally to $k_{vsg,p}$.

As seen from the figure, the VSHP with VSG control of the grid-connected inverter increases the damping of the interarea mode significantly as the gain of the VSG increases. Similarly, a larger VSHP will increase the damping more than a small VSHP. The local modes are less affected; however, a decrease of the damping of one of the modes in Area 1, where the VSHP is located, is observed.

Figure 9 compares the electromechanical modes of the MPC and VSG-based control system with a conventional VSHP control system as presented in [43]. The introduction of the VSG increases the damping of the power oscillation modes, especially the interarea mode between Area 1 and Area 2. It also causes additional oscillation mode in Area 1 between the VSG and the two generators in this area.

6 Transient simulations

In this section, the state-space representation of the MPC is compared to the original nonlinear MPC presented in [3] by transient simulation in the time domain. The motivation is to clarify the weak points and the limitations of the state-space representation of the

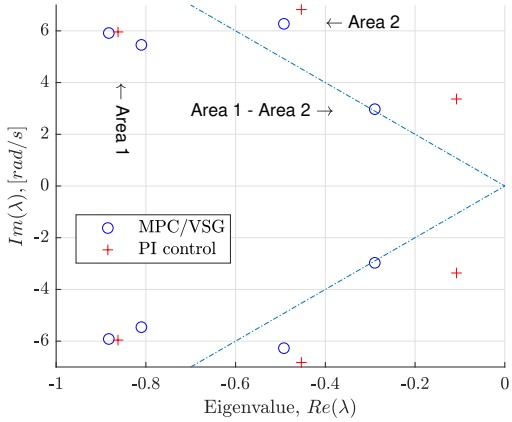

Fig. 9: Electromechanical modes for the proposed control system based on MPC and VSG compared to conventional PI control of VSHP

MPC. In addition, we investigate the consequences of the necessary assumptions for the derivation of this model.

The model of the nonlinear MPC is given by (1)-(3) and (13)-(18) while the state-space representation of the MPC in found in (8)-(12). Both cases utilise the same Kalman filter (19)-(24). They are also both tested on nonlinear models of the grid and VSHP as presented at the start of Section 4.

Figure 10 shows the transient behaviour of the two cases after a large disturbance in the grid; a 320 MW load increase at Bus 7 at $t = 0$. This corresponds to half of the rated power of the VSHP. From the figure, we recognize some differences in the internal variables of the VSHP. This is explained by the simplifications of the state-space representation of the MPC. Firstly, the turbine rotational speed reference ω^* is kept constant, while this is a function of VSHP output power P_g for the nonlinear MPC [3]:

$$\begin{aligned} 0.85 < P_g \qquad & \omega^* = 1 + 0.6(P_g - 0.85) \\ 0.73 < P_g < 0.85 \quad & \omega^* = 1 + 0.3(P_g - 0.85) \\ P_g < 0.73 \quad & \omega^* = 0.964 + 0.15(P_g - 0.73) \end{aligned} \tag{28}$$

Thus, the turbine rotational speed reference ω^* increases after the disturbance. This causes an overshoot in the turbine rotational speed ω and a higher steady-state value in the case of the nonlinear MPC.

Secondly, the power balance of the grid P_{pb} is assumed to be constant for the state-space representation of the MPC. For the nonlinear MPC, this value is a function of the grid frequency Δf and its derivative $\Delta \dot{f}$ (ROCOF - Rate of Change of Frequency), as given in [3]:

$$P_{pb} = -P_g + \frac{2H_g S_n}{\omega_s} \frac{\omega_{\dot{f}}}{s + \omega_{\dot{f}}} \Delta \dot{f} + D_m \frac{\omega_f}{s + \omega_f} \Delta f \tag{29}$$

Right after the disturbance, the frequency Δf decreases, causing the ROCOF to become negative and, thereby, the estimated value of the power balance P_{pb} decreases. From (13) and (16), we see that the predicted frequency Δf is lower for the nonlinear MPC, causing the nonlinear MPC to also predict a higher future VSHP output power P_g. Therefore, the nonlinear MPC increases the guide vane opening reference g^* more to limit the deviation in turbine rotational speed ω. This results in a higher deviation in the turbine mechanical power P_m, the turbine flow q, the head race tunnel flow q_{hr} and the pressure oscillations in the turbine head h and the surge tank head h_{st}.

Another main difference between the two models is that the nonlinear MPC reduces the VSHP power reference P_g^* the first 10 seconds after the disturbance. The reason for this is that the nonlinear MPC tries to limit the maximum deviation in the turbine rotational speed ω. Since the nonlinear MPC considers an estimated value of the power balance of the grid P_{pb}, it predicts a higher VSHP output power P_g. Thus, the nonlinear MPC reduces the VSHP power reference P_g^* more than the state-space representation of the MPC, that assumes a constant power balance of the grid P_{pb}.

After approximately 20 seconds, both MPC structures output the same guide vane opening reference g^*. At this point, the grid frequency Δf and the estimated power balance of the grid P_{pb} have stabilized and thereby the state-space representation of the MPC predicts the VSHP output power P_g more correctly. After the first 20 seconds, the flows are similar for both cases, and the oscillations in the heads are more or less equal. However, there is still a significant mismatch in turbine rotational speed ω since the reference turbine rotational speed ω^* is constant in the case of the state-space representation of the MPC.

7 Conclusion

A method for state-space representation of MPC is utilised in this paper in order to be able to perform small-signal analysis of a VSHP with a control scheme including MPC and VSG. The investigated MPC optimises the performance of the power plant by controlling the hydraulic system (guide vane opening) and the electrical power reference. By assuming a steady-state operation point of the VSHP within the constraints of the MPC where the reference values of the objective function are fulfilled, the MPC problem can be simplified to a linear system. Small-signal analysis on a power system with this linearised MPC demonstrates negligible dynamic interaction between the hydraulic system and the power system. This conclusion applies as long as the cost function of the MPC is defined such that the costs of deviations in the hydraulic system are low compared to the cost of deviations in the electrical power output.

The decoupling of the hydraulic and electrical system allows the possibility of tuning the VSG controller without considering the eigenvalues of the hydraulic system. Sensitivity analysis of the VSG parameters proves that the proposed VSHP control system is able to damp power oscillation significantly by correct tuning.

Damping of power oscillations by active power control requires the plant to change its output power within fractions of a second. VSHP is well-suited for this purpose since it can utilise the rotational energy of the turbine and generator. In future power systems with less directly connected synchronous generators contributing to inertia, it is expected that there will be an increasing demand for ancillary services providing fast frequency control to improve damping as well as rate of change of frequency variations.

8 Acknowledgments

This work was supported by the Research Council of Norway under Grant 257588 and by the Norwegian Research Centre for Hydropower Technology (HydroCen).

9 References

1 Kundur, P., Balu, N.J., Lauby, M.G.: 'Power system stability and control'. vol. 7. (McGraw-hill New York, 1994)
2 Reigstad, T.I., Uhlen, K.: 'Optimized Control of Variable Speed Hydropower for Provision of Fast Frequency Reserves', arXiv e-prints, 2020, arXiv:2003.06262
3 Reigstad, T.I., Uhlen, K.: 'Nonlinear Model Predictive Control of Variable Speed Hydropower for Provision of Fast Frequency Reserves', arXiv e-prints, 2020, arXiv:2006.02097
4 Zheng, Y., Zhou, J., Zhu, W., Zhang, C., Li, C., Fu, W.: 'Design of a multi-mode intelligent model predictive control strategy for hydroelectric generating unit', Neurocomputing, 2016, 207, pp. 287–299
5 Kishor, N., Singh, S.: 'Nonlinear predictive control for a nnarx hydro plant model', Neural computing and applications, 2007, 16, (2), pp. 101–108
6 Zhang, H., Chen, D., Xu, B., Wang, F.: 'Nonlinear modeling and dynamic analysis of hydro-turbine governing system in the process of load rejection transient', Energy Conversion and Management, 2015, 90, pp. 128–137

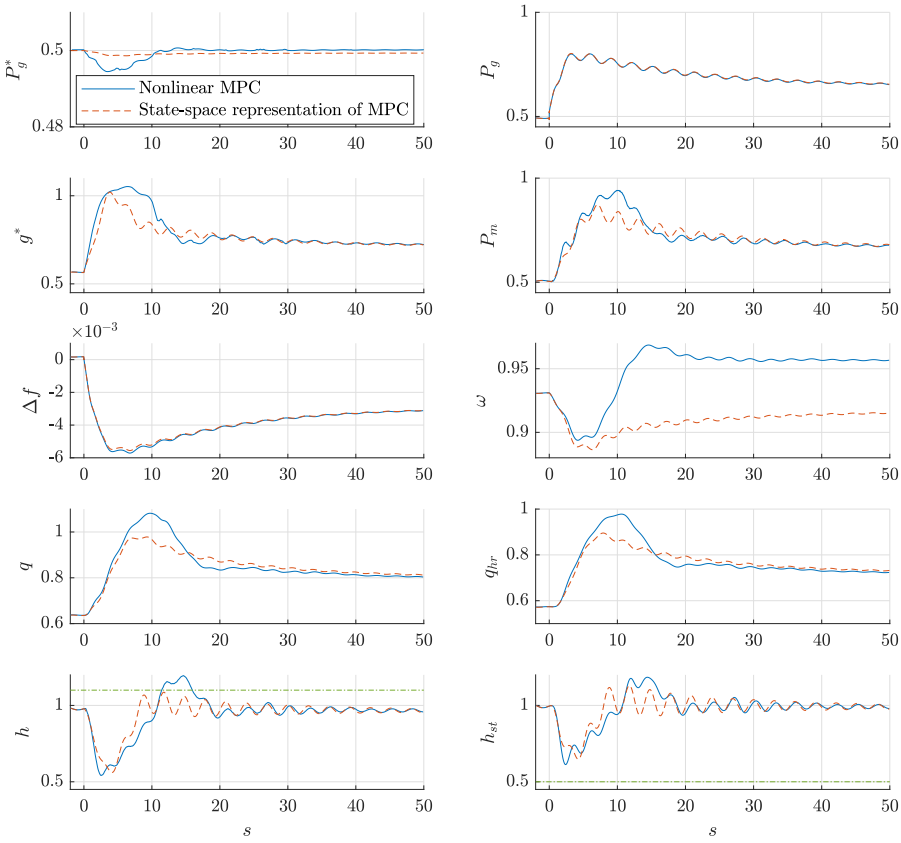

Fig. 10: Dynamic behaviour after 320 MW load increase at Bus 7 (at $t = 0$) for original nonlinear MPC (1)-(3) and state-space representation of MPC (Figure 3)

7 Beus, M., Pandžić, H.: 'Application of model predictive control algorithm on a hydro turbine governor control', 2018 Power Systems Computation Conference (PSCC), 2018, pp. 1–7

8 Fuchs, A., Imhof, M., Demiray, T., Morari, M.: 'Stabilization of large power systems using vsc–hvdc and model predictive control', IEEE Transactions on Power Delivery, 2014, 29, (1), pp. 480–488

9 Sanz, I.M., Judge, P., Spallarossa, C., Chaudhuri, B., Green, T.C., Strbac, G.: 'Effective damping support through vsc-hvdc links with short-term overload capability', 2017 IEEE PES Innovative Smart Grid Technologies Conference Europe (ISGT-Europe), 2017, pp. 1–6

10 Azad, S.P., Iravani, R., Tate, J.E.: 'Damping inter-area oscillations based on a model predictive control (mpc) hvdc supplementary controller', IEEE Transactions on Power Systems, 2013, 28, (3), pp. 3174–3183

11 Jain, A., Biyik, E., Chakrabortty, A.: 'A model predictive control design for selective modal damping in power systems', American Control Conference (ACC), 2015, pp. 4314–4319

12 Koul, S., Tiwari, S.: 'Model predictive control for improving small signal stability of a upfc equipped smib system', 2011 Nirma University International Conference on Engineering, 2011, pp. 1–6

13 Imhof, M., Fuchs, A., Andersson, G., Morari, M.: 'Voltage stability control using vsc-hvdc links and model predictive control', XIII Symposium of Specialists in Electric Operational and Expension Planning, XIII SEPOPE, Foz do Iguassu, Brazil, 2014

14 Ersdal, A.M., Cecilio, I.M., Fabozzi, D., Imsland, L., Thornhill, N.F.: 'Applying model predictive control to power system frequency control', 4th IEEE/PES Innovative Smart Grid Technologies Europe (ISGT EUROPE), 2013, pp. 1–5

15 Ersdal, A.M., Imsland, L., Uhlen, K.: 'Model predictive load-frequency control', IEEE Transactions on Power Systems, 2016, 31, (1), pp. 777–785

16 Ersdal, A.M., Imsland, L., Uhlen, K., Fabozzi, D., Thornhill, N.F.: 'Model predictive load–frequency control taking into account imbalance uncertainty', Control Engineering Practice, 2016, 53, pp. 139–150

17 Elsisi, M., Soliman, M., Aboelela, M., Mansour, W.: 'Improving the grid frequency by optimal design of model predictive control with energy storage devices', Optimal Control Applications and Methods, 2018, 39, (1), pp. 263–280

18 Reigstad, T.I., Uhlen, K.: 'Variable speed hydropower plant with virtual inertia control for provision of fast frequency reserves', arXiv e-prints, 2020, arXiv:2003.07062

19 Alipoor, J., Miura, Y., Ise, T.: 'Power system stabilization using virtual synchronous generator with alternating moment of inertia', IEEE Journal of Emerging and Selected Topics in Power Electronics, 2015, 3, (2), pp. 451–458

20 Poolla, B.K., Groß, D., Dörfler, F.: 'Placement and implementation of grid-forming and grid-following virtual inertia and fast frequency response', IEEE Transactions on Power Systems, 2019, 34, (4), pp. 3035–3046

21 Tielens, P., Van.Hertem, D.: 'The relevance of inertia in power systems', Renewable and Sustainable Energy Reviews, 2016, 55, pp. 999–1009

22 D'Arco, S., Suul, J.A., Fosso, O.B.: 'Small-signal modeling and parametric sensitivity of a virtual synchronous machine in islanded operation', International Journal of Electrical Power & Energy Systems, 2015, 72, pp. 3–15

23 Tamrakar, U., Shrestha, D., Maharjan, M., Bhattarai, B.P., Hansen, T.M., Tonkoski, R.: 'Virtual inertia: Current trends and future directions', Applied Sciences, 2017, 7, (7), pp. 654

24 D'Arco, S., Suul, J.A., Fosso, O.B.: 'A virtual synchronous machine implementation for distributed control of power converters in smartgrids', Electric Power Systems Research, 2015, 122, pp. 180–197

25 Torres L., M.A., Lopes, L.A.C., Moran T., L.A., Espinoza C., J.R.: 'Self-tuning virtual synchronous machine: a control strategy for energy storage systems to support dynamic frequency control', IEEE Transactions on Energy Conversion, 2014, 29, pp. 833–840

26 Mo, O., D'Arco, S., Suul, J.A.: 'Evaluation of virtual synchronous machines with dynamic or quasi-stationary machine models', IEEE Transactions on Industrial Electronics, 2017, 64, (7), pp. 5952–5962

27 Serban, I., Ion, C.P.: 'Microgrid control based on a grid-forming inverter operating as virtual synchronous generator with enhanced dynamic response capability', International Journal of Electrical Power & Energy Systems, 2017, 89, pp. 84–105

28 Liu, J., Miura, Y., Ise, T.: 'Comparison of dynamic characteristics between virtual synchronous generator and droop control in inverter-based distributed generators', IEEE Transactions on Power Electronics, 2016, 31, (5), pp. 3600–3611

29 Sakimoto, K., Miura, Y., Ise, T.: 'Stabilization of a power system with a distributed generator by a virtual synchronous generator function', 2011 IEEE 8th International Conference on Power Electronics and ECCE, Asia (ICPE & ECCE), 2011

30 Ullah, N.R., Thiringer, T., Karlsson, D.: 'Temporary primary frequency control support by variable speed wind turbines—Potential and applications', IEEE Transactions on Power Systems, 2008, 23, (2), pp. 601–612
31 Wang-Hansen, M., Josefsson, R., Mehmedovic, H.: 'Frequency controlling wind power modeling of control strategies', IEEE Transactions on Sustainable Energy, 2013, 4, (4), pp. 954–959
32 Wang, Y., Delille, G., Bayem, H., Guillaud, X., Francois, B.: 'High wind power penetration in isolated power systems—Assessment of wind inertial and primary frequency responses', IEEE Transactions on Power Systems, 2013, 28, (3), pp. 2412–2420
33 Wu, L., Infield, D.G.: 'Towards an assessment of power system frequency support from wind plant—Modeling aggregate inertial response', IEEE Transactions on Power Systems, 2013, 28, (3), pp. 2283–2291
34 Brisebois, J., Aubut, N.: 'Wind farm inertia emulation to fulfill Hydro-Québec's specific need', 2011 IEEE Power and Energy Society General Meeting, 2011
35 Soni, N., Doolla, S., Chandorkar, Mukul, C.: 'Improvement of transient response in microgrids using virtual inertia', IEEE Transactions on Power Delivery, 2013, 28, (3), pp. 1830–1838
36 Arani, M.F.M., El-Saadany, E.F.: 'Implementing virtual inertia in DFIG-based wind power generation', IEEE Transactions on Power Systems, 2013, 28, (2), pp. 1373–1384
37 Zhu, J., Booth, C.D., Adam, G.P., Roscoe, A.J., Bright, C.G.: 'Inertia emulation control strategy for VSC-HVDC transmission systems', IEEE Transactions on Power Systems, 2013, 28, (2), pp. 1277–1287
38 Zeni, L., Rudolph, A.J., Münster-Swendsen, J., Margaris, I., Hansen, A.D., Sørensen, P.: 'Virtual inertia for variable speed wind turbines', Wind Energy, 2013, 16, (8), pp. 1225–1239
39 Wang, S., Hu, J., Yuan, X., Sun, L.: 'On inertial dynamics of virtual-synchronous-controlled DFIG-based wind turbines', IEEE Transactions on Energy Conversion, 2015, 30, (4), pp. 1691–1702
40 Díaz-González, F., Hau, M., Sumper, A., Gomis-Bellmunt, O: 'Participation of wind power plants in system frequency control: Review of grid code requirements and control methods', Renewable and Sustainable Energy Reviews, 2014, 34, pp. 551–564
41 Wilches-Bernal, F., Chow, J.H., Sanchez-Gasca, J.J.: 'A fundamental study of applying wind turbines for power system frequency control', IEEE Transactions on Power Systems, 2015, 31, (2), pp. 1496–1505
42 Bao, W., Wu, Q., Ding, L., Huang, S., Teng, F., Terzija, V.: 'Synthetic Inertial Control of Wind Farm with BESS Based on Model Predictive Control', IET Renewable Power Generation, 2020
43 Reigstad, T.I., Uhlen, K.: 'Variable speed hydropower conversion and control', IEEE Transactions on Energy Conversion, March 2020, 35, (1), pp. 386–393
44 Endegnanew, A.G., Uhlen, K.: 'Global analysis of frequency stability and inertia in ac systems interconnected through an hvdc', 2016 IEEE International Energy Conference (ENERGYCON), 2016. pp. 1–6
45 Faanes, A., Skogestad, S.: 'State space realization of model predictive controllers without active constraints', Modeling, identification and control, 2003, 24, (4), pp. 231
46 Muske, K.R., Rawlings, J.B.: 'Model predictive control with linear models', AIChE Journal, 1993, 39, (2), pp. 262–287
47 Lewis, F.L., Xie, L., Popa, D.: 'Optimal and robust estimation: with an introduction to stochastic control theory', (CRC press, 2017)
48 MATLAB: 'version 9.5.0 (R2010a)', (Natick, Massachusetts: The MathWorks Inc., 2018)
49 Beerten, J., D'Arco, S., Suul, J.A.: 'Identification and small-signal analysis of interaction modes in vsc mtdc systems', IEEE Transactions on Power Delivery, 2016, 31, (2), pp. 888–897

Paper VIII

Variable Speed Hydropower for Provision of Fast Frequency Reserves in the Nordic Grid

This paper is awaiting publication and is not included in NTNU Open

ISBN 978-82-326-5323-2 (printed ver.)
ISBN 978-82-326-5870-1 (electronic ver.)
ISSN 1503-8181 (printed ver.)
ISSN 2703-8084 (online ver.)

NTNU

Norwegian University of
Science and Technology